Tsunami Hazard in Eastern Indonesia: Source Identification and Reconstruction for Historical Case Studies

Ignatius Ryan Pranantyo

A thesis submitted for the degree of
Doctor of Philosophy
The Australian National University

March 2020

Except where otherwise indicated, this thesis is my own original work.

Ignatius Ryan Pranantyo
3 March 2020

"Most people, if you describe a train of events to them, will tell you what the result would be. There are few people, however, who, if you told them a result, would be able to evolve from their own inner consciousness what the steps were which led up to that result. This power is what I mean when I talk of reasoning backwards*."*

Sherlock Holmes, A study in Scarlet, 1887; by Arthur Conan Doyle

Acknowledgments

Pursuing a PhD degree was not part of my dream in the past. I believed a Masters degree would give me enough expertise. However, while studying at the Australian National University over the past four years, my opinion has gradually changed. I have enjoyed the support of the relaxing and quiet environment of Canberra and I now want to keep on enhancing my expertise and conduct as much research as possible.

This research was only possible because of the dedicated guidance of my supervisor, Professor Phil Cummins. He worked very hard to make sure I would receive a letter of acceptance so that I would be able to arrive on time. He has suggested many ideas that have helped to solve problems and work effectively and efficiently. Working with him has been a beautiful experience; he has shown me how to have an optimistic attitude and to keep questioning every step in conducting research.

Thank you to Dr Sebastien Allgeyer, who has introduced me to the *snake* world. Even though I am not yet perfect, I am more confident with *Anaconda* and *Python*. In the early stages of my PhD study, he guided me in tsunami modelling and source inversion issues. In addition, he has taught me to be realistic.

I would like to thank Dr Gareth Davies, Dr Jonathan Pownall, Mr Jonathan Griffin, and Dr Hamzah Latief for our discussions to improve the results of my research. Special thanks to Dr Toshitaka Baba, who has developed the JAGURS code to the world. It was also a memorable experience to visit him at Tokushima University and learn about the first generation of the two-layers model in the JAGURS code.

My life in Research School of Earth Sciences (RSES) would never be happy without having friends. Particularly, *Kang Guru* Cipta, who has shown me around Canberra and helped me to make a crazy travelling trip, and the others who were always waiting for free food every week. Thanks to the staff in the Seismology and Mathematical Geophysics group and the other staff in RSES who have supported my academic life here.

I am a lucky student who gained the Australian Award Scholarship from the Australian Government's Department of Foreign Affairs and Trade. Without this scholarship, I would never have been able to come to Australia and undertake a PhD degree. Moreover, thanks to Elite Editing who has edited my English.

Last but not at the least, thanks to my family for your endless love. To my parents, I would not be here without your support and blessings. To my brother, who has introduced me to living overseas. To my sister, this is a teaser so that you can reach an even higher goal than mine. Lastly, my lovely wife, Dhinda. It was a great decision to bring you here to help and accompany me, as well as to start a new life together.

Abstract

The archipelagic country of Indonesia is vulnerable to tsunami hazard due to its tectonic setting. An updated tsunami catalogue numbers 133 tsunamis documented between 1608 and 2018. Approximately 80% of tsunamis in Indonesia were generated by earthquakes. Eastern Indonesia experienced almost double the number of tsunamis (88) than western of Indonesia (45), as separated by the Wallace Line. It is almost certain that the Sunda subduction zone and Krakatau (including Anak Krakatau) generated all tsunamis in the western part of Indonesia. However, it is more difficult to determine the primary source of many tsunamis in the eastern region. Observations of these tsunamis are documented in several tsunami catalogues. Most of the events begin with a description of ground motion felt by local people at various locations, which as then followed by a tsunami. For several major events, there was detailed information on the physical tsunami behaviour observed at several places. For events in eastern Indonesia, there is no detailed information on the primary source of the ground motion and the tsunami.

The aims of this study are 1) to develop techniques to optimise information from sparse and incomplete historical accounts using three case studies from eastern Indonesia: i) the Ambon Island 1674, ii) the Banda Sea 1852, and iii) the Flores Island 1992 tsunamis, and 2) to identify and reconstruct the primary source of the ground motion and tsunami for each event.

The Ambon Island 1674 earthquake and tsunami has the oldest detailed historical account in Indonesia. It was also the largest tsunami run-up height ever documented in Indonesia, reaching about 100 m only on the northern shore of Ambon, whereas minor tsunamis were observed at other locations. The accounts gave detailed information on the earthquake intensities and tsunami observations from Ambon and its surrounding islands. Through a process of eliminating the well-known faults around the island and tsunami modelling, the most credible source to explain the tsunami observation was determined to be a landslide from the northern shore of Ambon. The earthquake source is still unclear. However, the ground motions were caused by a local and shallow depth earthquake.

This study found that the Banda Sea 1852 earthquake and tsunami was the first event known in which a major tsunami was generated by a very low-angle normal fault, in this case known as the Banda Detachment. This conclusion is reached by combining a tsunami inverse travel time simulation, an earthquake intensity inversion, and tsunami modelling. An earthquake from the Banda Detachment can generate high intensity ground motion on the Banda Islands that gradually decreases towards Ternate in the north. Moreover, a landslide triggered by the Banda Detachment explains why people at Banda Neira and Ambon observed a tsunami that arrived with a positive phase polarity, unlike previous studies hypothesizing a source

on the Tanimbar Trough.

The source of the Flores Island 1992 earthquake and tsunami is constrained using a finite-fault source inversion technique. In this study, multiple data types are utilised together to provide an alternative solution to the rupture area, which has never been done in previous studies of this event. Through this technique and careful analysis of the fault plane model, the strike of the earthquake is confirmed to be 70°. This fault geometry raises new questions about segmentation on the Flores back-arc thrust.

Lastly, this study recommends a major modification for tsunami and earthquake hazard in eastern Indonesia. Firstly, all of events studied potentially involved landslides, so that landslides have to be considered in any tsunami hazard assessment. Secondly, the Banda Detachment is a major tsunami and earthquake source in the Banda Sea region. Lastly, the Flores back-arc thrust is a segmented zone. These factors will dramatically change the potential seismic and tsunami hazard distribution in this region.

Contents

List of Figures

List of Tables

Chapter 1

Introduction

1.1 Research background

Tsunamis are very low-frequency events but in comparison with other geohazards, they have high-severity effects [UNISDR, 2015]. Although tsunamis contribute to only a small portion of annual global economic loss, they cannot be neglected, particularly on a local spatial and temporal scale. The estimation of total annual economic loss from earthquakes, floods, storm surges, and wind hazards is about 310 billion USD (Figure 1.1). However, even a single devastating event can be very costly; for example, the Tohoku 2011 tsunami alone caused a loss of approximately 210 billion USD [UNISDR, 2015; Løvholt et al., 2014]. A tsunami risk assessment predicts that regions with a high level of economy activity near the coastline, such as Indonesia, Macau, and Hong Kong, will experience significant capital stock losses over a 50-year period because of tsunamis [UNISDR, 2015].

One global tsunami hazard study predicts that Indonesia, together with most of the Pacific Rim countries, will experience the highest tsunami hazard, with an exceedance rate of 1/500 and 1/2500 (Figure 1.2) [Davies et al., 2018]. The study estimates tsunami heights of approximately 5 to 10+ m along the Indonesia coastline, with the eastern region being the most tsunami-prone area. This finding is similar to that of an earlier study conducted by [Horspool et al., 2014]. However, both of those studies considered only tsunamis caused by earthquakes.

After the 2004 Indian Ocean tsunami, the Indonesia Tsunami Early Warning System (InaTEWS) was established. Since then, the system has been updated so that it can cover the eastern Indonesia region [Harig et al., 2019]. However, InaTEWS considers only tsunamigenic earthquake events. It failed to provide enough warning in the 2018 Palu and Sunda Strait tsunamis, which had other causes.

The Palu Bay tsunami was initiated by a Mw 7.5 strike-slip earthquake on the Palu-Koro fault. A tsunami warning was released approximately five minutes after the earthquake, but the tsunami, which was probably caused by submarine landslides in the bay [Sassa and Takagawa, 2019], arrived around two minutes earlier than the timing given in the warning. This region has experienced tsunamis in the past and older people have this knowledge, but it has not been transferred to the younger generations.

During the Sunda Strait event, InaTEWS gave no tsunami warning at all. This

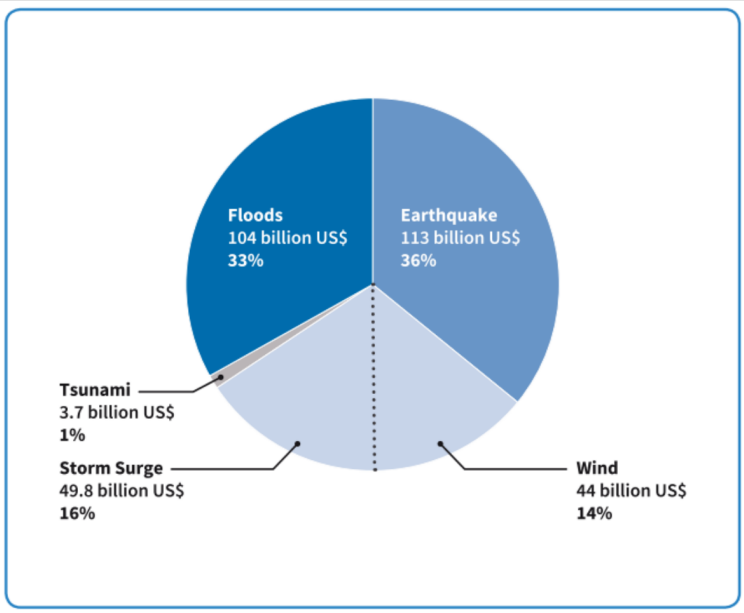

Figure 1.1: Global average annual loss from different types of geohazards (taken from UNISDR [2015])

silent tsunami was generated by a landslide on the Anak Krakatoa Volcano [Patton et al., 2018], which had been active during the previous months. In 1883, the Krakatoa Volcano generated a much larger tsunami in this region. A study from Paris et al. [2014] has apparently estimated the potential future tsunami hazard from the Anak Krakatoa Volcano.

These two events showed that the assessment of tsunami hazards is not yet adequate. As Indonesia is an archipelago country, with the Government building "maritime super highways" and port infrastructures across the country, conducting a comprehensive study to assess future tsunami hazards is essential. The simplest method for this is by examining past events.

Historical accounts show that at least 133 tsunamis have occurred in Indonesia since the 1600s according to tsunami catalogues available (discussed in Chapter 2). The catalogues describe tsunami heights and distribution, as observed by the local people at the time. While the data are sparse, they clearly indicate that all the coastline of Indonesia has been affected by tsunamis in the past. Unfortunately, crucial information regarding the sources of these tsunamis is incomplete, which means the historical accounts are not particularly useful. Scientific investigation is required to answer the questions; i) what was the source, ii) how big was it, and ii) how was it generated? The answers to these questions are needed for future hazard assessment.

Tsunami hazard studies in Indonesia have been conducted mostly for the islands of Sumatra and Java. However, approximately two-thirds of past events have occurred in the eastern region, separated by the Wallace Line that lies from Makassar

Strait at the north to Lombok Strait at the south, and this region is often described to the most complex tectonic region on Earth [e.g. Hamilton, 1979; McCaffrey, 1988; Spakman and Hall, 2010; Pownall et al., 2013, respectively]. As the Government of Indonesia is expanding economic activity into the eastern region [Coordinating Ministry for Economic Affairs, 2011], it is important to understand the tsunami hazard there, which is the reason for conducting this study in that area.

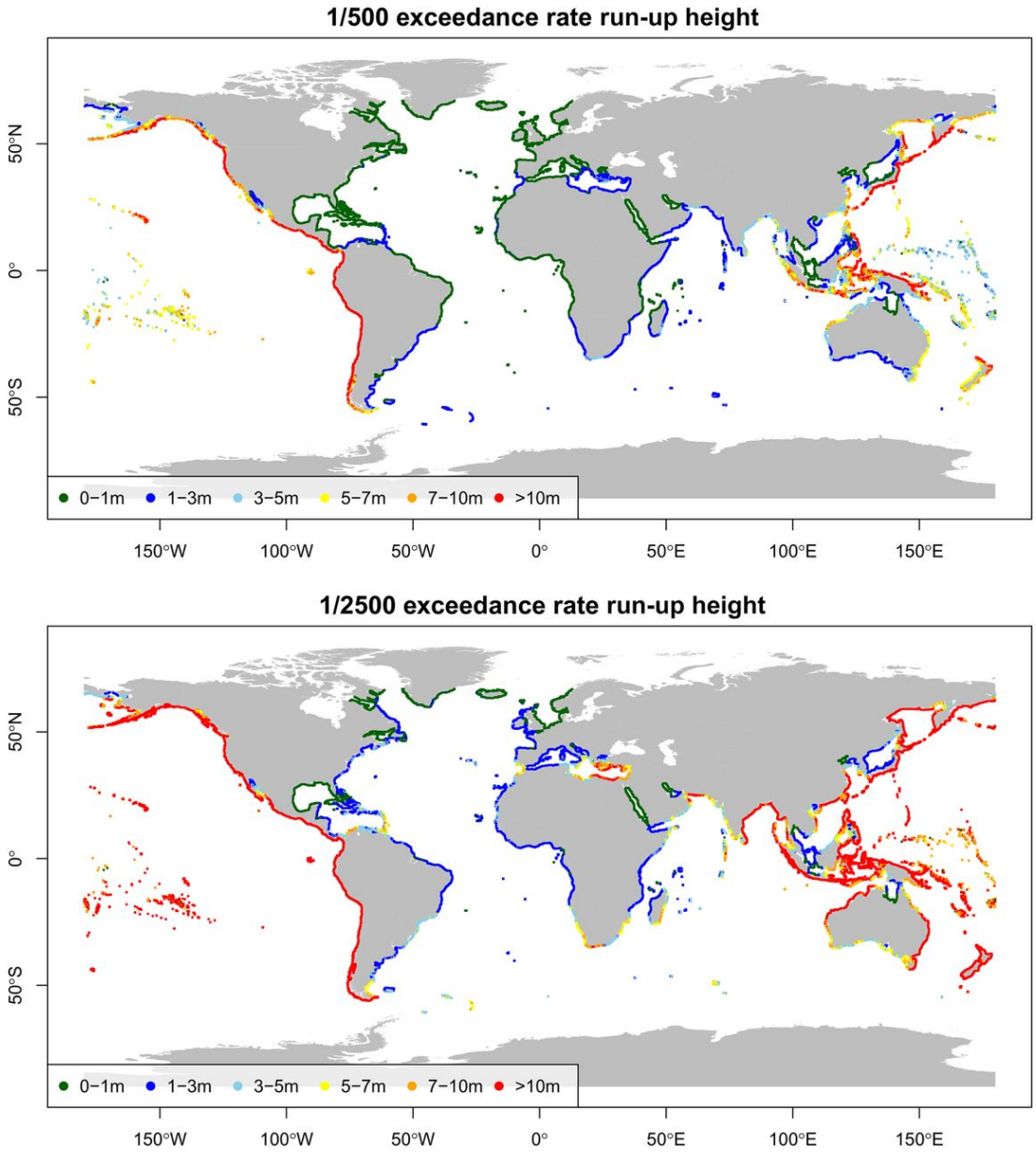

Figure 1.2: Tsunami run-up heights associated with 1/500 (top) and 1/2500 (bottom) exceedance rates (taken from Davies et al. [2018])

1.2 Research objectives

Understanding past events is the first important step in a tsunami hazard assessment [Glade et al., 2001]. The simplest way to calculate a potential hazard for the future is to use a tsunami event from the past.

In Indonesia, tsunami records have been documented since 1608 [e.g. Wichmann, 1918, 1922; Soloviev and Go, 1974; Soloviev et al., 1986; Latief et al., 2000; NGDC/WDS, 2019]. Relatively detailed information regarding ground motion perception and physical tsunami observations are available for some large and devastating events. However, these records do not mention the primary source of the tsunami, except for the modern events from the NGDC/WDS [2019].

The aims of this research are to (1) identify the sources of and (2) reconstruct historical tsunami events in the eastern Indonesia region. Three sub-questions have been defined to achieve these aims. First, what was the source of the event? Second, how was the event? Lastly, how was the tsunami generated?

The first activity is to review the tsunami catalogues of Indonesia. It leads to the creation of an updated tsunami catalogue. This updated catalogue provides information regarding the date of the event, the possible source, location of the affected areas, and qualitative interpretation of the intensity level.

Data of past tsunami events are sparse and incomplete, compared with data of more recent events. However, they contain beneficial information to guide us to answer the questions above. In this research, techniques to tackle these issues are developed through three case studies. The chosen events came from three different periods, to show how the techniques evolved according to the quantity and quality of data available. Then the reconstructed sources of these tsunami events are analysed to estimate the potential future tsunami hazard in this region.

1.3 Thesis organisation

The focus of this thesis is on three main issues relating to tsunamis in Indonesia. The first is a review of historical tsunamis and the tectonic setting of Indonesia, presented in Chapter 2 2. The second aspect is the presentation of the reconstruction and source identification of three cases of tsunamis in eastern Indonesia (Chapters 3 - 5). The third is an assessment of the future tsunami hazard for each region mentioned in these case studies. This is presented as a subsection in the chapter for each case study.

Chapter 2 is divided into two sections: a discussion of the tectonic setting of eastern Indonesia, and an updated tsunami catalogue of Indonesia (to December 2018), which is based on a review of all tsunami catalogues available for Indonesia. Some major and devastating tsunami events are discussed briefly.

Chapter 3 contains the first case study, the 17 February 1674 Ambon Island event. The oldest detailed historical accounts from Rumphius [1675] offer an opportunity to reanalyse the source of this tsunami. It shows that the tsunamigenic earthquake

scenario cannot generate the extremely high tsunami that observed on the northern coast of the island, except for the coastal landslide model.

Chapter 4 contains a study of the 26 November 1852 Banda Sea earthquake and tsunami. It is commonly believed that this event was caused by the Banda Arc megathrust earthquake. However, this study suggests different causes. The Banda Detachment, which has a very low-angle normal fault mechanism, is the most credible source of intense ground shaking at the Banda Islands. The Banda Detachment has never been considered a potential seismic and tsunami hazard source in the region. Therefore, if the Banda Detachment can be confirmed as an active fault, this will be the first study showing that a low-angle normal fault can generate a tsunami. The second possible source of the tsunami is a submarine landslide in the Weber Deep.

Chapter 5 contains a study from the 12 December 1992 Flores Island earthquake and tsunami, which has been studied by several authors. However, there has been no agreement regarding the primary fault source. It has been believed that the Flores back-arc thrust was the source. This study suggests an alternative interpretation of the event by optimising teleseismic waveforms, post-tsunami field surveys, and coastal subsidence datasets through the finite-fault source inversion technique. This created a new perspective on potential seismic and tsunami hazards in the region, which needs further investigation.

Chapter 6 contains a summary of this study. In addition, this chapter suggests further research work could be done.

1.4 Publication schedule

The findings of this research have been published elsewhere. The case studies in Chapters 3 and 5 have been published in the proceedings of academic conferences and Chapter 5 has been published as an article as well. Chapter 3 has been submitted to an academic journal. Chapter 4 soon be submitted to a peer-reviewed journal.

- Academic conferences:
  - A low-angle normal fault earthquake and tsunami: The 1852 Banda Sea, eastern Indonesia case study. AGU Fall Meeting 2018, Washington DC, USA.
  - Finite-fault source inversion for the 1992 Flores tsunami. International Tsunami Symposium, 2017, Bali, Indonesia.
  - Modelling of historical tsunamis in eastern Indonesia: 1674 Ambon and 1992 Flores case studies. International Symposium of Earth Hazard and Disaster Mitigation 2016, Bandung, Indonesia.

- Publications:
  - Cummins, P.R., **Pranantyo, I.R.**, Griffin, J., Pownall, J., Meilano, I. and Zhao, S. (2000) Earthquakes and tsunamis caused by low-angle normal faulting in the Banda Sea, Indonesia. Nature Geoscience (accepted), doi: 10.1038/s41561-020-0545-x
  - **Pranantyo, I.R.** and Cummins, P.R. (2019) The 1674 Ambon tsunami: Extreme run-up caused by an earthquake-triggered landslide. Pure and Applied Geophysics, doi: 10.1007/s00024-019-02390-2
  - **Pranantyo, I.R.** and Cummins, P.R. (2019) Multi-data-type source estimation for the 1992 Flores earthquake and tsunami. Pure and Applied Geophysics, doi: 10.1007/s00024-018-2078-4
  - **Pranantyo, I.R.** and Cummins, P., Griffin, J., Davies, G. and Latief, H. (2017) Modelling of historical tsunamis in eastern Indonesia: 1674 Ambon and 1992 Flores case studies. AIP Conference Proceedings 1857, doi: 10.1063/1.4987104

Chapter 2

Historical Tsunamis in Eastern Indonesia

2.1 Regional tectonic setting of Indonesia

Indonesia is an archipelago country that spans over 5,000 km from west to east (95°E–41°E) and 1,800 km from south to north, crossing the equatorial line (11°S–6°N). Water covers almost 75% of the area. It has 17,499 islands [KKP, 2017a] and over 99,000 km of coastline, which is the second-longest coastline in the world [KKP, 2017b]. Moreover, the archipelago is located at a strategic location between the Indian and the Pacific Ocean, as well as the Eurasia and Australia Continents.

Indonesia is a complex geological region. It is surrounded by five major tectonic plates: the Eurasia, India, Australia, Pacific, and Philippine Sea Plates [DeMets et al., 2010]. As shown in Figure 2.1, the Sunda Trench is the tectonic boundary in the western region between the Indian and Eurasian Plates. It lies parallel to the great strike-slip Sumatra Fault. The trench continues to the south as the Java Trench and ends to the south of Sumba Island.

The Flores back-arc thrust is the consequence of the collision process in the eastern Sunda-Java trench [Silver et al., 1983, 1986]. Earlier studies have shown the arc lying from the northern part of Lombok in the west, to the north of Wetar Islands in the east, as an intermittent long segement rather than continuous thrust zone [Hamilton, 1979; Usna et al., 1979; Silver et al., 1983, 1986; Breen et al., 1989]. McCaffrey and Nabalek [1987] argues that the Bali Basin is a part of the thrust zone, but the evidence for this is unclear. The most recent studies suggest that the arc might continue to eastern Java [Koulali et al., 2016]. In addition, there is a possibility that the Flores back-arc thrust is segmented [Pranantyo and Cummins, 2019].

The eastern region is often described as being the most complex tectonic region in the world [e.g. Hamilton, 1979; McCaffrey, 1988; Spakman and Hall, 2010; Pownall et al., 2013, respectively]. The convergence of the tectonic plates noted above occurs in the Banda Sea region, creating the Banda Arc. The Banda Arc is like a D-shaped sandwich, bending with a radius curvature of approximately 200 km [Sandiford, 2010]. The inner arc forms a volcanic chain, while the outer arc is a group of non-volcanic islands. The Pacific Plate is moving to the south, creating a subduction zone

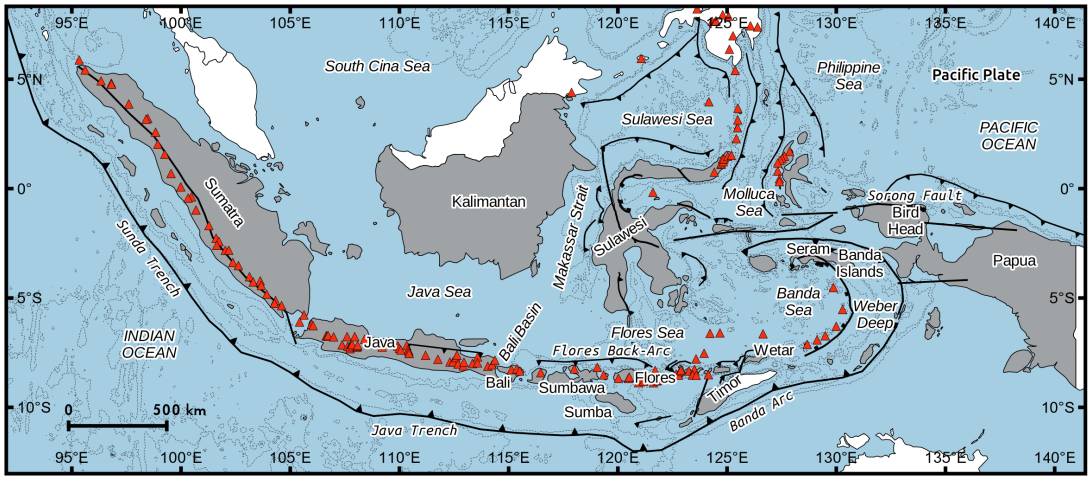

Figure 2.1: Tectonic setting of the archipelago of Indonesia. The dashed contours represent bathymetry at depth 500 m, 1000 m, 2000 m, and 5000 m with red triangles are active volcanoes.

to the north of Papua. In addition, it forms another significant strike-slip fault, the Sorong Fault.

The double subduction zone of Maluku (or Molluca) is formed between the Philippine Sea and the Eurasia Plates. It creates the subduction zone of northern Sulawesi as well. It has been suggested that Sulawesi Island consists of at least five microplates [Cipta et al., 2017]. One of the most prominent structures is the Palu-Koro fault, which has a left-lateral mechanism. It has a geodetic slip rate of approximately 41 to 45 mm per year [Socquet et al., 2006].

As Indonesia lies in a complex tectonic region, the country is vulnerable to many types of geohazard. First, it is a seismically active region. As shown in Figure 2.2, earthquakes are evenly distributed over the archipelago. At least 137 damaging earthquakes were reported between 2005 and 2017 [BMKG, 2018a]. About 33% of them were caused by earthquakes with magnitude less than 6.0, 6.1 to 6.9 (45%), and greater than 7.0 for the rest. Poor quality of the buildings and houses were the main cause of the large numbers of damaging earthquake events reported in Indonesia [e.g. Pribadi et al., 2008; The New Humanitarian, 2009; Mayberry, 2018](e.g. Pribadi et al. [2018], Mayberry, K. [2018], The New Humanitarian [2009]).

In addition, Indonesia has more than 160 active volcanoes. On Sumatra, Sinabung Volcano has been active since 2010, after an extensive dormant period. The activity of the Agung Volcano on Bali Island has fluctuated since 2017, with the latest massive eruption being in 1963 to 1964. In the northern region, the active Soputan and Karangetan Volcanoes are on warning level III/IV, meaning that they might erupt at any time. Further, there is a major threat of tsunami in the archipelago. The 22 December 2018 Sunda Strait tsunami was not the first event occurred from the Anak Krakatoa Volcano. A more devastating event happened in the 1883 when the Kraka-

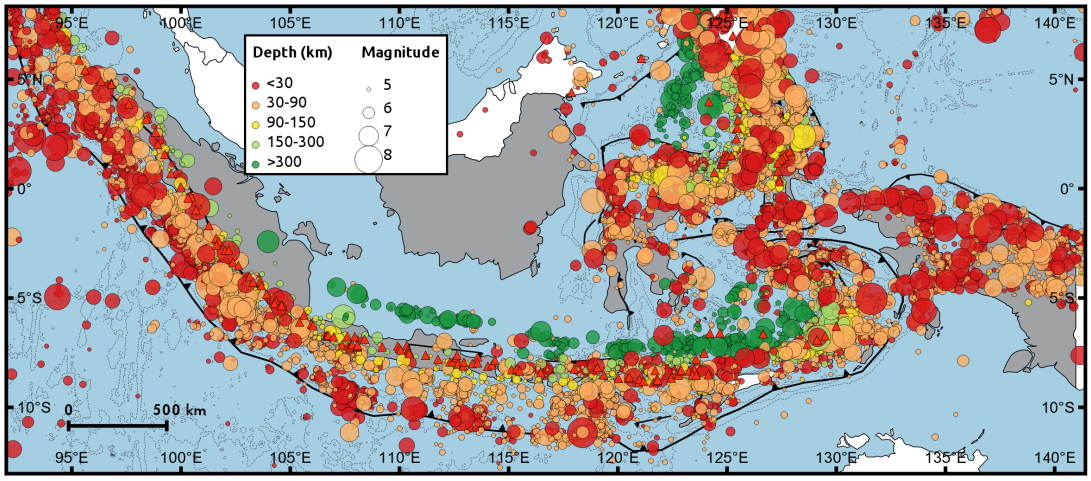

Figure 2.2: Seismicity of Indonesia with Mw greater than 5.0 in 1900–2018 (data taken from U.S. Geological Survey [2019]). Earthquake epicentre depth is indicated by colour and circle size represents its magnitude.

toa Volcano massively erupted and triggered tsunami. Similar to the 28 September 2018 Palu Bay tsunami, a more devastating event has occurred in 1927 that generated higher tsunami up to 15 m. These two examples show Indonesia's vulnerability to tsunami hazards.

2.2 Tsunami definition

A tsunami is an ocean wave caused by a sudden and massive vertical displacement of seawater. This displacement can be generated by a submarine earthquake, landslide, or volcanism. A tsunami has an extremely long wavelength compared with the ocean depth. As shown in Figure 2.3, tsunami amplitude on the open ocean is relatively small, making it difficult to detect tsunamis without using instruments. During propagation towards the coastal area, the shoaling process makes the wavelength shorter and increases the wave's amplitude.

Most of the tsunamis in the world are generated by earthquakes. Other causes of tsunami are volcanic activity and landslides. Generally, earthquakes with a significant vertical mechanism (normal or reverse) generate a larger tsunami than do earthquakes of a similar magnitude but with a strike-slip mechanism. However, a strike-slip earthquake can cause a secondary effect (such as a landslide) that can generate a tsunami, such as the 2010 Haiti [Hornbach et al., 2010] events.

Tsunamis that are generated by volcanic eruption or landslide have a more complex mechanism (Figure 2.5). There are up to eight mechanisms to describe the generation of a tsunami from a volcano [Paris et al., 2014]. Even though the 1883 Krakatoa and 2018 Anak Krakatoa tsunamis arose from a similar volcano, they were each generated by a different mechanism. The 1883 tsunami was a complex event

that involved multiple possible sources[Nomanbhoy and Satake, 1995; Paris et al., 2014], while flank failures caused the 2018 event [Patton et al., 2018].

Tsunamis that are caused by landslides can be generated through two mechanisms (Figure 2.5). The first mechanism is subaerial failure, which occurs when part of a mass slides down from above the seawater. Submarine failure occurs when a mass collapses under the sea surface. Moreover, according to Vernes [1978], there are six types of slope movement that can produce landslides, each of them giving rise to a different result.

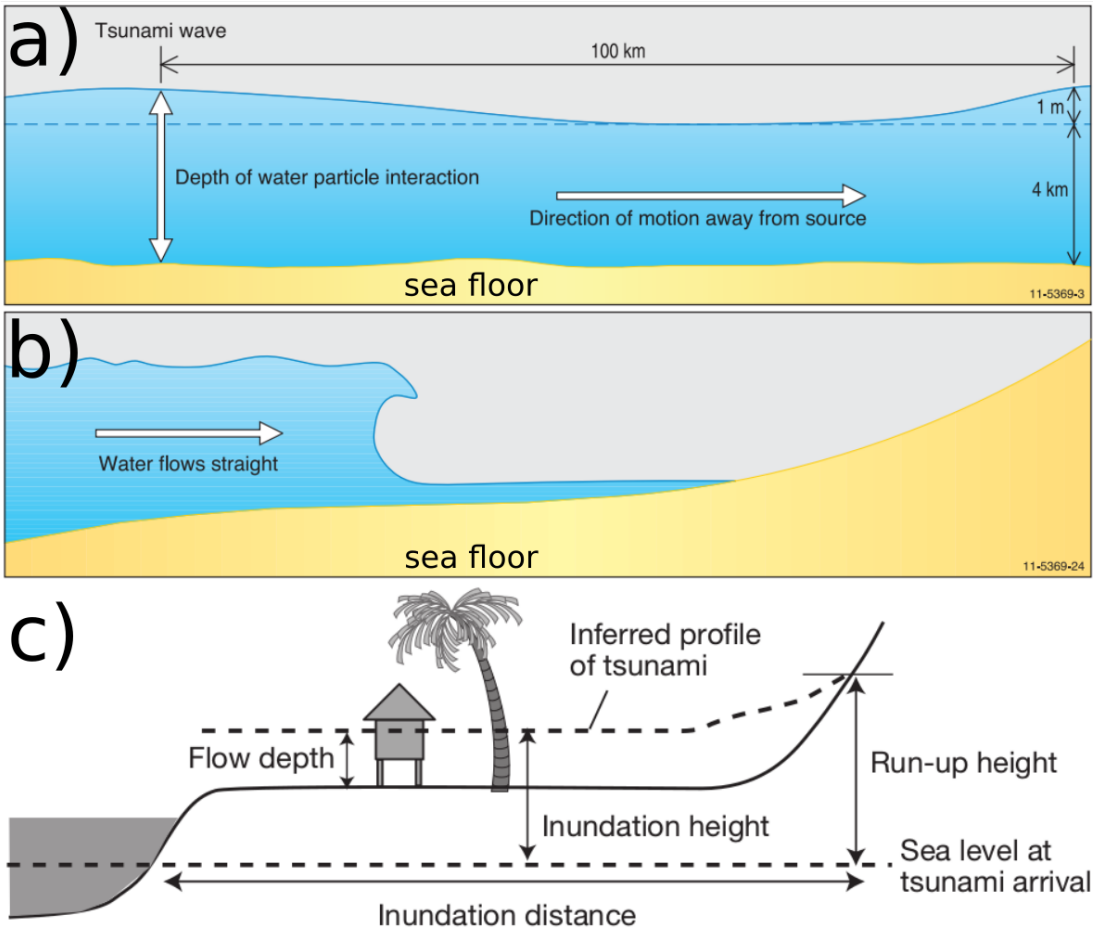

Figure 2.3: (a) Tsunami propagation from the open ocean to (b) the coastal region (modified from Sexton et al. [2011]) and (b) definitions of tsunami run-up heigh, flow depth, and inundation distance on land (taken Satake [2015])

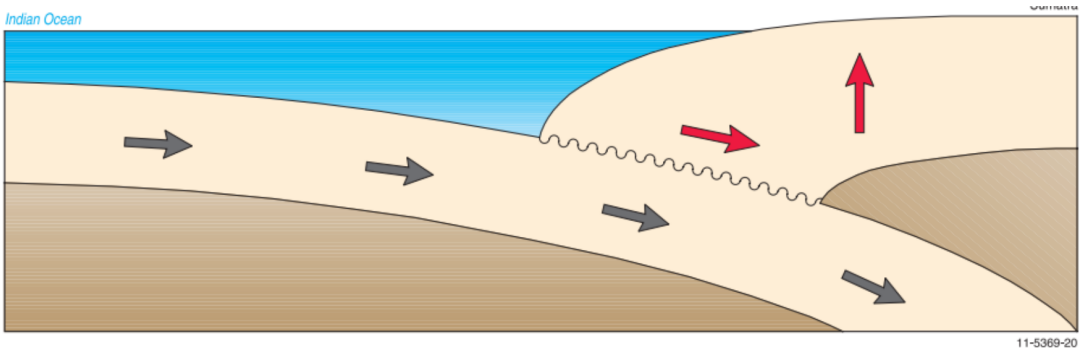

Prior to earthquake. Subduction zone earthquakes cause the most common source of destructive tsunami. They are generated when the lower subducting plate drags the upper plate down causing it to bend.

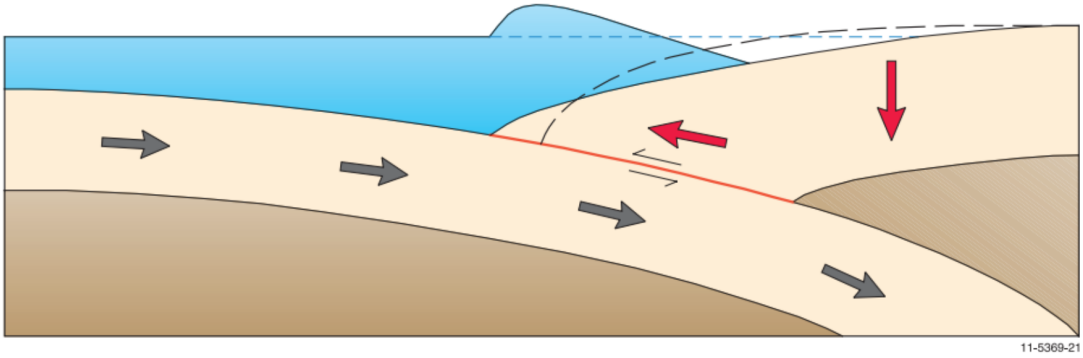

At time of earthquake. Release of stress on the plate boundary causes the upper plate to rebound to its initial, unflexed position, displacing upwards the column of water above. The arrows (shown on the upper plate) in the above pictures indicate the direction in which the upper plate is deformed due to drag and release of the lower plate.

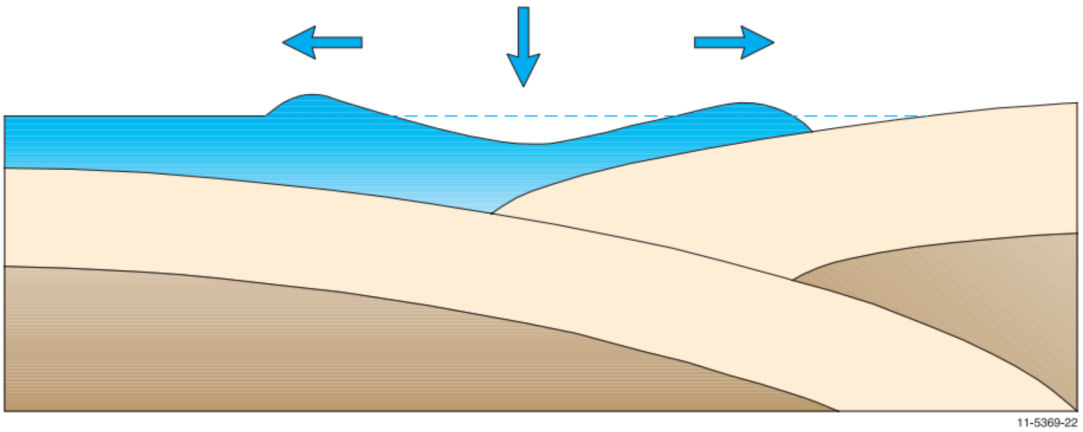

10 minutes after earthquake. The displaced sea surface propagates outward as a tsunami.

Figure 2.4: Earthquake tsunami-generation process (modified from Sexton et al. [2011])

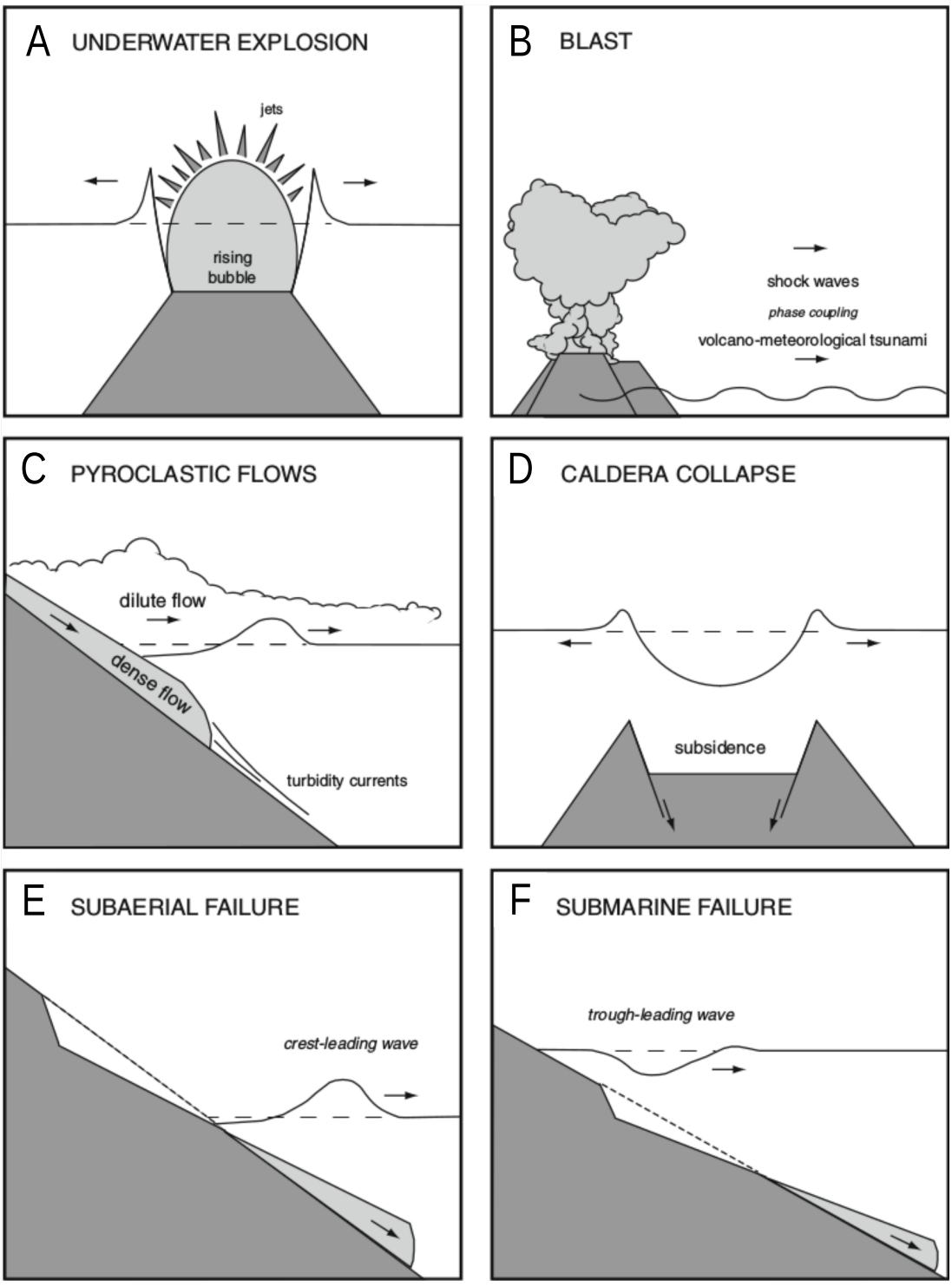

Figure 2.5: Six types of tsunami generation caused by volcanic activity. Subaerial and submarine failure can be the source of tsunami generation as well, due to landslide. (taken from Paris et al. [2014])

2.3 Tsunami in Indonesia

Majority of tsunamis in Indonesia have been caused by earthquakes, followed by volcanic activity and landslide (Figure 2.6). Historical accounts from Indonesia show that at least 133 tsunamis occurred between 1600 and 2018, including the 2018 Central Sulawesi and Sunda Strait tsunamis. Further, at least 61% of those occurred in the eastern Indonesia region from according to several catalouges available (Figure 2.6).

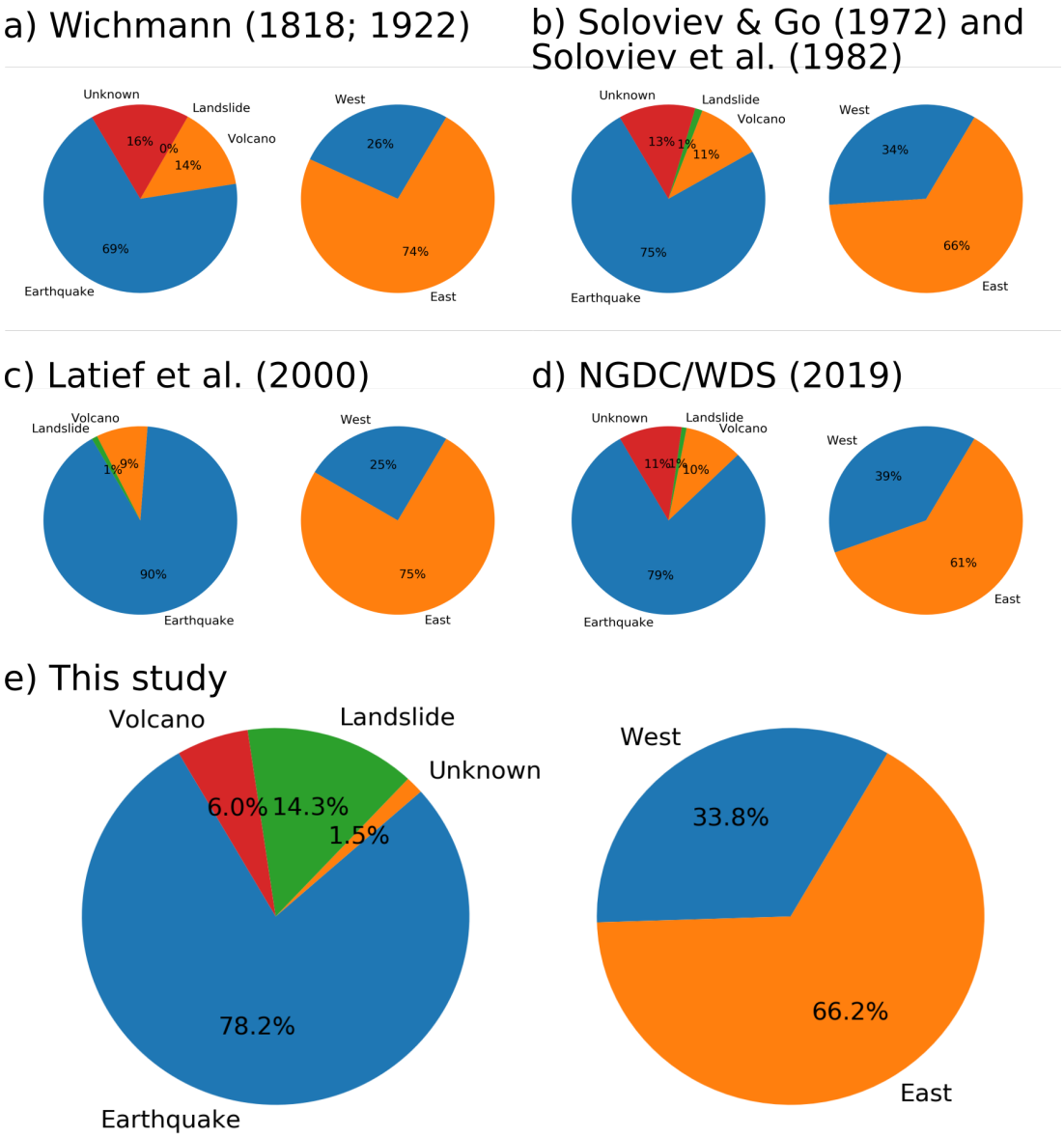

Figure 2.6: Tsunami in Indonesia according to the (left) mechanism and (right) location based on the Wallace line (Figure 2.9) from a) Wichmann [1918] and Wichmann [1922], b) Soloviev and Go [1974] and Soloviev et al. [1986], c) Latief et al. [2000], d) NGDC/WDS [2019], e) this study.

2.4 Tsunami catalogue of Indonesia

Historical tsunami accounts in Indonesia have been reported in several catalogues [e.g. Rumphius, 1675; Wichmann, 1918, 1922; Soloviev and Go, 1974; Soloviev et al., 1986; Latief et al., 2000; Paris et al., 2014; NGDC/WDS, 2019]. Some of those even

mention a tsunami that occurred in 416, according to the Javanese book of *Pustaka Radja* or Book of Kings [Wichmann, 1918; Soloviev and Go, 1974; NGDC/WDS, 2019]. The documents say that a huge explosion from the Kapi Volcano separated the islands of Java and Sumatra and generated a massive tsunami. It seems that the location of the Kapi Volcano would make it the *great-great-grandparent* of the Anak Krakatau Volcano in the Sunda Strait. However, further investigation regarding this event is required.

The historical accounts in Rumphius [1675]; Wichmann [1918, 1922]; Soloviev and Go [1974] and Soloviev et al. [1986] usually begin with a report by the local people about the ground motion felt in various locations. If an event was followed by a tsunami, the catalogues reported the tsunami observations in the affected area as well. However, the catalogues often use another word for tsunami, such as 'emphtidal wave, *sea wall*, *sea quake*, or *water oscillation*. Unfortunately, this can lead to different interpretations of an event. Further analysis would be required to ascertain whether the event described was, in fact, a tsunami or simply a common ocean phenomenon. In addition, there is no detailed information on the source of the ground motion and the tsunami

2.4.1 Tsunami catalogues available

The Rumphius book

A book by Rumphius [1675] is believed to be the oldest detailed tsunami accounts in Indonesia. This book reported a devastating earthquake on 17 February 1674 on Ambon Island, which was followed by a gigantic tsunami only on the northern coast of the island. The book focused on the effects of the earthquake and tsunami on Ambon, as well as some other islands such as Saparua, Haruku, and Seram.

The Wichmann catalogues

The Wichmann [1918] and Wichmann [1922] catalogues mainly describe the ground motion that preceded some tsunami events between 416 and 1877. These catalogues, which have been translated by Harris and Major [2017], record at least 87 tsunami events, most of them caused by earthquakes. Most of the events were in the eastern Indonesia region.

The Soloviev and Go and Soloviev et al. catalogues

Soloviev and Go [1974] and Soloviev et al. [1986] released a tsunami catalogue for the Pacific Ocean region, including Indonesia. Most of the historical accounts before 1877 were based on the Wichmann [1918] and Wichmann [1922] catalogues, with additional references from other authors. Unfortunately, it is difficult to trace back the original references that were used in the Soloviev and Go [1974] and Soloviev et al. [1986] catalogues. These catalogues noted 158 tsunami events between 1608 and 1982, with 103 of them in the eastern Indonesia region. Most of the tsunamis noted in

these catalogues had been generated by earthquakes. The catalogues provided their own interpretations of a level of authenticity to each tsunami report.

The Latief et al. catalogue

A tsunami catalogue published in 2000 by Latief et al. reported 105 tsunamis between 1600 and 1998, with most of the events caused by earthquakes. However, the catalogue has a gap between 1938 and 1961. The the catalogue divides the events into six zones according to the tectonic condition so that the frequency could be analysed. During that period, 23 tsunamis occurred in the western Indonesia region, (Zone A and B) while the rest occurred in the eastern region.

The Paris et al. volcano-tsunami catalogue

A review of tsunami generated by volcanic activity in the Southeast Asia region between 1550 and 2007 was conducted by Paris et al. [2014]. The study showed that Indonesia, Papua New Guinea, and the Philippines are vulnerable to tsunami hazard caused by volcanism. At least 23 historical tsunamis were caused by volcanoes in Indonesia were reported. The authors made suggestions about the main mechanism of tsunami generation in these events.

The NGDC/WDS tsunami database

The most up-to-date tsunami catalogue is from NGDC/WDS. This is a global historical tsunami database organised by the National Oceanic and Atmospheric Administration in the US. The database reports 247 tsunamis occurring in Indonesia between 1608 and 2018, which consider all validity levels from -1 to 4. The number of events reported by this catalogue is much higher than the other. Then majority of those events were caused by earthquakes in the eastern Indonesia region.

The summary of all tsunami catalogues above are shown in Table 2.1 and Figure 2.7 below.

Table 2.1: Summary of tsunami catalogues of Indonesia

		a) Wichmann [1918] b) Wichmann [1922] translated by Harris and Major [2017]			**a) Soloviev and Go [1974] b) Soloviev et al. [1986]**			**Latief et al. [2000]**			**NGDC/WDS [2019]**			**This study**		
Period	a) b)	416, 1608–1857 416, 1608–1857			416, 1608–1968 416, 1608–1968			1629–1998			416, 1608–2018			1608–2018		
		Total	West	East	Total	West	East	Total	West	East	Total	West	East	Total	West	East
Numbers of event	a) b)	69 18	15 8	54 10	158 5	55 1	103 4	105	26	79	247	96	151	133	45	88
Earthquake source	a) b)	46 17	12 8	33 9	119 4	45 1	74 3	95	23	72	195	73	122	104	39	65
Volcano source	a) b)	12 1	1 0	11 1	18 0	4 0	14 0	9	3	6	24	10	14	19	5	14
Landslide source	a) b)	0 0	0 0	0 0	1 1	0 0	1 1	1	0	1	2	2	0	8	1	7
Unknown source	a) b)	12 3	3 4	9 5	20 1	6 2	14 3	0	0	0	26	11	15	2	0	2

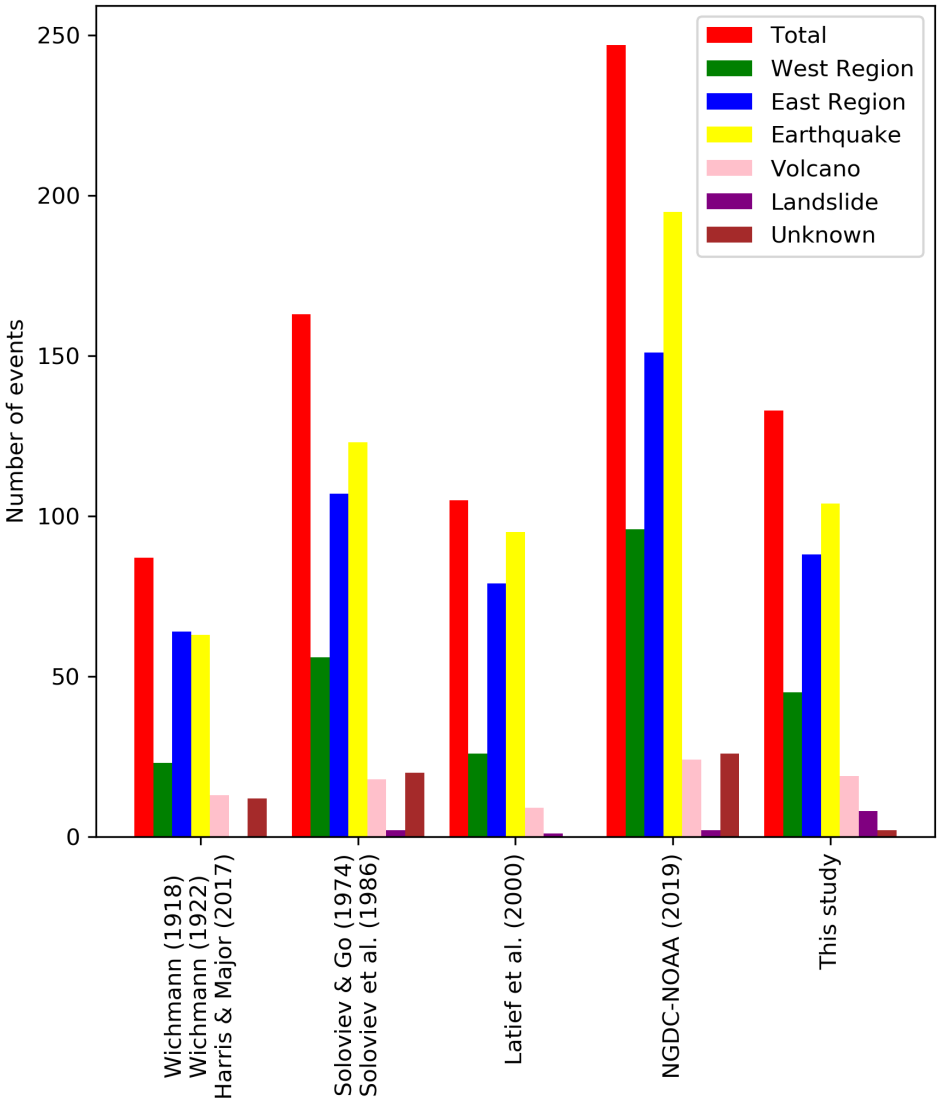

Figure 2.7: Number of tsunami events in Indonesia based on different catalogues

2.4.2 Updated tsunami catalogue

As shown in Table 2.1 and Figure 2.7, the number of events recorded in each catalogue is different. The newer data in the Latief et al. [2000] catalogue seem to suggest fewer events than those of the Soloviev and Go [1974] and Soloviev et al. [1986] catalogues. As previously mentioned, there is the possibility of misinterpretation of historical events in the Soloviev and Go [1974] and Soloviev et al. [1986] catalogues. As the Latief et al. [2000] catalogue used more recent references, such as from Berninghausen [1966, 1969]; Cox [1970]; Iida [1983], to build the database so that false events were rejected. However, it is unclear how it was done.

Interestingly, the NGDC/WDS [2019] database indicates a larger total number of events than the other catalogues. This number is based on all tsunami events with an event validity level between -1 (erroneous entry) and 4 (definite tsunami). If we consider only Level 2 (questionable tsunami) and above, or Level 3 (probable tsunami), the number of events reduces to 177 and 114, respectively, roughly compatible with other catalogues.

Several historical events were not reported in one catalogue while others clearly described it as a tsunami event and. Moreover, there are errors in the dates of some events. For example, three consecutive tsunamis occurred in the Bali Sea in 1815, 1818, and 1820 [Wichmann, 1918; Soloviev and Go, 1974]. However, Latief et al. [2000] has an event in 1816 that supposed to be the 1815 event and the author did not have the 1818 tsunami event. The 1674 Ambon Island tsunami was reported as being in 1675 in the English translation of Wichmann [1918] catalogue [Harris and Major, 2017], which contradicts the date in Rumphius [1675]. In addition, even though only minor tsunamis recorded on instruments, the NGDC/WDS [2019] reports it as an event.

Because of these issues in the catalogues, this study has updated the tsunami catalogue of Indonesia (see Table 2.2). The Latief et al. [2000] and NGDC/WDS [2019] databases were used as the basic data. Then historical accounts were cross-checked with the Wichmann [1918] and Wichmann [1922] catalogues, which have been translated by Harris and Major [2017], Soloviev and Go [1974], and Soloviev et al. [1986], as well as other available references [e.g. BMKG, 2018b,a; Lander et al., 2003; Lassa, 2009, respectively]. A study by Paris et al. [2014] was the basis for the volcanic-tsunami events.

The updated tsunami catalogue is simplified into two regions, seperated by the Wallace Line, instead of six zones as in Latief et al. [2000]. The Wallace Line is a boundary runs from the northern side of Makassar Strait to the southern part of Lombok Strait. It separates flora and fauna between the western and eastern Indonesia region. The flora and fauna in the western section have a similarity to the Asian species whereas the eastern region closes to the Australian. Apparently, this line has indirect correlation to the tectonic condition in this region.

The six zones used by Latief et al. [2000] explained the correlation between tsunami rate and the tectonic condition of each area. However, the historical accounts did not clearly describe the source of the tsunami. A tsunami generated from one zone might propagate across to and be reported only in the other area. Thus, the six classification zones could limit our interpretation of the source.

In my updated catalogue, the tsunami intensity is divided into three levels: minor, medium, and large. These interpretations were based on the historical accounts available. When there was an observation of a tsunami, but there was no detailed information on its height and it was reported only from a few locations, it was defined as a *minor* event. When there was information regarding the height of the tsunami, number of building damaged, and casualties, but it was reported at only few locations, this was defined as a *medium* level. A *large* tsunami event was when the tsunami and its devastating effects were reported from many locations.

Table 2.2: Updated tsunami catalogue of Indonesia (1600–2018)

Time			Tsunami source			Affected area			Refs:
YY	**MM**	**DD**	**Source**	**Location**	**Mag, VEI**	**Location (max tsunami in m)**	**Region**	**Level**	
1608	7	1	Volcano	Mt. Gamalama	3	Makian Island	East	Medium	a, c
1629	8	1	EQ	Seram megathrust		Fort Nassau, Banda Islands, Banda Sea (16)	East	Large	a, c, f
1659	11	11	Volcano	Teon Volcano	3	Ambon Bay (1.0-1.5)	East	Large	a, c, q
1673	8	12	Volcano	Ternate Volcano (Gamkonora)	5	Halmahera	East	Large	a, c
1674	2	17	Landslide	Northern coast of Ambon Island[1]		Ambon Island: between Lima and Hila (80–100), Larike (0.5), Nusatelo, Urien, Hitumala (3), Haruku - Saparua - Laot (1.5–2), Ceram Island: south west of the island, Loki (5.5), Kelang Island (5)	East	Large	a, c, e, g
1674	5	6	EQ			Ambon Bay (weak)	East	Minor	a, c
1708	11	28	Unknown			Ambon (minor)	East	Minor	a, c
1710	3	6	EQ			Banda Islands (local)	East	Minor	c
1711	9	5	EQ			Ambon Island eastern coast and Baguala Bay, Ambon Bay	East	Large	a, c
1754	8	18	EQ			Hutumuri, Haruku, Saparua	East	Minor	a, c
1754	9	7	EQ			Haruku Island	East	Minor	a, c
1763	9	12	EQ			Banda Neira (9)	East	Large	a, c
1770			EQ			Bengkulu, West Sumatra	West	Minor	a, c
1775	4	18 / 19	EQ			Ambon	East	Minor	a, c

[1] see Chapter 3

Continuation of Table 2.2

YY	MM	DD	Source	Location	Mag, VEI	Location (max tsunami in m)	Region	Level	Refs:
1797	2	10	EQ	West Bengkulu, Sunda Arc		Padang, West Sumatra (Strong)	West	Large	a, c, h, ad
1802	8	25	EQ			Ambon (very high)	East	Medium	a, c
1814			EQ			Kupang Bay	East	Minor	a, c
1815	4	11	Volcano	Tambora Volcano	7	Coast of Sumbawa (0.5–3), Bima (0.3), around Tambora (5–6), Sumenep (1–1.5),	East	Large	a, c
1815	11	22	Landslide			Buleleng, North Bali (damaging)	West	Large	a, c
1818	3	18	EQ			Bengkulu, West Sumatra	West	Large	a, c
1818	11	8	EQ			Bima Bay (3.5), Nusa Tenggara Barat	East	Large	a, c
1820	12	29	EQ			Bulukumba (20–25), Sumenep	East	Large	a, c
1833	11	24	EQ	West Bengkulu, Sunda Arc		Bengkulu, West Sumatra	West	Large	h, ad
1840	1	4	EQ	Sout of Java		Local tsunami at South Java	West	Minor	ad
1836	3	5	EQ			Bima	East	Minor	a, c
1840	2	14	Volcano	Mt. Gamalama	3	Ternate (water rushed inland)	East	Medium	c, q
1841	11	26	EQ			Banda Neira: south coast (2.5–3), Fort Nassau	East	Large	a, c
1841	12	16	EQ			Ambon (1.5), Buru, Ambelau	East	Large	a, c
1843	1	5–6	EQ			Nias Island (large)	West	Large	a, c
1845	2	8	Volcano	Mt. Soputan	2	Kema	East	Medium	a, c, q
1846	1	25	EQ			Ternate (1.2) and near Manado	East	Large	a, c
1846	2	14	EQ			Ternate (1.2-1.6)	East	Minor	al
1851	5	4	EQ			Teluk Betung, Lampung (1.5)	West	Minor	a, c
1852	1	9	EQ			Lampung Bay	West	Minor	a, c

Continuation of Table 2.2

YY	MM	DD	Source	Location	Mag, VEI	Location (max tsunami in m)	Region	Level	Refs:
1852	11	26	EQ	A low angle normal fault from Banda Detachment or a possibility of submarine landslide [2]		Banda Neira between Neira and Lonthor (up to 14), Ai Island (1), Ambon bay (0.2), Hila, Larike, Saparua Island, Haruku Island, Caroline Islands	East	Large	a, c, i
1854	9	27	EQ			Ternate	East	Minor	a, c
1855	4	14	EQ			Manggarai, Flores	East	Minor	a, c
1856	3	17	Volcano	Awu Volcano	3	Tahuna Island	East	Large	a, c
1857	5	13	EQ			Dili Bay (3)	East	Medium	a, c
1857	11	17	EQ			Menado, Kema, Ternate	East	Medium	a, c
1858	12	13	EQ			Djailolo Bay and entire eastern coast of Sulawesi from the Bangai arc in the south to the Sanighe	East	Large	a, c
1859	6	28	EQ			Kema, Sidangoli – western of Halmahera (10)	East	Large	b, c
1859	7	29	EQ			Kema, Bangai Island and Makian (moderate)	East	Medium	b, c
1859	9	25	EQ			Banda Islands (local and strong)	East	Medium	a, c
1859	10	20	EQ			Pacitan, East Java (strong)	West	Minor	ad
1861	2	16	EQ			W. Sumatera: Padang, Sibolga, Barus (0.5–1), Nias Islamd, Aceh (1.5), Anyerbangis, Panjang Island, Pulu Tello, Batu Island, Natal, Singkel, Fort Laundi (7), Lapau Island, Bengkulu (1), Citarum River (1.5)	West	Large	h, ad
1861	2	21	EQ			Lake Wanaidjas (1)	West	Minor	b, c

[2] see Chapter 4

Continuation of Table 2.2

YY	MM	DD	Source	Location	Mag, VEI	Location (max tsunami in m)	Region	Level	Refs:
1861	3	9	EQ			W. Sumatera: Simuk Island, Babanirege, Lakao,	West	Large	d
1861	4	26	EQ			Singkel, West Sumatra (0.25)	West	Minor	b, c
1861	6	17	EQ			Anyerbangis, West Sumatra	West	Minor	c
1861	9	25	EQ			Indrapura, West Sumatra	West	Medium	b, c
1864	5	23	EQ			Manokwari (3.5)Geelvink Bay, Papua	East	Large	b, c
1871	3	3	Volcano	Mt. Ruang	2	Tahulandang Island (25)	East	Large	c, q
1876	5	28	EQ			Buru Island, Kajeli (0.3)	East	Minor	b, c
1882	10	10	EQ			Banda Islands	East	Minor	c
1883	8	26 / 27	Volcano	Mt. Krakatoa	6	Sunda Strait (30), south of Sumatera Island (4), north and souther Java (0.5–1), south America (0.5–1)	West	Large	q, am
1885	4	30	EQ	There was an eruption from Maluku Island		Buru Island: Kajeli, Dijkomurasa (0.75), Wahai (0.3)	East	Medium	c
1889	9	6	Volcano	Mt. Banua Wuhu	2	N. Sulawesi: Manado (2), Kema and Amurang (3.5–4), Bentenan (0.5), Ternate Island, Tahuna (1.5),	East	Large	c, q
1891	6	20	Unknown			Saparua, Ambon, Banda Islands	East	Medium	c
1891	10	5–6	EQ			Kupang, Timor	East	Medium	c
1892	5	17	EQ			Sumatera	West	Minor	c
1892	6	2-Jul	Volcano	Mt. Awu	3	Ternate, Makassar, Maros, Bima, Flores, Ende, Ambon Bay (1.5)	East	Large	c, q
1892	11	18	EQ			Buru, Kajeli	East	Minor	c

Continuation of Table 2.2

YY	MM	DD	Source	Location	Mag, VEI	Location (max tsunami in m)	Region	Level	Refs:
1899	9	29	Landslide	Multiple landslides along the southern coast of Seram Island		Seram Island: south coast (9), Paulohi (9), Amahai bay (2), Uwalohi, Taumale, Teluti Bay, Laimu (7-9), Piru Bay (4), north of Hatusua, Kawa (1.7), Taniwil (4.6), Wahai, Saparua,Ambon Bay, Banda Islands, Lonthor (1), Kajeli.	East	Large	c
1904	7	5	EQ			Saparua Bay	East	Minor	c
1907	1	[4]	EQ	Thrust – West of Nias Is.	7.6	Sumatera: Simeleu Island, Aceh, Tapanuli Bay, Metnawai islands, Gunung Sitoli, Pulu Boanga, Natal, Barus, Meulaboh, Kealebu, Puluradja, PuluTello, Padang, Sibolga,	West	Large	c, j
1907	3	30	EQ			Talaud Island (4)	East	Large	c
1908	2	6	EQ			Sikakap Strait, Mentawai Island	West	Minor	c
1909	6	3	EQ			Tandjun, Pau, Mutti, Kambang, Kerinci-Jambi, West Sumatra	West	Minor	c
1914	5	26	EQ			Yapen, Papua	East	Medium	c, p
1917	1	20	EQ	Maybe triggered landslide		Klungkung to Benoa, Bali (2)	West	Medium	c
1918	7	18	Volcano	Mt. Banua Wuhu	3		East	Minor	c, q
1919	4	3	Volcano	Mt. Banua Wuhu	3		East	Medium	c, q
1921	5	14	EQ			Sekurau (1), Sangkurilang	East	Minor	c
1921	9	11	EQ			Local tsunami at Parangtirirs, Central Java (0.1)	West	Minor	c
1927	12	1	EQ	Palu-Koro fault (probably triggered landslide)		Palu Bay (15)	East	Large	c, k
1928	3	26	Volcano	Mt. Krakatoa	2		West	Minor	c, q
1928	8	4	Volcano	Rokatenda Volcano	3	Palu Island, north of Flores (10)	East	Large	a, c

Continuation of Table 2.2

YY	MM	DD	Source	Location	Mag, VEI	Location (max tsunami in m)	Region	Level	Refs:
1930	3	17	Volcano	Mt. Krakatoa	one event with March 1928		West	Minor	c
1930	6	19	EQ	??? - Sunda Strait	6.2	Teluk Betung, Lampung (1.5)	West	Minor	c
1931	9	25	EQ	??? - Southwest Sumatra	7.4	Enggano Island (1)	West	Minor	c
1936	4	1	EQ	??? - Talaud Is., Sulawesi Sea	7.8	Salebabu Island (3)	East	Large	c
1938	2	1	EQ	Thrust - Banda Sea	8.5	Fakfak (0.5)	East	Minor	c, l
1938	5	19	EQ	??? - Tomini Bay	7.7	Toribulu to Parigi (2–3), Lemo – Makatate	East	Large	c
1939	12	21	EQ	??? - Tomini Bay		Langoan	East	Medium	c
1948	6	1	EQ	??? - North Sumatra		Sabang, Sumatra	West	Minor	c
1950	10	8	Landslide	??? - Ambon		Ambon Bay	East	Large	m
1957	10	26	EQ			East of Kalimantan	East	Minor	c
1964	4	2	EQ	??? - Banda Aceh	7	Sumatra	West	Minor	c
1965	1	24	EQ	??? - South Sula Is., between Buru and Mangole	8.2	Sanana Island	East	Large	c
1967	4	11	EQ	Thrust - Makassar Strait	6.3	Tinambung, Sulawesi	East	Large	c, k
1967	4	12	EQ	??? - Sigli, North Sumatra	6.7	Sigli, Sumatra	West	Minor	c
1968	8	10	EQ	??? - Maluku Sea, between Halmahera and Manado	7.6		East	Minor	c
1968	8	14	EQ	Normal - Makassar Strait, Mapaga	7.2	Donggala, West central coast Sulawesi (10)	East	Large	c, k
1969	2	23	EQ	Thrust - Makassar Strait, Majene	7	Majene, Sulawesi (6)	East	Large	d, k
1977	8	19	EQ	Normal - southwest of Sumbawa Is.	8.3	Lunyuk, Sumba Island (8), Leterua, Sumba Island (5.5)	East	Large	d, n
1979	7	18	Landslide	Mt. Iliwerung, Lembata		Waiteba Bay (7)	East	Large	d, o
1979	9	12	EQ	Strike-slip - Yapen Is.	7.9	Local tsunami at Biak and Yapen Island	East	Medium	d, p

Continuation of Table 2.2

YY	MM	DD	Source	Location	Mag, VEI	Location (max tsunami in m)	Region	Level	Refs:
1981	10	20	Volcano	Mt. Krakatoa	II	Small tsunami (less than 2)	West	Minor	q
1982	12	25	Landslide	Larantuka, NTT		Larantuka	East	Minor	al
1983	3	12	EQ	Oblique Thrust - South of Ambon	6.7		East	??	al, an
1983	8	17	Volcano	Mt. Iliwerung	II		East	??	q
1984	1	8	EQ	Thrust - Makassar Strait, Mamuju	7	Mamuju, West central coast Sulawesi	East	Minor	k
1992	12	12	EQ	Thrust - North of central Flores Is.	7.8	Northern coast of Flores (26)	East	Large	r
1994	1	21	EQ	Strike-slip - Halmahera Is.	7	Western coast of Halmahera (2)	East	Medium	s
1994	6	3	EQ	Thrust - South of Eastern Java	7.8	South eastern coast of Java (14)	West	Large	t
1994	10	8	EQ	Strike-slip - between Halmahera and Obi Islands, Maluku	6.8	Kau, Halmahera (2) and damaging	East	Medium	u
1995	5	14	Landslide	Earthquake triggered coastal landslide	6.9	Dili (1.5) inundated 120 m	East	Medium	al, an
1996	1	1	EQ	Thrust - North West Sulawesi	7.9	Northwest central coast Sulawesi (4-10)	East	Large	k, v, w
1996	2	17	EQ	Thrust - North Papua	8.2	Biak Island (7.7)	East	Large	p, x
1998	11	28 / 29	EQ	Strike-slip - Taliabu Is.	7.7	Local tsunami at Mangole Island (2.75)	East	Medium	ah
2000	5	4	EQ	Strike-slip - east of Luwuk region, Sulawesi	7.6	Luwuk, Banggai (3)	East	Large	ai
2002	10	10	EQ	Strike-slip - southeast of the bird head of Papua Is.	7.6	Local and small tsunami at Manokwari	East	Minor	ak
2004	1	28	EQ	Strike-slip - between Buru and Seram Islands	6.7	Namlea (lokal)	East	Minor	an
2004	11	11	EQ	Thrust - Nort of Alor Is.	7.5	Local tsunami at Alor (2)	East	Medium	an

Continuation of Table 2.2

YY	MM	DD	Source	Location	Mag, VEI	Location (max tsunami in m)	Region	Level	Refs:
2004	12	26	EQ	Thrust - Nortwesth Sumatra	9.1	Aceh, northern Sumatra (25+)	West	Large	well known
2005	3	28	EQ	Thrust - Nias Is., Sumatra	8.6		West	Large	an
2006	3	14	EQ	Strike-slip - between Buru and Seram Islands	6.7	Local tsunami at Buru (5)	East	Minor	aj
2006	7	17	EQ	Thrust - south of Western Java	7.7	South coast of Western Java (20)	West	Large	y
2007	9	12	EQ	Thrust - Bengkulu, Southwest of Sumatra	8.4	Lais 50 km northwest of Bengkulu (3.9)	West	Large	z
2008	11	16	EQ	Thrust - North of Sulawesi Is.	7.4	North Sulawesi (local and small)	East	Minor	an
2009	1	3	EQ	Thrust - Head of Bird, Papua	7.7	Manokwari	East	Minor	aa
2009	8	16	EQ	Thrust - East of Mentawai Is.	6.7	Recorded at Padang (0.36)	West	Minor	an
2009	9	2	EQ	Thrust - Southwest Java	7.3	Pelabuhan Ratu (0.2), Pameng-peuk (1)	West	Minor	an, ao
2009	9	30	EQ	Oblique - West Sumatra	7.6	Padang (0.2), Tuapejat (0.07)	West	Minor	ab, an
2010	4	7	EQ	Thrust - between Nias and Sumatra	7.8	Banyak Is. (0.4), Nias Is. (0.2), Sibolga (0.1)	West	Minor	an, ao
2010	5	9	EQ	Thrust - West of North Sumatra	7.2	Meulaboh (0.2)	West	Minor	an, ao
2010	10	25	EQ	Thrust - Mentawai Is.	7.8	North and South Pagai Islands, Mentawai Islands, West Sumatra (9.3)	West	Large	ac
2012	4	11	EQ	Strike-slip - double earthquakes off-shore West Sumatra	8.6, 8.2		West	Minor	ae
2014	11	15	EQ	Thrust (a splay fault) - West of Halmahera	7.1	Jailolo (0.09)	West	Minor	ag

Continuation of Table 2.2

YY	MM	DD	Source	Location	Mag, VEI	Location (max tsunami in m)	Region	Level	Refs:
2018	8	5	EQ	Thrust - North of Lombok	6.9	Carik and Badas, North of Lombok	East	Minor	an
2018	9	28	Landslide	Palu-Koro Fault triggered landslides (?)	7.5	Palu Bay (10)	East	Large	af, an
2018	12	22	Volcano	Mt. Anak Krakatau		Sunda Strait	West	Large	an

Refs: a) Wichmann [1918]; b) Wichmann [1922]; c) Soloviev and Go [1974]; d) Soloviev et al. [1986]; e) Rumphius [1675]; f) Liu and Harris [2014]; g) **?**; h) Natawidjaja et al. [2006]; i) Fisher and Harris [2016]; j) **?**; k) Prasetya et al. [2001]; l) Okal and Reymond [2003]; m) Latief et al. [2016]; n) **?**; o) Yudhicara et al. [2015]; Lassa [2009]; p) Okal [1999]; q) Paris et al. [2014]; r) Yeh et al. [1993]; Tsuji et al. [1995b]; Hidayat et al. [1995]; Beckers and Lay [1995]; Griffin et al. [2015]; Pranantyo and Cummins [2019]; s) Schindelé et al. [1995]; Satake and Imamura [1995]; t) Tsuji et al. [1995a]; Maramai and Tinti [1997]; Abercrombie et al. [2001]; Synolakis et al. [1995] ; u) Satake and Imamura [1995]; v) Pelinovsky et al. [1997]; w) Gomez et al. [2000] ; x) Matsutomi et al. [2001]; Imamura et al. [1997]; Henry and Das [2002]; y) Fritz et al. [2007]; Ammon et al. [2006]; z) Borrero et al. [2009]; Lorito et al. [2008]; Fujii and Satake [2008]; Gusman et al. [2010]; aa) Fujii et al. [2011]; ab) McCloskey et al. [2010]; ac) Satake et al. [2013]; Newman et al. [2011]; Hill et al. [2012]; ad) Newcomb and McCann [1987]; ae) Singh et al. [2017]; af) Cipta et al. [2018]; Muhari et al. [2018]; Yalciner et al. [2018], etc.; ag) Gusman et al. [2017a]; Gunawan et al. [2016]; ah) Lander et al. [2003]; ai) Sull-Teng [2019]; aj) ITIC [2006] ; ak) OCHA/GVA [2002]; al) Latief et al. [2000]; am) Nomanbhoy and Satake [1995]; an) NGDC/WDS [2019]; ao) BMKG [2018b]

End of Table 2.2

The final number of tsunami events between 1608 and 2018 in the updated catalogue is 133. Earthquakes generated about 80% of the events, followed by volcanism (14%) and landslides. Unfortunately, particularly for historical events, detailed information regarding the source mechanism is unknown. During this period, the eastern Indonesia region experienced almost double events (88) than the western region (45). The Sunda subduction zone mainly caused tsunamigenic earthquake events in the western region. However, it is often difficult to identify the main fault that generated the tsunamis in the eastern region.

At least 14 tsunami events in the eastern Indonesia region were caused by volcanic activity. More than half these events were from volcanoes located on the Sangihe Islands and north of Maluku. Several events originated from volcanoes in the Banda Islands, the northern coast of Flores, and from Tambora Volcano. The family of Krakatoa Volcanoes was the primary source of volcanic tsunamis in the western Indonesia region.

The number of landslide-generating tsunamis in Indonesia noted in this updated catalogue is significantly more than the number recorded by Latief et al. [2000]. Previously, only the 1979 Lembata event was categorised as a tsunami caused by a landslide. However, after re-examining the historical accounts available, I determined that the main cause of other events was landslide, either with subaerial or submarine mechanism, even though the description of the events began by mentioning ground motion (probably caused by an earthquake): for example, the 1674 North Ambon Island, 1815 northern Bali, and 1899 Seram Island tsunamis.

Lastly, currently, more tsunamis likely occurred than in the past (Figure 2.8). Records from the past were collected mainly during the colonial era, coming from regions with high economy activity. It is possible that tsunamis affected other regions with fewer people but as they did not have a significant economic effect [Reid, 2015], they were not reported. The eastern Indonesia region has longer historical records than the western region. During the colonial era, the eastern region was famous for trading spices, which were transported by ship, with the centre of activity on islands such as Ambon, Banda Islands, and the Maluku Islands. Therefore, any unusual ocean phenomena that affected business were recorded. All historical accounts from the western region were from the west and south coast of Sumatra and Java, respectively. It was because less of a colonial presence and therefore fewer written records [Reid, 2015].

From historical accounts, distribution of tsunami heights and run-up from all of the region were plotted (Figure 2.9). It is clear that most of the coastline of Indonesia has been affected by tsunamis.

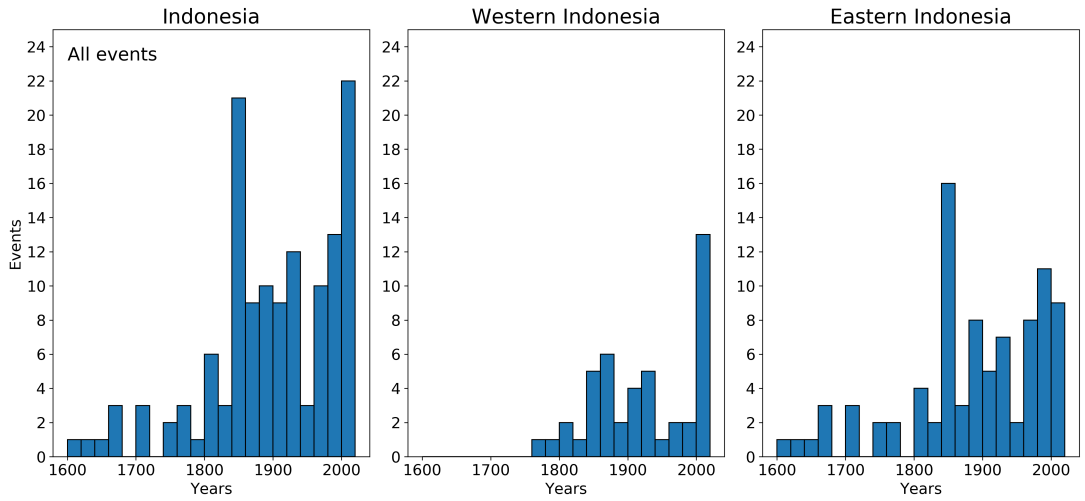

Figure 2.8: Histogram of tsunami by zone and period

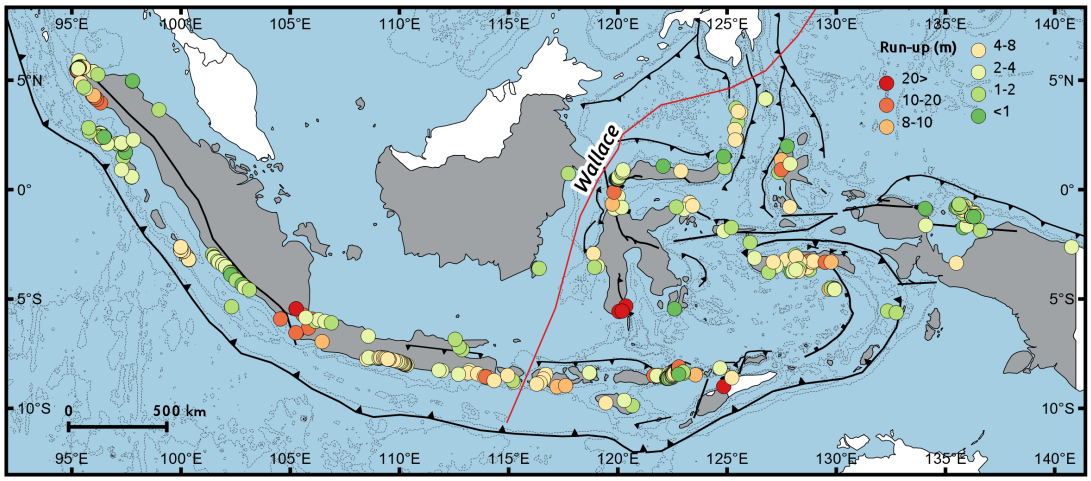

Figure 2.9: Tsunami run-up heights documented in Indonesia from 1600 to 2018. The red line represents the Wallace Line. The eastern Indonesia region lies to the east of the Wallace Line

2.5 Tsunamis in the western Indonesia

From the historical accounts, the west coast of Sumatra experienced two periods of big tsunamis; in the 1800s and early 2000s. A study of the coral micro-atolls from the Mentawai and Nias Islands confirmed the first period of three megathrust earthquakes of Mw 8.5 to 8.7 followed by tsunamis in 1797, 1833, and 1861 [Newcomb and McCann, 1987; Natawidjaja et al., 2004, 2006]. Then the second period was started by the 2004 Indian Ocean and followed by the 2005 Nias Island, the 2007

Bengkulu, and the 2010 Mentawai Islands tsunamis [e.g. Borrero et al., 2009; Lorito et al., 2008; Gusman et al., 2010; Fujii and Satake, 2008; Satake et al., 2013; Newman et al., 2011; Hill et al., 2012, respectively]. In 2012, there were twin large strike-slip earthquakes (Mw 8.2 and 8.8) generated minor tsunamis from Wharton Basin[3] [Singh et al., 2017; Gusman et al., 2017b; Hananto et al., 2018]. Except the latest one, all of these events were correlated with the Sunda subduction zone earthquakes.

Unlike Sumatra, the southern coast of Java is a 'calmer' earthquake region. Newcomb and McCann [1987] noted only three major earthquakes in this region, based on 300 years of data until 1984. The earthquakes on 4 January 1840 and 20 October 1859 produced only local tsunamis. Further, they noted no tsunamis until the eastern Java tsunami on 3 June 1994, which was generated by a Mw 7.6 earthquake that produced a tsunami run-up height of up to 9.5 m [Maramai and Tinti, 1997]. The last tsunami from the southern shore of Java was in 2006 caused by a Mw 7.8 earthquake. It was categorised as a tsunami earthquake event which had a slow rupture mechanism [Ammon et al., 2006] and generated more than 8 m tsunami height [Fritz et al., 2007; Hébert et al., 2012].

The latest tsunami event from the western Indonesia was from Anak Krakatau Volcano. The Anak Krakatau event on 22 December 2018 was a "silent tsunami" that killed more than 426 people along the western coast of Java and southern coast of Sumatera [detikNews, 2018]. Unlike a tsunami generated by an earthquake, there was no "natural warning", such as a strong ground shaking, even without a massive eruption. The volcano had been active since June 2018. A satellite photograph after the event suggested that a flank collapse was the main source of the tsunami [Williams et al., 2019; Grilli et al., 2019] (see Figure 2.10).

[3]Wharton Basin is located at the Indian Ocean between east of the Ninety East Ridge and western Australia.

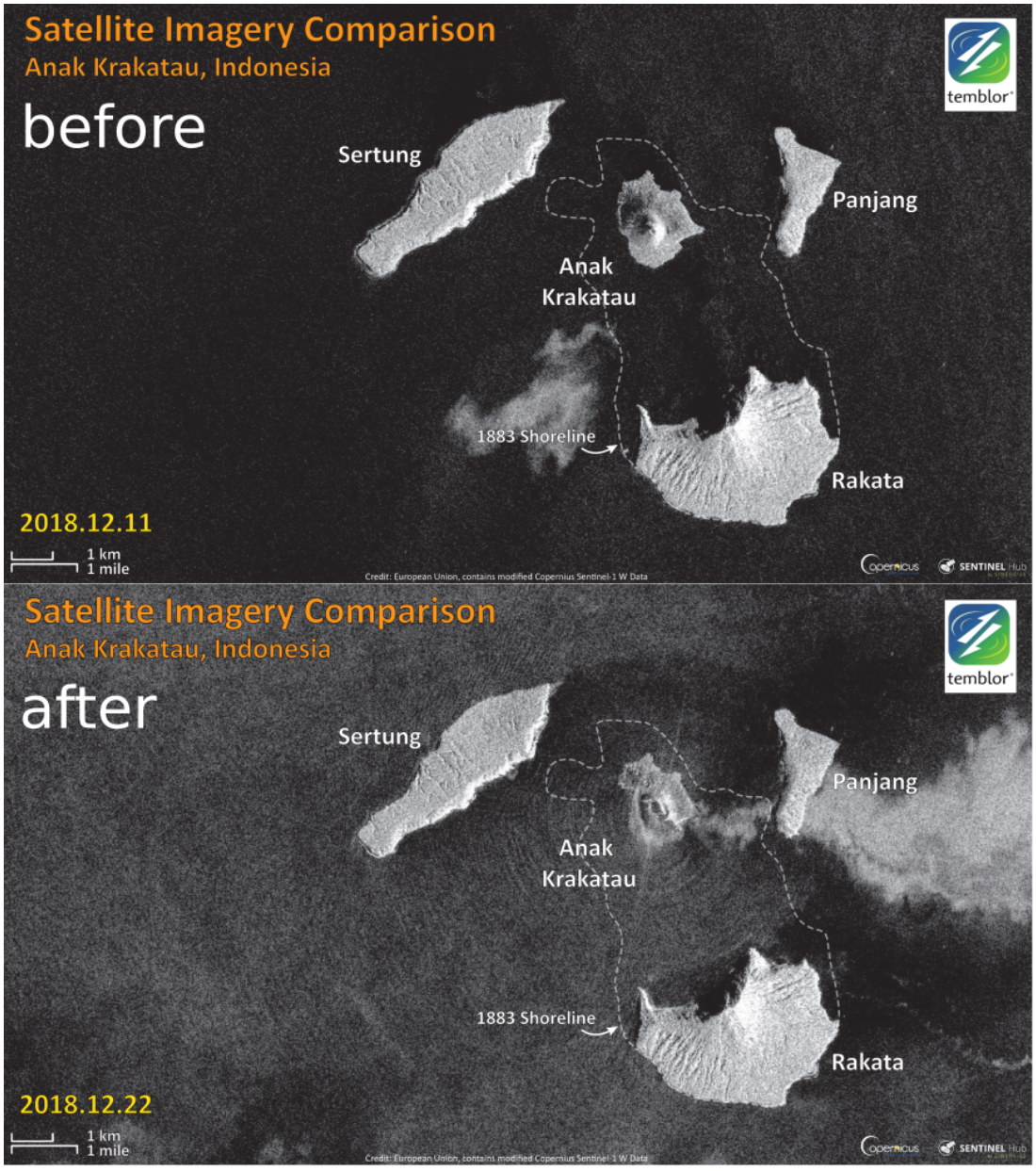

Figure 2.10: Satellite imagery of Anak Krakatau Volcano before and after the tsunami (modified from Patton et al. [2018]). The dashed line indicates the previous shoreline before the 1883 Krakatau tsunami.

2.6 Tsunamis in the eastern Indonesia region

The eastern Indonesia region had more tsunamis than the western region. Unlike the events in Sumatra and Java, the main source of most of the tsunamis is unknown and cannot be simply assumed being because of an earthquake. Some major historical accounts clearly described ground motion being felt, followed by a tsunami. However, there has been no detailed information recorded regarding the source of the ground movement. In the following section, some major past tsunamis are discussed briefly.

2.6.1 Banda Sea

Historical accounts from the Banda Sea have mostly reported on two regions: 1) Ambon Island and the surrounding area and 2) the Banda Islands. Figure 2.11 shows locations discussed in this section.

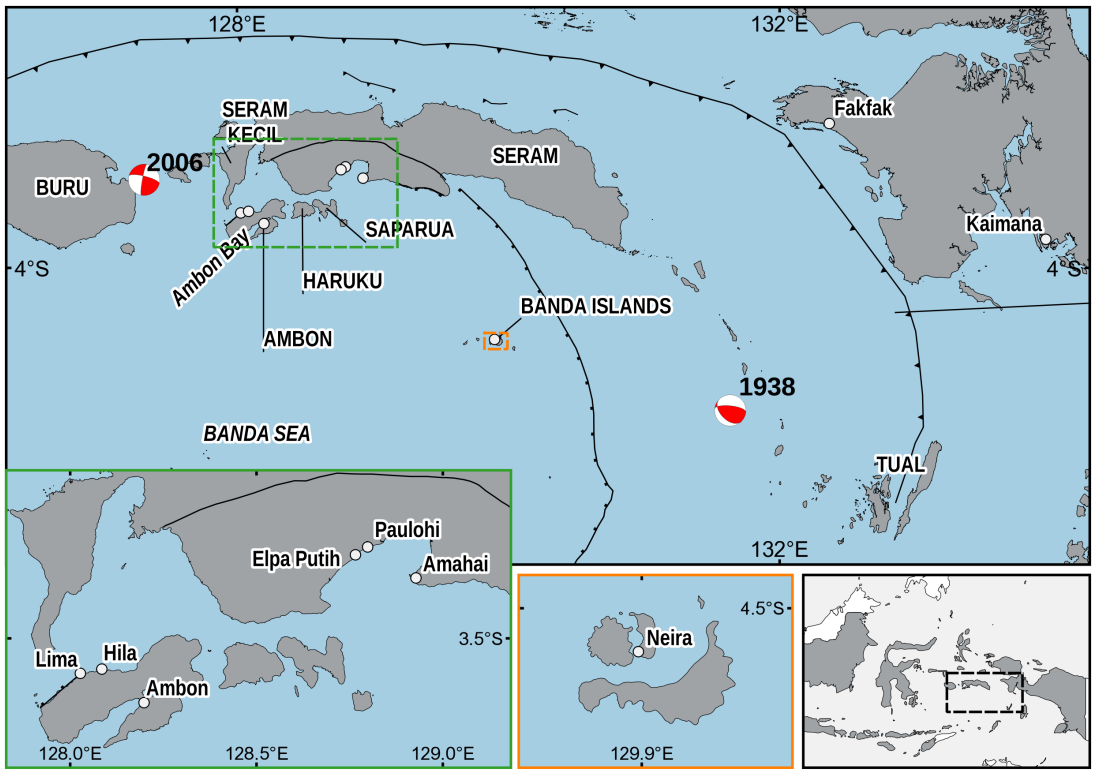

Figure 2.11: Locations discussed in Section 2.6.1 (Banda Sea region). The green box inset map shows locations discussed from Ambon and Seram Islands where the orange inset map shows location of Neira on the Banda Islands. Beach balls represent earthquake focal mechanism and their year of the event.

Ambon and the surrounding area

Rumphius [1675] reported that Ambon Island suffered a devastating earthquake on 17 February 1674 (discussed in Chapter 3). Many stone buildings collapsed because of the strong ground shaking. Very high tsunamis, with a run-up up to 100 m, were reported on the north coast of the island between Negeri Lima and Hila. Devastating tsunamis were reported only along the northern coast of Ambon and south of Seram Kecil; the rest of the island suffered only a minor tsunami. This event occurred during the Chinese New Year celebrations and killed more than 2,000 people.

Between 1674 and 1899, there were no significant tsunamis in the Ambon and Seram region, according to the Wichmann [1918] and Soloviev and Go [1974] catalogues. There were several minor events, mostly earthquakes felt on the islands followed by small oscillations observed near the coastline. However, there was little information available. A mysterious 'tidal wave' was seen on 5 September 1711, when the seawater rose quickly to 1.2 m but with no indication of an earthquake. A moderate tsunami occurred in Ambon Bay after an earthquake was felt over the entire island on 16 December 1841, with a 1.5 m ocean wave height washing away several huts at Galala, a village at Ambon.

On 30 September 1899, the south coast of Seram suffered a devastating earthquake and tsunami. According to the report by Verbeek [1901] in Soloviev and Go [1974], this event caused at least 3,700 deaths and an economic loss of more than 140,000 Dutch guldens at that time. The land-based earthquake triggered massive subaerial landslides at three places. These landslides generated a massive tsunami up to 9 m at the villages of Amahai, Paulohi, and Elpaputih, which suffered the most destruction. This event is known as *bahaya Seram* (the danger of Seram) and the story has been passed down through generations.

On 8 October 1950, three villages on Ambon Island suffered a devastating tsunami. Unfortunately, limited information on this event was available at the time because of the post-independence day war. According to eyewitness information compiled by Latief et al. [2016], the tsunami arrived about 15 minutes after an earthquake of Mw 7.4 that had epicentre on the south of the island [U.S. Geological Survey, 2019]. The massive tsunami was observed only at Galala in Ambon Bay. At that time, the villagers did not know tsunami terminology. This event is known as *banjir Galala* (Galala flood) or *air turun naik* (up-and-down water). [Mw 7.3; hypocentre = 128.23°E, 4.199°S, 20 km [Storchak et al., 2013]]

Banda Islands

The Banda Islands suffered a devastating tsunami on 1 August 1629 [Soloviev and Go, 1974; Harris and Major, 2017; Wichmann, 1918]. Thirty minutes after an earthquake with intense shaking, a tsunami with a height up to 16 m hit the islands. The earthquake was felt at Ambon but fishermen on the open sea did not see an unusual wave. Liu and Harris [2014] investigated this event and concluded that it was associated with the Seram megathrust earthquake.

The Banda Islands experienced another strong earthquake on 12 September 1763 [Soloviev and Go, 1974; Harris and Major, 2017; Wichmann, 1918]. About 75% of the houses on Neira Island collapsed. In less than three minutes, the island was flooded with seawater. A similar event occurred on 26 November 1841, when Fort Nassau on Neira Island was inundated by a tsunami up to 3 m in height. However, the ground shaking for that event was less intense than for the previous event.

On 25 November 1852 (discussed in Chapter 4), Banda Islands suffered a devastating tsunami [Wichmann, 1918; Harris and Major, 2017; Soloviev and Go, 1974] approximately 15 minutes after strong shaking was felt at Neira. The tsunami reached the footwall of Fort Belgica, which is located higher than Fort Nassau. At this location, a tsunami of approximately 8 m was observed. The wave was reported at Ambon, Haruku, and Saparua Islands as well.

A strong earthquake occurred in the Banda Sea on 1 February 1938 [Soloviev and Go, 1974]. The shaking was reported from Kaimana and Fakfak, southwest of Papua Island. It was reported that a small new island rose near the Kai Islands after the earthquake. The magnitude of this earthquake was equivalent to Mw 8.5, with a deep epicentre (60 km) [Okal and Reymond, 2003]. Even though the earthquake magnitude was large, a tsunami height of only 1 m (maximum) was reported from Tual, Kai Islands. [Mw 8.5; hypocentre = 131.63°E, 5.05°S, 25 km [Storchak et al., 2013]]

2.6.2 Bali and Flores Sea

The northern coast of Sumbawa Island was inundated up to 3.5 m by a tsunami following the eruption of Tambora Volcano on 10 April 1815 [Wichmann, 1918; Harris and Major, 2017; Soloviev and Go, 1974]. The wave height reached 0.3 m at Bima Bay and a strong wave oscillation was reported on Sulawesi and Java Islands. The 1815 Tambora eruption is the strongest modern volcanic explosion recorded in Indonesia.

Three consecutive tsunamis between 1815 and 1820 occurred in the Bali Sea [Wichmann, 1918; Harris and Major, 2017; Soloviev and Go, 1974]. First, the northern coast of Bali Island was rocked by a strong earthquake on 22 November 1815, which caused coastal mountains to collapse, which triggered a tsunami. More than 10,000 people were buried under the mudflow and 1,200 people were washed away by the tsunami. The earthquake itself was felt as far away as Surabaya and Bima (Figure 2.12).

Another strong earthquake was felt from eastern Java to Bima on Sumbawa Island on 8 November 1818 (Figure 2.12). Moments later, the sea level in Bima Bay rose rapidly up to 3.5 m. In addition, a seaquake[4] was reported in Bali Strait.

On 29 December 1820, Sumenep (Madura Island), Bima, and Makassar (Sulawesi) (Figure 2.12) felt a strong earthquake for approximately 2.5 minutes. Suddenly, up to 25 m of seawater rose and inundated land between Nipanipa and Terangterang villages along the Bulukumba coastline (south of Sulawesi) up to 400 m, then retreated

[4] underwater disturbance felt by floating object caused by an earthquake or volcano [Martin Jr., 1967]

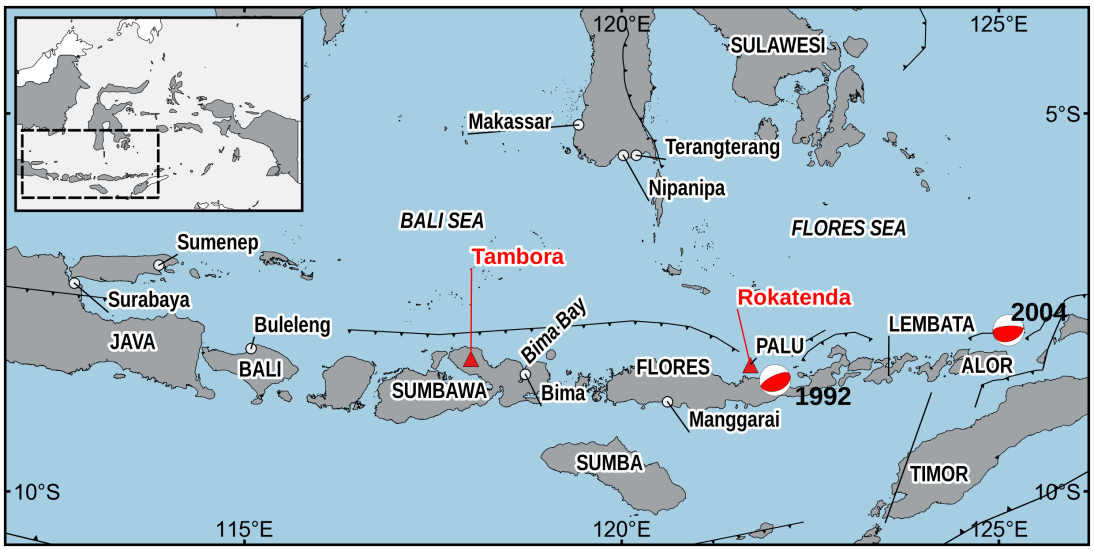

Figure 2.12: Locations discussed in Section 2.6.2 (Bali and Flores Sea region). Beach balls represent earthquake focal mechanism and their year of the event. The red triangles represent volcanoes discussed in this region.

for several kilometres. At Bima Bay, a ship was tossed far inland, over a house's rooftop.

During the years after these three devastating events, several minor tsunamis were reported. Two earthquakes followed by tidal waves occurred in Bima Bay (Figure 2.12) in 1836 but no damage was reported, [Wichmann, 1918; Harris and Major, 2017; Soloviev and Go, 1974] and an earthquake occurred at Manggarai in 1855.

A tsunami caused by volcano activity occurred on 4 to 5 August 1928, generated by Rokatenda Volcano [Wichmann, 1918]. The volcano ejected massive amounts of ash and lava and generated a tsunami up to 10 m in height on Palu Island (Figure 2.12) and the north coast of Flores Islands. More than 120 people died because of the tsunami.

A tsunami generated by landslide was reported on Lembata Island on 18 July 1979 [Yudhicara et al., 2015; Lassa, 2009]. According to Lassa [2009], at least 500 people were killed because of this tsunami. The maximum tsunami run-up at Waitabe Bay (Figure 2.12) was approximately 7 m.

The first "modern" tsunami[5] event in Indonesia was from the 12 December 1992 Flores earthquake and tsunami. It was the first time an International Tsunami Survey Team (ITST) conducted post-tsunami fieldwork to collect tsunami and earthquake evidence in Indonesia, and the second time in the world [Yeh et al., 1993]. The tsunami was generated by a Mw 7.8 earthquake and killed more than 2,000 people. Because of the earthquake's location, the tsunami arrived at the nearest coastline

[5]Here I define modern tsunamis as events were recorded by instruments (e.g. seismic, geodetic, oceanographic)

within less than five minutes. The tsunami height along the northern coast of Flores was between 3 and 5 m (Figure 2.13). However, an extreme run-up height of up to 26 m was reported at Riangkroko Village on the eastern side of the island [Tsuji et al., 1995b]. This event is discussed further in Chapter 5. [Mw 7.7; hypocentre = 122.025°*E*, 8.532°*S*, 16 km [Pranantyo and Cummins, 2019]]

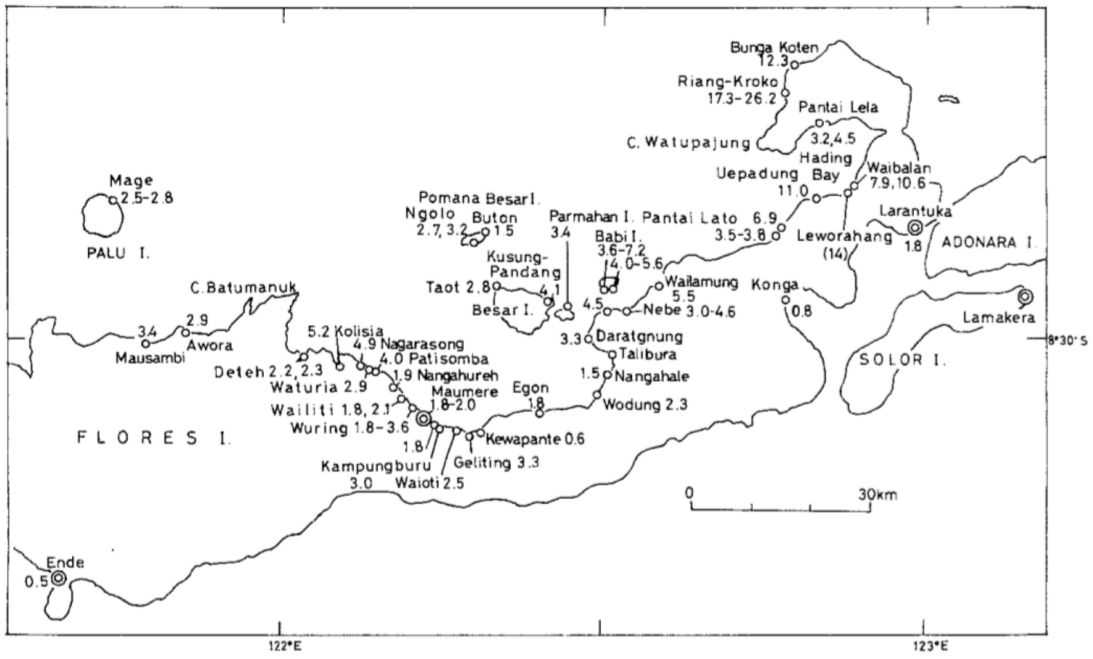

Figure 2.13: Tsunami heights meassured after the Flores 1992 tsunami (taken from Tsuji et al. [1995b])

A relatively strong Mw 7.5 rocked Alor Island on 11 November 2004 (Figure 2.12). It produced a local tsunami up to 2 m high in East Alor and inundated land to approximately 50 m from the coastline [NOAA/NWS, 2004]. At least 17 people died in this event. [Mw 7.5; hypocentre = 125.12°E, 7.87°S, 17 km [Ekström et al., 2012][Global CMT Catalog]]

2.6.3 Sulawesi and North Maluku

Historical tsunami accounts from Sulawesi and North Maluku can be divided into the following three regions: Makassar Strait, North Sulawesi and the northern Maluku Islands, and Tomini Bay and its surroundings. Figure 2.14 and 2.17 shows locations mentioned in this section.

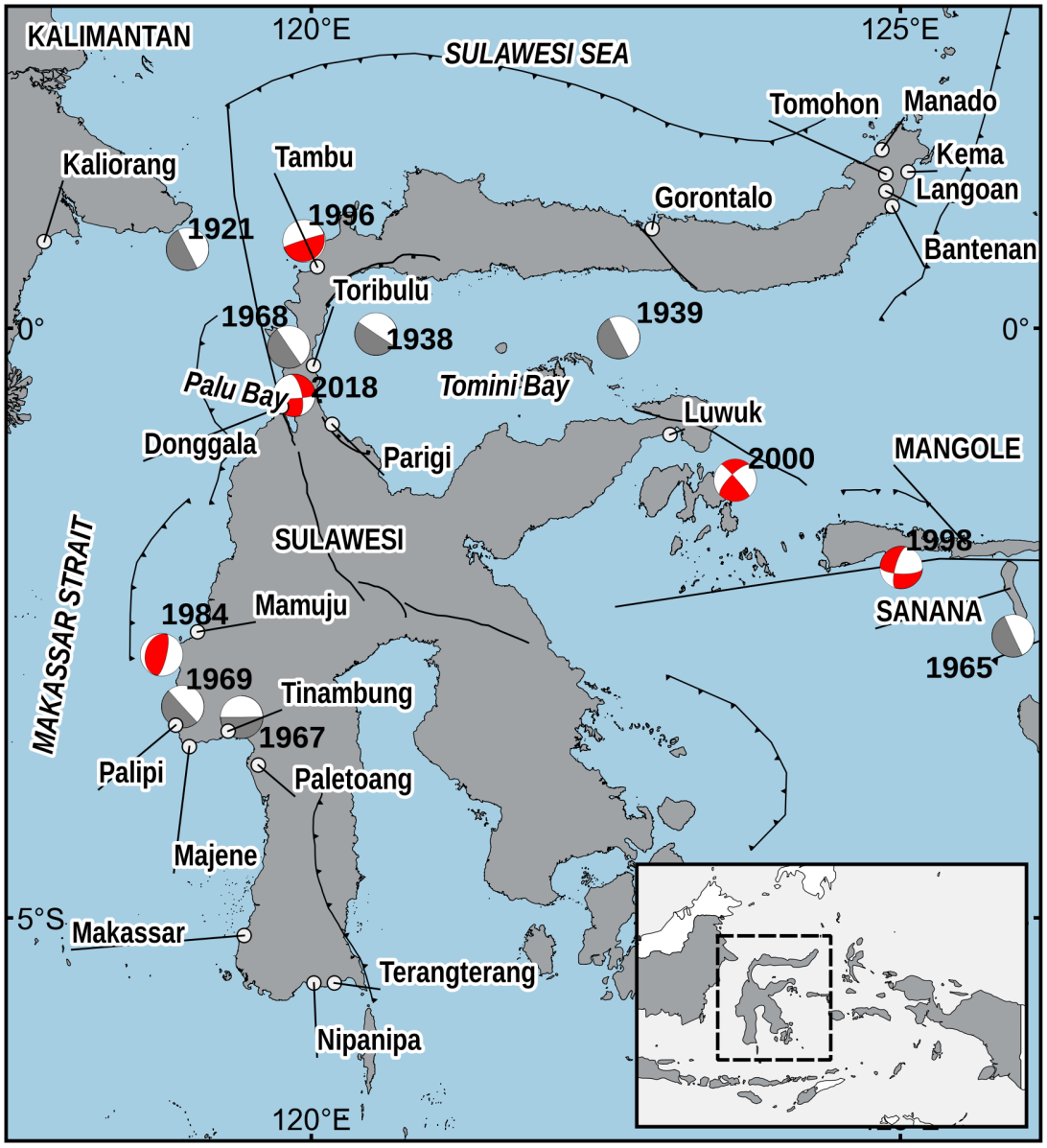

Figure 2.14: Locations mentioned in Sections 2.6.3 and 2.6.3 (Makassar Strait and Tomini Bay region). Red beach balls represent earthquake focal mechanism while grey beach balls only indicate the strike of the earthquake and their year of the event.

Makassar Strait

Two small tsunamis occurred in 1921 and 1957[6], reported from the east of Kalimantan Island [Soloviev and Go, 1974]. On 14 May 1921, an earthquake damaged houses and

[6] 26 October 1957 Mw 6.1; hypocentre = 116.01°E, 1.76°S, 20 km [Storchak et al., 2013]

a drill hole at Kaliorang (Figure 2.14), Kalimantan. A tsunami of approximately 1 m flooded the road. [Mw 6.52; hypocentre = 118.94°E, 0.67°N, 35 km [Storchak et al., 2013]]

A strong earthquake devastated Palu Bay (Figure 2.14) on 1 December 1927 [Soloviev and Go, 1974]. It caused land subsidence in several places and destroyed many buildings entirely. Almost at the same time, a tsunami as high as 15 m appeared in the bay and the sea became 12 m deeper. The tsunami killed at least 14 people. Prasetya et al. [2001] suggested that the earthquake had a magnitude of Mw 6.3. [Mw 6.2; hypocentre = 120.75°E, 0.88°S, 20 km [Storchak et al., 2013]]

Three consecutive tsunamis occurred on the western coast of Sulawesi in 1967, 1968, and 1969. At least 58 people died on the beaches between Tinambung and Majene (Figure 2.14) on 11 April 1967 [Soloviev and Go, 1974]. It was reported that the seawater first retreated and then rose to many times higher than the usual high-tide level. Prasetya et al. [2001] suggested that the preceding earthquake, with a thrust mechanism, had a magnitude of Mw 5.5 to 6.3. [Mw 6.2; hypocentre = 119.4°E, 3.3°S, 20 km [Prasetya et al., 2001]]

On 14 August 1968, an earthquake of magnitude Mw 7.4, with a normal focal mechanism (Figure 2.14), generated a tsunami [Prasetya et al., 2001]. Coastal subsidence between 2 and 3 m was observed between Tanjung and Sabang, The tsunami height was up to 10 m on the coast of Donggala, particularly around Tambu, and inundated up to 500 m inland [Soloviev and Go, 1974]. [Mw 7.4; hypocentre = 119.8°E, 0.16°S, 20 km [Storchak et al., 2013]]

The Majene region (Figure 2.14) felt strong ground shaking on 23 February 1969 and many buildings collapsed [Soloviev et al., 1986]. This was followed by a tsunami with a height of 4 m in Paletoang and 1.5 m in Parosanga and Palipi. Prasetya et al. [2001] suggested that it was due to a Mw 6.6 thrust earthquake. [Mw 7.0; hypocentre = 118.9°E, 3.21°S, 15 km [Storchak et al., 2013]]

A relatively small tsunami was reported in the Mamuju region(Figure 2.14) on 8 January 1984 [Latief et al., 2000; Prasetya et al., 2001]. It was due to a Mw 6.7 earthquake with a thrust mechanism. Unfortunately, no detailed information is available. [Mw 6.7; hypocentre = 118.72°E, 2.77°S, 14.8 km [Global CMT Catalog]]

A Mw 7.9 earthquake rocked the central region of Sulawesi, particularly at Tambu, on 1 January 1996 (Figure 2.14) and killed at least 63 people. The tsunami height was approximately 2 to 4 m (Figure 2.15), arriving within 10 minutes after the earthquake [Pelinovsky et al., 1997]. [Mw 7.9; hypocentre = 119.93°E, 0.74°N, 15 km [Global CMT Catalog]]

A devastating tsunami hit Palu Bay, Central Sulawesi, on 28 September 2018. An early tsunami warning was released after the Mw 7.6 strike-slip earthquake in the Palu-Koro fault. However, the tsunami arrived at the nearest coastline within less than five minutes. In general, the tsunami run-up heights along the bay varied up to 5.3 m [Cipta et al., 2018; Muhari et al., 2018], with a maximum run-up height of 9 m (Figure 2.16) [Yalciner et al., 2018]. The source of this tsunami remains questionable; it is believed that submarine landslide was the main source but this needs further investigation. [Mw 7.6; hypocentre = 119.86°E, 0.72°S, 12 km [Global CMT Catalog]]

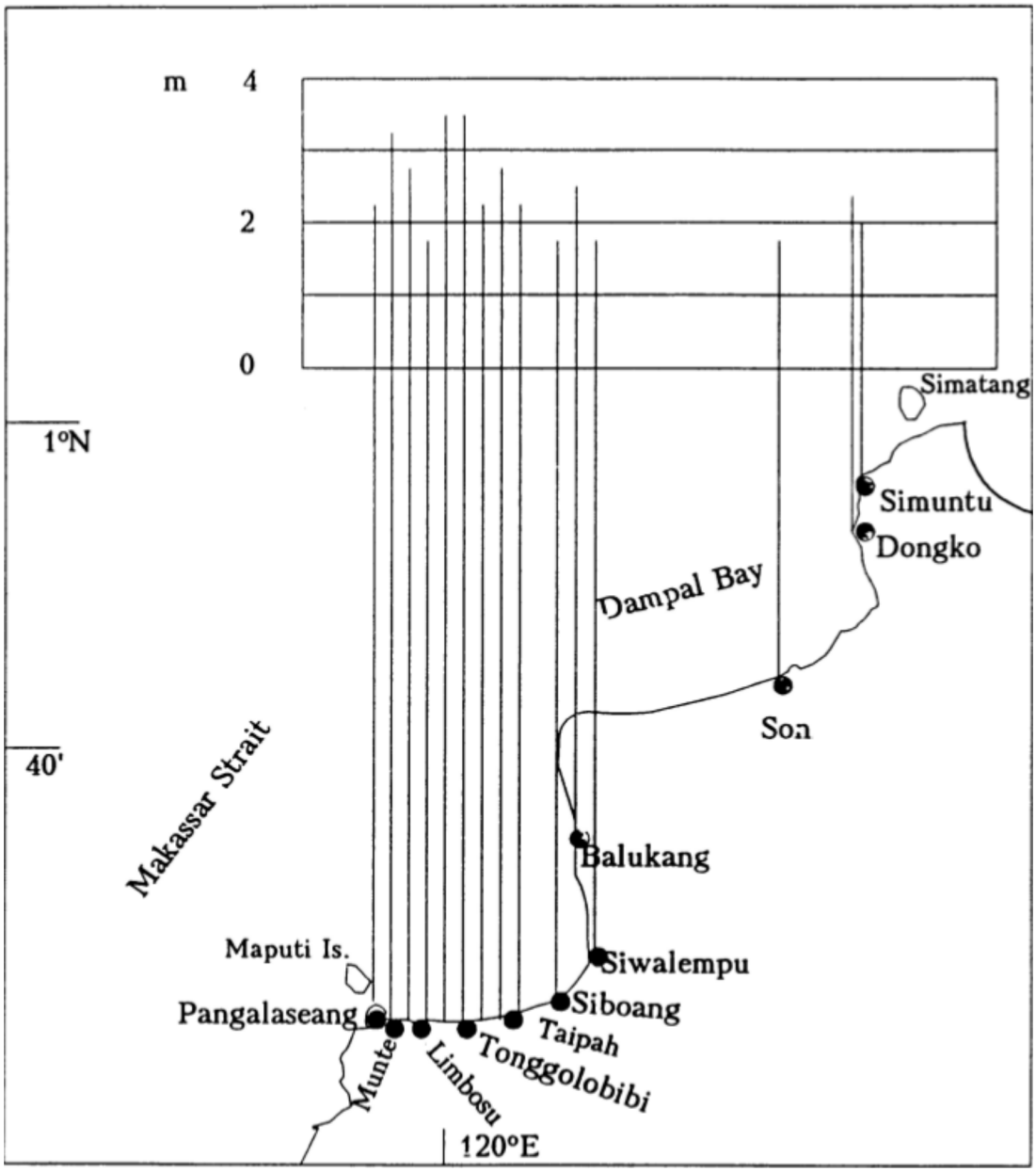

Figure 2.15: Tsunami heights meassured after the Sulawesi 1996 tsunami (taken from Pelinovsky et al. [1997])

Tomini Bay

On 19 May 1938, a destructive earthquake of Mw 7.6 was felt over almost all Sulawesi Island and as far away as east Kalimantan [Soloviev and Go, 1974]. The earthquake's epicentre was at Tomini Bay (Figure 2.14). Almost a thousand houses were destroyed or damaged and many ground cracks were observed. The earthquake was followed

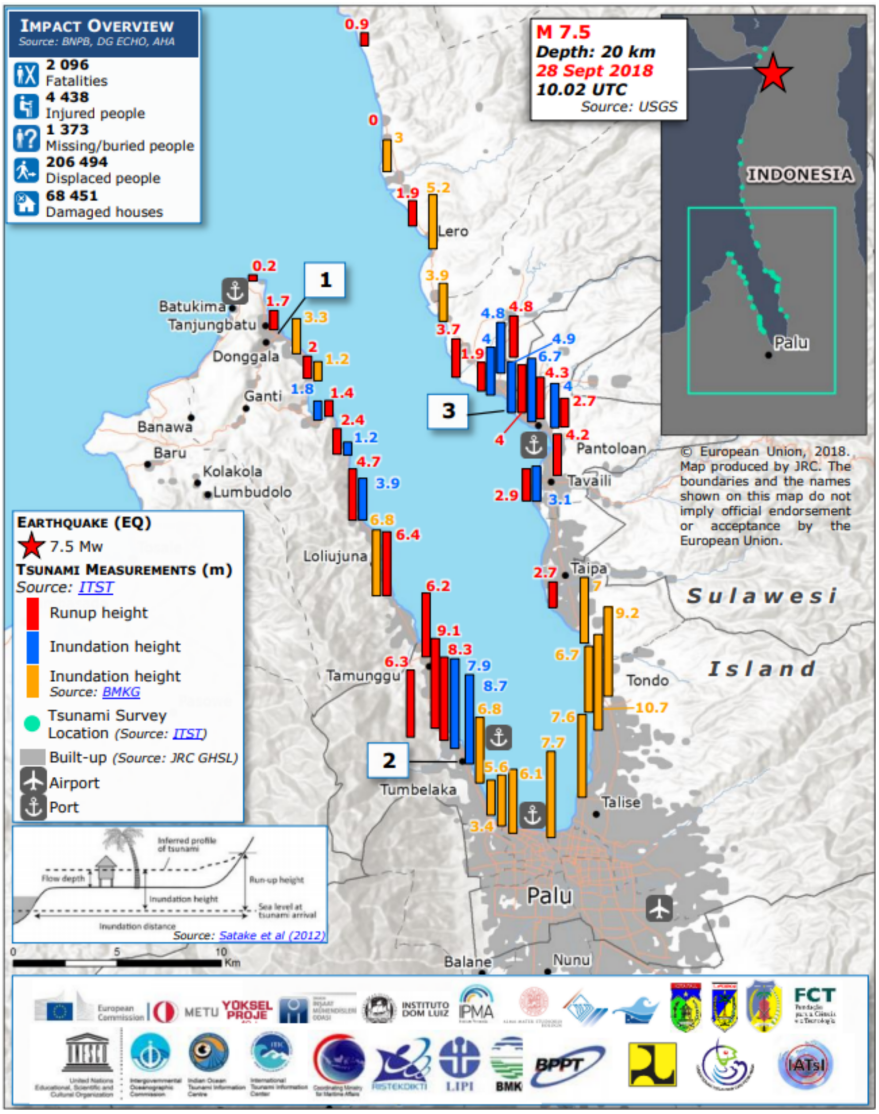

Figure 2.16: Post tsunami field survey data after the 2018 Palu Bay tsunami (taken from Yalciner et al. [2018]).

by a tsunami up to 3 m high on the coast of Toribulu to Parigi (Figure 2.14). It was reported that the sea retreated first and then inundated the land up to 80 m from the coastline. [Mw 7.7; hypocentre = 120.54°E, 0.05°S, 35 km [Storchak et al., 2013]]

Another devastating earthquake was registered in Tomini Bay (Figure 2.14) on 21 December 1939, with a magnitude of Mw 8.0 and a depth of 150 km [Soloviev and Go, 1974]. The ground shaking was reported from the east of Kalimantan Island as well. The sea oscillated and inundated rice fields at Langoan (Figure 2.17). [Mw 8.1; hypocentre = 122.6°E, 0.08°S, 35 km [Storchak et al., 2013]]

On 24 January 1965, a strong Mw 7.6 earthquake occurred on Sanana Island (Figure 2.17), an island between Sulawesi and Buru Islands [Soloviev and Go, 1974; NGD-

C/WDS, 2019]. It killed at least 71 people and destroyed more than 3,000 buildings. The earthquake was accompanied by a tsunami that destroyed 90% of the houses in Sanana City. [Mw 8.2; hypocentre = 125.95°E, 2.61°S, 20 km [Storchak et al., 2013]]

A local tsunami 2.75 m high was reported on Mangole Island (Figure 2.17) on 29 November 1998 [Lander et al., 2003]. It was caused by a Mw 7.7 earthquake with a strike-slip mechanism [NGDC/WDS, 2019]. [Mw 7.7; hypocentre = 125.00°E, 2.03°S, 16.4 km [Global CMT Catalog]]

A strong Mw 7.5 earthquake hit the area of Luwuk, Banggai (Figure 2.17), and the eastern part of Sulawesi on 4 May 2000. A tsunami height of around 3 m [Sull-Teng, 2019] was reported, even though the earthquake had a strike-slip mechanism. At least 38 people died and hundreds of buildings were destroyed in this event [OCHA/GVA, 2000]. [Mw 7.5; hypocentre = 123.59°E, 1.29°S, 18.6 km [Global CMT Catalog]]

A relatively small Mw 6.7 earthquake generated a local tsunami at Buru on 14 March 2006 [ITIC, 2006]. The maximum run-up measured was 5 m and at least three people died in this event. [Mw 6.7; hypocentre = 127.31°E, 3.35°S, 13 km [Global CMT Catalog]]

North Sulawesi and North Maluku

About eight of the 14 tsunamis were generated by a volcano were in this region. In July 1608, the first definite tsunami in Indonesia was reported by Dutch ships from Makian Island (Figure 2.17) [Soloviev and Go, 1974; Wichmann, 1918], who observed that the seawater was very rough and they had seen a run-up onto the shoreline. After this observation, the activity on Tidore Volcano intensified and it erupted.

On the 12 August 1673 in the late evening, the southern slope of Ternate Volcan[7] (Figure 2.17) collapsed [Wichmann, 1918; Soloviev and Go, 1974]. It distrubed a huge amount of seawater and tossed ships and fish on land. There was no indication of a volcano eruption.

A massive eruption of Awu Volcano (Figure 2.17), Sangihe Islands, occurred on 2 March 1856 [Wichmann, 1918; Soloviev and Go, 1974]. Lava flowed into the seawater and this, together with an earthquake, caused the seawater to surge towards the shoreline. The volcanic activity continued to fluctuate until a new eruption on 17 March 1856. The most devastation to settlement were Tahuna and Tabukan, with more than 2800 people killed from a combination of the eruption and tsunami after the 17 March eruption.

An enormous eruption of Ruang Volcano (Figure 2.17) occurred on 3 March 1871 [Soloviev and Go, 1974; Wichmann, 1922]. It generated a massive tsunami up to 25 m high and inundated the land to about 180 m from the coastline. Approximately 400 people were killed in this event.

From the evening of 6 September 1889 through to the next morning, recurring strong earthquakes were felt in the northern Sulawesi region [Soloviev and Go, 1974; Paris et al., 2014]. Then a strong earthquake from the direction of Sangihe Island

[7] Paris et al. [2014] describes it as Gamkonora Volcano

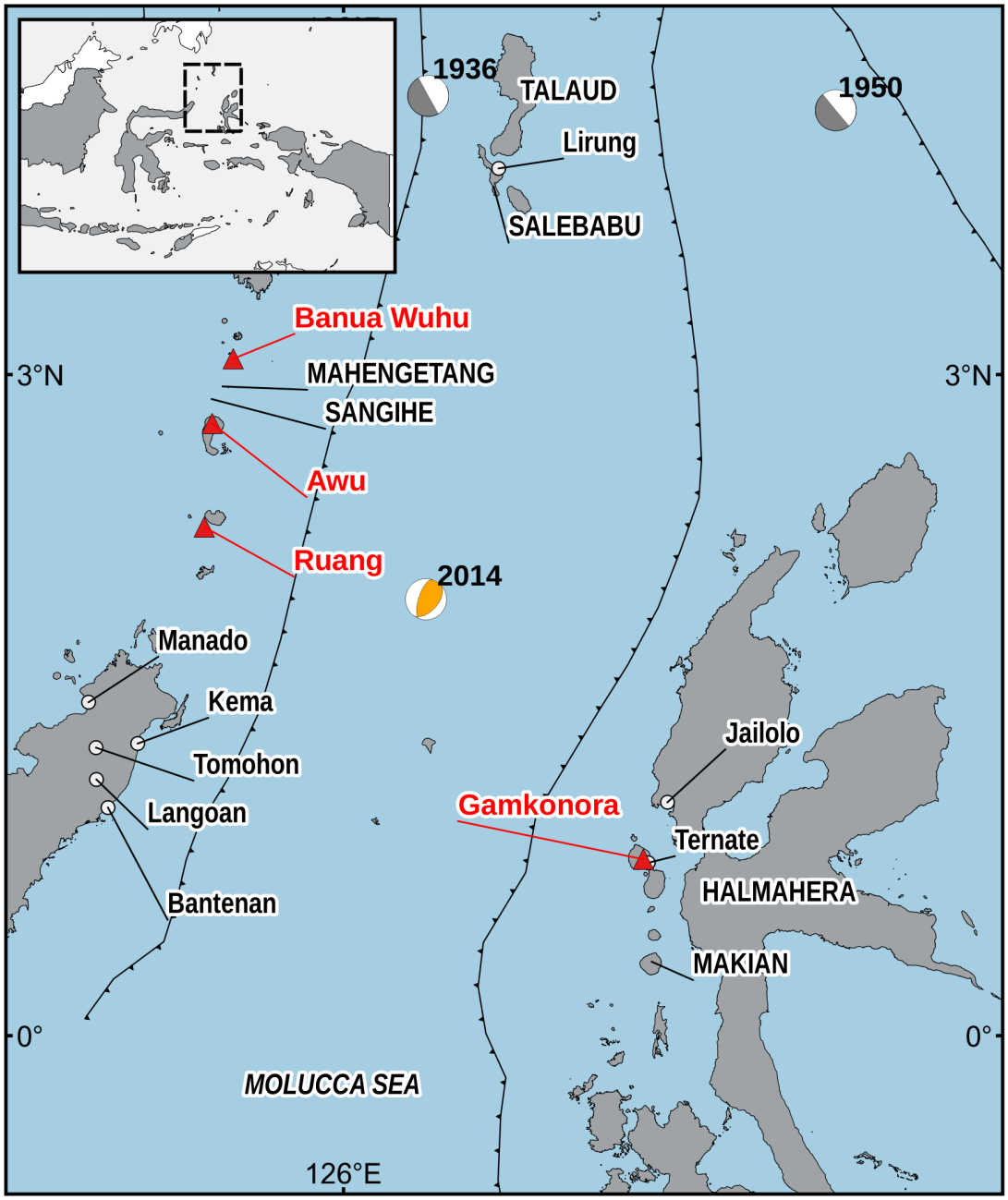

Figure 2.17: Locations mentioned in Section 2.6.3 (North Sulawesi and Maluku region). The yellow beach ball reprsents the 2014 earthquake's focal mechanism while the grey beach balls show only the strike angle of the earthquake and their year of the event. The red triangles are volcanoes discussed in this section.

occurred, followed by a tsunami that was observed in many locations. At Manado and Kema (Figure 2.17), the sea rose up to 3 m. At Bantenan, seawater oscillated 15

times within two hours and inundated houses. The wave amplitude was estimated at 9 m. Sangihe Island was heavily flooded soon after the earthquake when the sea rose about 1.5 m. The local people assumed that this was caused by the activity of the submarine volcano Banua Wuhu [Soloviev and Go, 1974].

A powerful eruption of Awu Volcano (Figure 2.17) was reported on 7 June 1892 [Soloviev and Go, 1974]. The eruption sound was heard at Ternate, Manado, Donggala, the southern region of Sulawesi, and even at Bima on Sumbawa Island. Weak seawater oscillations were noticeable at Bima. The sea rose by 1.5 m at Ambon Bay. However, there is no detailed information on the effects of the tsunami around the volcano.

Between 1918 and 1919, the underwater volcano Banua Wuhu (Figure 2.17) was active [Soloviev and Go, 1974], forcing the residents of Mahengetang Island to move to other islands. On 2 April 1919, the volcano erupted again, causing the sea to become rough. The sea rose by 2 m and occasional up to 5 m.

Earthquakes have been the source of tsunamis in this region as well. A moderate but long shaking was felt from Ternate (Figure 2.17) on 25 January 1846 Soloviev and Go [1974]. It was followed by a rise in sea level to 1.2 m. This was observed at Manado as well but with no detailed observation on the height.

Two tsunamis were noticed in the northern part of Sulawesi and Maluku in 1859. On 28 June, a strong earthquake was felt at Kema and Ternate, speculatively the source was from the Molucca Sea, (Figure 2.17) [Soloviev and Go, 1974; Wichmann, 1922]. Then the sea level oscillated. At the western coast of Halmahera Island, the tsunami reached a height of 10 m.

On 29 July, another strong earthquake was felt at Manado, Gorontalo, and Ternate, followed by a tsunami [Soloviev and Go, 1974; Wichmann, 1922]. The tsunami washed away houses on the northern coast of Sulawesi. At Ternate, the tsunami height reached 1 m.

An unusual wave oscillation, up to 4 m high, was seen around Talaud Islands (Figure 2.17) on 30 March 1907 [Soloviev and Go, 1974]. At the same time, a weak shaking was reported from Lirung, Tomohon, and Donggala.

On 1 April 1936, a devastating earthquake rocked the Talaud Islands [Soloviev and Go, 1974]. It destroyed more than 100 huts on the island. At Salebabu Island (Figure 2.17), the sea retreated to 500 m and then quickly rose to 3 m above the normal flood-tide level. The tsunami was less intense on the western coast of Sangihe Island than on the eastern side. [Mw 7.75; hypocentre = 126.38°E, 4.264°N, 35 km [Storchak et al., 2013]]

An early tsunami warning was issued after a Mw 7.1 earthquake in the Northern Moluccas Sea on 15 November 2014. Fortunately, only small tsunami waves were recorded at three tide gauges, with a maximum height of 9 cm at Jailolo (Figure 2.17), Halmahera [Gusman et al., 2017a]. A GPS study has shown that the earthquake came from an unmapped splay-fault in the double subduction zone of Maluku [Gunawan et al., 2016]. [Mw 7.1; hypocentre = 126.37°E, 1.98°N, 38.1 km [Global CMT Catalog]]

2.6.4 Papua

The first historical tsunami accounts from Papua was on 23 May 1864. Wichmann [1918] and Harris and Major [2017] reported that a strong earthquake was felt from Mansinam Island near Manokwari and Supiori Islands (Figure 2.18). The earthquake caused significant landslides around Manokwari, with the seawater rising three times (a maximum height around 3.5 m) and inundating huts.

An earthquake of magnitude 7.9 was registered on Yapen Island (Figure 2.18) on 26 May 1914 [Soloviev and Go, 1974]. The strong ground motion destroyed brick buildings and the sea level rose three times. The tsunami was recorded at a tide gauge at both Honolulu and Hawaii. Okal [1999] has argued that the main rupture was in the open Caroline Sea. [Mw 8.15; hypocentre = 136.94°E, 1.98°S, 15 km [Storchak et al., 2013]]

Another massive earthquake of magnitude 7.7 rocked Yapen Island (Figure 2.18) on 12 September 1979 [Soloviev et al., 1986]. It killed at least 15 people and generated a significant local tsunami at Biak and Yapen Islands. The earthquake had a strike-slip mechanism and it has been suggested that it is a segment of the Sorong Fault [Okal, 1999]. [Mw 7.52; hypocentre = 135.98°E, 1.67°S, 20 km [Storchak et al., 2013]]

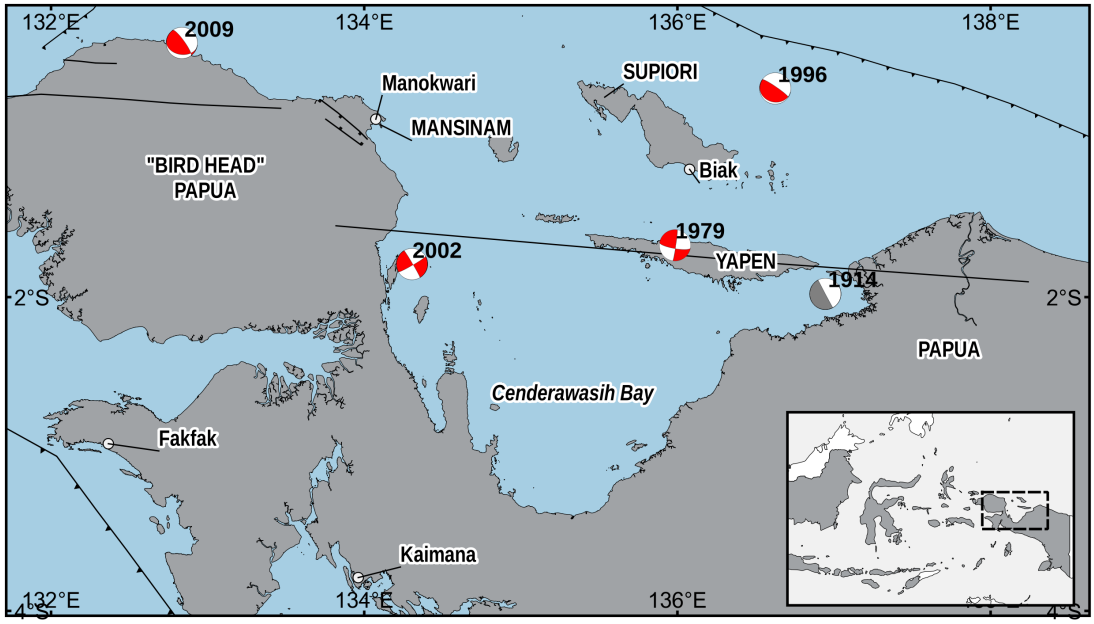

Figure 2.18: Locations mentioned in Section 2.6.4 (Papua region). The red beach balls represent earthquake focal mechanism while grey beach balls only indicate the strike of the earthquake and their year of the event.

The 17 February 1996 Biak Island (Figure 2.18) tsunami is the largest reported event from the Papua region. It was generated by a Mw 7.9 earthquake and killed over 107 people [Imamura et al., 1997]. An ITST group went to the field and measured tsunami run-up heights of approximately 1 to 4 m (Figure 2.19) [Matsutomi

et al., 2001]. The team found an extreme run-up height of 7.7 m on the southwest part of the island. A teleseismic study has shown that the earthquake had a complex rupture mechanism, with the largest slip of 12 m near the epicentre [Henry and Das, 2002]. [Mw 8.2; hypocentre = 136.62°E, 0.67°S, 15 km [Global CMT Catalog]]

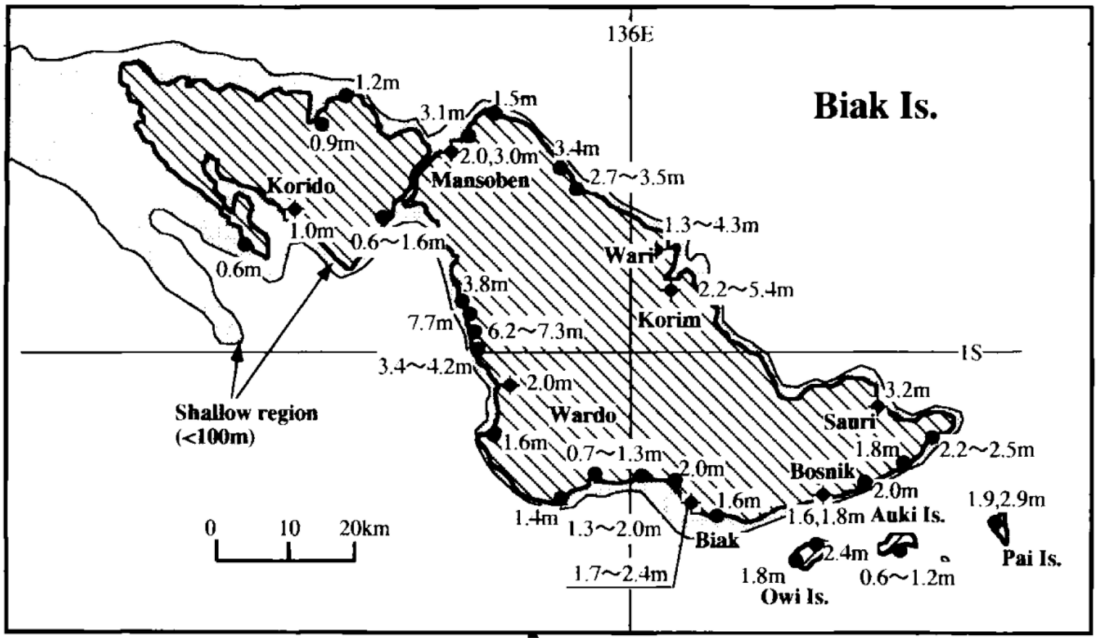

Figure 2.19: Tsunami heights meassured after Biak 1996 tsunami (taken from Imamura et al. [1997])

A Mw 7.6 earthquake struck the Manokwari region (Figure 2.18), Papua, on 10 October 2002. It generated a moderate tsunami, but no official publication was released about this event. At least eight people died and hundreds of houses were damaged [OCHA/GVA, 2002]. [Mw 7.5; hypocentre = 134.30°E, 1.79°S, 15 km [Global CMT Catalog]]

Another strong earthquake of Mw 7.7 hit the Head Bird of Papua Island (Figure 2.18) near Manokwari on 3 January 2009. It generated small tsunamis observed on the northern shore of Papua, particularly at Manokwari region, with the wave recorded at stations around the western side of the Pacific Ocean [Fujii et al., 2011]. The majority of the rupture area was on land and four people were killed when buildings collapsed after the earthquake [Nathalia and Ismar, 2009]. [Mw 7.7; hypocentre = 132.83°E, 0.38°S, 15.2 km [Global CMT Catalog]]

2.7 Remarks

Indonesia is located in a complex tectonic zone. It is a very seismically active region, as well as having many volcanoes. As an archipelagic country with water covering about 75% of its territory, Indonesia is very vulnerable to tsunami hazards. At least

133 tsunamis have been recorded in Indonesia between 1608 and 2018, although this undoubtedly underestimates the true number due to the paucity of older historical records. Almost 80% of these were caused by an earthquake and 14% by volcanic activity, while the rest of these events were associated with submarine or subaerial landslides. Moreover, 66% of these tsunamis occurred in the eastern Indonesia region.

Historical accounts of tsunamis in Indonesia have been published in several catalogues [e.g. Wichmann, 1918, 1922; Soloviev and Go, 1974; Soloviev et al., 1986; Latief et al., 2000]. These accounts usually begin with a brief description of ground motion for an event. For some significant events, the catalogues give detailed information regarding the tsunamis' physical behaviour, such as arrival time, wave period, and run-up heights. However, there is often no detailed information regarding the source of the tsunami.

The source of a tsunami is an essential input for hazard assessment. The simplest method is to use the source of past events. Therefore, understanding a past event is the first essential step. Even though no detailed information is given in the historical accounts, they can be optimised to identify the likely source of an event.

Unlike the western Indonesia region, it is a challenging task to identify the primary source of a tsunami for the eastern region events because of the complexity of the tectonic nature of the area. The primary tsunami source in the western region is certain to be the Sunda subduction zone for a tsunamigenic earthquake event.

Eastern Indonesia is one of the most complex tectonic areas in the world, with many tectonic features to be considered. Even though the historical accounts of tsunamis begin with a description of strong ground movement, it cannot be assumed that the primary source of each tsunami was an earthquake. There have been significant events in the region that could lead to a false impression of the source. Only a few events in the eastern Indonesia that we really know about the details of the source; such as the 1629 Banda Islands, the 1992 Flores Island, the 1996 Biak Island, and the 2009 Manokwari tsunamis.

For example, the 1674 Ambon event began with a strong earthquake. However, an extremely high tsunami was observed only on the northern coast of the island. In 1820, a very high tsunami was seen at Bulukumba to Bantaeng on the southern side of Sulawesi. A study conducted by Nguyen et al. [2015] was unable to define a proper tsunamigenic earthquake model to fit the data. In the 1852 Banda Sea event, the incoming tsunami wave had a positive polarity that was observed at both the Banda Islands and Ambon. While a megathrust earthquake scenario has been selected as the most likely source of this event [Fisher and Harris, 2016], any thrust earthquake from the suggested location would always produce a negative phase. While a devastating tsunami occurred in 1938 at Tomini Bay, Sulawesi, after a strong earthquake was felt, no major fault in the bay has been identified as its cause.

These examples raise a new question that needs to be addressed, 1) what was the primary source of the tsunami? This is followed by further issues: 2) how to identify the source? and 3) how to optimise limited historical accounts of an event? In the following chapters, these questions will be addressed through three case studies: the

Ambon Island 1674, the Banda Sea 1852, and the Flores Island 1992 tsunamis.

Chapter 3

The 1674 Ambon Tsunami: Extreme Run-up Caused by an Earthquake-triggered Landslide

Published: *Pranantyo, I.R. & Cummins, P.R. (2019) Pure and Applied Geophysics*

We present an analysis of the oldest detailed account of tsunami run-up in Indonesia, that of the 1674 Ambon tsunami (Rumphius, 1675). At 100 m this was the largest run-up height ever documented in Indonesia, and with over 2,300 fatalities even in 1674, it ranks as one of Indonesia's most deadly tsunami disasters. We consider the plausible sources of earthquakes near Ambon that could generate a large, destructive tsunami, including the Seram Megathrust, the South Seram Thrust, and faults local to Ambon. We conclude that the only explanation for the extreme run-up observed on the north coast of Amon is a tsunami generated by an earthquake-triggered coastal landslide. We use a two-layer tsunami model to show that a submarine landslide offshore the area on Ambon's northern coast where dramatic changes in coastal landscape were observed can explain the observed tsunami run-up along the coast. Thus, the 1674 Ambon tsunami adds weight to the evidence from recent tsunamis, including the 1992 Flores, 2018 Palu and Sunda Strait tsunamis, that landslides are an important source of tsunami hazard in Indonesia.

3.1 Introduction

Eastern Indonesia, and the Banda Sea in particular, is a region of very active and complex tectonics [Hamilton, 1979; McCaffrey, 1988; Spakman and Hall, 2010; Pownall et al., 2013]. Despite a historical record rich in major, destructive earthquakes and tsunamis, during the more recent era of instrumental seismology most of the major events have occurred in western Indonesia. The only way to better understand the tsunami threat in eastern Indonesia is therefore to glean as much information as we can from the historical record, which often consists of accounts that are sparse

and difficult to interpret.

The oldest detailed tsunami account in Indonesia was documented by Rumphius [1675]. A devastating earthquake rocked Ambon and its surrounding islands on 17 February 1674. The earthquake was followed by a massive tsunami about 100 m in run-up height which was only observed on the northern coast of Ambon Island while other areas experienced only minor tsunamis. The earthquake and tsunami caused more than 2,300 fatalities, mostly on the northern shore of Ambon.

The source of the tsunami and earthquake is unknown. Løvholt et al. [2012] and Harris and Major [2017] speculated that it was triggered by an earthquake from south of Ambon and a landslide triggered by an earthquake from inside Ambon Bay, respectively. However, no attempt has been made to investigate this event further, particularly to answer why the extreme run-up was observed only on the northern coast of Ambon. Therefore, the primary source of the tsunami and earthquake remains open to question.

In the following sections of this chapter, the tectonic setting around Ambon is discussed first, followed by our interpretation of the accounts of this event. The primary source of the earthquake and tsunami is investigated through analysis of the Rumphius document. Tsunami modelling is then performed to confirm the analysis. Lastly, the result of the analysis and the implications of the findings are discussed.

3.2 Tectonic setting around Ambon

Ambon is a small volcanic island that lies southwest of Seram Island. It consists of two small islands, Hitu and Leitimor, which are connected by a short isthmus. Ambon is located to the southwest of Seram Island which is part of the outer Banda Arc. The islands are surrounded by major faults, namely the Seram Megathrust, Kawa Fault and the Banda Detachment (Figure 3.1).

As summarised in Patria and Hall [2017], the Seram Megathrust stretches from Kai Islands in the east side to the northwest of Seram Island (Figure 3.1). It is often described as a subduction zone [e.g. Hamilton, 1979; Honthaas et al., 1998]. However, others have argued that it is a foredeep produced by loading from a developing fold and thrust belt [Audley-Charles et al., 1979; Pairault et al., 2003; Spakman and Hall, 2010]. Through high-resolution bathymetry and seismic data, Patria and Hall [2017] confirmed the second hypothesis: that it is a result of oblique intra-plate convergence.

The Kawa Fault is the most prominent structure in central Seram Island (Figure 3.1). The fault runs from Piru Bay, on the northern shore of Ambon, to the central south of the island on the northern side of the Banda Sea. The fault has a major left-lateral movement identified through geological observations [Pownall et al., 2013]. A large earthquake reported on Seram Island in 1899 was suspected to have ruptured the Kawa Fault [Soloviev and Go, 1974].

At the southern end of Seram, Pownall et al. [2016] argues that the Kawa Fault continues to the Banda Sea and is related to the Banda Detachment (Figure 3.1). The Banda Detachment is a recently discovered low-angle normal fault identified from

geological observations and high-resolution bathymetry data. Moreover, the Banda Detachment exhibits rapid extension as indicated by a very thin sediment layer in the Weber Deep [Pownall et al., 2016].

On Ambon, Watkinson and Hall [2017] identified several faults via a digital elevation model of the Shuttle Radar Topography Mission (SRTM). First, a normal fault with a very steep angle was identified on the northern shore of the island. Then a lineament with NE–SW trend, crossing the city of Ambon was observed. Last, a suspected quaternary normal fault was observed on the southern side of Ambon Bay.

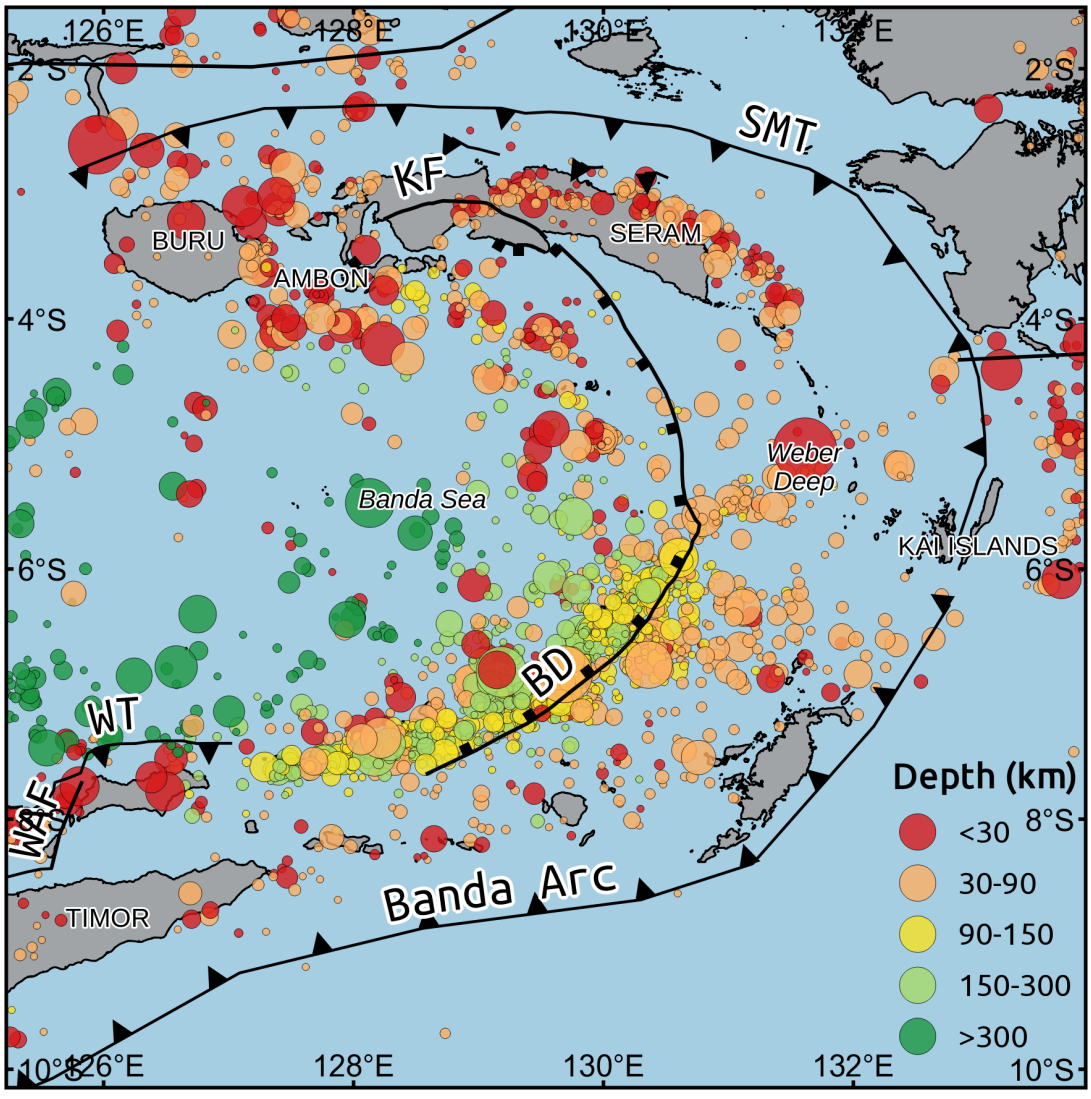

Figure 3.1: Tectonic setting of Ambon and its surrounding islands; *SMT* Seram Megathurst, *KF* Kawa fault, *BD* Banda Detachment, *WT* Wetar thrust, *WAF* Wetar-Atauro fault.

Ambon and its surrounding islands (Seram, Haruku, Saparua, Nusa Laut, and

Buru) have experienced at least 14 tsunamis in the past (Table 3.1). There were two events each were generated by volcano activities and landslides, earthquakes (7 events), and three events with an undetermined source. The majority of the events are categorised to be minor tsunamis with a maximum height up to 2 m, except for the 1674 and 1899 events. The 1674 tsunami event was started by strong ground motion felt on Ambon Island. An extreme tsunami run-up up to 100 m was observed only on the northern shore of the island with minor tsunamis at the other areas [Rumphius, 1675]. The source of this tsunami would be discussed in the following sections. In the 1899 event, settlements on Seram Island were devastated by an earthquake that was suspected originating from the Kawa Fault [Soloviev and Go, 1974]. It triggered multiple landslides which were generated tsunamis along the northern shore of Seram Island. The tsunami rose up to 9 m at villages of Amahai, Paulohi, and Elpaputih, with no reports of tsunami on the north coast of Ambon.

Table 3.1: Historical tsunamis on Ambon and its surrounding islands

Date	**Source**	**Description**	**Refs:**
9–11 November 1659	Volcano: Mt Teon	A tsunami was noticed at Ambon Bay (1–1.5 m).	a, b
17 February 1674	Landslide triggered by an earthquake	Strong ground motion devastated Laitimor refion followed by an extreme tsunami only on the northern shore of Hitu (100 m). A prolonged sequences of aftershocks was reported, with the largest occurring on 6 May generating a weak tsunami at Ambon Bay.	a, b, c
28 Novmber 1708	Undertermined	A strong "tidal wave" suddenly burst into Ambon Bay and oscillated throught the night until the following morning. An earthquake was felt a day before.	a, b
5 September 1711	Earthquake	A strong earthquake was felt on Haruku, Saparua, Nusa Laut, and Banda Islands. At Paso Baguala, eastern shore of Ambon, seawater rose by 1.2 m and destroyed two houses.	a, b
18 August 1754	Earthquake	Houses on Ambon were destroyed by an earthquake. It was followed by a tsunami observed at Hutumuri, Haruku, and Saparua.	a, b
19 April 1775	Earthquake	In the morning, a strong ground motion felt at Ambon Bay made the seawater oscillate.	a, b

Continuation of Table 3.1

Date	Source	Description	Refs:
25 August 1802	Earthquake	Seawater rose and damaged the coast of Ambon after a strong earthquake was felt on the island.	a, b
16 December 1841	Earthquake	A moderate earthquake was felt on Ambon, Buru, and Amblau Islands that generated a tsunami. The tsunami rose up to 1.5 m in height and swept away houses at Ambon Bay and Amblau. The aftershocks were reported until 21 December.	a, b
26 November 1852	Earthquake	The Banda Islands were devastated by strong ground motion that was felt on Ambon. A tsunami arrived 15 minutes later on the Banda Islands and was reported at Ambon Bay up to 2 m height.	a, b
10 June 1891	Undertermined	In the evening, seawater at Saparua Bay retreated about 200 m and then rapidly returned, inundating the shore. An earthquake was felt a day before.	b
7 June 1892	Volcano: Mt Awu	A 1.5 m tsunami was noticed at Ambon Bay caused by the eruption of Awu Volcano. The volcano is located at the Sangihe Island, north of Sulawesi (see Figure 2.17). The distance between Ambon and Awu Volcano is 800 km, roughly.	b
30 September 1899	Landslide triggered by an earthquake	A strong earthquake was suspected as originating from the Kawa Fault devastated the settlements of Seram Island. It generated a tsunami that swept away villages at Elpaputih and Taluti Bays on the southern shore of Seram up to 9 m height. The tsunami was reported in a village on the eastern shore of Piru Bay as well, and noticed on Ambon.	b
5 July 1904	Undertermined	In the morning, seawater suddenly retreated and then rapidly returned, inundating the shore. An earthquake was felt a day before.	b

Continuation of Table 3.1

Date	Source	Description	Refs:
8 October 1950	Earthquake	An Mw 7.4 earthquake [USGS] at south of Ambon generated a tsunami that arrived about 15 minutes later at Ambon Bay	d
Refs: a) Wichmann [1918], b) Soloviev and Go [1974], c) Rumphius [1675] d) Latief et al. [2016]			

End of Table 3.1

3.3 Historical accounts of the Ambon Island 1674 earthquake and tsunami

Historical accounts of the 17 February 1674 Ambon earthquake and tsunami were documented in the book "Waerachtigh Verhael Van de Schlickelijcke Aerdbebinge" written by Rumphius [1675]. The book was translated into English with the title "The true history of the terrible earthquake". Rumphius was a scientist in the field of biology and worked for the Dutch East Indies Company [de Wit, 1952]. He lived on Ambon and experienced the disastrous earthquake which killed his wife and youngest daughter. Even though he had gone blind because of glaucoma several years before this event, he carefully collected and documented all the accounts available around the island. The historical accounts described below are based on the English translation and summarised in Figure 3.2 and Table 3.3 below.

The event occurred at about 7:30 pm local time when people in Laitimor were celebrating Chinese Lunar New Year. In Ambon, the bells in Victoria Castle swung by themselves and people who were standing fell to the ground as the earth heaved up and down like the sea. Stone buildings collapsed and buried up to 80 people. Strong shaking was felt on the mountains in Laitimor, with rocks falling and ground cracking open. In Hutumuri near the coast, on the eastern side of Laitimor, seawater burst into the air like a fountain.

The earthquake was reported from Hitu as well. In Waytome River, on the northern side, the river water spurted to 6 m high. People in the north to northwest of Hitu heard a loud sound like canon-fire. They noticed two long, thin marks in the sky, extending from Luhu to Seith, shortly before the earthquake. Less than 15 minutes after the earthquake, villages between Lima and Hila were wiped away by a gigantic mountain of seawater. The seawater rose about 50 to 60 fathoms (approximately 90–110 m) to the top of the surrounding hills, and more than 2,300 people perished.

This unusual phenomenon was reported at the other places, but with much less intensity. Hitu Lama village, located approximately 15 km to the east of Hila, reported that the seawater rose only about 3 to 5 metres, killing 35 people. A little further to the east, 40 houses in Mamala were swept away without fatalities. The settlement of Orien (or its present name, Ureng), which is located less than 10 km west of Lima reported that the seawater rose and inundated land but it did not enter

the houses. People in Larike, a village in the westernmost of Hitu, observed that the seawater rose less than 1 m at the Rotterdam Redoubt. In the southern and eastern areas of Ambon Island, there was much less seawater oscillation reported, apart from some small boats being tossed over each other.

At Luhu in Seram Kecil, the seawater inundated trees and the dwellings of a company. The waster rose with a hight just over 5 m. At the northernmost of Piru Bay, half of the houses in Tanuno were engulfed by water, but without fatalities. Fishermen in Piru Bay said the sea remained calm with a noticeable ripple. A much lower seawater oscillation was noticed by people from Manipa, Salati, Haruku, Nusa Laut, and Banda Neira Islands compared with the oscillation that was was observed in Hitu and Laitimor.

What were the source of the ground motion and seawater phenomena described above, particularly on 17 February 1674? In the following sections, we will make use of the historical accounts of ground motion and tsunami observation to answer that question.

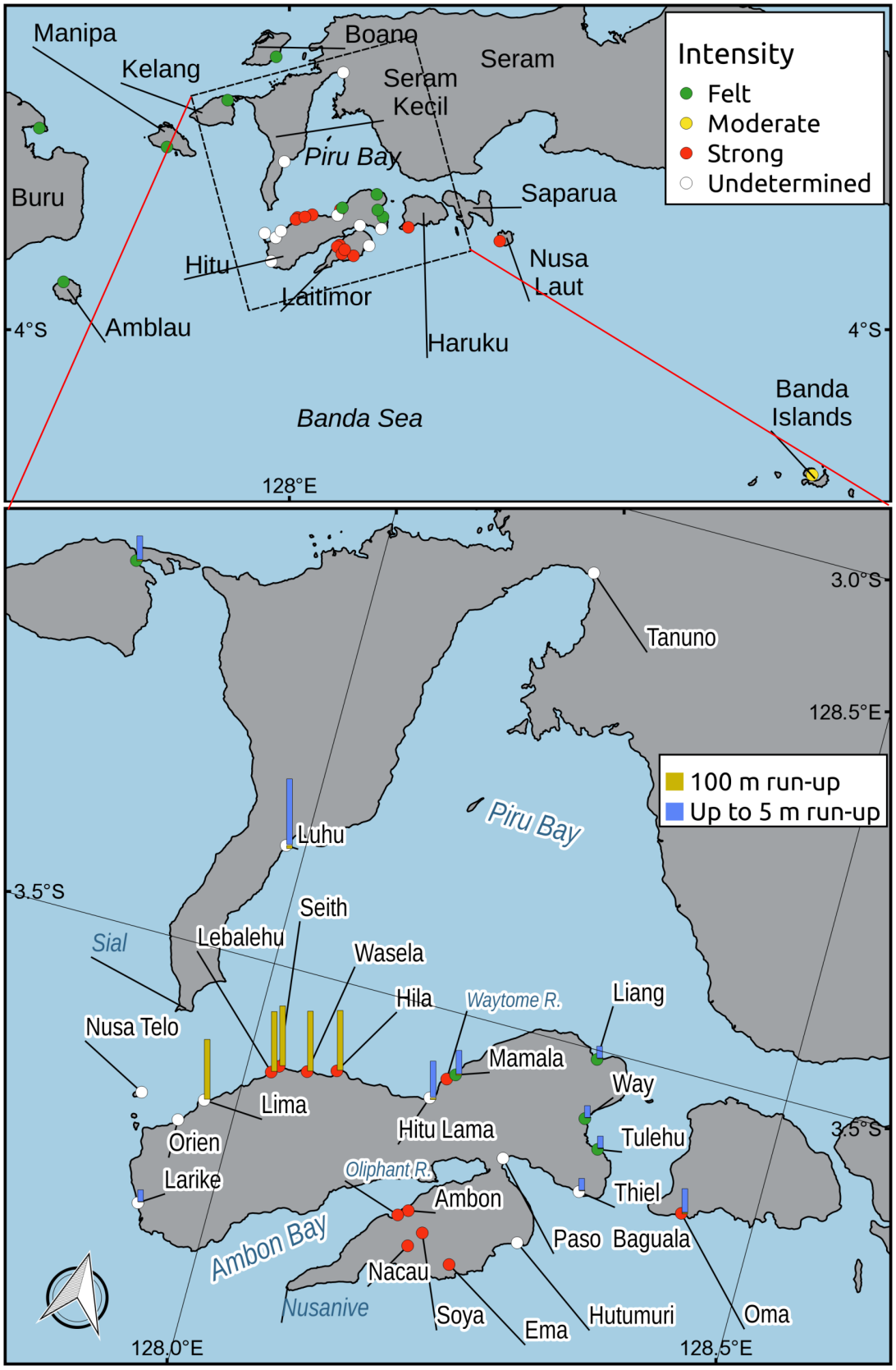

Figure 3.2: Historical accounts of the 1674 Ambon Island earthquake and tsunami. Colour circles represent interpreted earthquake intensity. Tsunami heights are indicated by the gold colour bar (up to 100 m) and the blue bar (up to 5 m).

Table 3.2: Tsunami and ground motion interpretation from Rumphius [1675]

Location (Region: Village)	**Description**	**Estimated tsunami height (m)**	**Estimated earthquake intensity**
Hitu: Larike, Rotterdam Redoubt	Seawater rose to 2 feet high around the redoubt. The water rose three times without causing major damage other than crashing a boat.	<1 (inundation depth)	Undetermined
Hitu: Nusa Telo	Seawater rose suddenly after first withdrawing in the direction of Orien. The water oscillated three times from two directions.		Undetermined
Hitu: Orien	A loud roar was heard in the air. The seawater rose then was drawn in the direction of Nusa Telo. The water did not enter houses but only surrounded the barricades.		Undetermined
Hitu: Lima, Haarlem Redoubt	Seawater came from the direction of Lebalehu and rose about 50 or 60 fathoms around the redoubt, carrying stones, mud, and sand. Large boulders were thrown on the first floor of the redoubt. A woman was swept away 20 fathoms behind the redoubt. Lime kilns were washed away, with at least 86 fatalities.	90–110 (run-up height)	Undetermined
Hitu: Seith	Seawater rose about 50 to 60 fathoms, up to the windows of the fort. Villages between Seith, Lebalehu, and Wasela were washed away (but Hautunua village at a higher location was safe). Lime kilns were washed away, with more than 619 fatalities.	90–110 (run-up height)	Strong

Continuation of Table 3.2

Location	**Description**	**Estimated tsunami height (m)**	**Estimated earthquake intensity**
Hitu: Lebalehu	A 200 m-wide region around Lebalehu collapsed, making the beach very steep. This also happened between Seith and Hila (west of Fort Amsterdam), including Nukunali, Taela, and Wawani. An upwelling of seawater (to about 50 or 60 fathoms originated from here, dividing into three: i) east – Seith and Hila, ii) west – Lima and Orien, iii) to the sea. The water glowed like fire but was as black as coal and noisy. Lime kilns were destroyed.	90–110 (run-up height)	Strong
Hitu: Hila, Fort Amsterdam	At least 1461 people were killed. Seawater rose between 50 and 60 fathoms high to the gallery of the fort and overtopped the roof. All the houses around the fort were swept away, particularly to the west and south. A grinding wheel, a drum, a large coral, fish cages, and cattle were swept away.	90–110 (run-up height)	Strong
Hitu: Hitu Lama	Seawater rose 10 feet and swept away several houses. About 35 people were killed.	3–5 (inundation depth)	Undetermined
Hitu: Mamala and Waytome River	40 houses were swept away, without fatalities. Limekilns were destroyed. Strong ground motion toppled equipment inside a warehouse. Eastern shore of Waytome River split open and water spurted 18–20 feet high.	<2 m (inundation depth)	Felt (Mamala) - Strong (Waytome River)
Hitu: Liang	The earthquake was felt with no damage to the houses.		Felt
Hitu: Way	The earthquake was felt with no damage to the houses.		Felt
Hitu: Tulehu	The earthquake was felt with no damage to the houses.		Felt
Hitu: Thiel	A few houses were carried away by seawater		Undetermined

Continuation of Table 3.2

Location	**Description**	**Estimated tsunami height (m)**	**Estimated earthquake intensity**
Laitimor: Paso Baguala, Fort Middleburg	Weapons and equipment were damaged. The earth around Baguala and Hutumuri cracked. Seawater came from the direction of Fort Victoria but did not overflow the isthmus.		Strong
Laitimor: Hutumuri, near to the shore	Seawater burst upwards like a fountain		Strong
Laitimor: Cape Nusanive	Boats were tipped over and fishermen noticed the waves were a little higher than normal.		Undetermined
Laitimor: Ambon, Victoria Castle	Bells in the castle swung by themselves. People around the castle fell over and saw the ground heaving up and down like the sea. Central walls of the town hall collapsed. A hospital was badly damaged. Boats at the mouth of Oliphant River were thrown into the stream. The bridge close by was almost shaken loose. Goods in houses shifted 3 to 4 feet without breaking. 79 people were killed and more than 35 injured when at least 75 buildings collapsed.		Strong
Seram Kecil: Cape Sial	Seawater caused damaged.		Undetermined
Seram Kecil: Luhu, Overburg Redoubt	Villages and boats were swept away. Seawater rose 3 fathoms above normal.	5.5	Undetermined
Seram Kecil: Tanuno	Seawater rose once and half the houses were swept away, without fatalities. Fishermen claimed that the sea in Piru Bay was calm.		Undetermined
Haruku: Oma	Earthquake described as violent, small rocks fell into the sea and a large boulder was moved. Seawater rose 6 feet above normal.	2	Strong
Nusa Laut	Earthquake described as violent.		Strong

Continuation of Table 3.2

Location	**Description**	**Estimated tsunami height (m)**	**Estimated earthquake intensity**
Banda Islands: Neira	Earthquake described as moderate. Seawater rose a little, but no damage.		Moderate
Buru	Earthquake was felt.		Felt
Amblau	Earthquake was felt.		Felt
Manipa	Earthquake was felt. Seawater rose at Fort Manipa. 40 houses swept away, but no fatalities.	1–2	Felt
Kelang: Salati	Earthquake was felt. Seawater rose 6 feet above normal.	2	Felt
Boano	Earthquake was felt.		Felt
Laitimor: Nacau	Strong earthquake made 7 houses collapse, large rocks fell.		Strong
Laitimor: Ema - Soya	Road was cracked 2 to 3 feet wide in several places.		Strong

End of Table 3.2

3.4 Source identification

3.4.1 Earthquake source

With regard to the tectonic setting around Ambon, there are five candidate faults that could have generated a large earthquake with intensities and effects shown in Figure 3.2: 1) the north Seram Megathrust, 2) the Kawa Fault, 3) an intraslab fault 4) the purported South Seram Thrust Fault, or 5) a local fault on Ambon. Each of these is qualitatively analysed below to identify the most credible source of this event.

In general, the strongest ground motions were felt on Laitimor, Oma (Haruku), and Nusa Laut (Figure 3.2). Then the intensity of ground motion decreases toward Neira, the Banda Islands in the south, and Boano in the north. Many buildings collapsed and ground cracked in various places on Laitimor. There was liquefaction at Hutumuri and Waytome Rivers according to the accounts of *'water spurted high [in]to the air'*. Recurring aftershocks were reported until at least 10 May. Judging by these observations, the source must have been a moderate to large earthquake with a local and shallow epicentre.

A shallow earthquake on the north Seram Megathrust would have been too far from Ambon to have these effects and if the earthquake had occurred on this fault, the islands of Boano, Kelang, and Manipa would have experienced stronger ground shaking than Ambon and Neira. If the earthquake had originated from the Kawa Fault, the villages on Seram Island would have experienced more intense ground shaking as in the 1899 earthquake and tsunami event [Soloviev and Go, 1974]. A deep instraslab earthquake would generate ground motion that felt over a broader region. However, an intraslab earthquake typically do not cause ground cracking and the long aftershock sequences. The Benioff zone is over 100 km beneath Ambon [Spakman and Hall, 2010], and intraslab earthquake at this depth would likely generate strong ground motion distributed over a wider area than Ambon.

Therefore, the most credible source for this event would have been the South Seram Thrust Fault or a local fault on Ambon. The South Seram Thrust is a fault line that runs from the south shore of Buru to Nusa Laut and then dips northward. An earthquake on this fault could have generated effects such as the ones that were observed. However, it is not clear whether this fault actually exists even though it has been used in seismic and tsunami hazard maps of Indonesia [Irsyam et al., 2010; Horspool et al., 2014]. Brouwer [1921] and Watkinson and Hall [2017] have identified quartenary faults on Ambon itself. Harris and Major [2017] identified one of these faults as the primary source of this earthquake, but without a clear explanation of why. All of these faults on Ambon could have generated this type of earthquake but further investigation is required to determine exactly which one.

3.4.2 Tsunami source

If we consider which of the five candidate faults previously mentioned might have been capable of directly generating the observed tsunami, it is immediately obvious that an intraslab event could not, since an earthquake at the greater than 100 km

depth of the Benioff zone beneath the Banda islands could generate only a weak tsunami at best. Okal and Reymond [2003] showed that the largest intraslab event ever recorded, the Mw=8.5 Banda Sea event at 60 km depth, generated only a weak tsunami. A tsunami generated by the Seram Megathrust or South Seram Thrust would have to enter Piru Bay through narrow straits around Ambon Island, which would greatly attenuate the tsunami arriving on the north coast of Ambon. As we show in Section 3.7 below, instead of having highest run-up long the north coast of Ambon, the tsunami energy generated by these two scenarios would be concentrated between the western and southern coast of Hitu and Laitimor, respectively. The Kawa Fault has a strike-slip mechanism that would generate insignificant vertical displacement for tsunami generation.

The only fault that might generate a large tsunami on the northern coast of Ambon and nowhere else would be a local fault on the northern shore of Hitu [Brouwer, 1921; Watkinson and Hall, 2017]. The fault has a normal mechanism that could generate vertical displacement of a water column for tsunami generation. However, the fault under consideration is only 16 km long, and therefore unlikely to generate an earthquake with magnitude greater than 7 and slip much higher than 2 m [Wells and Coppersmith, 1994], far too small to generate the observed tsunami run-up. Therefore, if none of the potential tsunamigenic earthquakes could have been capable of directly generating a tsunami with the observed run-up, the most plausible source of the tsunami is from aan earthquake-triggered landslide in Piru Bay.

There is an indication in the accounts that a massive coastal landslide occurred on the northern shore of Hitu, between Seith and Hila mentioned in the accounts [Rumphius, 1675]:

> The country around Lebalehu, a region once famed for its market and for being the most important Muslim meeting place, collapsed the width of a Musquet shot. There is no longer any beach there, but only a very steep precipice. Just the same is true between Ceyt (Seith) and Hila, even as far as the beach at the later place, along the west side of the Fort Amsterdam and beneath the Residence of Intche Tay. Including the Negeris Nukunali, Taela and Wawani, all this disappeared along with [the] roadstead where ships used to anchor. It seems likely that the aforementioned wall of water arose in the place just indicated, to wit directly below Lebalehu. It might even have come from Hitu because various people on board ships that were not far off shore, reported only a rippling of the waves. The mass of upwelling water divided into three parts. One went east to Ceyt (Seith) and Hila, the other west to the villages of Lima and Oried. The water stank so horribly that people on board ships close to the coast became ill, and it was so filthy that anyone who had been immersed in it looked as if he had been hauled out of a mudbath.

In other words, there was a major change in the landscape around the coastal region: a gentle beach became very step. Moreover, people saw that the water was dark and a roaring sound was heard from this area, which indicates that the seawater

mixed with sediment and the tsunami source was near the people. The seawater colour and loud sound described in the accounts are similar to those described after the 1998 Aitape, Papua New Guinea (PNG) tsunami [Davies et al., 2003], which is thought to have been generated by a landslide. Unfortunately, there is no further information with regard to parameters of the landslide. According to the accounts, it was a subaerial landslide, with about 200 m of the previous shoreline collapsing into the sea. The lateral extent is thought to be at least 5 km along the coastline between the villages of Seith and Hila.

Further, the majority of the fatalities in this event were in this region and not many buildings collapsed in the earthquake. In addition, an extreme run-up laterally along the coastline can only be explained by a landslide. These observations are similar to the 1998 Aitape, PNG tsunami, which was generated by an underwater landslide [Okal and Synolakis, 2004; Synolakis et al., 2002].

3.5 Landslide-generating tsunami

Tsunamis generated by landslides were not widely considered before the 1998 Aitape, PNG tsunami even though evidence of them has been identified at various locations [Tappin, 2017; Okal and Reymond, 2003]. This is because of the lack of adequate technology to map bathymetry underwater and it was thought that a landslide would generate only an insignificant tsunami [Tappin, 2017].

As noted in Synolakis et al. [2002], the Aitape, PNG 1998 tsunami was initiated by a relatively small earthquake of Mw 7.0. About 20 minutes later, a tsunami swept away more than 2,100 people with a maximum run-up of 15 m extending 25 km along the coastline. However, at tidal gauges in Japan, the tsunami was recorded only reaching 25 cm [Synolakis et al., 2002]. Based on the tsunami height observation and moment energy analysis, the initiating mechanism is considered to be an underwater landslide, which was confirmed by a series of marine seismic surveys. The surveys found a massive slump scarp with an estimated volume of 4 km^3 located about 40 km from the western end of the fault [Tappin et al., 1999, 2001]. The authors used tsunami modelling to show that an underwater landslide was the only source needed to explain the tsunami observations: an extreme run-up with a very narrow extent along the shore.

Tsunami generation is affected by both the vertical and length extent of the bathymetry displacement. Vertical displacement due to an earthquake normally reaches only a few metres at most, whereas it can easily reach hundreds of metres in a mass failure event. The dimensions of an earthquake rupture can extend to hundreds of kilometres but it is rare to see a huge landslide up to 100 km length. Therefore, a tsunami generated by an earthquake has a long wavelength as it travels across the ocean. On the other hand, a tsunami generated by a landslide loses its energy quickly as it travels because of its shorter wavelength, but it has a much larger amplitude in a local area. Therefore, tsunamis generated by earthquakes can observed over a wide area, with a relatively similar run-up along the coastline. In

contrast, a narrow region of extreme run-up is observed in a tsunami event generated by a landslide.

Okal and Synolakis [2004] investigated tsunami height profiles along a coastline from some past tsunami events. They found similar patterns in the 1946 Unimak (Alaska) and 1998 Aitape (PNG) tsunamis profile, which were both generated by landslides. The profiles had extreme run-up heights over a very narrow along-shore extent. Based on these findings, Okal and Synolakis [2004] developed a criterion for identifying landslide-generating tsunami based on the aspect ratio $I_2 = \frac{b}{a}$ between the maximum tsunami run-up height b and the distance a of the lateral extent of high tsunami run-up along the coastline. Thus, any event with I_2 larger than 0.0001 should be considered a tsunami generated by a landslide.

Accordingly, we calculate the I_2 of the tsunami observations on the northern coast of Hitu. It was difficult to determine the exact values of a and b because of the sparse data available (Figure 3.3a). However, the data clearly shows a very rapid drop in run-up to the east and west of the maximum run-up height location between Lima and Hila. The estimated I_2 was greater than 0.006, which was 60 times larger than the limit suggested by Okal and Reymond [2003]. Therefore, this event is almost sure to have been a tsunami generated by a landslide.

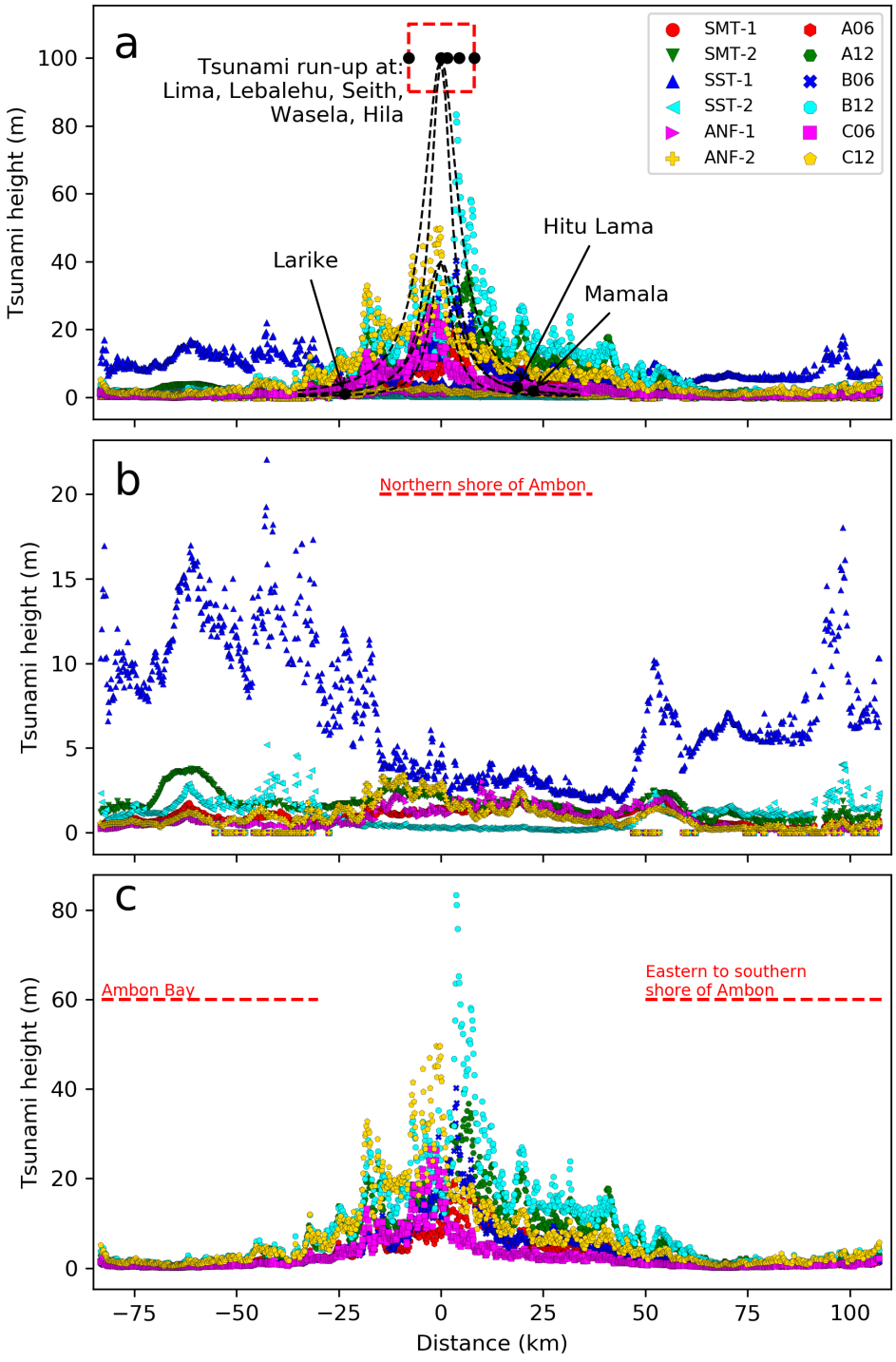

Figure 3.3: Tsunami height profiles along the coastline: a) data and all scenarios the dashed lines indicate *a*= 3–5 km with *b*= 40–100 m; b) only from tsunamigenic earthquake scenarios; c) selected landslide-generating tsunami scenarios. Symbols with colour indicate the scenario codes as shown in Tables 3.3 and 3.4.

3.6 Tsunami modelling

Tsunami modelling was performed to confirm the analysis above using the JAGURS tsunami simulation code [Baba et al., 2015, 2017]. The code numerically solves non-linear shallow water wave equations in a spherical coordinate system with a finite-difference scheme. The digital elevation model (DEM) was built from a combination of nautical charts, a 90-m commercial bathymetry dataset provided by the TCarta Marine, the General Bathymetric Chart of the Oceans (GEBCO), and the SRTM-90m in a domain of nested grids (Figure 3.4). The coarsest and finest grid resolution of the domain is approximate 1,500 and 167 m, respectively. A time-step of 0.5 s is set to satisfy the Currant stability condition. Due to the unavailability of a high-resolution topography dataset, tsunami inundation is not performed.

Tsunami simulations were conducted for a tsunamigenic earthquake (Table 3.3) and landslide-generating tsunami scenarios in this area (Table 3.4). The initial sea surface elevation from the earthquake scenarios were assumed to be equal to the earthquake deformation calculated from the Okada [1985] formula, using the parameters discussed below. A two-layer model was utilised to simulate tsunami generation and propagation due to a landslide [Baba et al., 2019]. Because of an instability issue, simulation of tsunami generated by a landslide was performed in a single grid domain model. A detailed explanation of this technique is discussed in Appendix A.

Table 3.3: Tsunamigenic earthquake scenarios for the 1674 Ambon event

Scenario	Position[1]	Length	Width	Strike	Dip	Rake	Slip
SMT-1	2.97°S, 126.13°E, 0 km	202 km	80 km	73°	20°	90°	8.0 m
SMT-2	2.55°S, 127.25°E, 5 km	180 km	90 km	83°	20°	90°	5.0 m
SST-1	4.15°S, 128.61°E, 0 km	179 km	80 km	-85°	40°	90°	7.0 m
SST-2	4.31°S, 128.61°E, 5 km	70 km	40 km	-90°	30°	90°	1.5 m
ANF-1	3.58°S, 128.19°E, 2 km	25 km	10 km	-98°	70°	-90°	5.0 m
ANF-2	3.58°S, 128.04°E, 2 km	20 km	10 km	-135°	70°	-90°	5.0 m

Position[1]: Top-right corner coordinate of a fault plane (Figure A.2).

3.6.1 Tsunamigenic earthquake scenarios

SMT-1 and SMT-2 (Figure 3.5) represent two earthquake scenarios from the Seram Megathrust zone. The Mw 8.2 parameters of SMT-1 [Løvholt et al., 2012] were speculated to be the source of the events documented in 1657, 1708, 1876, and 1965. According to Horspool et al. [2014] and Irsyam et al. [2010], the Seram Megathrust zone is capable of generating an earthquake with a maximum of Mw 7.9 to 8.2. Here, SMT-2 represents an earthquake of Mw 8.1 with the fault parameters taken from Horspool et al. [2014].

SST-1 and SST-2 (Figure 3.5) represent two scenarios from the South Seram Thrust Fault. Løvholt et al. [2012] assumed the 1674 Ambon tsunami was caused by an Mw 8.1 earthquake from South Seram Thrust Fault. The authors suggested that the same fault zone triggered the 1950 and 1983 events. The source parameters of the SST-1

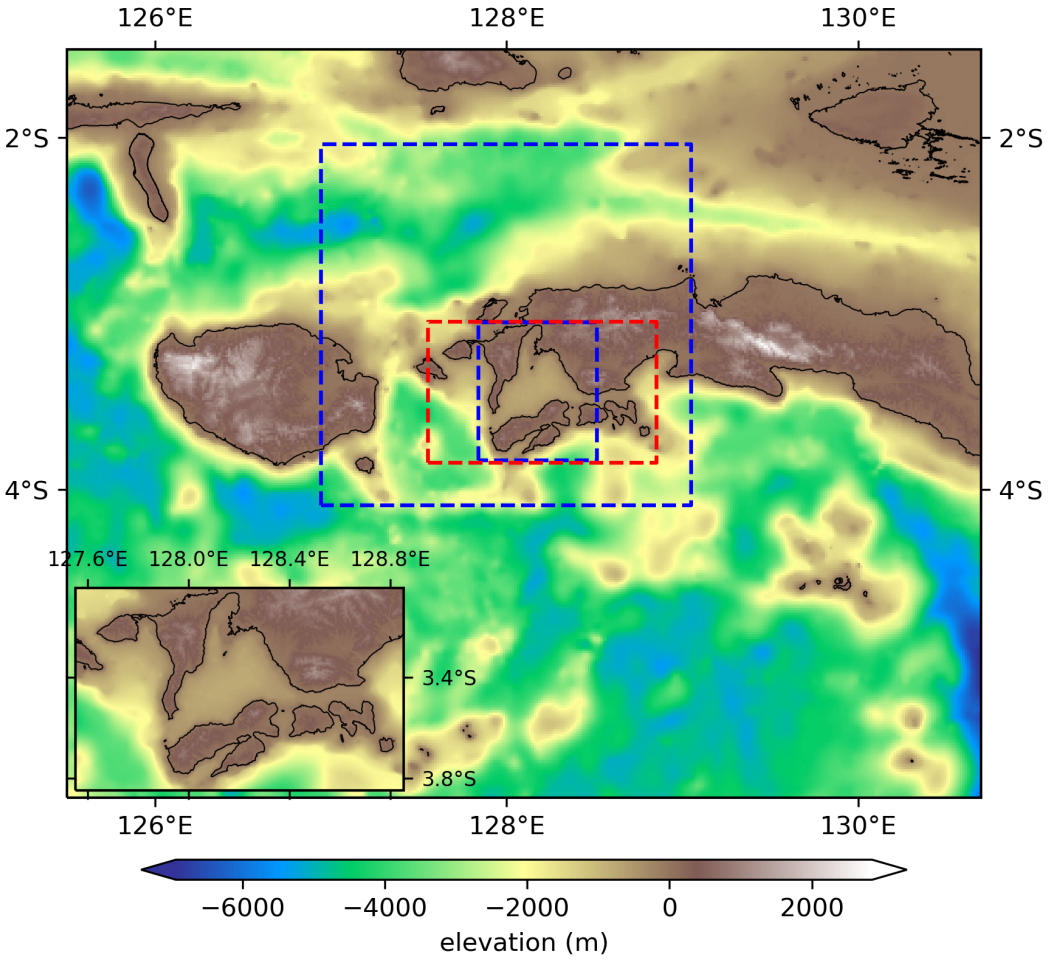

Figure 3.4: Domain model of tsunami modelling. The dashed blue boxes are the nested-grids domain for the tsunamigenic earthquake model. The red box shows the domain model for landslide-generating tsunami scenarios; the elevation model is shown in the inset map.

scenario were taken from their study. Another study conducted by Latief et al. [2016] indicated the source of the 1950 Ambon tsunami being from the South Seram Thrust Fault, but it was located a little further south, with a smaller fault plane. The SST-2 scenario followed the parameters used in Latief et al. [2016] and is represented as an Mw 7.5 earthquake.

Finally, ANF-1 and ANF-2 (Figure 3.5) were designed to follow the normal fault, as indicated by Brouwer [1921] and Watkinson and Hall [2017], respectively. These two scenarios represent Mw 6.0 to 6.5 earthquake, respectively. They are only hypothetical scenarios because no detailed study has been conducted on these faults, other than categorisation as quaternary faults [Watkinson and Hall, 2017]. Here a dip

of 70° was selected as the optimum angle of a normal fault earthquake to generate maximum vertical displacement.

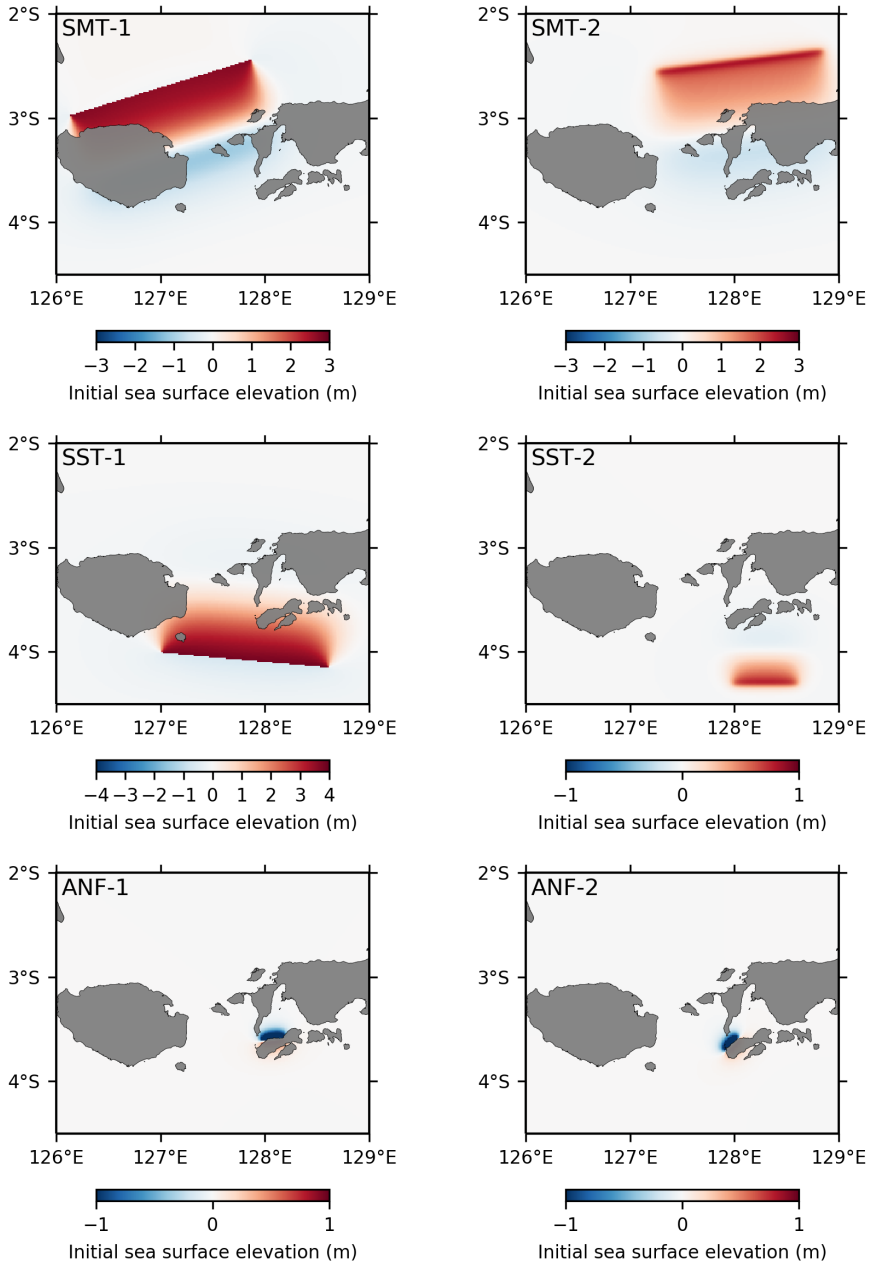

Figure 3.5: Initial sea surface elevation from tsunamigenic earthquake scenarios shown in Table 3.3. SMT-1 and SMT-2 represent the Seram Megathrust; SST-1 and SST-2 are the South Serahm Thrust; and ANF-1 and ANF-2 are local faults on the Ambon scenarios. Each figure has a different colour scale.

Table 3.4: Landslide-generating tsunami scenarios

Centre of the Gaussian

Location	Longitude	Latitude
A	128.07° E	3.585° S
B	128.03° E	3.585° S
C	128.02° E	3.585° S

Gaussian parameters

ID	Radius (m)	Thickness (m)
1	500	100
2	500	200
3	500	300
4	1000	100
5	1000	200
6	1000	300
7	2000	100
8	2000	200
9	2000	300
10	2500	100
11	2500	200
12	2500	300

3.6.2 Landslide-generating tsunami scenarios

We tested 36 synthetic scenarios of landslide-generating tsunami models (Table 3.4). The landslide layer was assumed to have a Gaussian function on top of the recent DEM with a deformable material type. The radius and thickness of the Gaussian varied from 500 to 2,500 m and between 100 and 300 m, respectively. It was located at three different places (A, B, C) near the shoreline between Seith and Hila. The locations were selected according to the accounts previously discussed. To satisfy the stability of the model, the landslide layer needed to be 'clipped', so that the landslide would always below the at-rest level of the sea surface. Therefore, the landslide layer looked like a half of the Gaussian (Figure 3.6).

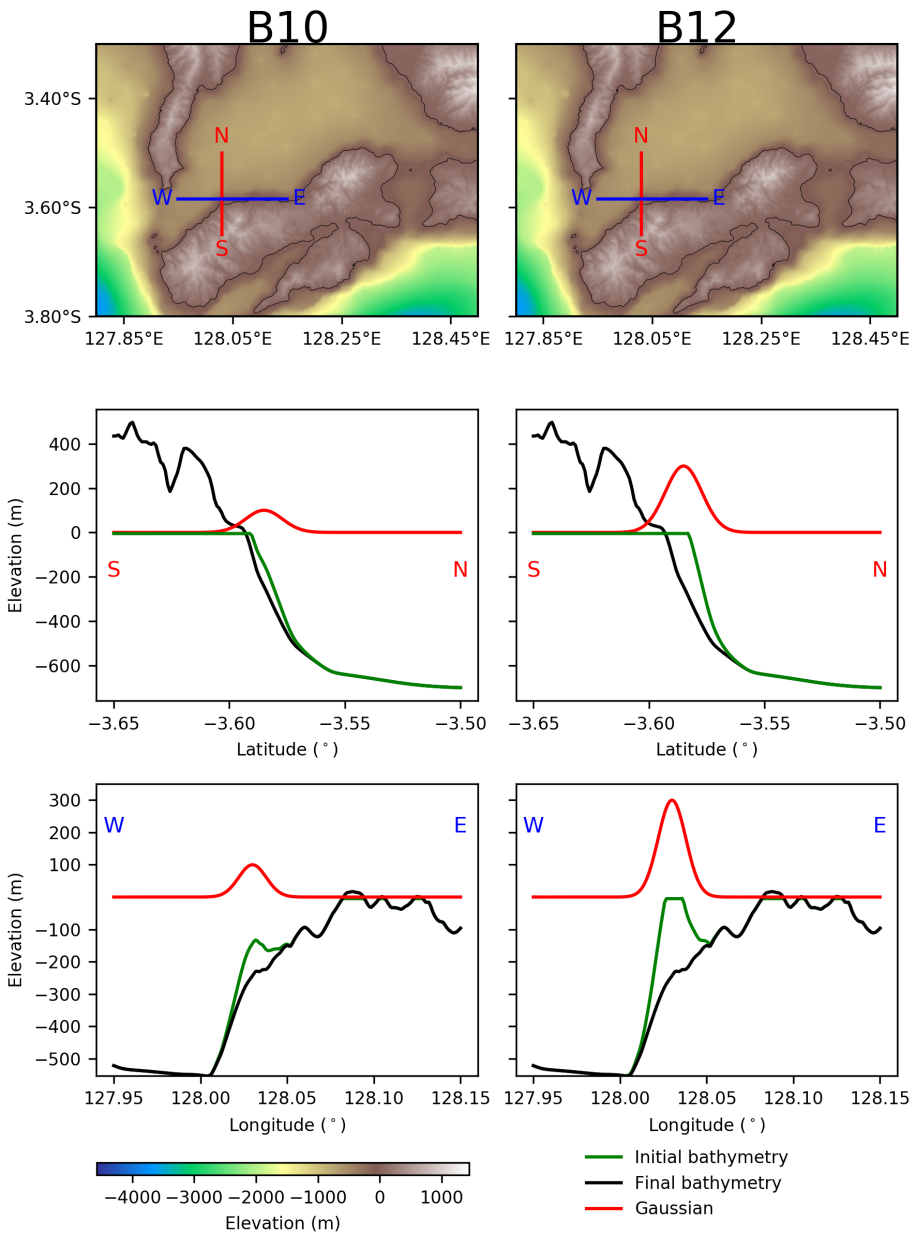

Figure 3.6: Illustration of selected tsunami landslide scenarios shown in Table 3.4. B10 and B12 are landslides with the centre of the Gaussian located at Point B (128.030°E and 3.583°S) with each radius of 2,500 m and maximum thickness of 100 and 300 m, respectively. The middle and bottom figures are final bathymetry (black), the Gaussian (red), and 'clipped' initial bathymetry (green) profiles along the W–E and N–S direction.

3.7 Results and discussion

Piru Bay is a closed sea surrounded by several narrow straits surround Ambon Island. It is difficult for much tsunami energy to propagate from outside the bay to Ambon's northern shore, particularly for the SMT-1, SMT-2, SST-1, and SST-2 scenarios. Therefore, the maximum tsunami amplitude simulated was relatively small (Figure 3.7). These results meant that a tsunami source inside the bay is required.

As suspected, no tsunamigenic earthquake model could generate a high tsunami inside Piru Bay only, with the maximum height located on the northern shore of Ambon, except the normal fault scenarios (Figure 3.3b). However, the fault length limits the magnitude, requiring a huge slip to produce very high tsunami. This would be an unrealistic model. The normal fault model scenarios in this study were already unrealistic, with a five-meter slip.

All the landslide-generating tsunami simulations result in a maximum tsunami height concentrated inside Piru Bay between Seith and Hila with minor tsunamis at the other places (Figure 3.8). Through these simulations, we confirm the tsunami height distribution mentioned in the [Rumphius, 1675] accounts. The largest tsunami height near the shoreline is almost 80 m from the B12[1] landslide scenario, with an approximate volume of 1 km^3 (Figure 3.3c). We understand that the B12 scenario can be considered as a very large landslide. However, we still assume that the B12 is the best scenario according to the historical account of *"...villages between Seith and Hila collapsed..."* and *"...with a width of a musket shot..."*. The distance between those two villages is approximately 2.5 km and the shot range of a musket shot varies from 100 to 300 m (see Table3.3).

The 100 m tsunami run-up between Seith and Hila villages could not be reconstructed for several reasons. First, there was no high-resolution DEM available to accommodate detailed inundation modelling. Therefore, the tsunami height profiles were extracted along the depth of 20 m and Green's law [Synolakis, 1991] was used to estimate the run-up height on the shoreline. Second, the DEM did not represent the actual elevation at that time. Third, it was possible that the tsunami run-up reported had been exaggerated. For example, *'the water rose especially between those villages (Lima and Hila) and Seith to the top of the surrounding hills, estimated to be some 50 to 60 fathoms [90–110 m] high'*. This account could have meant a maximum run-up height due to water splash. According to the recent DEM, the closest hill with a height above 100 m was located about 500 to 1,500 m from the shoreline, meaning the northern coast had a narrow strip coastal area followed by steep topography. Moreover, some accounts noted seawater rising as high as the window of a redoubt in Seith and over-topping Fort Amsterdam in Hila. According to the online photos available, all the redoubts and forts are located near the coastline and are two to three floors high (approximately 20–30 m; Figure 3.9). Therefore, our simulated landslide scenario produced a reasonable tsunami height.

Although the primary source of the ground motion was still unclear, it was most likely from a local and shallow earthquake. From the reports of ground cracking and

[1] A landslide located at Point B from ID-12 – Table 3.4

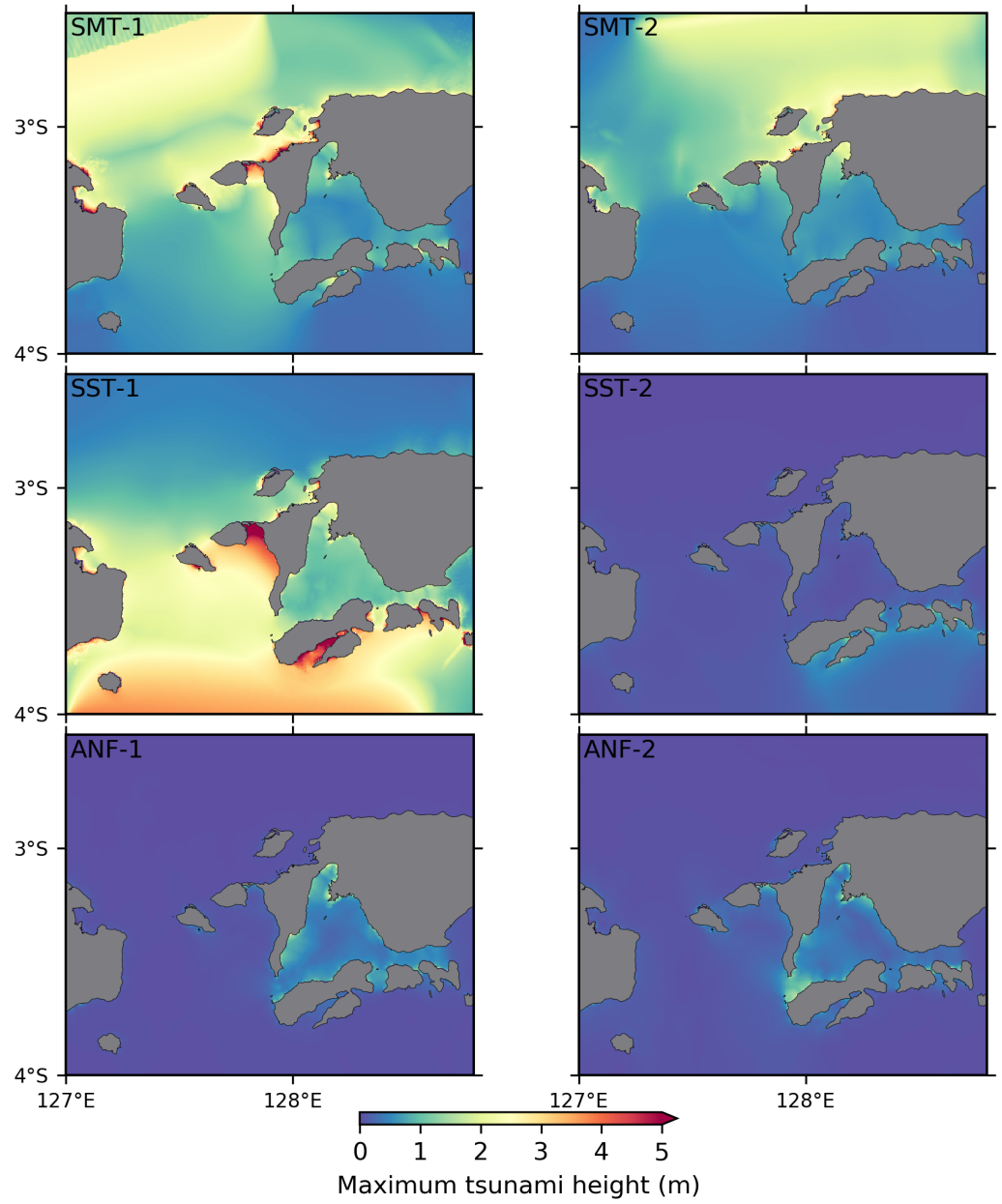

Figure 3.7: Maximum tsunami heights from the tsunamigenic earthquake scenarios shown in Figure 3.5.

building damage in Laitimor region, the earthquake location was most likely south of Ambon or Nusa Laut, with the northern limit in the Laitimor region. Further investigation is highly recommended.

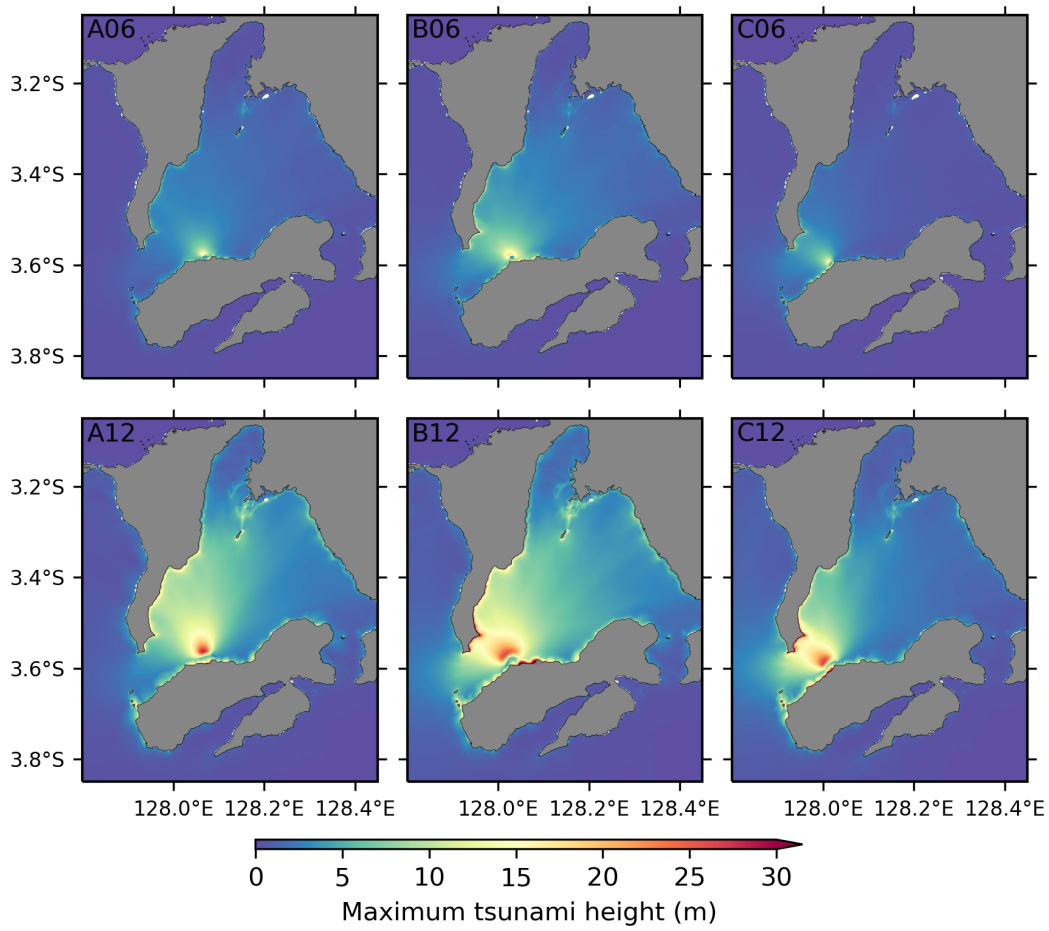

Figure 3.8: Selected maximum tsunami height from landslide scenarios shown in Table 3.4. Scenario C3 is the best source parameter to describe this event.

3.7.1 Limitations

Because our DEM cannot resolve evidence of a slump, confirmation of this finding through a high-resolution bathymetric survey, as well as a more sophisticated landslide-generating tsunami model is needed. The two-layer model in the JAGURS code considered only a submarine landslide type. Therefore, as noted earlier, the landslide layer had to be 'clipped' to keep it below sea level, for code stability, which may have resulted in an underestimate the actual condition. In addition, the code was a friction-less model, so the slide layer did not stop moving during the simulation.

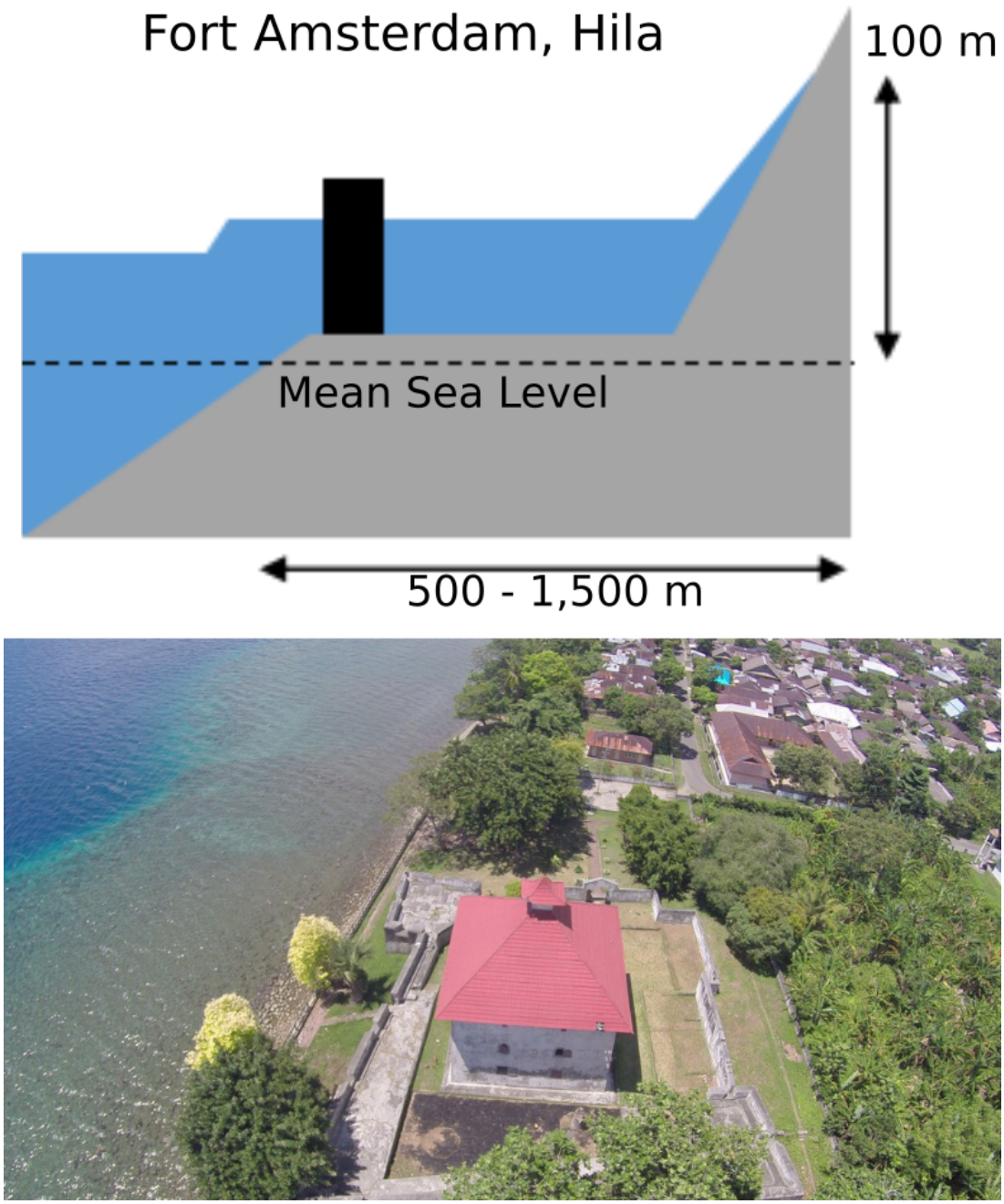

Figure 3.9: Illustration of tsunami run-up at Fort Amsterdam, Hila and a photo of the fort in the present condition (source: Indonesia Kaya [2019]).

3.7.2 Implications for the other historical accounts

The primary source of this earthquake and tsunami was confirmed from the sparse historical accounts [Rumphius, 1675]. While the precise mechanism of the earthquake remained unclear, the source of the tsunami could be confirmed to be a coastal

landslide.

This study has shown a technique for optimising sparse and incomplete accounts. The historical accounts of tsunamis in Indonesia have been documented in several catalogues [e.g Wichmann, 1918, 1922; Soloviev and Go, 1974; Soloviev et al., 1986]. Generally, all accounts of tsunami events began by describing ground motion felt at various places with different intensities. These were followed by tsunami heights observation along the coastline. As with the 1674 Ambon event, there is no detailed information regarding the source of the ground motion, nor the tsunami. By using on similar to that used in this study, the primary source of the tsunamis noted in the catalogue might be changed and/or updated in more detail. For example, the primary source of the devastating 1899 Seram tsunami was associated with an earthquake from the Kawa Fault. However, because the Kawa Fault has a strike-slip mechanism and the majority of the earthquake would be on land, this could generate only an insignificant tsunami. By investigating accounts available in detail, such as in Soloviev and Go [1974], the primary source of the tsunami could be seen as beeing a landslide occuring at different places along the southern shore of Seram. The accounts indicated the locations and sizes of the landslides on land.

Investigating other historical accounts will help to reveal more about the most likely primary source of the tsunami in each region. This will allow a comprehensive tsunami hazard assessment.

3.8 Conclusion

In this study we have shown how historical accounts of the 1674 Ambon tsunami, one of Indonesia's largest and deadliest tsunami disasters, can be used to better understand its earthquake source and mechanism of generation. We have shown that, although the reports of ground motion intensity and damage fail to definitively identify the earthquake source, it is almost certain that it was local and shallow, probably either a crustal fault on Ambon itself or the putative South Seram Thrust Fault off its southern coast.

More significantly, we have shown that the only way to explain the extreme run-up only on the northern shore of Ambon, and in particular the very narrow lateral extent along the coast over which it occurred, is by attributing the tsunami generation to a submarine landslide. Tsunami scenario simulations showed that plausible earthquake sources could not generate such a run-up profile, but a submarine landslide of about 1 km^3 volume, consistent with eyewitness accounts of dramatic changes in the coastal landscape (between Seith and Hila), could produce run-up commensurate with the historical observations.

Our analysis of the 1674 Ambon tsunami suggests that, as suggested by more recent events like the 1992 Flores and 2018 Palu and Sunda Strait tsunamis [Pranantyo and Cummins, 2019; Sassa and Takagawa, 2019; Giachetti et al., 2012; Patton et al., 2018, respectively], submarine landslides are an important component of the tsunami threat in Indonesia and should be considered in future tsunami hazard as-

sessments. We believe further work on this and other historical events, especially when combined with paleotsunami and bathymetric surveys, can provide important constraints on the unique nature of the tsunami threat in regions of particularly complex and active tectonics like eastern Indonesia.

Chapter 4

The Banda Detachment: A Major Source of Earthquake and Tsunami Hazard in the Banda Sea

This chapter is a part of an accepted journal: *Cummins, P.R., Pranantyo, I.R., Griffin, J., Pownall, J., Meilano, I. and Zhao, S. (2000) Nature Geoscience*

4.1 Introduction

The Banda Arc, eastern Indonesia, is often described as the most complex tectonic feature in the world. It was previously assumed the only potential earthquake and tsunami sources in the region were associated with the putative subduction megathrust in the Outer Banda Arc, until the world's largest normal fault, the Banda Detachment, was discovered in the Inner Banda Arc [Pownall et al., 2016]. This discovery brings us an opportunity to revisit historical earthquakes and tsunamis that have occurred in the Banda Sea.

A devastating earthquake rocked the Banda Islands on 26 November 1852 that lasting for 5 minutes [Wichmann, 1918; Soloviev and Go, 1974]. The earthquake ground motion was so severe that people were unable to stand, fissures appeared in the ground, and many buildings collapsed on the islands. The ground motion was also felt on Ambon and its surrounding islands as far as Ternate at the north. The earthquake was then followed by a tsunami that arrived fifteen minutes later after the ground shaking stopped with no indication of a draw-down phase of the seawater at the Banda Islands. A similar phenomena was also reported at Saparua and Ambon.

The 1852 earthquake and tsunami event has been ascribed to a megathrust earthquake on the Banda Arc [Løvholt et al., 2012; Fisher and Harris, 2016]. However, the Banda Arc has a reverse mechanism that would not generate a tsunami without the draw-down phase at the observation sites. Moreover, the Banda Arc is unlikely able to generate a megathrust earthquake because of its tectonic setting [Spakman and Hall, 2010; Pownall et al., 2013; Hall and Spakman, 2015]. The discovery of

the Banda Detachment, the largest normal fault system exposed anywhere in the world's oceans, and evidence of slumps in the Weber Deep [Pownall et al., 2016] suggests there are major earthquake and tsunami sources that have never previously been considered. Therefore, we can say that the source of the 1852 event remains open to question.

In this study, we suggest a new hypothesis of the earthquake and tsunami source of the 1852 Banda Sea event. First, tectonic setting of the Banda Sea is given. Then it is followed by description and analysis of the ground motion and tsunami accounts of the 1852 event. Then we discuss the findings to the tsunami and earthquake hazard implications to the Banda Sea.

This chapter was arranged to be submitted to Nature Geoscience journal. I therefore discuss the methodology in Appendix B.

4.2 Tectonic setting

The Banda Arc is a product of complex convergence tectonic plates in the Eastern Indonesia region (Figure 4.1). It is shaped like a "sandwich", and bends like a "D-shape" with a radius of curvature of 200 km [Sandiford, 2010]. The inner arc forms a volcanic chain while the outer arc is a group of non-volcanic islands. The northern side of the arc is associated with a subducting zone while the southern side is a result of arc-continent collision.

There are two main hypotheses about the Banda Arc evolution, as due to : i) southward subduction on the northern and northward subduction on the southern sides of the arc, and ii) rollback of a single slab associated with the Proto-Banda Sea into the Banda Embayment [Spakman and Hall, 2010; Pownall et al., 2013; Hall and Spakman, 2015], requiring crustal extension. Pownall et al. [2013] showed that only the latter hypothesis can explain how the Weber Deep was formed, by substantial lithospheric extension driven by eastward subduction rollback. This extension in the upper plate was accommodated by a major, previously unidentified, low-angle normal fault system they named the "Banda detachment", whose scarp forms the eastern wall and floor of the Weber Deep.

There are two key observations for the existence of the Banda Detachment [Pownall et al., 2016]. Firstly, parallel striations across the Weber Deep are seen from high-resolution bathymetry (Figure 4.1), aligned along the direction of hypothesized slab rollback. Secondly, low-angle (12°) fault scarps observed in southeast Seram and on Fadol Island can be interpret as surface expressions of the Banda detachment. On Fadol, a normal-shear-sense fault is the only way to account for the exhumation of upper-mantle-lower-crustal rocks (plus overlying Quaternary reefs) immediately adjacent to the 7 km Weber Deep. In addition, the striations in the Weber Deep run parallel to strike-slip faults of the Kawa Shear Zone (KSZ) on Seram, a major lithospheric fault zone incorporating slivers of exhumed mantle [Pownall et al., 2013]. Pownall et al. [2016] propose that the Banda detachment converges with the KSZ, and interpret them as part of the same system, with KSZ once functioning as a right-lateral

continental transform east of 129.5°E that separated northwest-southeast extension on the Banda detachment from contraction on land in northern Seram. The Kawa Fault, as evidenced from $^{40}Ar/^{39}Ar$ dating of adjacent mylonites [Linthout et al., 1996; Pownall et al., 2017] has had a long, complex history of operating with both left- and right-lateral motions, the most recent phase of which facilitated the opening of the Weber Deep.

An important consequence of arc-continent collision around the Tanimbar Trough is that an oceanic trench is no longer preserved. The bathymetric depressions around the outer arc islands are troughs, *not trenches*, and represent the frontal thrust of the Seram and Timor fold-and-thrust belts - alone of continental convergence, *not of oceanic subduction* [Spakman and Hall, 2010; Pownall et al., 2013; Hall and Spakman, 2015]. In contrast to some previous proposals [Liu and Harris, 2014; Fisher and Harris, 2016], it is therefore not possible that either the Seram or Tanimbar troughs could produce a megathrust earthquake. As shown by Pownall et al. [2016], based on the locations of seismicity within the Banda Slab, the over-thrust ocean-continent boundary (the former trench location) is most likely located immediately below the Weber Deep, a 7.2 km deep fore-arc basin within the easternmost Banda Sea, and the deepest point of the Earth's oceans that is not located within an oceanic trench.

Considering the extremely high erosion rates occurring in the wet, tropical region, it is striking that these fault scarps are so sharply preserved in the topography. Furthermore, it is notable that so little sediment has accumulated in the Weber Deep, less than a 1 km thickness based on seismic reflection data [Hamilton, 1979; Bowin et al., 1980], especially as 100 km wide submarine landslides are currently present along the eastern rise [Pownall et al., 2016]. These two observations indicate the Weber Deep, and therefore the Banda Detachment must be young features. However, as noted by [Pownall et al., 2016], no focal mechanisms determinable from any seismic catalogue are consistent with being produced by an earthquake on this low-angle fault. Moreover, there is notoriously a complete absence of seismic evidence for rupture of any normal fault occurring at a low angle.

There are two ways to explain the lack of recent seismic evidence for fault slip on the Banda Detachment. Firstly, the detachment might slip aseismically or during frequent low-magnitude events. Alternatively, the detachment might slip during infrequent but large-magnitude earthquakes, the most recent of which must have occurred prior to the modern seismic record. The hypothesis we test here is that the second of these possibilities might be true.

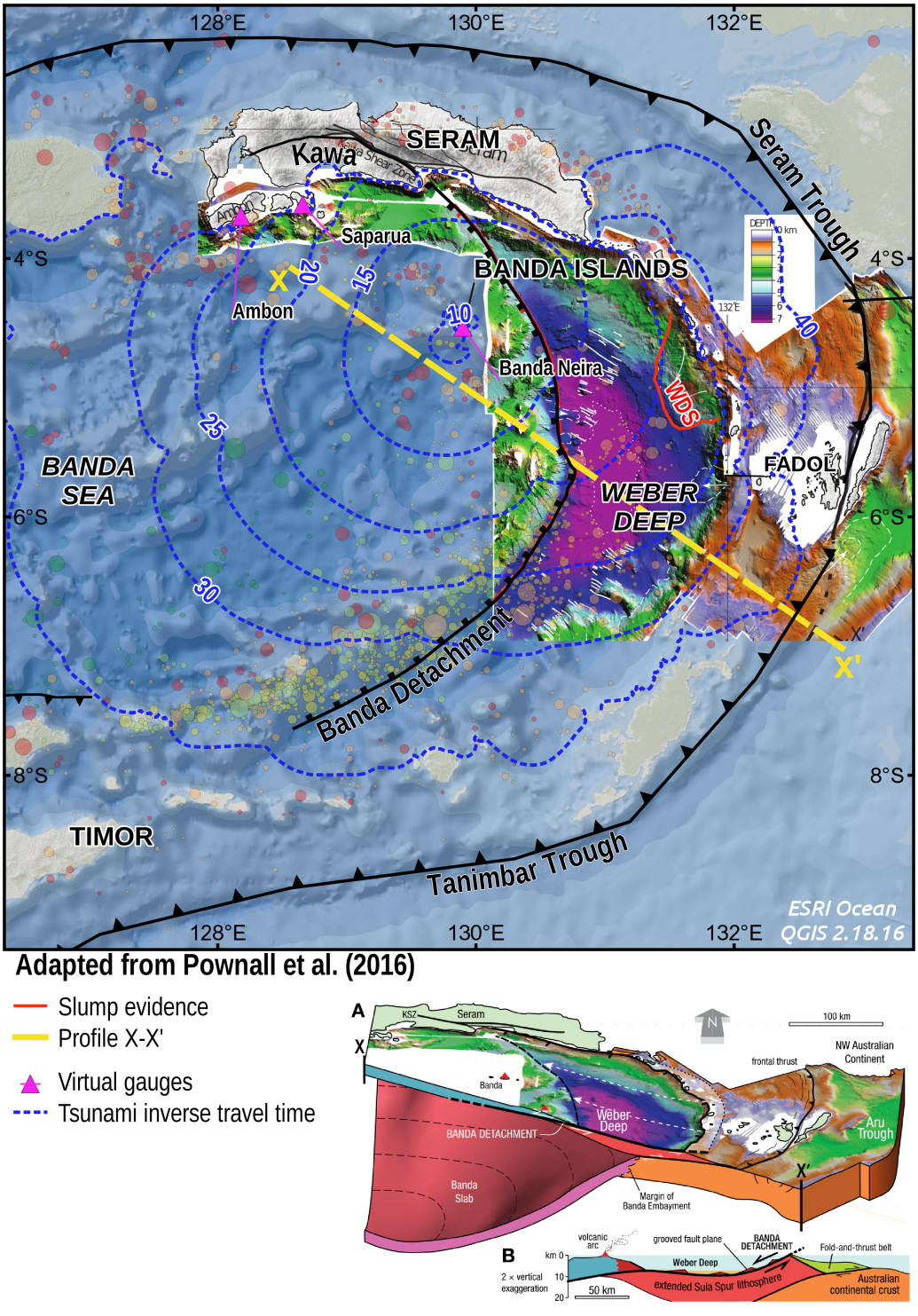

Figure 4.1: Tectonic setting of the Banda Sea. Contours are inverse travel-time from Banda Neira. The A and B inset figures show illustration of the Banda Slab and the Banda Detachment profile along the yellow dashed line, whereas WDS, discussed in Section 4.5, represents landslide scarp in the Weber Deep identified on high-resolution bathymetry imaged (adapted from Pownall et al. [2016]). The pink triangles are the virtual tide gauges where tsunami waveforms are calculated. Background seismicity (1900–2018; Mw >5.0 with epicentre depth of <30 km (red), 30–90 km (orange), 90–150 km (yellow), 150–300 km (light green), and >300 (green)).

4.3 Banda Sea earthquakes

While the Banda Sea is widely regarded to be an area of high seismicity [Spakman and Hall, 2010; McCaffrey, 1988], since the late 19th century no earthquake has caused widespread damage in the Banda Islands themselves. The majority of large, instrumentally recorded earthquakes are intermediate and greater depth intraslab events (Figure 4.1), that are weakly if at all felt in the Banda Islands. The largest intraslab event ever recorded, the 1938 Mw=8.5 Banda Sea earthquake, was only weakly felt in the Band Islands. Historical accounts from the 17th to 19th centuries, however document at least 5 earthquakes that caused widespread destruction in the Banda Islands (1683: "most houses became rubble heaps", 1710: "most houses were damaged irreparably", 1763: "three-quarters of all houses of Banda Neira were transformed to rubble heaps", etc.). These and other earthquakes felt strongly in the Banda Islands were often accompanied by ground cracking or fissuring, tsunamis, and prolonged sequences of felt aftershocks, none of which are normally associated with intraslab earthquakes. Thus, we conclude at least some of the 5 earthquakes that devastated the Banda Islands were shallow.

Two violent earthquakes that occurred in 1629 and 1852 were accompanied by large and destructive tsunamis. Because major tsunamigenic earthquakes are most often associated with subduction zone megathrust, and because prior to the discovery of the Banda Detachment the only plausible source of major shallow earthquakes in the Banda Sea seemed to be the putative Banda Megathrust. Liu and Harris [2014] and Fisher and Harris [2016] attribute the 1629 and 1852 events to the Seram and Tanimbar Troughs, respectively. As discussed above, these are actually frontal thrust unrelated to subduction and therefore unlikely to generate major thrust earthquakes. Here we consider what constraints historical accounts place on the source of the 1852 earthquakes, since it is the event that has the most detailed accounts available.

4.4 Ground motion intensity of the 1852 earthquake

Accounts of the 1852 Banda Sea earthquake and tsunami were documented in Wichmann [1918], which has been translated into English by Harris and Major [2017], and Soloviev and Go [1974]. These documents have also been interpreted by Fisher and Harris [2016]. A summary of the accounts and our interpretation are given below and shown on Table 4.1 and Figure 4.2. Note that our MMI (Modified Mercalli Intensity) assignments are generally more conservative than those of Fisher and Harris [2016]; for example, we cap MMI at VIII since it is likely this would result in collapse of masonry built in 1852. However, this means when we assign MMI VIII it is often as a lower; because of the already pervasive collapse of masonry structures, there is no way to distinguish between MMI VIII and higher values.

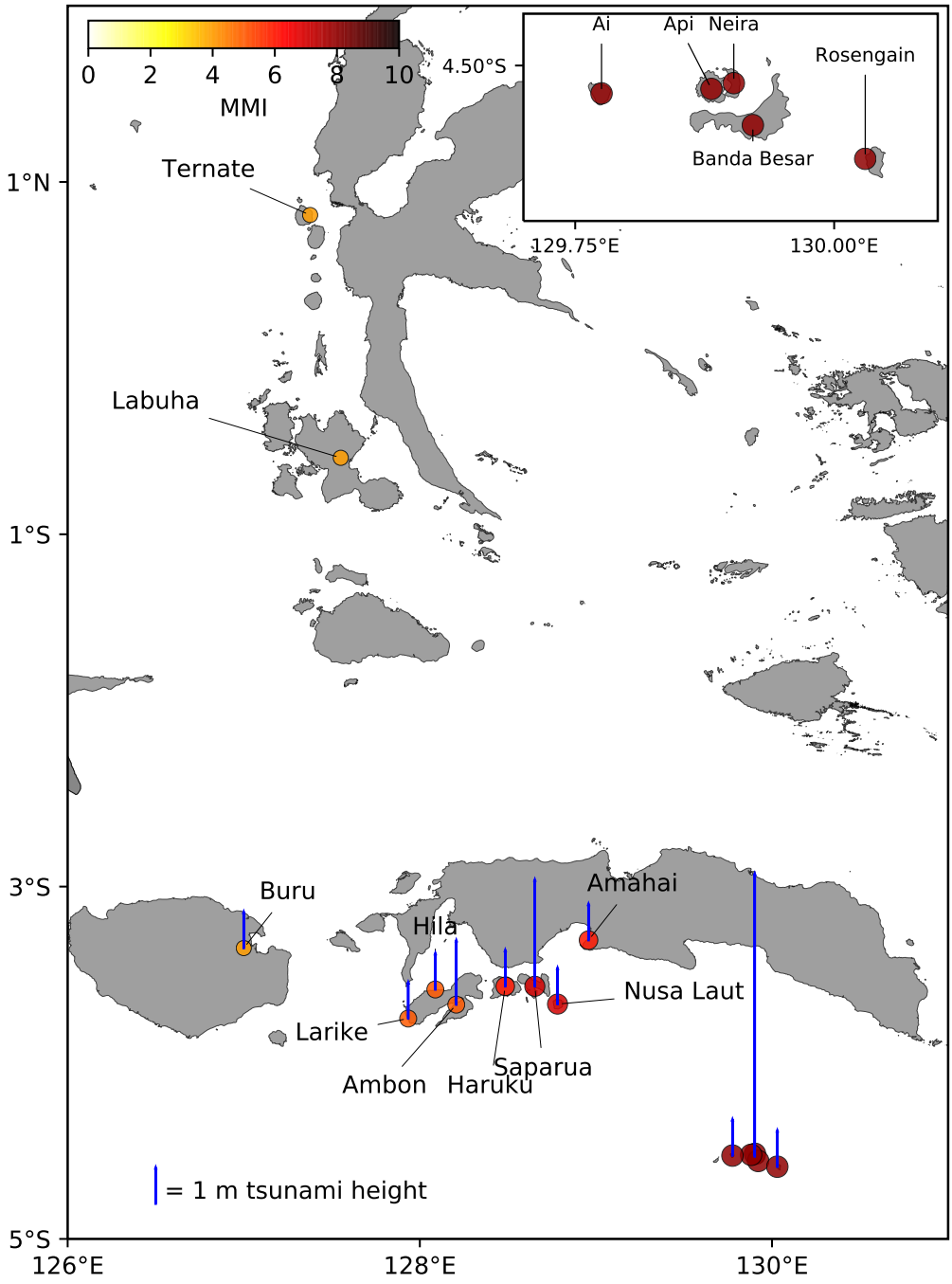

Figure 4.2: Historical accounts of the 1852 Banda Sea earthquake and tsunami. Coloured circles represent earthquake ground motion intensity. Black vertical bars indicate observed tsunami height. (This revised figure has been submitted to Nature Geoscience journal.)

Table 4.1: Ground motion and tsunami accounts of the 1852 Banda Sea event

Location (Region)	**Description**	**MMI**[1]	**TH**[2]
Banda Islands: Banda Neira and Banda Besar	7:50 am earthquake with a duration of 5 minutes. Majority of the buildings were destroyed and ground cracking appeared around the island. Then it was followed by at least 9 aftershocks during the day. A flood wave surged into the bay fifteen minutes later. The seawater rose as high as the foot wall of Fort Belgica and the foot mountains at Banda Besar (Lonthor) (approx. 8.2 m). The north coast of Banda Neira and the southern shore of Banda Besar noticed minor tsunamis only.	VIII (X)	8.2[a]
Banda Islands: Rosengain and Ai	Strong earthquake was felt at the islands of Rosengain and Ai. Seawater rose but only a few feet above the usual level.	VIII (VIII)	<1[a]
Ambon: Ambon Town, Hila, Larike	7:30 am, the town of Ambon felt violent ground motion lasting for 5 minutes. Shortly after, the water in the bay rose and oscillated until 2:00 pm. It reached up 1.8 m in the first five times. The ground motion was also felt at Hila and Larike without causing any damage.	V (Ambon: VIII; others: VI)	1.8[a] (Ambon Bay)
Saparua: Tijau, Hatuana, Porto, Kulor, Siri Sori, Boi	7:30 am, island of Saparua felt an earthquake. A flood wave surged into Saparua Bay, oscillated between 8:30 and 11:00 am, rose up to 3 m, and inundated about 127 inland at settlements around the bay and Tijau. Villages of Porto,Kulor, Siri Sori noticed a weak flood. A village of Boi, where was located in the bay, heard rumble sound from southeast direction.	VII (V)	3.0[a] (Saparua Bay)

Continuation of Table 4.1

Location (Region)	Description	MMI[1]	TH[2]
Haruku: Fort Zeelandia (Haruku), Hulaliu, Oma, Wasu	7:30 am, island of Haruku felt vibration causing cracks at Fort Zeelandia. Villages of Hulaliu, Oma, and Wasu noticed a flood wave together with a rumble sound.	VII (VI)	<2[a]
Nusa Laut: Amet, Akoon, Leinitu	Earthquake was felt and instantaneous flooding noted at Amet, Akoon, and Leinitu.	VII (V)	<2[a]
Buru	Earthquake was felt and followed by a flood wave without causing any damage.	V (V)	<2[a]
Seram: Amahai	8:00 am violent shaking was felt at Amahai.	VI (VI)	<2[a]
Halmahera: Ternate, Labuha	Ground motion was felt at Ternate and Labuha	IV (Labuha: V; Ternate: III)	–
Kai Islands and its surroundings	Two small risen islands were observed in 1853 had soft and yellow golden colour surface. Three smalls islands were discovered between Tayandu and Kaimer islands. Another new islands was discovered in 1854.	–	–
Java: Semarang, Pasuruan, Grati, Sumenep	6:45 am, a weak shock felt[3].		

[1] This study (Fisher and Harris [2016])
[2] Estimated tsunami height (m)
[3] Caused by other earthquake from Grati Fault [Marliyani et al., 2019]
a) Fisher and Harris [2016]

End of Table 4.1

Figure 4.2 shows that the earthquake generated its strongest felt intensity at the Banda Islands, which we have assigned MMI VIII. Then the earthquake intensity decreases northward to MMI IV at Ternate. Wichmann [1918] described ground motion felt in Java, almost 2,000 km distant, which Fisher and Harris [2016] used to ascribe an enormous felt area to the event. However, Marliyani et al. [2019] have since shown that these observations are more likely associated with a Mw 5.7 to 6.0 earthquake on the Grati Fault in eastern Java. Similarly, Wichmann [1918] noted the appearance of small islands in the archipelago observed in 1853, which Fisher and Harris [2016] argue indicated coseismic displacement in the rupture area of the 1852 earthquake. However, these islands are more likely to be associated with mud volcanoes, similar to one that appeared in the Makran subduction zone after a Mw 7.7 earthquake 400 km in Balochistan, Pakistan in 2013 [Kassi et al., 2017]. Like the Makran mud volcano islands, small islands have appeared in the Kai Archipelago repeatedly, often following regional earthquakes. We therefore discount Kai Islands mud volcano as indicative of the rupture area of the 1852 earthquake.

The felt area we consider for the 1852 Banda earthquake is therefore more restricted that that of Fisher and Harris [2016] (see Figure 4.3a). We used the approach of Griffin et al. [2018], a grid search for earthquake source parameters that uses Bayesian inference to characterise the uncertainties, to estimate the source parameters of the 1852 earthquake. The results are shown on Figure 4.3a, very clearly indicating the earthquakes that best explain the intensity data are just north of the Banda Islands, with Mw 7.5 to 8.0. The only major fault identified so near the Banda Islands is the Banda Detachment, and in Figure 4.4 we have considered a Mw 7.5 earthquake in the area of the maximum a *posterior* probability and aligned along the Banda Detachment. We used the subduction Interface Prediction Equation (IPE) of Dowrick and Rhoades [2005], simply because it is based on MMI observed in an island arc setting and accommodates large earthquakes on shallowly-dipping faults (and to our knowledge there is no corresponding IPE for normal-faulting earthquakes).

Figure 4.4b shows why the observed felt intensities constrain the earthquake to on or near the Banda Detachment. Even a very large earthquake on the Tanimbar Trough or elsewhere on the Banda "Megathrust" is too far away to produce intensities as strong as those observed: the earthquake must have been not only large, but very close to the Banda Islands. In order to produce the rapid fall-off intensities northward, towards Ambon, Seram, and Ternate, the rupture area must have been relatively compact; the much larger rupture area of Fisher and Harris [2016] generates intensities that do not decrease sufficiently with distance northward.

While only the 1852 earthquake as enough observations to undertake detailed analysis, we believe our conclusion that it ruptured to the Banda Detachment, or some other major but as yet undiscovered fault adjacent to the Banda Islands, is inescapable in light of reports of the other destructive Banda Islands earthquakes. Of the other 4 events causing widespread damage in the Banda Islands, as well as others described as "violent", none have generated reports of strong ground motion felt anywhere else. Many have resulted in ground cracking or fissuring, and prolonged sequences of aftershocks – lasting months in the case if the 1853 earthquake – that

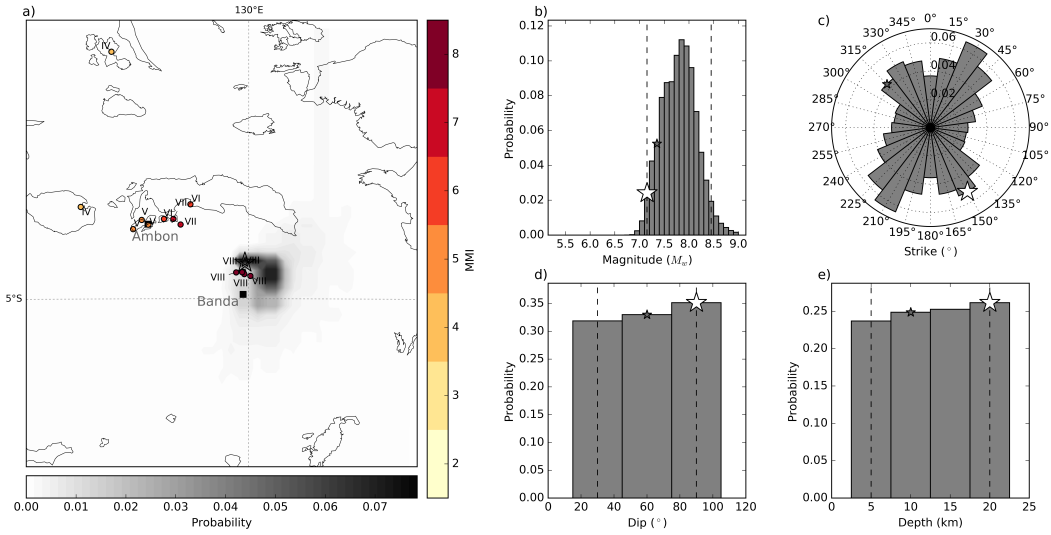

Figure 4.3: Posterior distributions of source parameters for the 1852 Banda Sea earthquake (a) location, (b) magnitude, (c) strike, (d) dip, and (e) depth. Large stars indicate the most probable parameters from the posterior distribution; small stars indicate the least-squares solution. Dashed lines in (a) indicate the spatial extent of the source location considered in the grid search. Vertical dashed lines in (b, d, e) indicate the bounds of 95% of the posterior distribution.

were again felt only in the Banda Islands. All of these observations indicate a source of shallow, large earthquakes very close to the Banda Islands. We believe the Banda Detachment is the best candidate fault to explain essentially all of the earthquakes that have caused extensive damage in the Banda Islands, other than those which appear to have been associated with eruptions of Gunung Api.

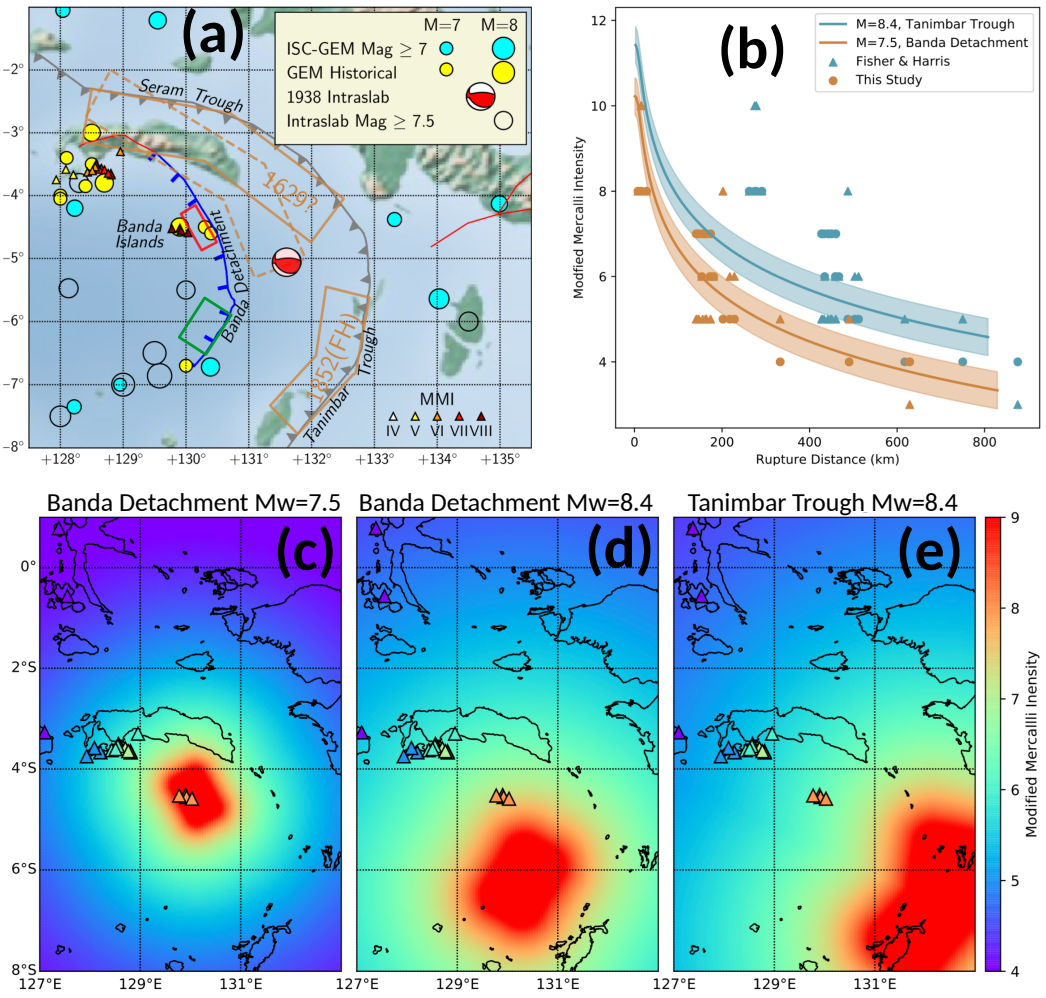

Figure 4.4: Banda Sea earthquakes and seismic intensity modelling. (a) Earthquake activity in the Banda Sea, including hypothesised Banda "megathrust" rupture areas for the 1629 (dashed: Liu and Harris [2014]; solid: modified to follow the actual deformation front), and 1852 [Fisher and Harris, 2016] earthquakes. Red box is the Banda Detachment rupture area for the 1852 earthquake proposed here, see (c), and green box for (d). (b) modelling of observed intensities vs rupture area using the Dowrick and Rhoades [2005] Intensity Prediction Equations (IPE) for the Mw 7.5 Banda Detachment and Mw 8.4 Tanimbar Trough [Fisher and Harris, 2016] models for the 1852 Banda Sea earthquake (c), (d), and (e): Seismic intensity fields calculated for the Mw 7.5 and Mw 8.4 Banda Detachment and the Mw 8.4 Tanimbar Trough models, respectively, for the 1852 Banda Sea earthquake

4.5 Banda Sea tsunamis

4.5.1 Qualitative analysis

The Banda Islands have experienced at least eight tsunamis in the past (see Table 4.2) [Wichmann, 1918, 1922; Soloviev and Go, 1974]. The largest of these occurred in 1629 (16 m at Banda Neira), while the second largest was generated by the 1852 earthquake. For these largest events, and particularly for the 1852 event, the descriptions of sea level changes are reasonably detailed, including information about height, arrival time, and period. They also describe the first motion – i.e. "tsunami polarity" of sea level change, which for the 1852 event is described as: "a flood wave" (Banda Neira, Saparua, and Haruku), and "a rising of the water in the bay" (Ambon). We note that for at least one other event in 1763 which had the opposite polarity, it was so described: "the sea level fell 9 m (30 feet), and then quickly rose".

Again, because of the faults are most frequently responsible for generating such large tsunamis are subduction zone megathrusts, Liu and Harris [2014] and Fisher and Harris [2016] considered that the 1629 and 1852 tsunamis were generated by giant (Mw 8.4) earthquakes in the Seram and Tanimbar Troughs, respectively. Above we have indicated that these interpretations are unlikely based on geological and seismological grounds; here we show that they are also inconsistent with the tsunami observations.

Any tsunamis in the Banda Sea generated by subduction megathrust earthquakes on the Banda Outer Arc, whether the Seram Trough to the north or the Tanimbar Trough to the south, will have negative polarity (i.e. "draw-down"). This is a consequence of the arc-inwards dip of the fault, which generates a pattern of seafloor subsidence that is downwards in the direction of the Banda Sea and upwards along the rim of the outer arc. This can be seen from the tsunami waveforms calculated by Liu and Harris [2014] (their Figure 8) and Fisher and Harris [2016] (their Figure 11), which have pronounced draw-downs as first-arriving tsunami energy, and also in our Figure 4.5. While it might be possible to argue that the polarity observation for the 1629 tsunami in Banda Neira was ambiguous ("a wall of water"), the observations for the 1852 event were more numerous and always indicated positive polarity, showing that the source was not a megathrust event in the outer arc.

The accounts of the 1852 tsunami in Banda Neira includes a particularly clear description of its arrival time relative to the earthquake: after "vertical shocks ... of 5 minutes duration", "the ground had been calm for a quarter of an hour when a flood wave crashed in". This 20 minutes delay time between the occurrence of the earthquake and the arrival of the tsunami is an important constraint on the locus of the tsunami generation. In Figure 4.1 we show an inverse tsunami travel time map, which shows where a tsunami arriving at Banda Neira at various times would have originated (see Appendix B.2). The 20 minutes contour of this map highlights 2 potential locations where the tsunami could have originated: (1) the Banda Detachment, where it emerges on the western side of the Weber Deep about 100 km south-southeast of Banda Neira; and (2) a large submarine landslide scarp at the

base of the Weber Deep's eastern scarp.

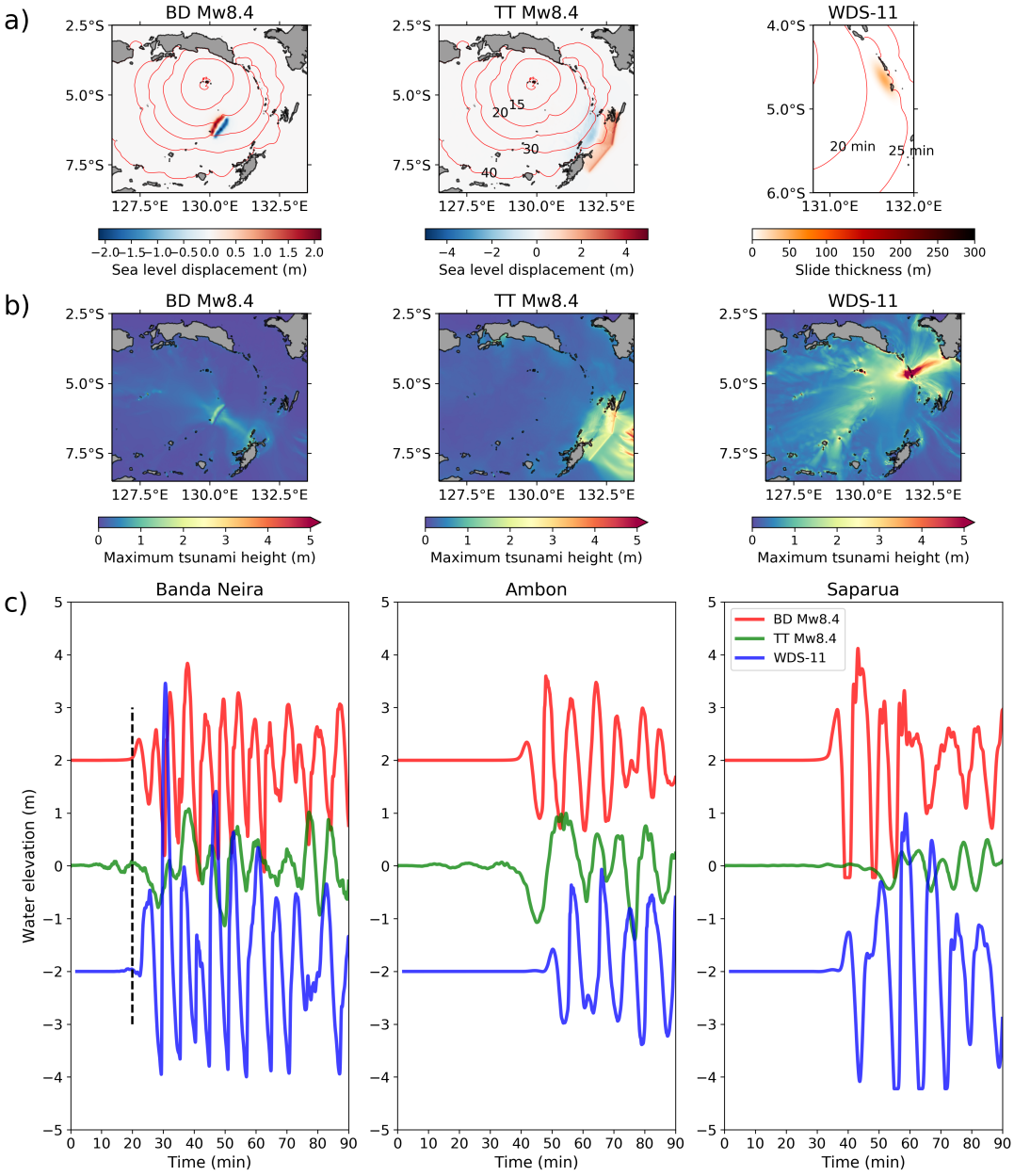

Figure 4.5: Selected tsunami models of the 1852 Banda Sea event; a) scenarios from the Banda Detachment Mw=8.4 (BD Mw8.4), the Tanimbar Trough Mw=8.4 of Fisher and Harris [2016] (TT Mw8.4), and a landslide from Weber Deep (WD-14) – note that the scale bars are different; b) simulated maximum tsunami height from scenarios in a; c) simulated tsunami waveform at three virtual gauges. The red line in (a) represent travel time contours of the tsunami inverse travel time contours.

4.5.2 Tsunamigenic earthquake modelling

To model a tsunami generated by an earthquake on the Banda Detachment south of Banda Neira, we assume an elliptical fault area and calculate the vertical motion of the seabed caused by a set of candidate ruptures having magnitude ranging from Mw 7.4 to 8.5, with a corresponding range of fault lengths from 40 to 100 km. We assigned each rupture an elongated elliptical area oriented along the strike of the Banda Detachment, and use the method of Meade [2007] to calculate vertical coseismic displacement of the seafloor due to normal fault slip on a triangular mesh following the irregular geometry of Pownall et al. [2016]. It is important to note that only a normal fault having the extremely shallow dip of Pownall et al. [2016] results in a significant positive polarity tsunami to match the observations. Lastly, the vertical deformation calculated is then assumed to be equal to the initial sea surface elevation required for the tsunami simulation.

None of the earthquake scenarios considered resulted in simulated sea level variations as large as those observed in Banda Neira and Saparua (8 m peak-to-peak and 3 m maximum, respectively). The best agreement was obtained with the largest Mw 8.4 earthquake, which resulted in the tsunami waveforms shown in Figure 4.5c (blue curves). Like the other Banda Detachment earthquake scenarios, this tsunami has positive initial polarity at all observation locations – Banda Neira, Ambon, and Saparua – and this relatively weak first arrival is followed by a prominent draw-down, as was observed. The maximum tsunami height at Saparua is 2 m, smaller than the 3 m observed, while the peak value at Banda Neira height is about 3.5 m, close to half the value of the observed peak-to-peak variation (note that the maximum draw-down is below the depth of the virtual tide gauge). Given the high level of uncertainty that should be ascribed to the historical account, as well as to the variability inherent in the modelling due to the unknown details of rupture as well as poorly resolved bathymetry, we regard this agreement with the observations as acceptable, i.e., the actual tsunami could plausibly have been caused by a large earthquake on the Banda Detachment south-southeast of Banda Neira.

4.5.3 Landslide generating tsunami

When considering a submarine landslide on the eastern scarp of the Weber Deep, we were guided by the extensive landslide scarp, about 100 km along-scarp length and 50 km down-scarp width (WDS in Figure 4.1), noted as 'slump' in Figure 1 of Pownall et al. [2016]. It is the largest of at least four such scarps evident on both west and east sides of the Weber Deep and its deepest edge coincides with the 20 minutes inverse travel time contour, so its triggering at the time of the earthquake should match the observed arrival time well. As discussed in the Methodology section (see B.5), we simulate landslide-generated tsunami using a two-layer approach of Imamura and Imteaz [1995] with the JAGURS software [Baba et al., 2019]. The landslide layer is assumed to be a Gaussian function on top the current elevation model, elongated along the top of the eastern scarp of the Weber Deep. We considered a wide variety of lengths (10–75 km), aspect ratios (2–10) and thickness (50–300

m). Tsunami waveforms for one of the models that best matched the observations, a slump initially of 40 km long by 15 km wide, and of 50 m thickness (i.e. volume 30 km^3), are shown in Figure 4.5c (green curves).

Like the earthquake-generated tsunami waveforms, the landslide-generated tsunami waveforms in Figure 4.5c (blue curves) have positive initial polarity followed by a rapid draw-down, which matches the historical accounts. At Saparua, the tsunami height builds over several cycle to 3 m, while at Banda Neira the second peak is highest at 5.5 m, giving a peak-to-peak sea level variation of 7.5 m that matches at the observations well (Soloviev and Go [1974] is reporting of the account from the brig "Hai", refers to the ship anchored in 11 m water depth before the tsunami, which fell on the ebb to 7 m depth and then rose later to 14.5 m depth; Wichmann [1918] also reports: "the difference between the highest and the lowest water level was 26 rh. feet (fuss) [8.2 m]"). The reported sea level variations at Ambon are more ambiguous, but not inconsistent with the simulated 1.5 m height. In general, the tsunami waveforms simulated from the landslide-generated match the observations better than those of the earthquake-generated tsunami.

We should note that what is among the most precise quantitative reports in the historical accounts is difficult to match. Soloviev and Go [1974]'s report for Banda Neira states: "A ship riding at anchor at a depth of 9 m (5 fathoms) sat on the bottom twice". Although several of the scenarios considered here produced draw-down off Banda Neira of 2 to 3 m, none came close to the 9 m reported.

Finally, we note that Figure 4.5c (blue curves) also shows the tsunami waveforms have calculated for the Mw 8.4 Tanimbar Trough model of Fisher and Harris [2016]. As indicated above, the polarity of the first-arriving tsunami is a prominent draw-down at all three virtual tide gauges, in contrast to those observed. The first positive polarity tsunami energy arrives at about 35 minutes, much later than the observed arrival of 20 minutes, and the height of the tsunami at Ambon is much lower than was observed (about 3 m peak-to-peak, as opposed to 8 m observed), and likewise at Saparua (<1 m maximum height, as opposed to 3 m observed). As with seismic intensity, the tsunami observations are difficult to reconcile with an earthquake on the Tanimbar Trough.

Table 4.2: Historical tsunamis on Ambon and its surrounding islands

Date	**Source**	**Description**	**Refs:**
1 August 1629	Earthquake (Seram Trough)	A strong earthquake devastated the Banda Islands. About 30 minutes later, a tsunami arrived at the islands and rose up to 16 m.	a, c, d
10 March 1710	Earthquake	A long earthquake sequences up to a month felt at Banda Neira that caused seawater repeatedly surged on to the land.	a, c

Continuation of Table 4.2

Date	Source	Description	Refs:
12 September 1763	Earthquake	75% of houses at Banda Islands were destroyed by a large earthquake lasting for four minutes which then followed by a tsunami.	a, c
26 November 1841	Earthquake	A relatively weak earthquake lasting for three minutes felt at Banda Neira which was followed by a tidal surge fifteen minutes later that rose up to 3 m.	a, c
26 November 1852	Earthquake	A strong and longer earthquake followed by a tidal surge that rose up to 8.2 m on Banda Neira that arrived twenty minutes later after the earthquake stopped.	a, c, e
25 September 1859	Earthquake	A rather strong earthquake was felt at Banda Islands that caused seawater oscillated and rose onto land.	b, c
10 October 1882	Earthquake	A similar phenomena as the previous one.	c
1 February 1938	Earthquake (Mw 8.4)	The largest earthquake recorded by instruments, occurred in the Banda Sea. It was a deep earthquake of 60 km that caused a relatively small intensity near the epicentre (Kai and Banda Islands) but felt as far as Darwin to the south and Merauke to the south east and only triggered minor tsunami less than 1 m.	c, f

Refs: a) Wichmann [1918]; b) Wichmann [1922]; c) Soloviev and Go [1974]
d) Liu and Harris [2014]; e) Fisher and Harris [2016];
f) Okal and Reymond [2003]

4.6 Results and discussion

The analysis of historical accounts of ground motion and tsunami observations described above establishes two alternative scenarios for the 1852 Banda Sea earthquake and tsunami. On the one hand, the seismic intensity in the Banda Islands was too strong and falls of too rapidly in Ambon and other islands to the northwest for the earthquake to have been a giant earthquake as distant as the Tanimbar Trough. The observations are best fit by a more compact source much closer to the Banda Islands, such as the Mw 7.5 earthquake on the Banda Detachment indicated by the Bayesian

inversion for earthquake parameters described in Appendix B.1.

While less optimal, a Bayesian analysis that excludes the area within the 20 minutes inverse travel time contour shows that a Mw 8.4 earthquake on the Banda Detachment 200 km south of the Banda Islands can also provide a reasonable fit to the seismic intensity observations, while also satisfying the requirement that any tsunami it generates arrive at the Banda Islands 20 minutes after it occurs. The analysis of tsunami waveforms above also shows that a tsunami generated by such an earthquake has some of the features described in the historical accounts, such as a positive initial polarity followed by rapid draw-down. However, the modelled variations in sea level are not as strong as those observed.

The second hypothesis for tsunami generation is via an earthquake-triggered, submarine landslide on the eastern side of the Weber Deep, where there is a major submarine landslide scarp evident in the bathymetry data. Modelling of the tsunami waveforms generated by such a landslide can explain both the timing and character of the observed tsunami and is more commensurate with strength of the observed sea level variations than is the earthquake-generated tsunami scenario. Thus, the scenario that best explains both the seismic intensity and the tsunami observations is a large, $\approx$ Mw 7.5 earthquake on the Banda Detachment immediately adjacent to the Banda Islands, which triggered a submarine landslide on the opposite side of the Weber Deep.

Can the mechanism for earthquake and tsunami generation of the 1852 event apply also to other historical earthquakes in the Banda Sea? As discussed above, in the 17th to 19th centuries, at least four other earthquakes have caused widespread destruction in the Banda Islands. These earthquakes did not generated felt reports from elsewhere, were often accompanied by ground cracking or fissuring and prolonged sequences of felt aftershocks, and in some cases caused tsunamis. All of these factors argue for a shallow source of major earthquakes near the Banda Islands, and the Banda Detachment is the only known active fault large enough to support such earthquakes. For this reason, we suggest that the Banda Detachment is likely to be the source of not only the 1852 earthquakes but also the four other earthquakes known to have devastated the Banda Islands.

It is more speculative to suggest that other major tsunamus that have affected the Banda Islands, in 1629, 1763, and 1841, were caused by earthquake-triggered submarine landslides. To understand the propensity for such landslides to occur, it is important to appreciate the unique character of the Weber Deep, a 7.2 km deep forearc basin which is the deepest point of the Earth's oceans not within a trench. The Weber Deep began to open at 2 Ma (million years ago) [Hall, 2011, 2012], as forearc extension driven by the final stages of eastward rollback of the Banda slab [Pownall et al., 2016]. The floor of the Weber Deep is therefore thought to consist of hyper-extended lower crust metamorphic or even exhumed upper mantle ultramafic rocks, with only a thin cover of basin-floor sediments.

In Figure 4.6, we display several cross sections across the Weber Deep, in which maximum slopes are calculated on either side of the basin. Maximal slopes range from 3 to 14°, with half being greater than 6°. ten Brink et al. [2009] undertook a

systematic study of the propensity for earthquakes to trigger submarine landslides along the eastern continental slope of the US, finding that earthquakes of Mw 7.5 can trigger submarine landslides at greater than 150 km distance – about the distance from our hypothesised Banda Detachment earthquake to the slump scarp on the eastern slopes. While this results depends on properties of the sediment and depth to the landslide failure plane, it suggests that the possibility of earthquakes on the Banda Detachment triggering landslides on the steep sides of the Weber Deep is not unrealistic.

The propensity for accumulations of sediment along the edges of the Weber Deep to slump down its steep slopes is evidenced by several large slump scarps on both western and eastern side of the Weber Deep (Figure 4.1; indicated by the white dashed lanes on the high-resolution bathymetry image). The one identified as a potential source of the 1852 tsunami is the largest (WDS), but there are at least three others, two on the western and an additional one on the eastern side. The other tsunamis associated with the historical Banda Islands earthquakes could be associated with these slumps, or it could also be that the slump we have suggested as the source of the 1852 tsunami occurred in multiple stages. Soloviev and Go [1974] report for the tsunami of 1763 that: "during the first shocks, the sea level fell 9 m (30 feet) and then quickly rose (in less than 3 minutes)". This initial draw-down of sea level could be associated with a slump on the western sides of the Weber Deep, much closer to Banda Neira than was the case for the 1852 tsunami, which had positive polarity at Banda Neira due to its location on the eastern side of the Weber Deep.

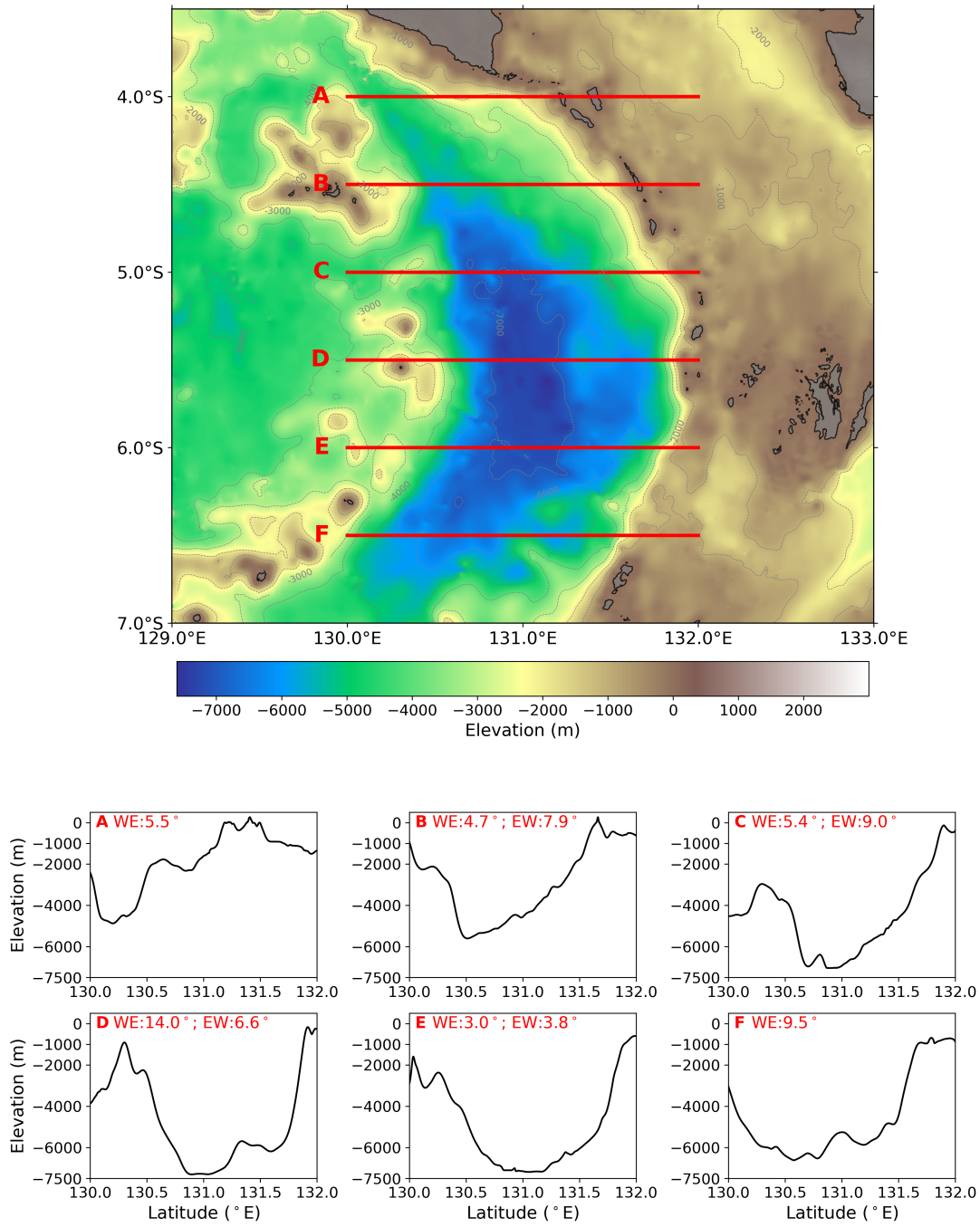

Figure 4.6: Elevation profiles in the Weber Deep. The red lanes indicate cross sections location with the elevation profile is shown at the bottom. Number on top of the profile shows maximum slope angle from west to east (WE) and east to west (EW) along the profile. The contours show the elevation at every 1,000 m deep.

4.7 Conclusion

While previous studies have ascribed the major source of earthquake and tsunami hazard to the putative megathrust in the Banda Outer Arc [Løvholt et al., 2012; Fisher and Harris, 2016], this study suggests that the Banda Detachment, a huge recently discovered low-angle normal fault (LANF) along the inner Banda Arc, is a much more likely source of the historical earthquakes and tsunamis affecting the Banda Islands. In particular, we have analysed historical accounts of a major earthquake and tsunami event in 1852 for which detailed historical accounts are available, to show that it was most likely caused by a Mw 7.5 earthquake along the Banda Detachment, that generated a tsunami by triggering a large submarine landslide along the eastern side of the Weber Deep (which is in fact the exposed scarp of the Banda Detachment).

Activity and seismicity on LANFs has been controversial, since there are few examples of LANF earthquakes in the seismic record, and the mechanics of LANF slip are difficult to explain [Axen and Karner, 2004; Wernicke, 1995; Collettini and Sibson, 2001], while occurrence of a Mw 7.5 event on a LANF would be the largest ever considered, we note that large LANF earthquakes are not without precedent. Earthquakes as large as Mw 6.8 have been documented in New Guinea's Woodlark Basin [Abers, 1991; Abers et al., 1997] and Mw 6.4 in the western Gulf of Corinth [Abers, 2001]. We also note that the Banda Detachment is by far the largest and potentially most active LANF in the world, and is the only known fault near the Banda Islands that is large enough to host earthquakes capable of causing extensive damage. On the other hand, the earthquake we associate with the Banda Detachment does not necessarily have to have occurred on the low-angle detachment itself. It is possible that it was confined or at least nucleated on a more steeply-dipping normal fault above the Banda Detachment that has yet to be identified. Axen [1999] discusses how such faults may serve as triggers to slip on an underlying LANF.

Finally we address the question of why, if the Banda Detachment is a major source of earthquake and tsunami hazard, is there no evidence of earthquakes rupturing the Banda Detachment in available earthquake catalogues? Our only answer is that the absence of recent seismicity does not preclude the occurrence of infrequent, large earthquakes. Indeed, the same question could have been raised regarding lack of seismicity on the Sumatra megathrust prior to the occurrence of the 2004 Sumatra-Andaman earthquake. In the case of Sumatra, a series of earthquakes in the mid 19th century was followed by a period of quiescence throughout the 20th century, until the Sumatra megathrust "re-awakened" in 2004 (discussed in Chapter 2). It could be that the same is true of the Banda Detachment, that the series of destructive earthquakes and tsunamis from the period 1629 to 1852 was followed by a long period of seismic quiescence. The same has been noted for Java, where despite the occurrence of many large, destructive earthquakes in 1681 to 1877, only one has occurred since [Griffin et al., 2018]. Regardless of which fault caused the Banda Sea earthquakes of 1629 to 1852, it would be a mistake to assume they will not happen again simply because there have been few if any recorded earthquake since.

Chapter 5

Multi-Data-Type Source Estimation for The 1992 Flores Earthquake and Tsunami

Published: *Pranantyo, I.R. & Cummins, P.R. (2019) Pure and Applied Geophysics.*

We revisit the source of the 1992 Flores earthquake and tsunami using finite-fault inversion. We simultaneously invert teleseismic body and surface waves together with coseismic uplift/subsidence datasets. Then we verify the inverted source against tsunami run-up heights along the northern coast of Flores Island and the only tide gauge recording of the tsunami. Our preferred source model provides a good fit to all the datasets, whereas previous models only explained a subset of the available data. We show that the fault geometry implies segmentation of the back-arc thrust system in the eastern Sunda Arc.

5.1 Introduction

A devastating earthquake with moment magnitude (Mw) of 7.8 followed by a tsunami severely impacted the northern coast of Flores Island, Nusa Tenggara Timur, Indonesia on 12 December 1992. It killed more than 2000 people and left thousands injured, with more than 25,000 buildings and much infrastructure destroyed [World Bank, 1993; Yeh et al., 1993; Tsuji et al., 1995b].

To understand why this event had such a major impact, we need to know those details of its source characteristics that determine the generation of tsunami and strong ground motion, viz. which fault ruptured, how large the slip was, and how it was distributed over the fault surface. Several studies have attempted to constrain these details using different datasets: Beckers and Lay [1995] used seismic waveforms, Hidayat et al. [1995] and Imamura and Kikuchi [1994] used a combination of seismic and tsunami data, and Griffin et al. [2015] used a combination of seismic and uplift data. However, it can be argued that none of these models fit all the data well.

In this chapter, the source of the Flores 1992 earthquake and tsunami is revisited

by conducting finite-fault source inversion using teleseismic waveforms and coastal uplift data. The estimated source is then adjusted systematically to fit tsunami run-up along the northern coast of Flores Island and a tide gauge waveform at Palopo, Sulawesi. First, the tectonic setting of the Flores region is discussed. Second, a brief explanation is given of the methodologies used, followed by the results of the inversion. Lastly, further investigations that could be done and the implications for the tsunami and seismic hazard associated with the Flores Back-Arc Thrust are discussed.

5.2 Tectonic framework

Eastern Indonesia encompasses a complex tectonic environment, involving the convergence of four major and at least four minor tectonic plates (Figure 5.1). Its southern margin is dominated by convergence of the Australian Plate with the Sunda Block and other minor plates comprising Nusa Tenggara (aka the Lesser Sunda Islands) and the Banda Island Arc. Flores Island lies in the Nusa Tenggara region, where the style of plate convergence transitions from ocean-continent subduction in the Java Trench to arc-continent collision near Timor.

The plate boundary along Indonesia's southern margin is often depicted as a contiguous subduction zone running offshore Sumatra and Java and continuing along the Timor Trough and its extension along the Banda Arc (the heavy grey curve in Figure 5.1). Although there is a well-developed Benioff zone along the southern Banda Arc [Sandiford, 2008], recent interpretations of tomography and the plate tectonic evolution of the region suggest that active subduction ceased along the Banda Arc 4 Myr ago [Spakman and Hall, 2010], while the Timor Trough has been recognized as a foreland basin of the Banda orogeny rather than a subduction trench [Audley-Charles, 2011]. Plate convergence east of the Java Trench, to the extent that it is not accommodated by the Timor Trough or Banda Arc, must be accommodated elsewhere.

An alternative for accommodating Australian-Sunda Plate convergence is the Flores Back-Arc Thrust, first identified in marine seismic and seismicity studies [Hamilton, 1979; Silver et al., 1983, 1986; McCaffrey and Nabalek, 1984]. These surveys showed clear evidence of back-arc thrusting along two distinct segments, viz. the 450-km-long Flores Thrust north of Sumbawa and western Flores, and the 350-km-long Wetar Thrust north of Timor (see Figure 5.1b). It was thought that, elsewhere, convergence may be accommodated by strike-slip faults that cut the arc at angles oblique to the convergence.

The Flores Back-Arc Thrust is depicted in the global plate model of Bird [2003] (see Figure 5.1a) as a continuous back-arc thrust stretching from western Flores to the Tanimbar Islands in the eastern Banda Arc. Koulali et al. [2016] (see also Nugroho et al. [2009]) used Global Positioning System (GPS) measurements of present-day crustal movement to suggest that a continuous zone of back-arc thrusting extends all the way from the Kendeng Thrust zone in eastern Java, through the Flores Thrust

zone, to the Wetar Thrust zone in the east. According to Koulali et al. [2016], convergence between the Australian Plate and Indonesia is progressively transferred from over 90% accommodation on the Java Trench west of Lombok, to over 90% accommodation on a back-arc thrust system along the southern margin of the Flores Sea east of Timor. Near Flores, the accommodation of convergence is roughly equally split between the Timor Trough and the Flores Back-Arc Thrust, with 33 and 26 mm/year convergence, respectively. This implies that a slip deficit of 10 m could accumulate on the back-arc thrust north of Flores every 400 years.

The detailed geometry of the Flores Back-Arc Thrust, including its segmentation and orientation of faulting, is important for understanding the earthquake and tsunami hazard of the Nusa Tenggara region. Does earthquake rupture occur only offshore, so that tsunami generation is enhanced but the seismic hazard onshore is reduced? Or does earthquake rupture extend onshore, so that both tsunami and ground shaking are major perils? Over 20 shallow (<40 km depth) earthquakes of magnitude 6.5 or larger have been recorded on the Flores Back-Arc, and many of these have caused damage through ground shaking. Although a few historical events causing major tsunamis have been attributed to the Flores Back-Arc Thrust [Griffin et al., 2018], the only instrumentally recorded event causing a major tsunami is the Mw 7.9, 1992 Flores earthquake [Tsuji et al., 1995b].

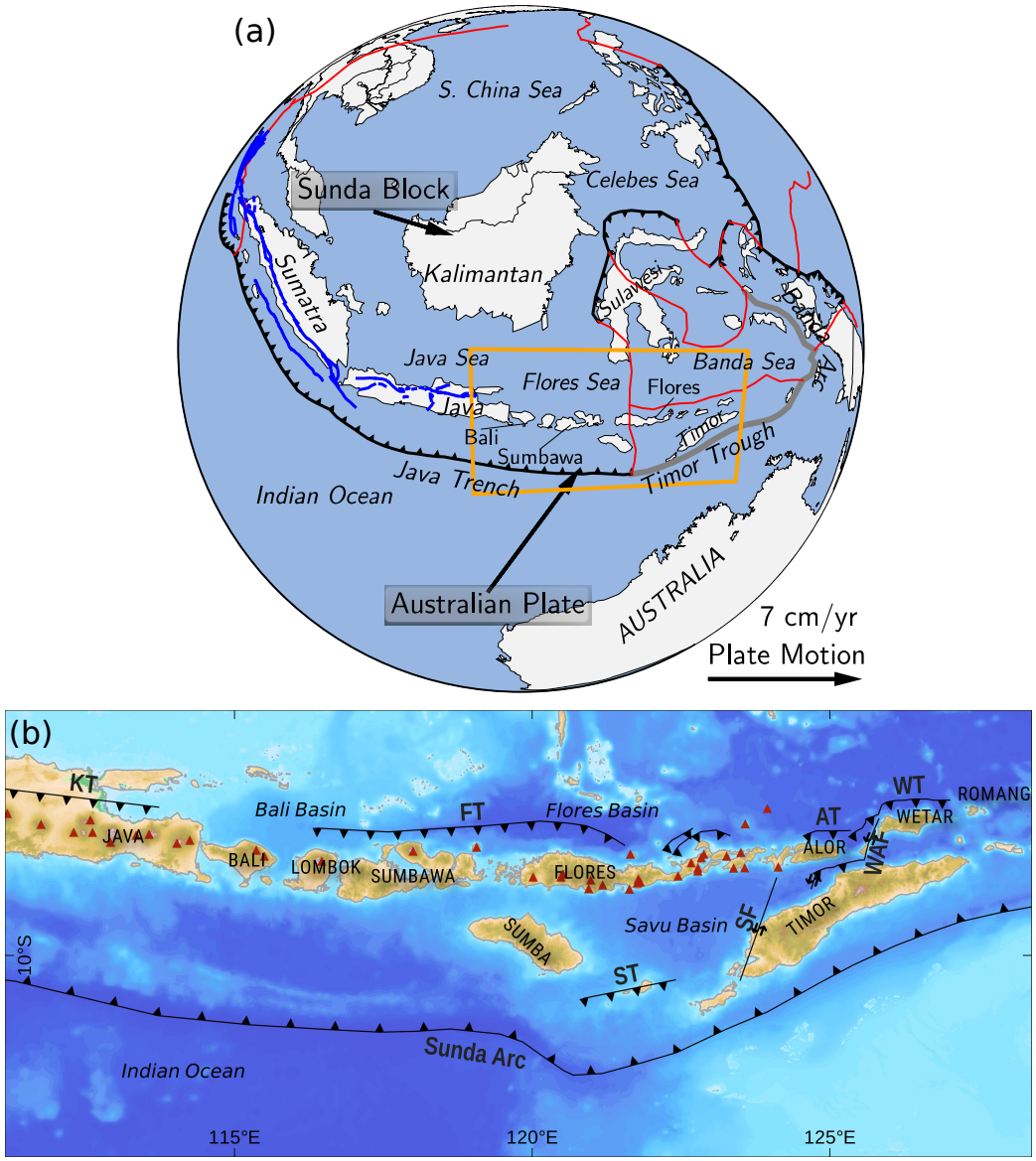

Figure 5.1: (a) Summary of the tectonics of Indonesia, with major plates and plate boundaries from Bird [2003], with the Nusa Tenggara region indicated; (b) Inset indicated in (a), illustrating details of the Flores back-arc thrust zone. The faults are compiled from Hamilton [1979]; Silver et al. [1983, 1986]; Koulali et al. [2016]; Breen et al. [1989]. KT = Kendeng Thrust, FT = Flores Thrust, AT = Alor Thrust, WT = Wetar Thrust, WAF = Wetar-Atauro Fault, SF = Semau Fault, ST = Savu Thrust.

5.3 Data for the 1992 Flores earthquake

Because it occurred prior to the post-2004 expansion of broadband seismographic networks worldwide, the number of stations that recorded seismic waveforms of the 1992 Flores earthquake is fewer than are typically available for more modern earthquakes. Similarly, there is only one tide gauge that recorded a waveform of the tsunami generated by the earthquake. On the other hand, because it was the target of one of the world's first detailed post-tsunami surveys by an international team of experts [Tsuji et al., 1995b], considerable data exist in the from of tsunami run-up and coastal uplift and subsidence.

5.3.1 Teleseismic body and surface waveforms

Seismic waveform data from 26 stations of the Global Seismographic Network (GSN) were retrieved from the Incorporated Research Institutions for Seismology's (IRIS) Data Management Center (Figure 5.2). Only stations at distance between 30° and 90° were used, to reduce the influence of either upper mantle or core-mantle boundary structure on the modeled waveforms. Waveforms were corrected for instrument response, and bandpass Butterworth filters with passbands of 0.002–0.0125 and 0.004–0.5 Hz were applied to surface and body wave data, respectively.

5.3.2 Coseismic uplift/subsidence

The post-tsunami survey of Tsuji et al. [1995b] documented extensive coastal uplift on the northern side of Flores Island due to the 1992 earthquake. The maximum uplift and subsidence was 1.1 and -1.6 m, respectively (see 5.3). The distance over which the maximum uplift shifted to the maximum subsidence was about 15 km, so the point where the "hinge line" (i.e., between uplift and subsidence where there is no change in elevation) crosses the coast is very well constrained. In total, there are eight locations where coastal uplift data collected by Tsuji et al. [1995b] are used in the source inversion. Tsuji et al. [1995b] note that the 1.6 m subsidence measurement at Kolisia may be biased by liquefaction, while the 0.75 m subsidence at Babi Island was reported by a local and may therefore be less accurate. However, these measurements both fit in well with the overall spatial pattern of the other measurements made by the team, so we include them in the inversion.

5.3.3 Tsunami run-up heights

Tsunami run-up heights of up to 5.2 m were measured near the epicentre along Maumere Bay, with the highest measurements on its western side and gradually decreasing run-up towards the east (Figure 5.4). Due to its circular shape, Babi Island appears to have experienced the remarkable phenomenon of edge waves that flowed around either side of the island and constructively interfered at its far side, resulting in particularly strong tsunami inundation that killed 700, about 25% of Babi Island's population [Liu et al., 1995]. Finally, extremely high tsunamis were observed around

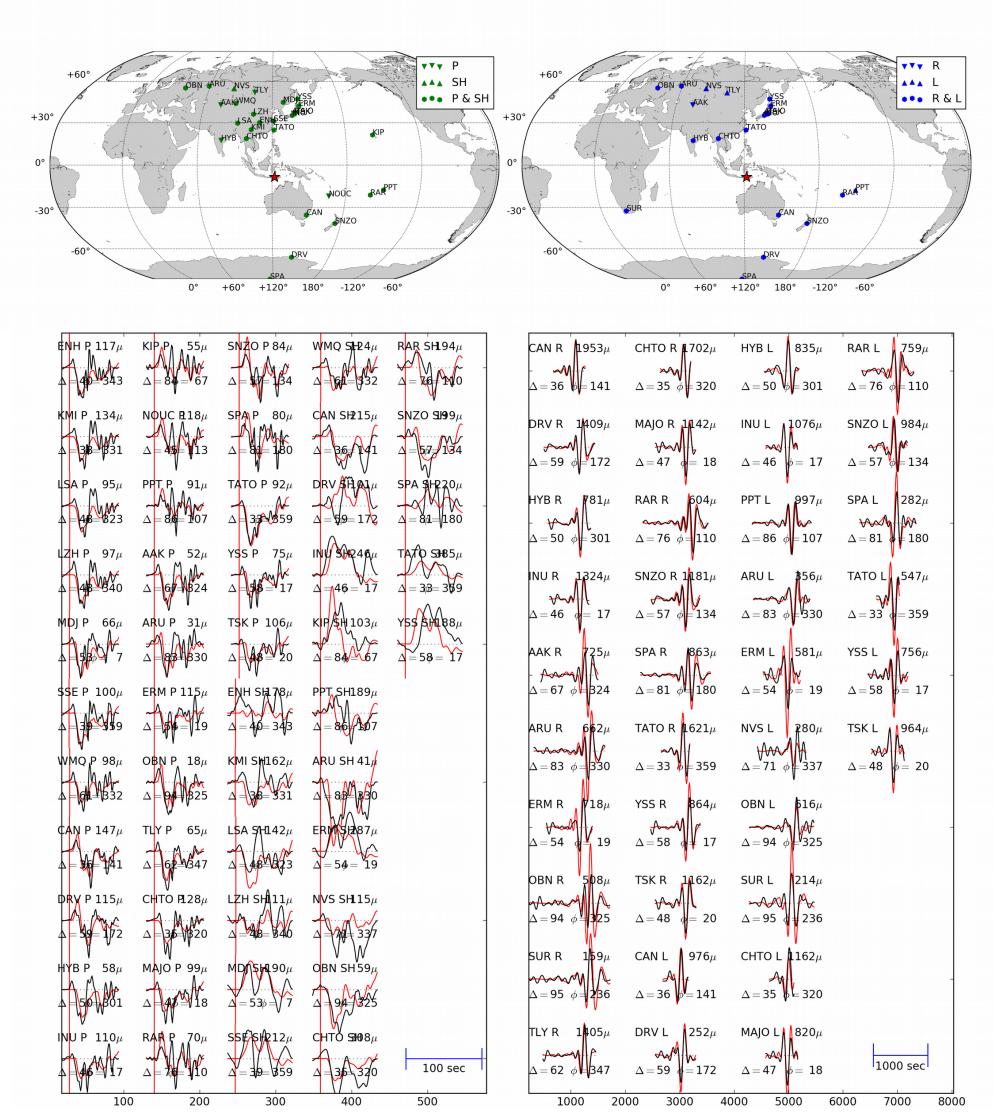

Figure 5.2: Teleseismic data coverage. Black and red curves show the original and inverted waveform fit for each station, respectively. The station and wave phase are indicated at the top left of each waveform, and the maximum peak value at the top right; Δ, and ϕ are the distance and azimuth from the epicenter, respectively

Hading Bay, with tsunami run-up of up to 26.2 m measured at Riangkroko. Yeh et al. [1993]; Hidayat et al. [1995] and [Tsuji et al., 1995b] suggested that these high run-ups were due to landslides, which were observed at several locations along Hading Bay. All tsunami run-up data used here to verify the inverted source model are taken from [Tsuji et al., 1995b].

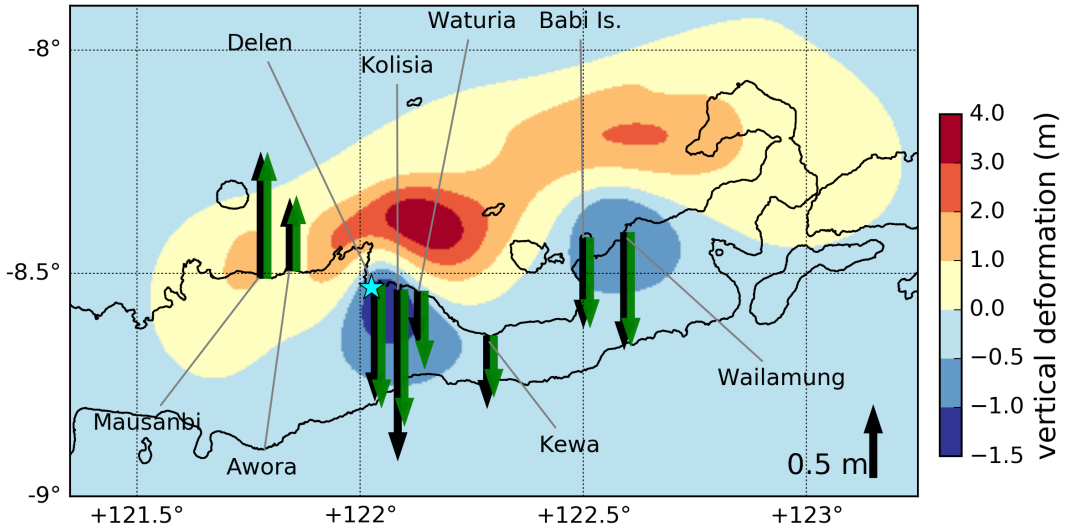

Figure 5.3: Coastal uplift/subsidence. Black arrows are coastal uplift observations from Tsuji et al. [1995b], and green arrows are uplift simulated from the preferred sip model.

5.3.4 Tsunami waveforms

Gonzalez et al. [1993] reported that only one tsunami waveform for this event is available, from the Palopo tide gauge at Bone Bay in Sulawesi, Indonesia, just over 600 km NNE from the earthquake epicentre. The tsunami arrived 104 min after the earthquake, with a predominant wave period of 69 min. The maximum and minimum peak amplitude recorded are 27 and −47 cm, respectively. Unfortunately, it is difficult to retrieve the original data, so the tsunami waveform is digitized from Hidayat et al. [1995]. However, it has poor resolution, and the accuracy of its timing is unknown. We found that all of the plausible fault models we tested resulted in a tsunami that arrives about 9 min later than the observed waveform. We therefore shifted all simulated tsunami waveform forward by 9 min in order to align the peaks in observed and modeled waveforms (Figure 5.5), and ascribe this to a timing error at the Palopo tide gauge.

5.3.5 Digital elevation model

A digital elevation model (DEM) is used as input for the numerical simulation of the tsunami (Figure 5.6). We used the high-resolution DEM developed by Griffin et al. [2015], available only for the north coast of Flores Island. This DEM was extended to the Palopo tide gauge using a combination of data from the General Bathy-

metric Chart of the Oceans (GEBCO), the 90-m Shuttle Radar Topography Mission (SRTM-90), and a 90-m commercial bathymetry dataset provided by TCarta Marine for depths shallower than 100 m [see Griffin et al., 2015].

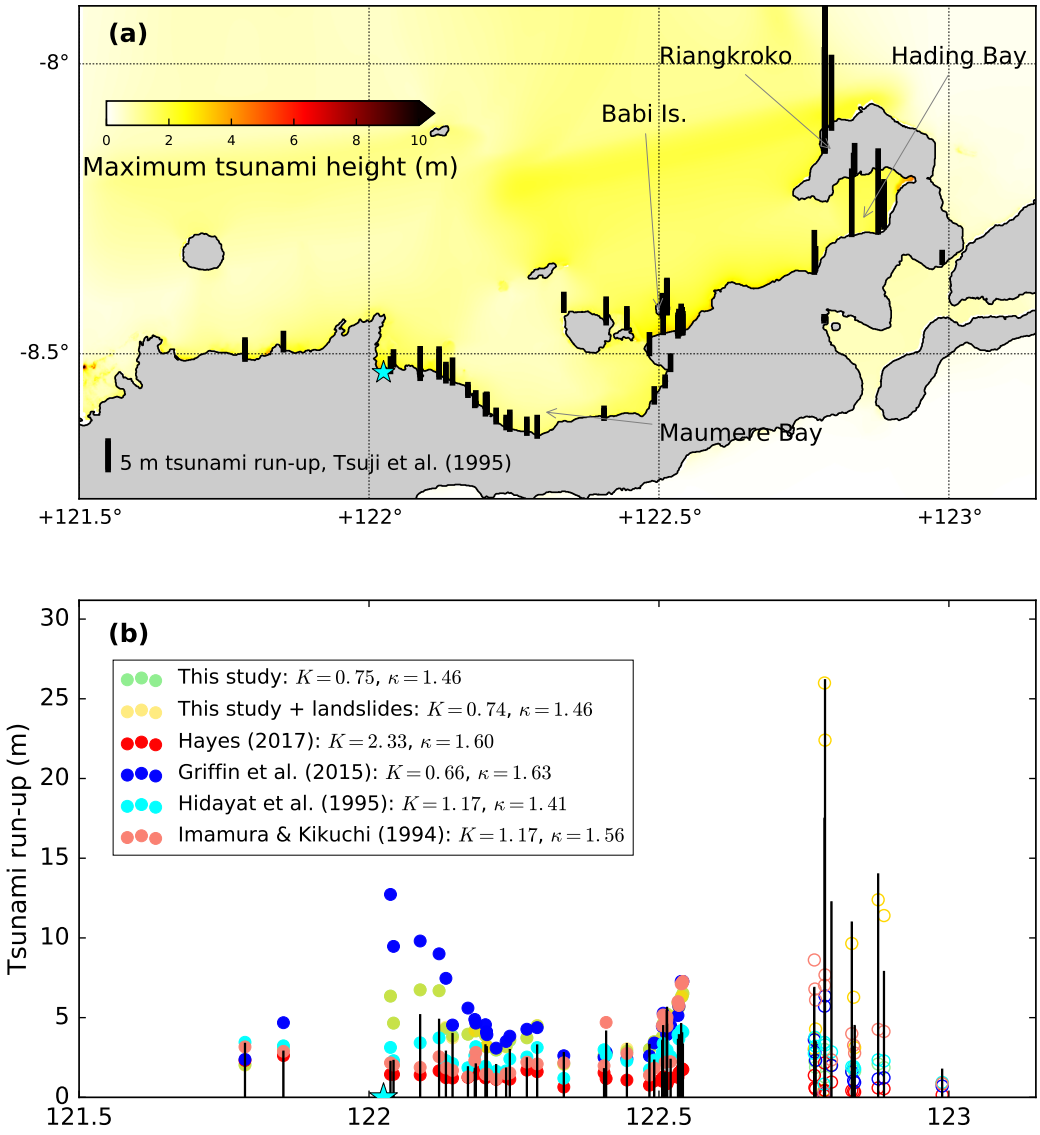

Figure 5.4: (a) Maximum simulated tsunami heights of this study. Bar charts show tsunami run-up heights data from Tsuji et al. [1995b]. (b) Comparison simulated tsunami run-up heights from previous studies. Solid coloured circles are simulated run-up heights used in the K and κ calculation, will be discussed in the next section. The hollow circles are excluded from the calculation.

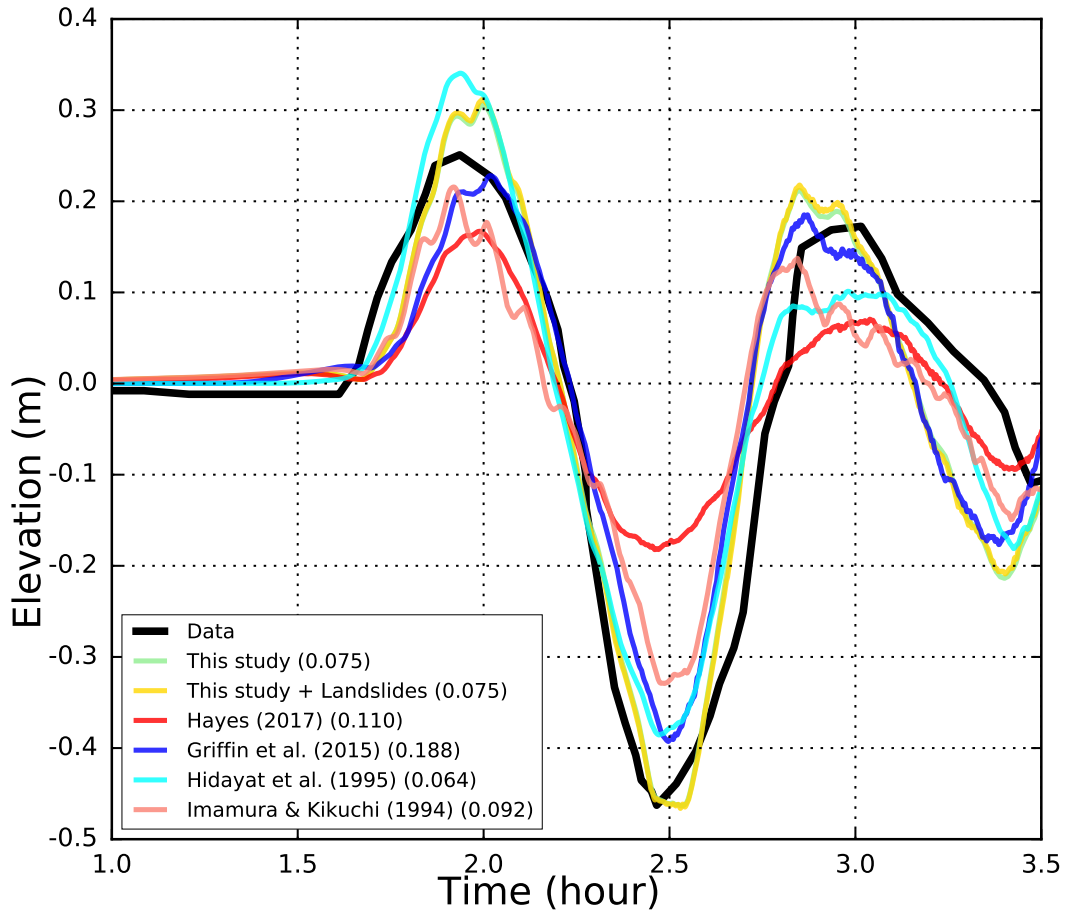

Figure 5.5: Tsunami waveforms at Palopo tide gauge of all sources. Tsunami waveform data is digitised from Hidayat et al. [1995]. Simulated waveform is shifted forward by 9 minutes in order to match the maximum peak arrival time (discussed in Sec. 5.6). Numbers on the legend are the RMS erros value for each models.

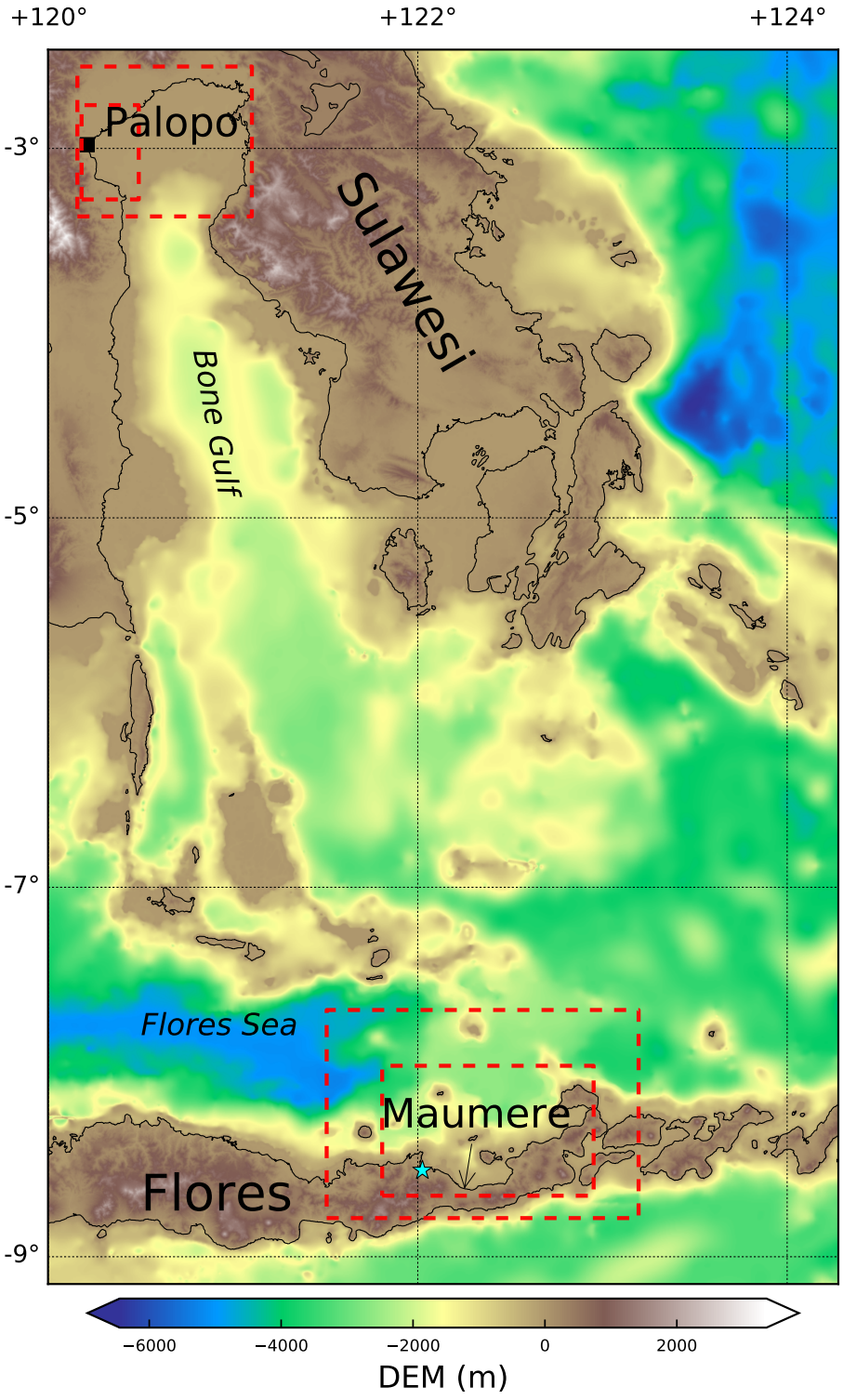

Figure 5.6: Elevation model for tsunami modelling. Red boxes are the nested grids. Resolution of the DEM from the finest are 55 m, 167 m, and 500 m, respectively.

5.4 Methodologies

5.4.1 Finite fault source inversion

TTrifunac [1974] and then Olson and Apsel [1982] introduced the finite-fault source inversion (FFI) technique, utilizing near-field seismic waveform datasets to invert for subsurface slip of an earthquake of a known discrete fault model. A stable inverted slip is obtained by applying a constrained linear least-squares method, and the basic methodology is similar in many subsequent studies. Satake [1987] proposed the use of tsunami waveform data for FFI, and Satake [1993] extended FFI by jointly inverting tsunami and geodetic data. After these early studies, FFI utilizing two or more datasets have been commonly done [Johnson et al., 1996; Konca et al., 2007; Baba et al., 2009; Tanioka et al., 1995; Gusman and Tanioka, 2014; Hill et al., 2012; Benavente and Cummins, 2013].

We utilise teleseismic waveform ($\mathbf{d_s}$) and coseismic uplift ($\mathbf{d_u}$) data to invert for a fault slip model ($\mathbf{m}$). Since two data types are used, proper weighting coefficients (γ_s, γ_u) are needed to balance the different datasets. To obtain a stable inverse solution we also need to regularise using a physically reasonable spatial smoothing operator. We apply a Laplacian smoothing matrix ($\mathbf{S}$) multiplied by a smoothing coefficient (β) to minimise the second spatial derivative of the slip. Our inversion problem is written as Eq. 5.1, where $\mathbf{I}$ is an identity matrix, N_s and N_u are the number of seismic waveform and uplift data points, respectively, and $\mathbf{G_s}$ and $\mathbf{G_u}$ are subfault "Green's function" matrices, the columns of which predict the data that would be observed if unit slip occurred on a single subfault. $\mathbf{G_s}$ includes rows for body and for surface waves, which are are numerically calculated using Kikuchi and Kanamori [1991, 1982, 1986] and Kanamori and Stewart [1976] (including phase velocity corrections for 3D structure from Ekström et al. [1997]), respectively. The elements of $\mathbf{G_u}$ are calculated using the Okada [1985] formulae.

$$\begin{pmatrix} \gamma_s \mathbf{I}_{N_s} & 0 & 0 \\ 0 & \gamma_u \mathbf{I}_{N_u} & 0 \\ 0 & 0 & \beta \mathbf{I}_{N_m} \end{pmatrix} \begin{pmatrix} \mathbf{G_s} & 0 & 0 \\ 0 & \mathbf{G}_u & 0 \\ 0 & 0 & \mathbf{S} \end{pmatrix} \mathbf{m} = \begin{pmatrix} \gamma_s \mathbf{d}_s \\ \gamma_u \mathbf{d}_u \\ 0 \end{pmatrix} \tag{5.1}$$

A systematic series of inversions are conducted to reproduce the best-fit source model, with trial-and-error adjustment of the weighting parameters γ_s, γ_u, and β. The earthquake epicentre is also adjusted by 15 km in all directions to account for potential error in epicentre location. This is followed by analysing the fault plane orientation (strike and dip angles as well as epicenter depth). Lastly, rupture propagation of the earthquake source is investigated. In addition, tsunami propagation and inundation modelling is considered to analyse the run-up heights along the northern coast of Flores Island and tsunami waveform at Palopo tide gauge.

5.4.2 Tsunami modelling

The JAGURS code is utilized for tsunami propagation and inundation simulation [Baba et al., 2015]. The code numerically solves the nonlinear shallow water wave

equations in spherical coordinates. An initial sea surface elevation as the input is assumed to be equal to the seafloor deformation due to fault rupture calculated using the Okada [1985] formula.

Tsunami simulation is conducted on a nested grid domain model. The coarsest and finest grid resolution approximately is 500 m and 55 m, respectively (Figure 5.6). Each simulation is run for 4 h with a 0.15 s time step to satisfy the Courant stability condition.

We validate simulated tsunami run-up heights using the Aida numbers of K and κ (Eq. 5.2) [Aida, 1978; Nakamura, 2009; Gusman et al., 2014]. K represents the mean ratio between data measurements (Obs_i) and simulation (Sim_i), whereas κ represents the standard deviation. In addition, we calculate the root-mean-square (RMS) misfit of observed and calculated tsunami waveforms at the Palopo tide gauge. We consider K of 1 ± 0.4 and a smaller κ as well as a small RMS value as indicating an acceptable source model.

$$\begin{aligned} \log K &= \frac{1}{N}\sum_{i=1}^{N} \log K_i \\ \kappa &= \sqrt{\frac{1}{N}\sum_{i=1}^{N}((\log K_i)^2 - (\log K)^2)} \\ K_i &= \frac{Obs_i}{Sim_i} \end{aligned} \tag{5.2}$$

5.5 Results and discussions

5.5.1 Original fault plane (ORI)

As a starting model, we use a fault plane with 150 km along-strike length and 60 km down-dip width, discretized into 30 and 12 rectangular subfaults in these respective directions with dimension of 5 km $\times$ 5 km. The strike and dip angles as well as hypocentre depth are set at 70°, 28°, and 16 km, respectively, taken from the seismic waveform analysis of Beckers and Lay [1995]. The epicentre is taken at $121.902°E$ and $8.475°S$ [IRIS, 2018]. These parameters are referred to below as the ORI fault plane model.

5.5.2 Weighting and smoothing

There are only eight coastal uplift data available. In contrast, the body and surface waves have about 3900 and 3200 data points (i.e., $N_S = 3900 + 3200$ and $N_u = 8$ in Eq. 5.1). Therefore, while γ_s for the seismic waveforms (both body and surface waves) is fixed at 1.0, γ_u for the coastal uplift needs to be adjusted to ensure that the misfits in the two datasets are reasonably balanced.

Figure C.1 shows how the misfit of the different datasets varies with γ_u and β. As might be expected, misfits for all datasets are low when β is small, $\beta = 0.01$,

and increase with increasing β. Misfits for seismic waveforms are low and that for uplift data is high when γ_u = 1, while the opposite is true for $\gamma_u = 500$. Some of the corresponding slip models are depicted in Figure C.2, which shows that slip models with $\beta = 0.01$ have very high spatial variability, while some of the models obtained using $\beta = 1.0$ have slip that is almost uniform over the rupture plane. Furthermore, the fit to the uplift data becomes unacceptably high for $\gamma_u <= 20$, while Figure C.1 shows that the misfit of the seismic waveform data begins to increase rapidly at around $\gamma_u = 40$.

Thus, visual inspection of the variation of both data misfit and model roughness with γ_u and β in Figs. C.1 and C.2 suggests that acceptable ranges for γ_u and β are $20 - 40$ and $0.3 - 1.0$, respectively. Since $\beta = 0.3$ is the minimal smoothing that gives rises to models with a reasonable level of spatial variability, and $\gamma = 20$ and 40 bound the region for which misfits to both uplift and seismic waveform data area acceptable, these values are taken for further analysis. ORI20 and ORI40 are named for models with the ORI fault orientation and $\gamma_u = 20$ and $\gamma_u = 40$, respectively.

5.5.3 Variations in hypocenter and fault plane orientation

From their body wave analysis, Beckers and Lay [1995] suggested best-fitting strike and dip angles of $70 \pm 30^\circ$ and $28 \pm 10^\circ$, respectively. Although the distribution of aftershocks is in rough agreement with this fault plane orientation (see Figure 5.7), the uncertainties on the estimated parameters are large. Furthermore, although the various published hypocentral solutions are in good agreement and have small (5–15 km) formal uncertainties, the lack of near-field data suggests a potential for bias in the hypocentre estimate. It therefore seems prudent to investigate the sensitivity of our source model to variations in the hypocentre as well as to azimuth and dip angles.

Figure C.3 shows the variance reductions that result from moving the epicentre 15 km from the original epicentre in different directions, with $\gamma_u = 20$ (S20, SE20, SW20, etc.) and $\gamma_u = 40$ (S40, SE40, SW40, etc.). Again, applying a larger γ_u produces a much better fit to the coastal uplift data with S40 being the model that best fits the uplift data (Figure C.4). Furthermore, by validating the inverted slip model against tsunami run-up data, we note that simulated tsunami run-up heights along the northern coast of Flores are smaller by moving the epicentre to the north (Figure C.5). Then by giving more weight on the coastal uplift data, it produces a better fit to the tsunami amplitude at the Palopo tide gauge (Figure C.6). Because $\gamma_u = 40$ improves the fit to both uplift and tsunami data, this value is chosen for further analysis. Moving the epicentre to the southeast also gives a better fit to the tsunami data. Therefore, SE40 is chosen as the preferred model.

The misfits to data are also sensitive to depth and fault plane orientation, as indicated in Figure C.7. A fault plane with 10 km hypocentral depth and strike greater than 80° produces smaller variance for all datasets. However, a shallower depth tends to overfit the uplift data (Figure C.9). A larger strike angle also results in simulated tsunami waveforms at the Palopo tide gauge with amplitude much smaller

than is observed (Figure C.11). This waveform amplitude is reduced as well by using dip angles other than 28°, but the fit is slightly improved by a deeper hypocentre depth. However, a 16 km depth is least preferred by the Rayleigh waves Figure C.7). The simulated tsunami run-up heights are self less sensitive to the fault plane orientation (Figure C.10). Therefore, SE40 is still regarded as the best fault plane model.

5.5.4 Rupture propagation

Compared to other datasets, the P-waveforms are more sensitive to the rupture propagation variables, viz. the maximum rupture velocity Vr, half-duration of subfault rise times t_h, and number of time windows NTW (see Figure C.12). With $NTW \leq 5$, the smallest variance is obtained with $Vr = 2.0^{km}/_s$. At larger NTW, $Vr = 2.5^{km}/s$ is preferred. However, the other datasets prefer a slower Vr. Furthermore, P-waveforms are fit better using $t_h = 2.0s$. On the other hand, other datasets produce small variance with a longer t_h. In general, a large NTW is preferred by all datasets.

Changing the rupture variables - NTW, t_h, and Vr - does not significantly change the fit of the model *SE40* to the coastal uplift data (Figure C.13). It also has only a small effect on the tsunami run-up heights (Figure C.14). However, it has a significant influence on the tsunami amplitude at the Palopo tide gauge (Figure C.15). By decreasing Vr and increasing NTW, the tsunami waveform amplitude is increased. From the P-wave variances, $NTW = 9$ and $Vr = 2.5^{km}/_s$ produces the smallest variance. However, the $NTW = 7$ with $Vr = 2.5^{km}/_s$ model results in only slightly higher variance than the best fit one. Even though this model slightly overestimates the maximum amplitude at the Palopo tide gauge, it generates a good fit to the minimum amplitude. In addition, to keep the rupture model as simple as possible while still fitting the data, $NTW = 7$ is selected as the preferred rupture propagation model.

Table 5.1: Final inversion parameters used

Parameters	Flores 1992
Strike	70°
Dip	28°
Hypocenter	122.025°E,8.532°S, and 16 km
Fault dimension	150 km × 60 km
Number of subfaults	32 × 12
NTW	7
t_h	2.0
Vrmax	$2.5^{km}/_s$
β	0.3
γ_s	1
γ_u	40

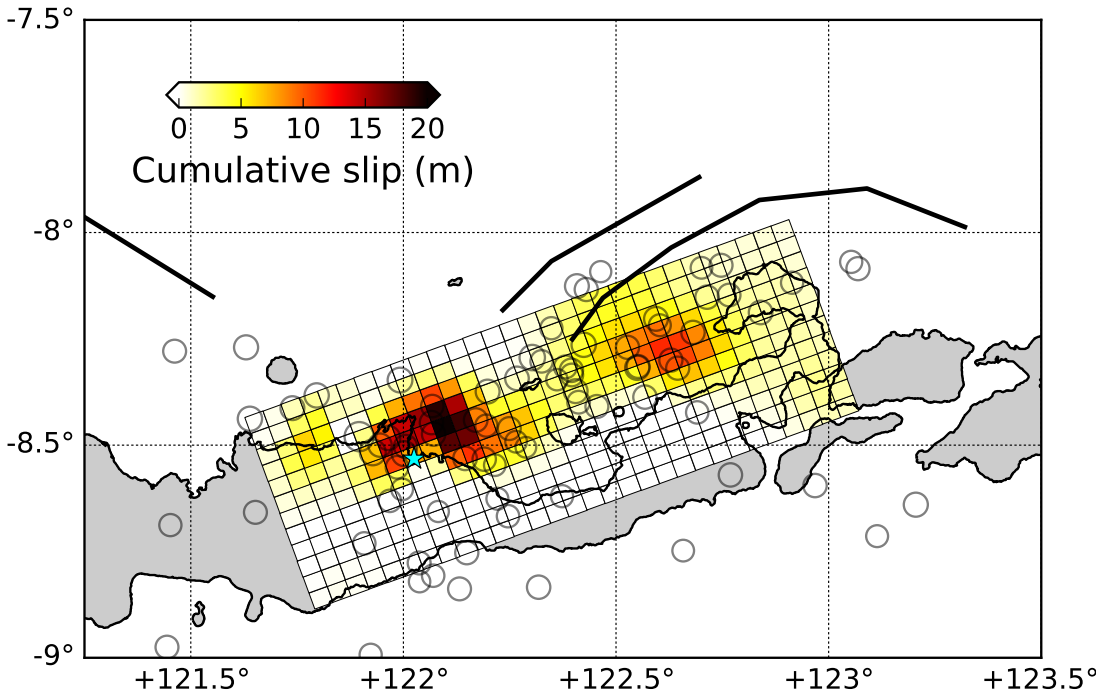

Figure 5.7: Final inverted slip model for Flores 1992 earthquake

5.6 Comparison with previous models

Our preferred rupture model SE40 for the 1992 Flores Earthquake has two patches of high slip resulting from the inversion. The highest slip patch is located near the hypocentre. The second patch is located about 70km northeast from the first one. This result is similar in some respects to those of Imamura and Kikuchi [1994], Beckers and Lay [1995], Hidayat et al. [1995], and Griffin et al. [2015]. Imamura and Kikuchi [1994] and Hidayat et al. [1995] used simpler fault models, although they estimated a higher slip on the northeast part from the epicentre. Most previous studies also have a similar fault plane orientation in the ENE direction to fit the aftershock distribution, with the exception of the Hayes [2017] model. The latter causes the Hayes [2017] model to have three high slip regions but the maximum slip is much smaller than other studies. We consider these models in more detail below.

The Hayes [2017] was constructed by inverting seismic waveform data, so it fits these observations very well. However, it grossly underpredicts both the tsunami run-up and tide gauge waveform data (Figs. 5.4 and 5.5, respectively), as well as the uplift data (Figure 5.3).

The models of Imamura and Kikuchi [1994] and Hidayat et al. [1995] were constructed to fit both seismic waveform and tsunami run-up data (and, in the case of Hidayat et al. [1995], the Palopo tide gauge waveform). Their fit to the seismic waveforms is similar to that of this study and Hayes [2017], and they also fit the tsunami run-up data better (17% under-prediction) than the model obtained here (30% over-prediction). However, their fits to the coastal uplift data are very poor (Figure 5.3). Although they provide better fits to the Palopo tide gauge waveform than Hayes [2017], they do not fit these data substantially better than the model obtained here.

Of the previous published models for the 1992 earthquake, the model of Griffin et al. [2015] is most similar to our preferred model. Griffin et al. [2015] optimised the fit of their model to the seismic waveform and coastal uplift data, and also compared its predictions to the tsunami run-up data. Although their model indeed provides excellent fit to the seismic waveform and coastal uplift data, its fit to the tsunami run-up data as well as the Palopo tide gauge waveform are considerably poorer than those of our preferred model (Figs. 5.4 and 5.5, respectively). We suspect that the Griffin et al. [2015] model overfits the coastal uplift data, which Tsuji et al. [1995b] note are subject to some uncertainty (Figure 5.8).

In summary, we believe that our preferred model (SE40) provides a better fit to all of the datasets, even though its fit to, e.g., the tsunami run-up data is marginally poorer than some of the previous models. Moreover, even though the Hidayat et al. [1995] model gives the smallest RMS for the tsunami waveform fit at the Palopo tide gauge (Figure 5.5), the RMS of our preferred model is only slightly greater and is much less than those of the other three models (Figure 5.5). We also attempt to match the macroseismic observations of Tsuji et al. [1995b] at Maumere and Ende, where Modified Mercalli Intensity (MMI) of 9-10 and 8-9, respectively, was estimated. Comparison with the MMI modelled using the fault modelling of Pagani et al. [2014] showed that these were matched only by the SE40 model, with the Griffin et al. [2015] model slightly underpredicting the MMI at Maumere but the other models giving values almost a unit of intensity too low at both locations (see Table 5.2).

Table 5.2: Modified Mercalli Intensity (MMI) calculated for the different published source models at Maumere and Ende, where Tsuji et al. [1995b] estimated MMIs of 9-10 and 8-9, respectively.

Source Model	Maumere	Ende
Hidayat et al. (1995)	7.8	8.3
Imamura & Kikuchi (1994)	8.3	7.1
Hayes (2017)	7.1	6.8
Griffin et al. (2015)	8.7	8.2
This study (*SE40*)	9.1	8.0

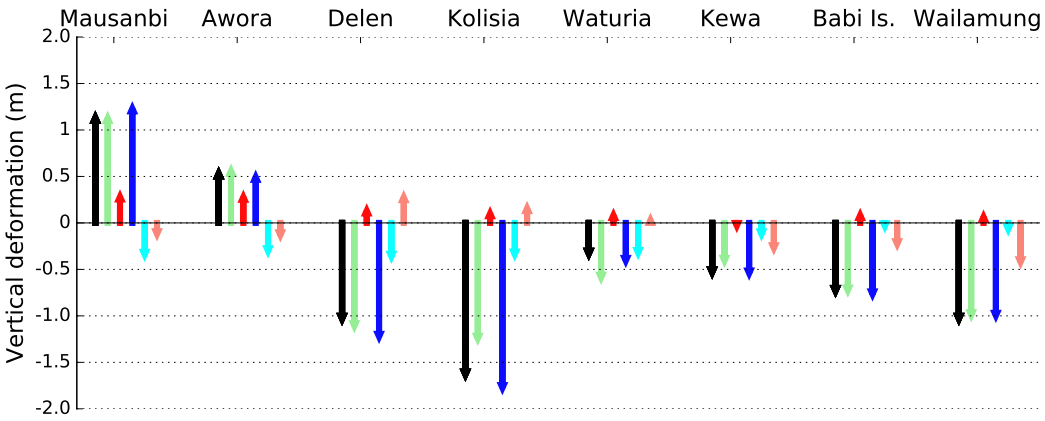

Figure 5.8: Vertical deformation comparison from all studies. Black=data, green=this study, red=Hayes [2017], blue=Griffin et al. [2015], cyan=Hidayat et al. [1995], salmon=Imamura and Kikuchi [1994]

5.7 Further investigation

5.7.1 Tsunami landslide model

Because our preferred source model is unable to explain the extreme run-up heights observed around Hading Bay, we agree with previous studies in ascribing these to coastal landslides [Yeh et al., 1993; Tsuji et al., 1995b; Hidayat et al., 1995; Imamura and Kikuchi, 1994]. Even though the locations of suspected coastal landslides are reported, it is difficult to build a tsunami landslide model without more detailed information.

We generate models for four landslides based on the limited information available in Yeh et al. [1993]. We can produce very high tsunami run-up around Hading Bay (Figure 5.9a). However, it is not an ideal model. Initial sea surface elevation is estimated using Watts et al. [2005] by assuming a Gaussian shape model with a slump mechanism (Figure 5.9b). The equations estimate the maximum acceleration and duration of the mass movement as well as the maximum initial sea surface elevation. But the equations do not consider the details of the dynamic process, which is crucial in a tsunami landslide model. However, these four landslides have very little effect on the Palopo tide gauge waveform, and we believe this is unlikely to change with more careful consideration of landslide physics. Therefore, modelling of the Palopo tide gauge waveform using a fault source alone, as considered above, seems justified.

5.7.2 Segmentation of the Flores Back-arc Thrust

Back-arc thrusting north of the eastern Sunda Arc is portrayed in the literature as southward-dipping thrusting that emerges at the surface in the Flores Sea. Beginning

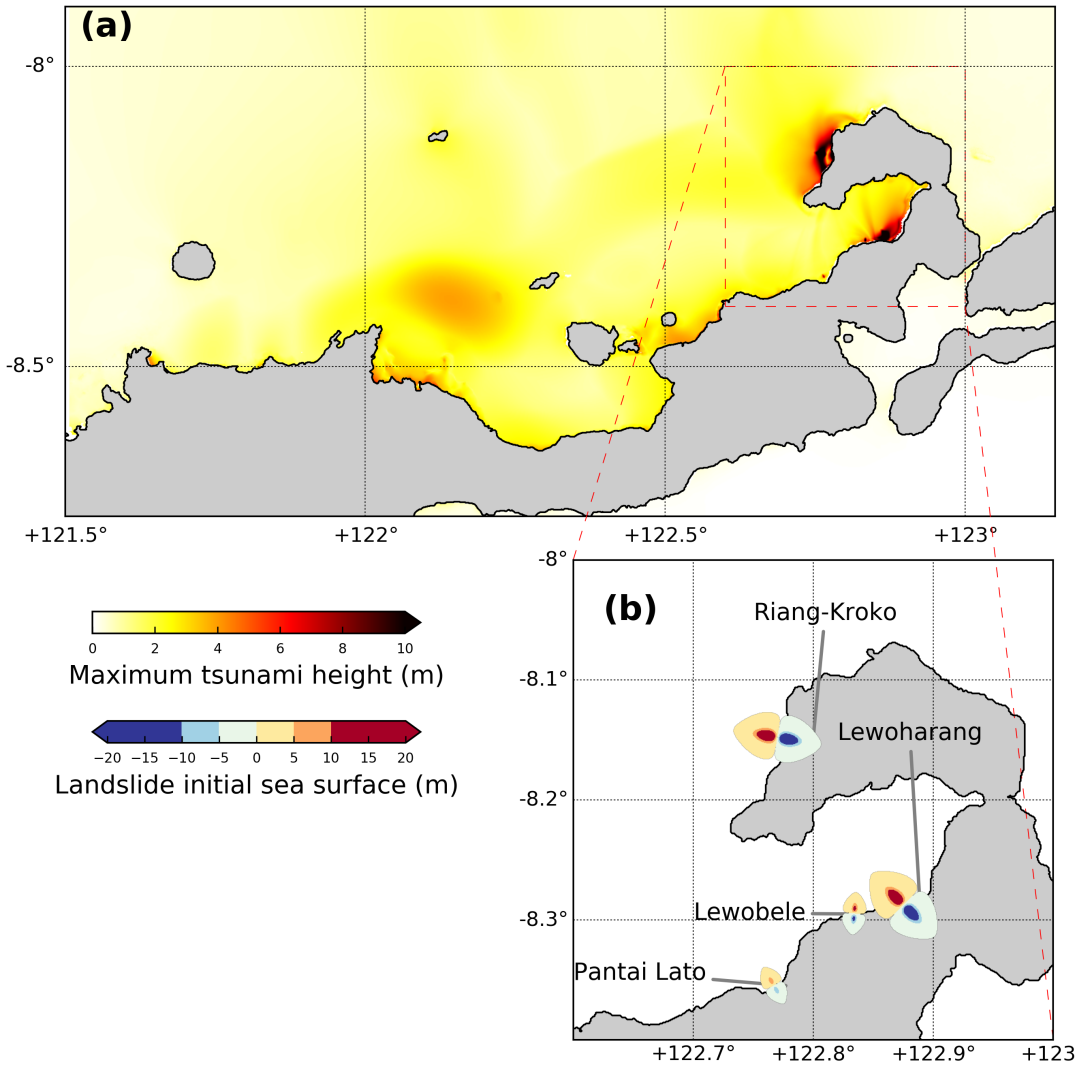

Figure 5.9: (a) Maximum tsunami heights by adding landslide sources, (b) arbitrary landslide initial sea surface elevation.

north of Bali in the west, its surface trace follows the bathymetric low that extends eastward to the western end of Flores, after which it appears only intermittently before reappearing north of the Island of Wetar in the east (see Figure 5.1b, and [McCaffrey and Nabalek, 1984; Silver et al., 1986]). Every published reference to the 1992 Flores earthquake we are aware of ascribes it to the Flores Back-Arc Thrust, but none have explained how the western end of the fault rupture extending beneath Flores can be connected to the surface expression of the Flores Back-Arc Thrust off the northern shore of the island's western end.

There seems to us no question that the 1992 Flores earthquake ruptured a major fault inclined at about 70° azimuth, extending onshore at its western end but offshore

at its eastern. Beckers and Lay [1995] first showed that the seismic data are best fit by a strike of 70°, that the aftershock zone is aligned ENE extending from onshore in the west to offshore in the east, and that the point where the "hinge line" (i.e., boundary between coseismic uplift ad subsidence) crosses the coast is consistent with this geometry. Finally, a substantial portion of the fault's eastern end must extend offshore in order to generate a large tsunami.

Whatever the relationship of the earthquake fault's onshore western end to the eastern end of the Flores Back-Arc Thrust offshore, it seems clear that the 1992 Flores earthquake ruptured a distinct segment of the back-arc thrust system. This implies a limit to the maximum magnitude of thrust earthquakes in Flores, and suggests that the back-arc thrust system may be more complicated than previously thought. We note that the 2004 Mw 7.5 Alor earthquake had a strike of 67°, implying it may have ruptured a separate, en echelon segment of the thrust system to the east. If such ENE-oriented segments exist elsewhere along the back-arc thrust system, the implications for hazard are important. As with the 1992 earthquake, the western end may extend onshore, where it can threaten population centres with strong ground shaking.

5.8 Conclusion

The earthquake and tsunami source of the 1992 Flores event are revisited in this study using a joint finite-fault source inversion technique that systematically explores the misfit of model predictions to all the datasets available: seismic and tsunami waveforms, tsunami run-up, and coastal uplift. It is shown that careful consideration of the constraints imposed by the multiple datasets allows resolution of the details of the source that were not well resolved by previous models (i.e., the larger slip near the hypocentre).

The study also establishes unequivocally that the 1992 Flores earthquake ruptured a fault that was inclined to the ENE, deviating from the overall EW trend of back-arc thrusting in the eastern Sunda Arc. This implies that the event ruptured a distinct segment of the back-arc thrust system. We suggest that this segment may not be the only part of the back-arc thrust system that is more complicated than previously thought, and that the detailed geometry of the system may have important implications for seismic and tsunami hazard, by limiting the maximum magnitude of events and directing rupture close to population centres onshore.

Chapter 6

Summary and Future Work

6.1 Summary

6.1.1 Tsunamis in Indonesia

The tsunami catalogue of Indonesia has been updated in this study (Chapter 2). The catalogue now documents 133 tsunamis occurring in Indonesia between 1608 and 2018. Approximately 80% of these were generated by earthquakes. As separated by the Wallace Line, the eastern Indonesia region had almost twice the number of tsunamis (88) than the western region (45). Further, the number of tsunamis associated with volcanic and landslide sources has been significantly increased in the updated catalogue to nineteen and eight events compared to the Latief et al. [2000] catalogues, respectively.

It is certain that the primary source of the tsunamis in western Indonesia is the Sunda subduction zone; from either the west shore of Sumatra or the south coast of Java. The only other tsunamis in western Indonesia are known with certainty to have been generated by the volcanic and landslide activity of Krakatau and its descendent, Anak Krakatau. It has been more difficult to determine the primary source of the tsunamis in eastern Indonesia. While tsunamis in the east have almost certainly been generated by earthquakes, for many events the specific faults that generated these tsunamis remains unclear.

6.1.2 Historical tsunamis and earthquakes in eastern Indonesia

Three historical events from eastern Indonesia have been studied; the 1674 Ambon Island, the 1852 Banda Sea, and the 1992 Flores Island earthquakes and tsunamis (Figure 6.1). The summary of each events is given below.

Ambon Island 1674

The oldest detailed account of an earthquake and tsunami in Indonesia is that of the 17 November 1674 event on Ambon Island, written by Rumphius [1675]. This account provides a detailed description of the ground motion and tsunami observations from Ambon and its surrounding islands. However, there is no detailed information on

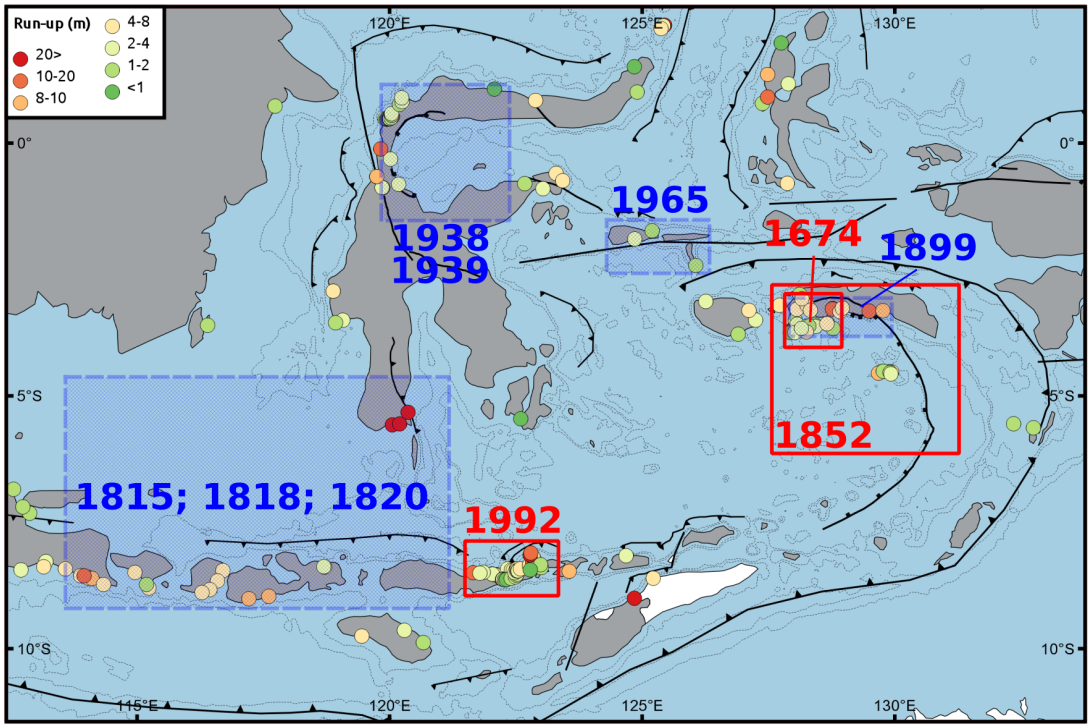

Figure 6.1: Locations of historical tsunamis have been studied (red rectangle) and suggested events should be investigated (blue rectangle).

the primary source of the earthquake and tsunami. It has been speculated that this event was caused by an earthquake from the South Seram Thrust Fault [Løvholt et al., 2012] or a landslide triggered by an earthquake from a local fault inside Ambon Bay [Harris and Major, 2017], but no further explanations have been available.

The relevant ground motion and tsunami observations for this event have been carefully analysed in this study (Chapter 3). Two candidate faults that could explain the earthquake intensity data are the purported South Seram Thrust Fault or a local fault on Ambon. However, the only references to the existence of the South Seram Thrust Fault have been from Irsyam et al. [2010] and Horspool et al. [2014]. Moreover, further investigation is required to determine which local fault could have generated this event.

As shown in Chapter 3, the only possible source of the observed tsunami, with a local extreme run-up confined to a narrow lateral extent along the coastline, is an earthquake-triggered landslide on the northern shore of Ambon. This analysis was supported by the historical accounts, which described a massive coastal landslide on the northern shore of Ambon causing major changes in the landscape. Tsunami simulation confirmed this analysis. The only source model that could explain the tsunami observations was a landslide with a volume of 1 km^3 between Seith And Hila villages, on the northern shore of Ambon.

Banda Sea 1852

It has been believed that the Tanimbar Trough, a section on the Banda Arc, was the source of the 1852 Banda Sea earthquake and tsunami event [Fisher and Harris, 2016], which involved very strong ground motion and a high tsunami in the Banda Islands. However, a thrust mechanism earthquake from the Banda Arc cannot produce a tsunami that has the positive polarity at the Banda Islands and Ambon Bay that was clearly described in the historical accounts. Therefore, a megathrust earthquake on the Banda Arc would not fit to the observations. Moreover, the arrival time of a tsunami generated in the Tanimbar Trough is later than that reported (20 minutes).

The historical earthquake and tsunami accounts of the 26 November 1852 Banda Sea have been revisited in this study (Chapter 4). Earthquake intensity inversion, tsunami inverse travel time simulation, ground motion and tsunami modelling constraint the source parameters of the 1852 Banda Sea event. A 'small' Mw 7.5 earthquake on the Banda Detachment, a huge low-angle normal fault recently discovered (Figure 6.2), is the most credible source to explain the intense ground motion in the Banda Islands, instead of the Mw 8.4 Tanimbar Trough earthquake [Fisher and Harris, 2016]. However this Banda Detachment could not generate a tsunami that fits the observations, particularly with respect to the arrival time. The most plausible tsunami source would be a massive landslide with a volume of 31.5 km^3 in the Weber Deep (Figure 6.2), which has been identified by Pownall et al. [2016]. Plausibly, the landslide was triggered by the Banda Detachment earthquake of Mw 7.5 which then generate the tsunami.

Flores Island 1992

The 12 December 1992 Flores Island earthquake and tsunami event has been revisited in this study (Chapter 5). A systematic finite-fault inversion of teleseismic and coseismic displacement dataset was verified against the reported tsunami run-up heights and waveform to constrain the rupture area to be inclined with an east-northeast trend. This trend deviated from the overall east to west trend of the back-arc thrusting in the eastern Sunda Arc (Figure 6.3). This result suggests that the earthquake ruptured a segment along the Flores back-arc thrust and implied that the back-arc has a more complex structure than has been previously thought. This would significantly change the potential seismic and tsunami hazard in this region, by limiting the maximum magnitude of an event and directing the rupture close to population centres onshore.

This part of the study has shown that source identification and reconstruction of historical events can be more detailed when an event has been recorded by instruments. A more sophisticated technique, such as a finite-fault source inversion can be optimised to constrain the source mechanism, making verification of the model much more accurate.

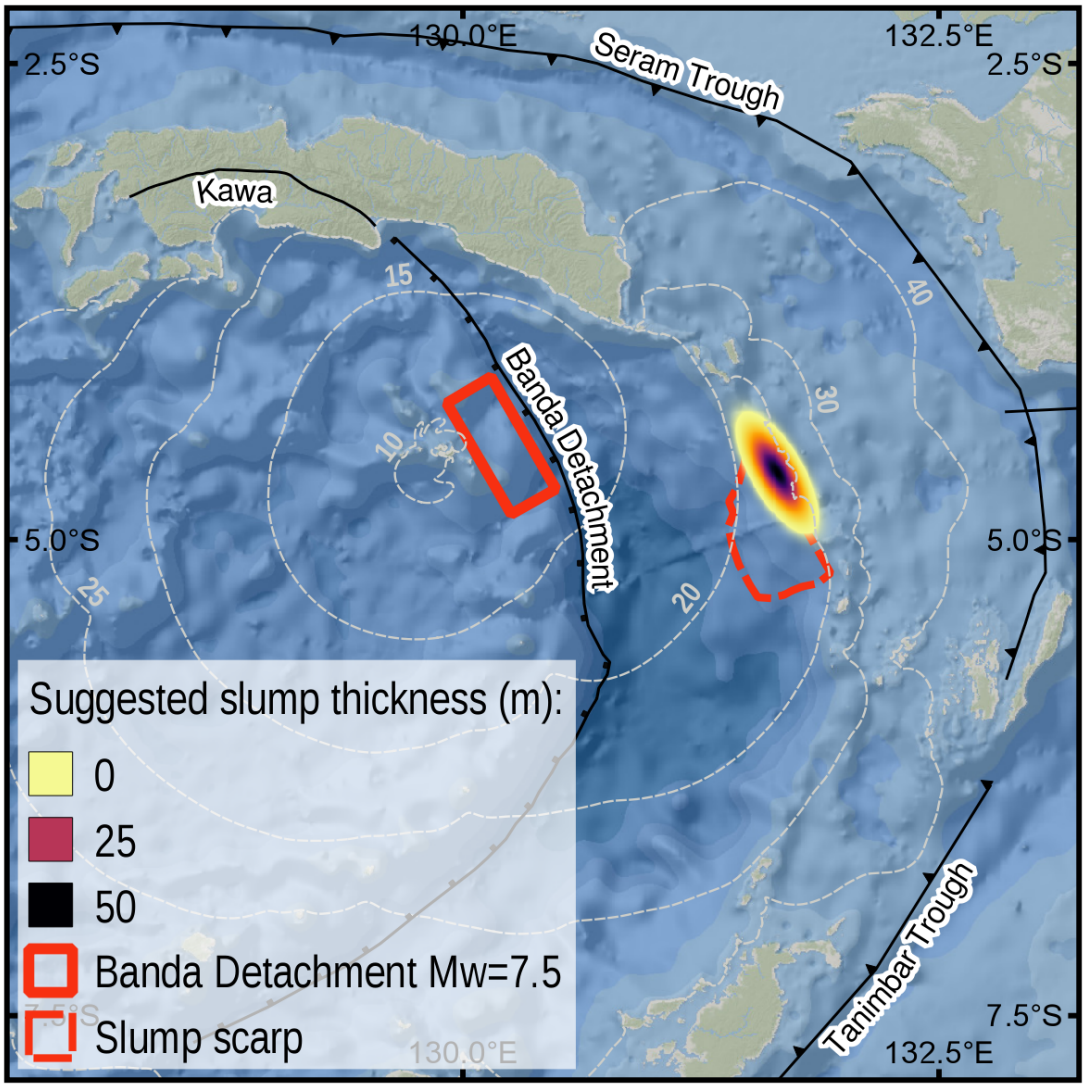

Figure 6.2: Earthquake and tsunami source of the 1852 Banda Sea event suggested from this study. The solid red box represents a rupture area of M7.5 earthquake from the Banda Detachment that triggered a landslide on the eastern slope of the Weber Deep, the yellow to black colours indicates the suggested slump thickness of this study. The dashed white contours show tsunami inverse travel time modelling result (number is in minutes).

6.1.3 Seismic and tsunami hazard implications

This study has introduced new perspectives to the implications for the seismic and tsunami hazard in eastern Indonesia region. It has previously been assumed that the eastern part of Sunda and Banda Arcs were the primary sources of earthquake and tsunami in the region. The recent discovery of a huge low-angle normal fault known as the Banda Detachment [Pownall et al., 2016] has shown that this type of

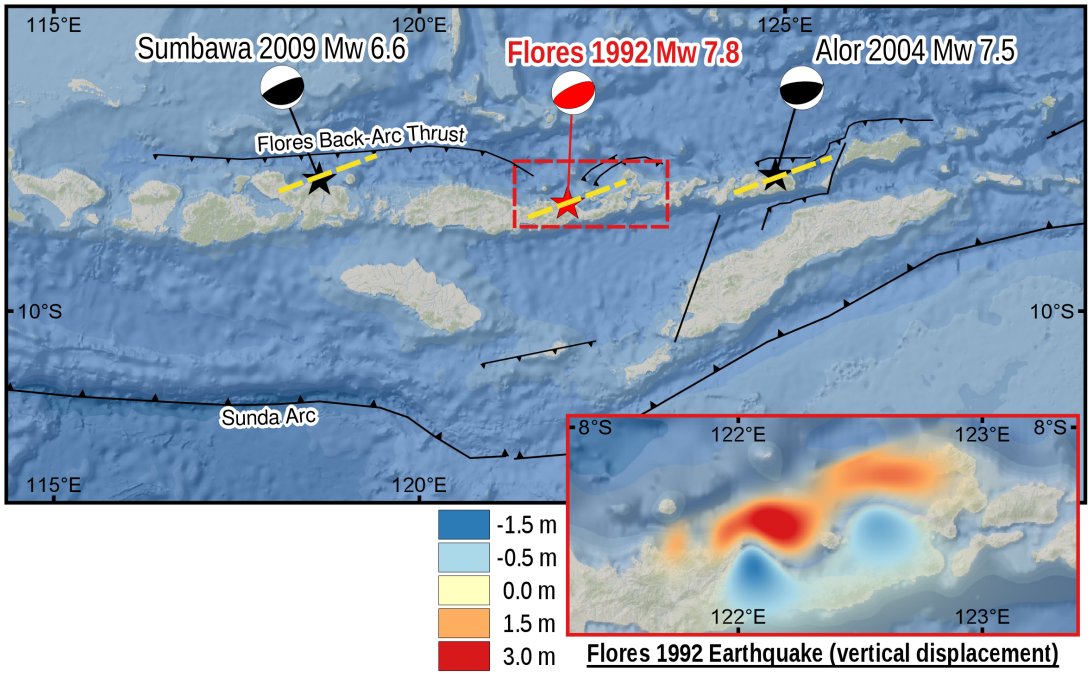

Figure 6.3: Suggested complex structure of the Flores back-arc thrust. Stars show three historical earthquakes and their focal mechanism that have a similar trend of inclination indicated by the yellow dashed line. The inset map shows vertical displacement of the Flores 1992 earthquake and tsunami from this study.

fault could generate a devastating earthquake and tsunami such as the 1852 Banda Sea event. Such a low-angle normal fault has not been considered to be the source of tsunamis in any published hazard assessment studies we are aware of.

Further, the Flores back-arc has previously been depicted as an intermittent thrust zone. However, it has often been simplified as a continuous thrust fault with east to west trends. It has been shown that the rupture area of the 1992 Flores Island earthquake had a strike of 70°, which is different from what was previously thought. This suggests that the Flores back-arc thrust is a segmented fault zone, with a series of en-echelon thrusts extending from Alor in the east to Flores and possibly Sumbawa in the west. This segmentation can generate a distinct pattern of seismic and tsunami hazard in this region.

6.2 Future work

6.2.1 More events need to be investigated

This study has explored techniques for optimising sparse and incomplete historical accounts to identify the primary source of tsunami, through three case studies. As discussed in Chapter 2, the details of the sources of only a few events in eastern

Indonesia are really known. Therefore, many events still need to be investigated.

A good place to begin would be with large-intensity events, from the early 1900s to before the 1992 Flores Island tsunami, that have "enough" data, such as the 1938 and 1939 Tomini Bay tsunamis, as well as the 1965 Mangole Island tsunami (Figure 6.1). These events would have been generated by earthquakes that could have been recorded by distant seismographic stations. With the combination of tsunami and earthquake waveform data, the focal mechanism could be well constrained.

The 1899 Seram Island tsunami was another interesting event from eastern Indonesia that could be studied (Figure 6.1). There is an indication that an earthquake from the Kawa Fault triggered multiple landslides along the southern coast of Seram. The story of this event has been passed through generations and therefore, many local accounts could be used to enhance the quality and quantity of the data.

Three consecutive tsunamis in the Bali Sea, occurring in 1815, 1818, and 1820 (Figure 6.1), indicate another source of tsunamis that should be studied. The 1815 Bali tsunami was generated by an earthquake that triggered a massive landslide, which buried the Buleleng region on the northern coast of the island. As Buleleng was one of the large kingdoms in Bali, written historical accounts of the event are likely available. The 1818 and 1820 tsunamis could have had correlations to the segmentation of the Flores back-arc thrust. As has been noted in Nguyen et al. [2015], earthquake models used have unable to resolve the tsunami height observations for these events.

6.2.2 High-resolution elevation data

Detailed tsunami inundation modelling requires high-resolution elevation data (DEM), which was not available for the cases examined in Chapter 3 and 4. Therefore, accurate verification of the model could not be conducted. On the basis of this study, it is recommended that high-resolution bathymetry data should be acquired where necessary and used for future tsunami modelling, particularly for the coastal region.

Having high-resolution bathymetry data would allow other analysis around the region. For example, Brune et al. [2010] and Pownall et al. [2016] discovered evidence of underwater landslide scarps that might had generate tsunamis in the past or potential landslide locations that could trigger tsunamis in the future. A similar technique could be applied to confirm the landslide evidence for the 1674 Ambon Island tsunami event (Chapter 3). Griffin et al. [2015] showed that modelling of tsunami inundation could be affected by the bathymetry and DEM used in the modelling. Moreover, Watkinson and Hall [2017] and Daryono et al. [2019] were able to identify active faults that could generate earthquake and tsunami in the future.

6.2.3 Paleotsunami and paleoearthquake studies

Paleotsunami studies are recommended to validate the past events that have been reported in the catalogues. Rhodes et al. [2006] noted that paleotsunami studies can reveal past-tsunamis that have not yet been documented in any catalogues. Further,

it could be used to interpret the tsunami time-period and its source mechanism. However, one problem is that it can be difficult to distinguish the source of a sediment deposit, particularly whether it been caused by a tsunami or a storm surge.

Paleogeodetic studies, which uses growth patterns of specific coral microatoll species to reconstructe a history of relative sea level, has been used to identify past megathrust earthquake sequences along the western shore of Sumatra [Natawidjaja et al., 2004, 2006]. Moreover, interseismic strain around the region can be well constrained by adding accurate measurements of crustal strain using GPS or InSAR techniques [Chlieh et al., 2008]. As almost 75% of Indonesia is covered by seawater and coral reefs are fairly evenly distributed across the archipelago [Giyanto et al., 2017], it should be possible to apply these techniques from the western coast of Sumatra to other areas. Thus, the sequences of large earthquakes and tsunamis could be investigated thoroughly.

6.2.4 Updating the tsunami hazard assessment of Indonesia

Tsunami hazard assessment now has shifted from a deterministic to a probabilistic technique, known as Probabilistic Tsunami Hazard Assessment (PTHA). The first PTHA of Indonesia was conducted in 2014 [Horspool et al., 2014], based on earthquake scenarios taken only from the 2010 seismic hazard map of Indonesia [Irsyam et al., 2010]. The seismic hazard map has since been updated [PUSGEN, 2017] by adding more earthquake parameters that could produce tsunamis, resulting in significantly different patterns of hazard than the previous maps. Moreover, this current study has identified additional sources that should be considered. Therefore, the PTHA of Indonesia should be updated again and used to investigate the uncertainty with regard to the sources of the tsunamis.

This updated PTHA should incorporate multiple sources such as those investigated: earthquake, landslide, volcano, meteotsunami, and asteroid impact [Grezio et al., 2017]. However, for the Indonesia region, meteotsunami and asteroid impact could be excluded because they are very infrequent events. Identifying the potential landslide and return periods of volcanic activity are other challenges that should be considered.

Appendix A

Tsunami modelling

A.1 Two-dimensional shallow water wave equations

The JAGURS code [Baba et al., 2015, 2017] is utilised to simulate tsunami propagation and inundation model. The code solves a two-dimensional non-linear shallow water wave equations [Satake, 2002] with seawater density stratification [Allgeyer and Cummins, 2014]. Moreover, the effect gravitational potential change is adapted by using the Green's function developed by Vinogradova et al. [2015]. Furthermore, a dispersive term with a Boussinesq-type [Peregrine, 1972] is added to compromise the short wavelength component of a tsunami.

In this study, I use non-dispersive equations without the seawater density stratification. The shallow water wave equations in spherical coordinate system are shown in Eq.(A.1) – (A.3)[1]. M and N represent the depth-integrated of flow quantities ($[H+\eta]u$ and $[H+\eta]v$) along the θ (latitude) and φ (longitude) directions. H is the water depth, u and v indicate the water velocities, R is the Earth's radius, η is the difference in water elevation at time t, and g is the gravitational acceleration. Then, f and n are the Coriolis parameter and Manning's roughness coefficient.

$$\begin{aligned}\frac{\partial M}{\partial t} + \frac{1}{R\sin\theta}\frac{\partial}{\partial \varphi}\left(\frac{M^2}{H+\eta}\right) + \frac{1}{R}\frac{\partial}{\partial \theta}\left(\frac{MN}{H+\eta}\right) = \\ -\frac{g(H+\eta)}{R\sin\theta}\frac{\partial \eta}{\partial \varphi} - fN - \frac{gn^2}{(H+\eta)^{7/3}}M\sqrt{M^2+N^2}\end{aligned} \tag{A.1}$$

$$\begin{aligned}\frac{\partial N}{\partial t} + \frac{1}{R\sin\theta}\frac{\partial}{\partial \varphi}\left(\frac{MN}{H+\eta}\right) + \frac{1}{R}\frac{\partial}{\partial \theta}\left(\frac{N^2}{H+\eta}\right) = \\ -\frac{g(H+\eta)}{R}\frac{\partial \eta}{\partial \theta} - fM - \frac{gn^2}{(H+\eta)^{7/3}}M\sqrt{M^2+N^2}\end{aligned} \tag{A.2}$$

$$\frac{\partial \eta}{\partial t} = -\frac{1}{R\sin\theta}\left[\left(\frac{\partial M}{\partial \varphi} + \frac{\partial (N\sin\theta)}{\partial \theta}\right)\right] \tag{A.3}$$

Eq.(A.1) and (A.2) represent momentum equations whereas Eq.(A.3) is the continuity formula. The code solves these equations in a finite difference method using a

[1] taken from Baba et al. [2017]

staggered grid leap-frog finite differential scheme. Moreover, it has been developed for a parallel computation. I use the Raijin supercomputer (www.nci.org.au) to simulate all tsunami models of this study. In addition, the code has a nesting algorithm to allow a fine-resolution simulation at the interested location.

A.2 Two-layers model for landslide-generating tsunami

The code is recently developed to model landslide-generating tsunami [Baba et al., 2019]. It uses a two-layers model scheme of Imamura and Imteaz [1995] illustrated on Figure A.1. I use the default numbers of seawater ($\rho_1 = 1000kg/m^3$) and slide layer density ($\rho_2 = 1065kg/m^3$). The two-layers model equations in cartesian coordinate system are shown in Eq.(A.4) – (A.9). I use this model for Chapter 3 and 4.

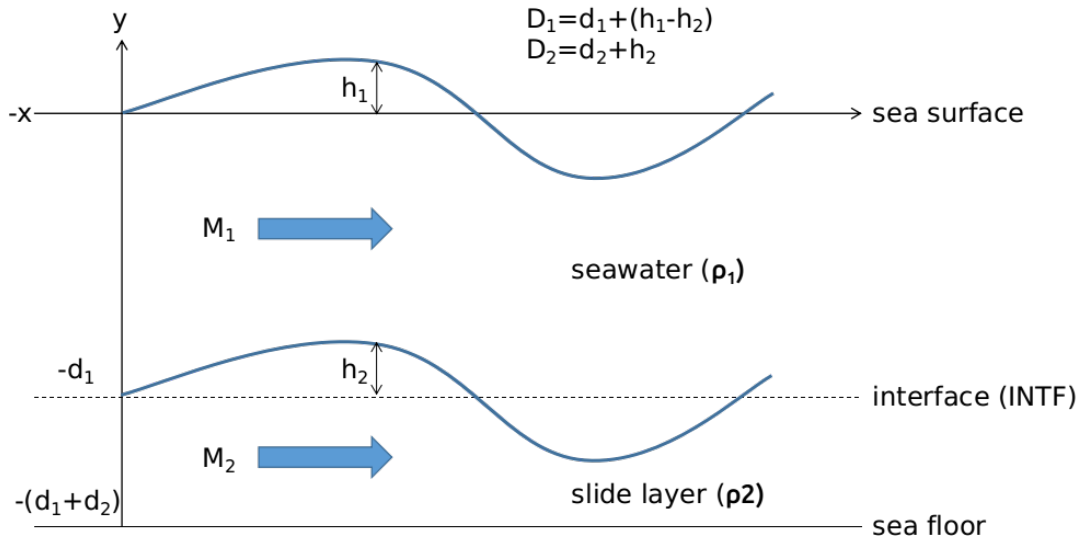

Figure A.1: Illustration of two layers model in JAGURS

$$\frac{\partial M_1}{\partial x} + \frac{\partial N_1}{\partial y} + \frac{\partial (h_1 - h_2)}{\partial t} = 0 \tag{A.4}$$

$$\frac{\partial M_1}{\partial t} + \frac{\partial (M_1^2/D_1)}{\partial x} + \frac{\partial (M_1 N_1/D_1)}{\partial y} + gD_1\frac{\partial h_1}{\partial x} - INTF = 0 \tag{A.5}$$

$$\frac{\partial N_1}{\partial t} + \frac{\partial (M_1 N_1/D_1)}{\partial x} + \frac{\partial (N_1^2/D_1)}{\partial y} + gD_1\frac{\partial h_1}{\partial y} - INTF = 0 \tag{A.6}$$

$$\frac{\partial M_2}{\partial x} + \frac{\partial N_2}{\partial y} + \frac{\partial (h_2)}{\partial t} = 0 \tag{A.7}$$

$$\begin{aligned}\frac{\partial M_2}{\partial t} &+ \frac{\partial (M_2^2/D_2)}{\partial x} + \frac{\partial (M_2 N_2/D_2)}{\partial y} \\ &+ gD_2\left[\alpha\left(\frac{\partial h_1}{\partial x} + \frac{\partial d_1}{\partial x} - \frac{\partial h_2}{\partial x}\right) + \frac{\partial h_2}{\partial x} - \frac{\partial h_1}{\partial x}\right] - INTF = 0\end{aligned} \tag{A.8}$$

$$\begin{aligned}\frac{\partial N_1}{\partial t} &+ \frac{\partial (M_2 N_2/D_2)}{\partial x} + \frac{\partial (N_2^2/D_2)}{\partial y} \\ &+ gD_2\left[\alpha\left(\frac{\partial h_1}{\partial y} + \frac{\partial d_1}{\partial y} - \frac{\partial h_2}{\partial y}\right) + \frac{\partial h_2}{\partial y} - \frac{\partial h_1}{\partial y}\right] - INTF = 0\end{aligned} \tag{A.9}$$

where

$$\begin{aligned}\alpha &= \frac{\rho_1}{\rho_2} \\ INTF &= f_{inter} = 0.025\end{aligned} \tag{A.10}$$

Unfortunately, it has a few instability issues in this first generation of the code for a landslide-tsunami model. Firstly, it is a frictionless ($n = 0$) model. Therefore, the slide layer keeps moving during the simulation and will not finish. Secondly, setting-up a nested grids model is "tricky". The setup model is unable to use for all types of scenarios. Therefore, I only use a single grid domain model to simulate landslide-generation in Chapter 3 . In Chapter 4, I run the two-layer model for up to five minutes then extract the sea surface elevation at t=2 minutes and use it to be the initial sea surface elevation for the nested grid model. Thirdly, the code only able simulates a submarine landslide type.

Other landslide tsunami codes

Tsunami landslide modelling can be categorised into three groups according to the generation process [Heidarzadeh et al., 2014]. First, the landslide motion is treated like another fluid motion assigned by different density. Secondly, initial sea surface elevation is defined based on a semi-empirical equation. Lastly, the landslide generation is modelled from transient bathymetry deformation in a period of time. As summarised by Heidarzadeh et al. [2014], all tsunami landslide codes, to some degrees, are able to reproduce model that fit to the data. However, the selected code will depend on the purpose of the application: (i) the needs of dispersion equations, (ii) computation facilities, (iii) high-resolution bathymetry, and (iv) accuracy and purpose of the modelling.

The first approach is similar to the two-layers model used in this thesis (Chapter 3 and 4). This technique has been widely used in many publications, such as Imamura and Imteaz [1995]; Xiao et al. [2015]; Yamanaka and Tanioka [2017]; Ioki et al. [2019].

The second approach is applied by utilising semi-empirical equations obtained from a laboratory experiment [e.g. Watts et al., 2005]. The experiment measures the

maximum initial sea surface elevation generated from different types of landslide parameter then an empirical equation is analysed. The second approach is used in Chapter 5 of this thesis.

The last approach probably is the most complex technique (in my opinion). It requires detail information of the sea floor deformation in a period of time. Therefore, high-resolution bathymetry is needed. Moreover, it may be difficult to exactly know this condition after an event. For example, this approach has been applied by Ward and Day [2003] and Lynett et al. [2003].

A.3 Digital elevation model

Digital elevation model (DEM) in this study is compiled from different sources. The GEBCO [Sandwell et al., 2002] and commercial T-Carta Marine dataset provided by the Australia-Indonesia Facility for Disaster Reduction and BATNAS [BIG, 2018] are the main data to build the bathymetric model. Then, the SRTM 90m [Jarvis et al., 2008] and DEMNAS [BIG, 2018] are used to build the topographic model. I also use IFSAR-Intermap elevation model provided by the Australia-Indonesia Facility for Disaster Reduction for the 1992 Flores Island earthquake and tsunami case study.

All the data is then manually compiled using Quantum GIS (QGIS) software. Furthermore, I use Generic Mapping Tools (GMT) software to interpolate the DEM using the *surface* function. Lastly, I create a nested grids domain model according to the interested location. Table A.1 shows the domain setup model used in Chapter 3 – 5.

Table A.1: Domain model of this study

Child grid	Parent grid	Resolution (°)	Resolution (m)	Xmin	Xmax	Ymin	Ymax	Zmax (m)	dt (s)
Tsunamigenic-earthquake model - Chapter 3 - the 1674 Ambon Island tsunami									
bathy.d00	bathy.d00	0.01350	1500.00	125.50000	130.69750	-5.75000	-1.49750	6938	1.83
bathy.d01	bathy.d00	0.00450	500.00	126.94450	129.05050	-4.08950	-2.03750	5585	0.68
bathy.d02	bathy.d01	0.00150	166.67	127.84000	128.51500	-3.83300	-3.05000	3964	0.27
Two-layers model - Chapter 3 - the 1674 Ambon Island tsunami									
dem.d00	dem.d00	0.00100	111.11	127.50000	128.85000	-4.10000	-3.05000	4573	0.17
Tsunamigenic-earthquake and landslide models - Chapter 4 - the 1852 Banda Sea earthquake and tsunami									
dem.d00	dem.d00	0.00450	500.00	125.00000	134.00000	-9.25000	-1.49650	7599	0.58
dem.d01	dem.d00	0.00150	166.67	129.59450	130.25150	-4.81750	-4.18750	4983	0.24
dem.d11	dem.d01	0.00050	55.56	129.80900	130.00100	-4.62250	-4.45000	1706	0.14
dem.d02	dem.d00	0.00150	166.67	127.71800	129.03200	-3.96250	-3.45850	4500	0.25
dem.d12	dem.d02	0.00050	55.56	128.01500	128.25350	-3.82750	-3.62050	2813	0.11
Tsunamigenic-earthquake and landslide models - Chapter 5 - the 1992 Flore Island earthquake and tsunami									
dem.G00	dem.G00	0.00450	500.00	120.00000	124.27500	-9.15000	-2.46750	6447	1.41
dem.G01	dem.G00	0.00150	166.67	121.50675	123.19575	-8.79075	-7.66425	5260	0.52
dem.G11	dem.G01	0.00050	55.56	121.80725	122.95225	-8.66975	-7.96625	4299	0.19
dem.G02	dem.G00	0.00150	166.67	121.15675	121.10175	-3.36825	-2.55675	1365	1.02
dem.G12	dem.G02	0.00050	55.56	120.17975	120.48925	-3.27625	-2.76575	90	1.32

A.4 Scenarios

Tsunamigenic earthquake scenario

Tsunamigenic earthquake is a tsunami generated by an earthquake. The JAGURS code has a function to calcuate the earthquake deformation model using the Okada [1985] formula. It requires a fault plane model as illustrated on Figure A.2. Strike is the azimuth angle of the fault plane toward North with a clockwise direction. Fault dip is the angle between a horizontal plane and the fault. The dip direction is always prependicular to the strike to the right hand side. Then, a fault rake is a movement direction of the hanging wall block during the ruptures. A rake of 0° or 180° indicates a strike-slip movement whereas 90° and -90° represent a reverse and normal mechanism, respectively. Coordinates indicated in this study (such as on Table 3.3) represent the *Position*, where is at the top-right corner of the fault plane. I use this assumption for Chapter 3 and 5.

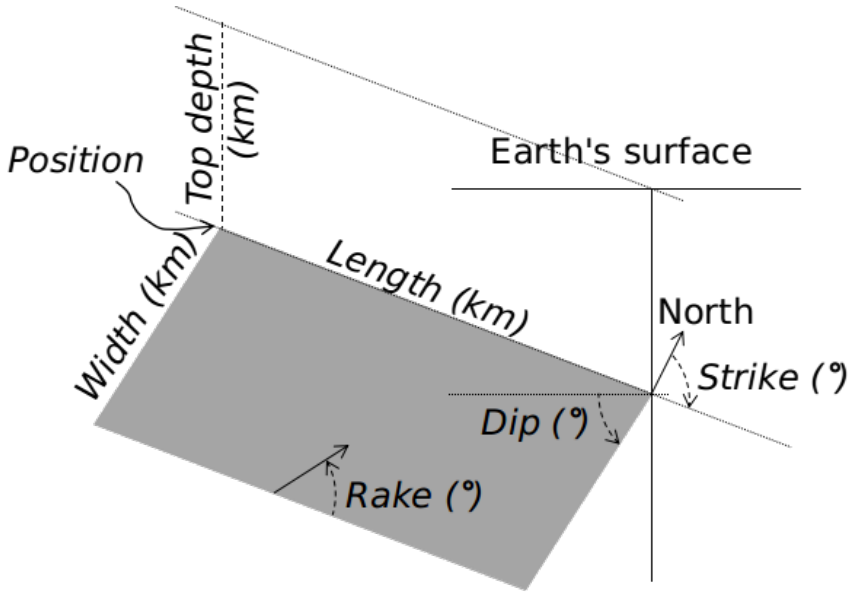

Figure A.2: Fault plane illustration in JAGURS

Empirical equations of landslide-generating tsunami

I use empirical equations of Watts et al. [2005] for Chapter 5 to simulate tsunami-generation caused by landslide. The equations were developed based on a laboratorium experiment. The equations provide a maximum initial sea surface elevation profile at the peak of the tsunami generation. However, the sea surface velocity at that time can not be included in the simulation.

Appendix B

Methodologies of Chapter 4

B.1 Earthquake intensity inversion

This study follows Griffin et al. [2018] to constrain the 1852 Banda Sea earthquake parameters: hypocentre, magnitude, and focal mechanism. First, description of ground shaking and damage reported by Wichmann [1918] at various places are converted into a Modified Mercalli Intensity (MMI) value (see Figure 4.2). A brute force approach of ground motion simulations are conducted using the OpenQuake Engine software [Pagani et al., 2014] to search the source parameters and then converted to intensity using the Atkinson and Kaka [2007] ground motion to intensity conversion equations. A Bayesian framework (Equation B.1–B.3) is then applied to calculate the posterior probability distribution of the source parameters Figure 4.3, rather than simply finding a single best-fit source model. Due to the unique nature of the Banda Sea, it is unclear which Ground Motion Prediction Equations (GMPE) are most appropriate. Therefore we use a weighted combination of subduction interface (Abrahamson et al. [2016], 0.55; Zhao et al. [2016], 0.2) and active shallow crustal (Boore et al. [2014], 0.125; Chiou and Youngs [2014], 0.125) GMPEs. Weights are chosen based on our subjective belief about the relative suitability of each GMPE to the Banda Sea region.

The posterior probability of the earthquake parameters $P(\mathbf{m}|\mathbf{I})$ are estimated using Bayes theorem as Kruschke [2011] for a given vector of model parameters $\mathbf{m}$ and vector of intensity data $\mathbf{I}$ (Equation B.1). From the given parameter combination $\mathbf{m}$, $P(\mathbf{I}|\mathbf{m})$ is the likelihood of the data. Then $P(\mathbf{m})$ is the a priori probability of the given parameter from the given parameter $\mathbf{m}$.

$$P(\mathbf{m}|\mathbf{I}) = \frac{P(\mathbf{I}|\mathbf{m})P(\mathbf{m})}{\int_M P(\mathbf{I}|\mathbf{m}')d\mathbf{m}'} \tag{B.1}$$

Further, we assume that the observed intensity data points contain errors with Gaussian distribution and uncorrelated between sites, with the likelihood is shown in Equations B.2 following Bevington and Robinson [1992]. N, I_{mi}, and I_{oi} are number of intensity data points, the modelled intensity at the ith data point, and the observed intensity, respectively. Then we assume the errors on the data σ using Equation B.3,

with n is free parameters.

$$P(\mathbf{I}|\mathbf{m}) = \left(\frac{1}{\sigma\sqrt{2\pi}}\right)^{N} e^{-0.5\left(\frac{\Sigma_{i=1}^{N}(I_{mi}-I_{oi})^2}{\sigma^2}\right)} \tag{B.2}$$

$$\sigma = \frac{1}{N-n}\sum_{i=1}^{N}(I_{mi}-I_{oi})^2 \tag{B.3}$$

B.2 Tsunami inverse travel time

We optimise the only tsunami arrival time data from Banda Neira to constraint the tsunami source location. The tsunami arrival time of 20 minute is based on the reports: ”vertical shocks ... of 5 minutes duration”, and ”the ground had been calm for a quarter of an hour when a flood wave crashed in” [Wichmann, 1918]. We performed a tsunami inverse travel time simulation following [e.g. Heidarzadeh and Satake, 2014]. A Gaussian function with a radius and maximum height of 500 m and 1 m, respectively is assumed to be an initial source located at the Banda Neira. Then numerical tsunami modelling is conducted and we extract tsunami travel time contour at various times shown in Figure B.1.

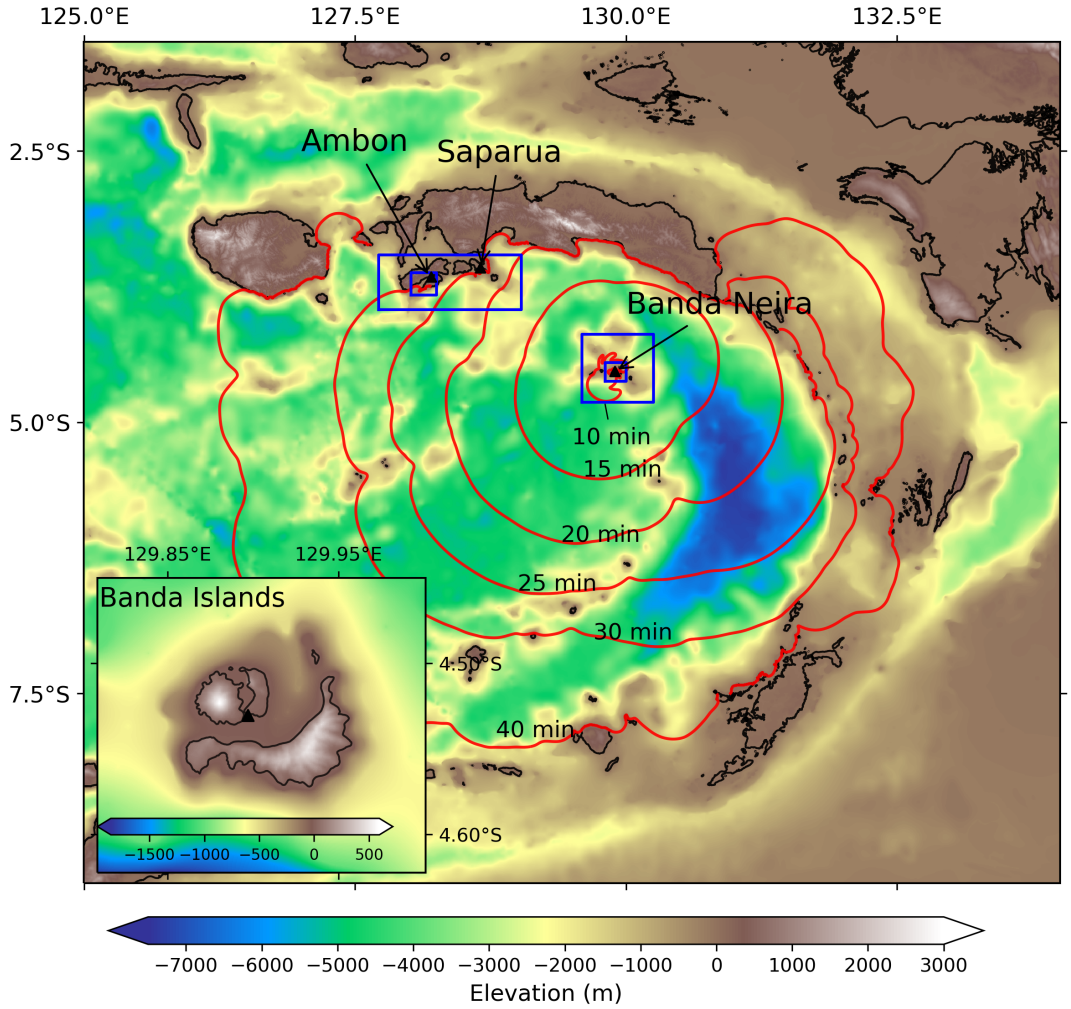

Figure B.1: Domain of tsunami modelling and inverse travel time result. The solid blue boxes are the nested grid domains model; black triangles represent virtual gauges; and red contours are tsunami inverse travel time result.

B.3 Tsunami modelling

Tsunami modelling is performed using the JAGURS tsunami simulation code [Baba et al., 2015, 2017]. The code numerically solves the non-linear shallow water wave without dispersive equations in a spherical coordinate system using a finite-difference scheme (see Appendix A.1). Tsunami simulation is performed on a nested grid domain with the coarsest and finest grid resolution approximately 450 and 50 m, respectively (Figure B.1). A time-step of 0.2 s is set to satisfy the Courant stability condition. A digital elevation model (DEM) (Figure B.1) is built from combination of National Bathymetry (BATNAS) [BIG, 2018], a marine chart around the Banda Islands (see Figure B.2; Reclus [1885]), and the SRTM-90m [Jarvis et al., 2008]. Detailed tsunami inundation modelling is not conducted due to unavailability of high-resolution DEMs around the region of interest [Griffin et al., 2015].

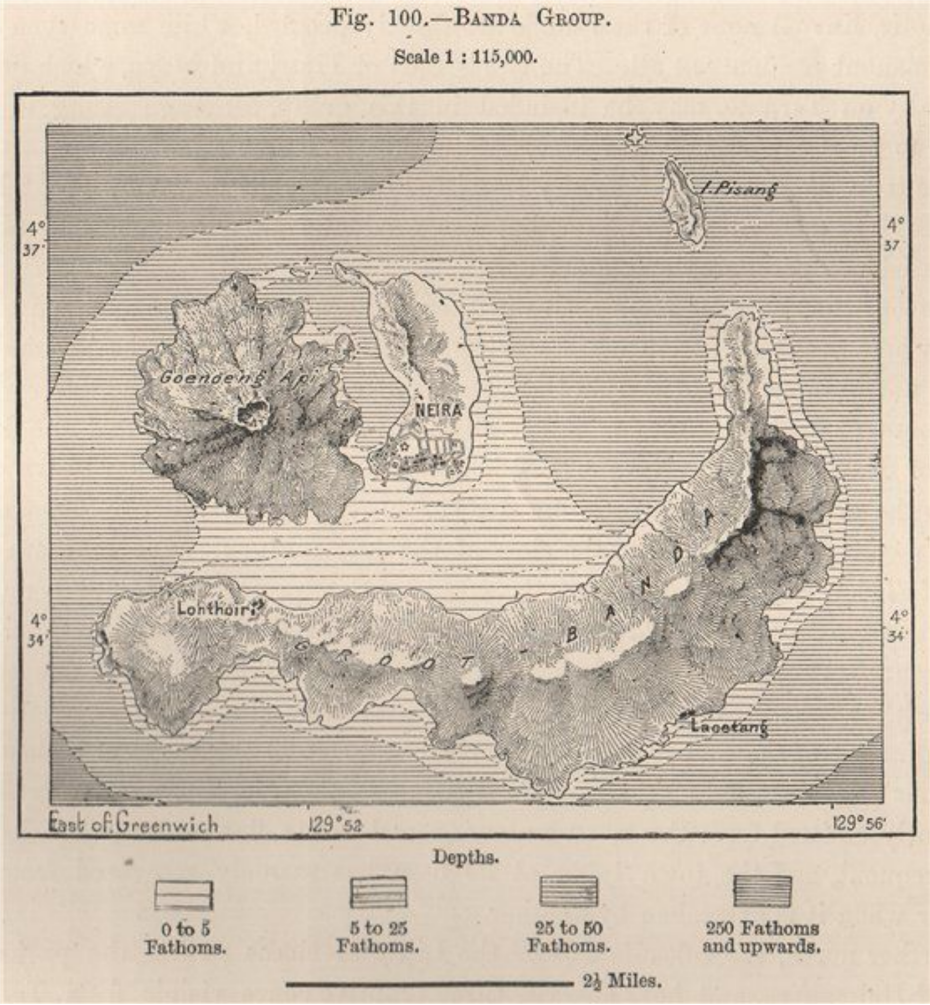

Figure B.2: Nautical chart of the Banda Islands from 1885 (taken from Reclus [1885]). Remarkably, this appears to be the most detailed bathymetry model available for the channel between the Banda Islands.

B.4 Tsunamigenic earthquake scenarios

We designed a set of earthquake scenarios of Mw 7.4 to 8.4 to model the tsunami. We assume an ellipse fault plane with length varied from 40 to 100 km and a width as half of the length. We assume the earthquake has a homogeneous slip that ranges from 2 to 15 m by assuming a rigidity of 30 GPa. The vertical deformation of the earthquake is modelled using the method of Meade [2007] on a triangular mesh following the irregular fault geometry of Pownall et al. [2016]. In this study, we use a python package library provided from https://github.com/cossatot/tri_dislocations_python. Further, we run a Tanimbar Trough Mw 8.4 scenario taken from [Fisher and Harris, 2016] (their M05 scenario) to compare the results using the Okada [1985] on a rectangular fault plane model (see A.4). Selected tsunamigenic earthquake modelling scenarios are shown on Figure B.3.

Figure B.3 shows that only the Banda Detachment earthquake can generate tsunami with a positive polarity that matches the observations. The Banda Detachment Mw 7.5 earthquake represents a scenario based on the earthquake intensity inversion. The earthquake rupture area is directly beneath the Banda Islands so that the tsunami arrival time does not fit the observations. The rupture area location of the Banda Detachment Mw 8.4 earthquake is designed to fit the tsunami arrival time, but it is not at the highest posterior probability location from the earthquake intensity inversion. However, even though a large magnitude is used, the maximum simulated tsunami height at Banda Neira is a little bit smaller than at Saparua.

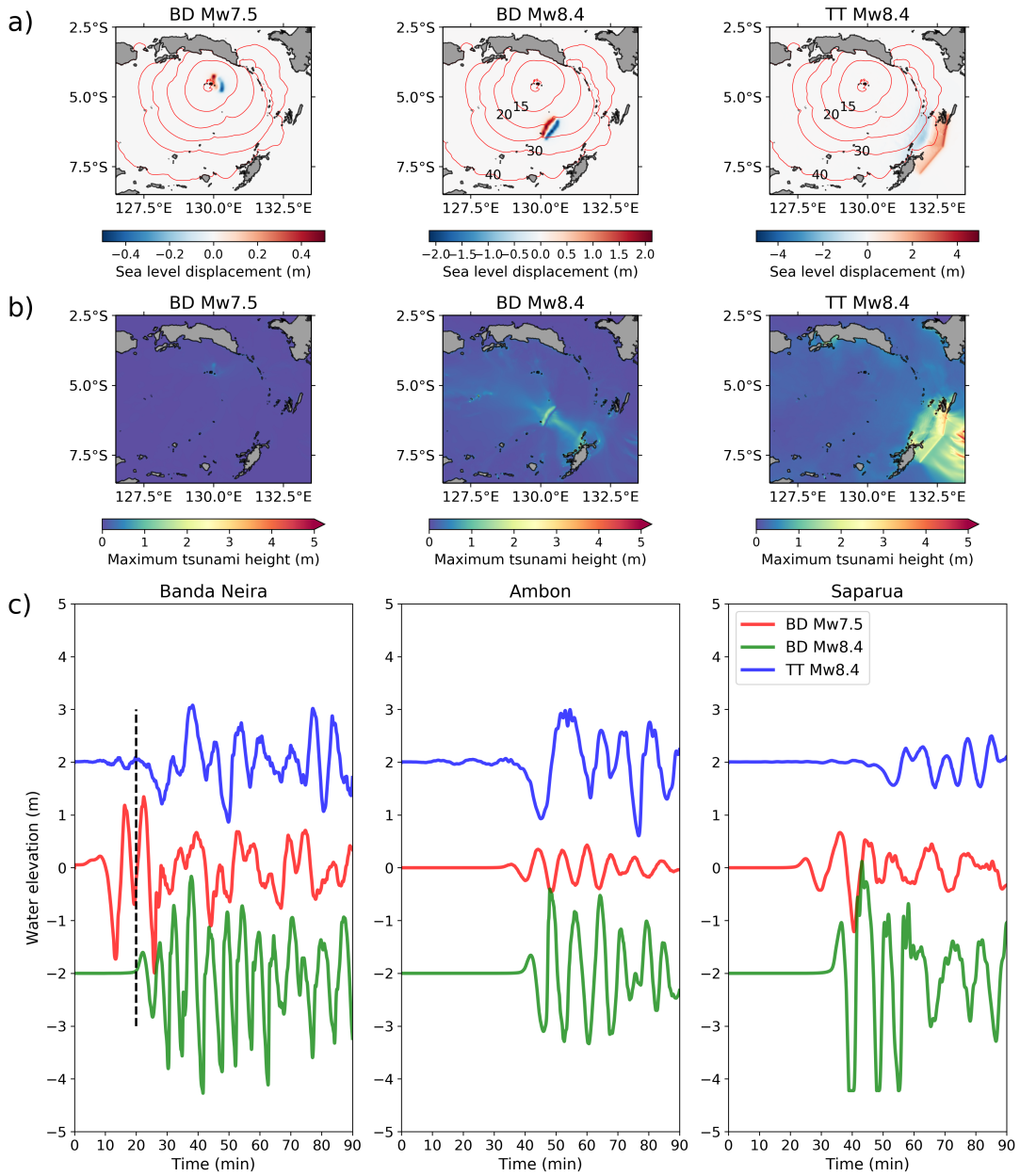

Figure B.3: Selected tsunamigenic earthquake models of the 1852 Banda Sea event: a) coseismic sea level displacement from the Banda Detachment (Mw7.5 and 7.8) and the Tanimbar Trough of Fisher and Harris [2016] (Mw8.4); b) simulated maximum tsunami height from scenarios in a; c) simulated tsunami waveform at three virtual gauges shown. The red line in *a* represent travel time contours of the tsunami inverse travel time.

B.5 Landslide-generated tsunami

Landslide-generated tsunamis and their propagation are simulated using a two-layer approach [Imamura and Imteaz, 1995] in the JAGURS code [Baba et al., 2019] (see A.2). The landslide layer is assumed to be a deformable material on top of the current elevation model (illustrated on Figure B.4). We designed two set of landslide scenarios from Weber Deep: the WD and WDS. WD is located at the top-right corner whereas WDS is along the top-scarp of the landslide identified by Pownall et al. [2016] (see WDS in Figure 4.1). The WD landslide has a circular (Table B.1) while the WDS landslide with an elliptical shape of a Gaussian function.

Figure B.5 and B.6 show the selected landslide of the WD and WDS scenarios generate tsunamis with positive polarity at all locations. The maximum simulated tsunami varies depend on the parameters used. The WD scenario represents only a 'small' part of the massive slump has been identified in Weber Deep. Unfortunately, there is no detailed information, such as age and landslide dimension, available of the massive slump from Pownall et al. [2016]. We noticed that the code used has a few issues that might affect the result. First, it is a frictionless model so that the landslide movements will not finish during the simulation. The code has an instability issue on a nested grids simulation. We therefore simulate the tsunami generation caused by the landslide for five minutes in a single grid domain. Further, we extract the sea surface elevation at time of 2 minutes and then use it to be the initial sea surface elevation for the nested grid simulation.

Table B.1: Landslide-generating tsunami scenarios from Weber Deep with a circular type (WD)

Scenario	**Radius (km)**	**Thickness (m)**	**Volume (km^3)**
Centre = 131.525°E and 4.47°S			
WD-1	5	100	2.62
WD-2	5	200	5.24
WD-3	5	300	7.85
WD-4	5	500	13.10
WD-5	10	100	10.47
WD-6	10	200	20.94
WD-7	10	300	31.42
WD-8	10	500	52.36
WD-9	15	100	23.56
WD-10	15	200	47.12
WD-11	15	300	70.69
WD-12	15	500	117.81
WD-13	12.5	100	16.36
WD-14	12.5	200	32.73
WD-15	12.5	300	49.09
WD-16	12.5	500	81.81

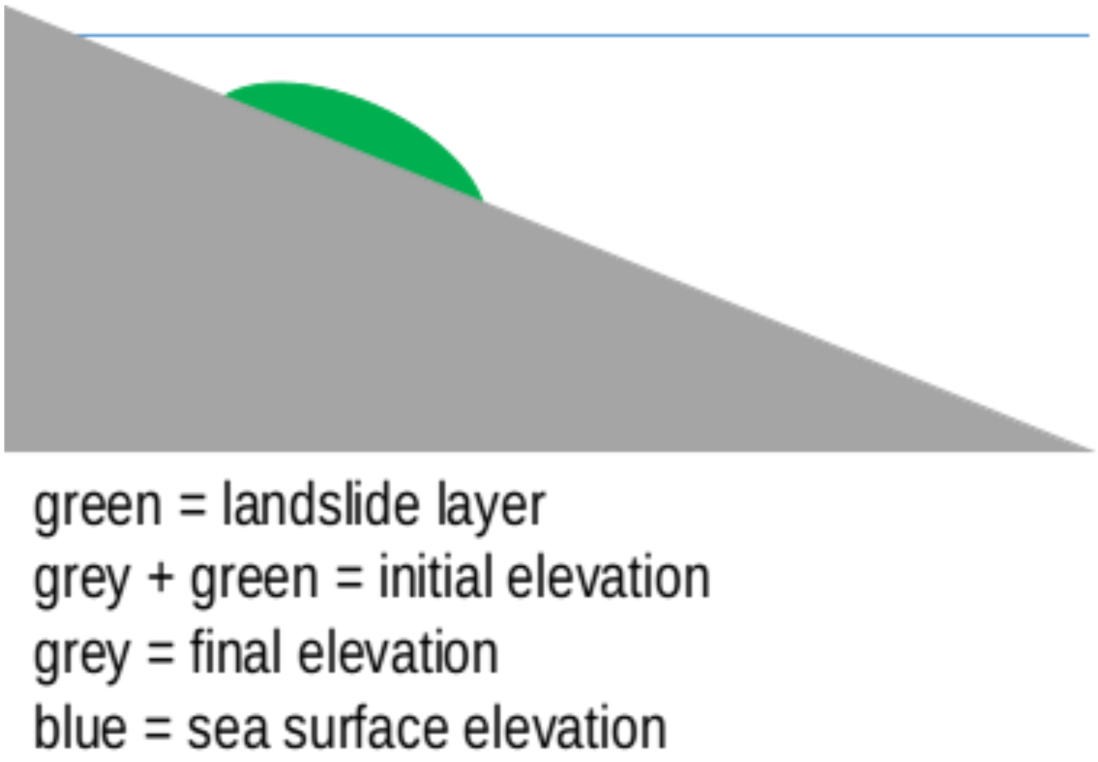

Figure B.4: Illustration of the two-layer approach in landslide-generating tsunami simulation.

Table B.2: Landslide-generating tsunami scenarios from Weber Deep with an elliptical type (WDS)

Scenario	**Length (km)**	**Width (km)**	**Thickness (m)**	**Volume (km^3)**
Centre = 131.65°E and 4.65°S				
WDS-1	30	5	50	7.85
WDS-2	30	5	100	15.71
WDS-3	30	10	50	15.71
WDS-4	30	10	100	31.42
WDS-5	30	15	50	23.56
WDS-6	30	15	100	47.12
WDS-7	40	5	50	10.47
WDS-8	40	5	100	20.94
WDS-9	40	10	50	20.94
WDS-10	40	10	100	41.89
WDS-11	40	15	50	31.42
WDS-12	40	15	100	62.83
WDS-13	40	20	50	41.89
WDS-14	40	20	100	83.78
WDS-15	50	5	50	13.09
WDS-16	50	5	100	26.18
WDS-17	50	10	50	26.18
WDS-18	50	10	100	52.36
WDS-19	50	15	50	39.27
WDS-20	50	15	100	78.54
WDS-21	50	20	50	52.36
WDS-22	50	20	100	104.72
WDS-23	50	25	50	65.45
WDS-24	50	25	100	130.90
Centre = 131.70°E and 4.73°S				
WDS-25	75	10	50	39.27
WDS-26	75	10	100	78.54
WDS-27	75	20	50	78.54
WDS-28	75	20	100	157.08

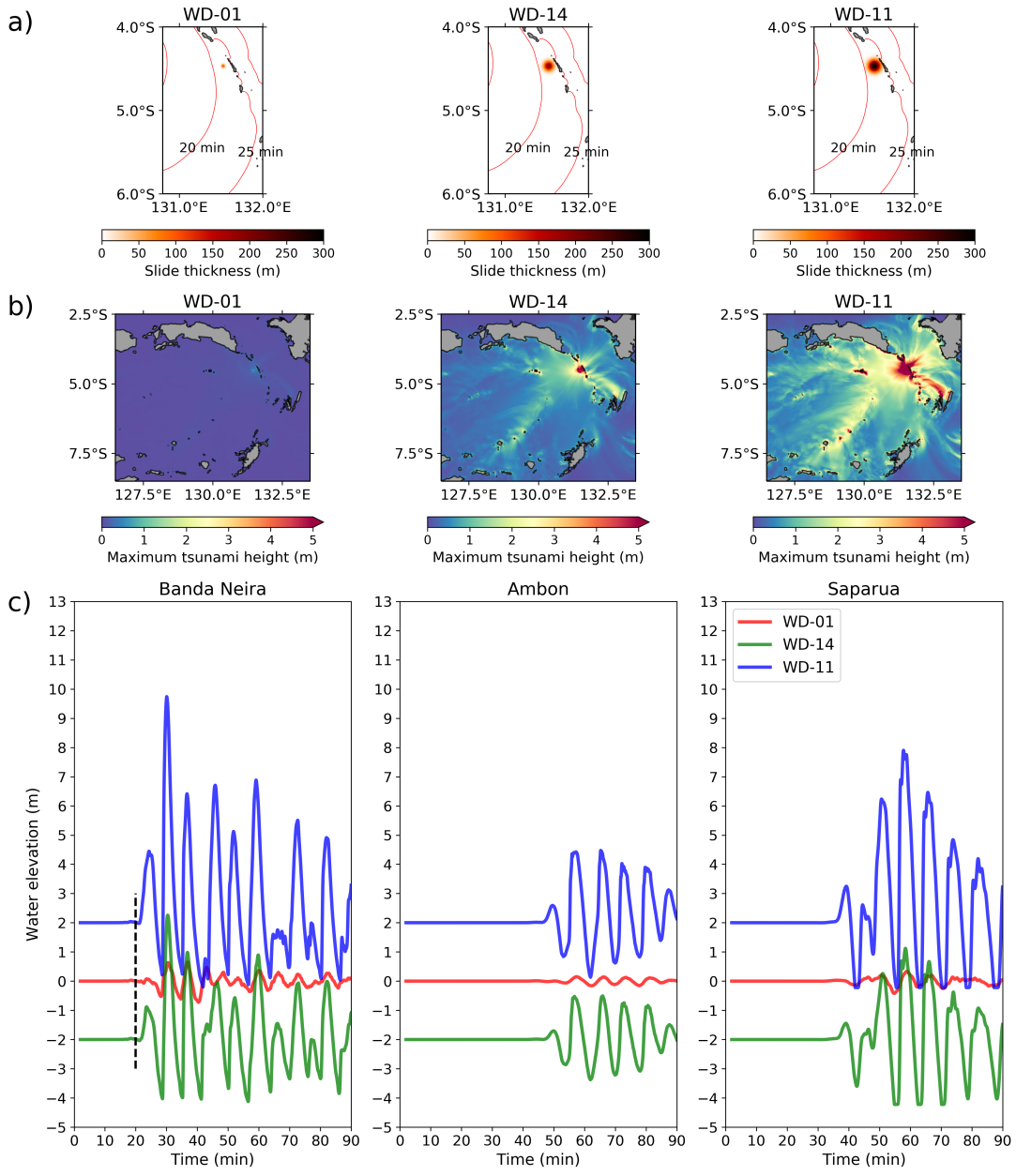

Figure B.5: Selected landslide-generating tsunami models of the WD scenarios: a) landslide locations and their thickness layer ; b) simulated maximum tsunami height from scenarios in (a); c) simulated tsunami waveform at three virtual gauges. The red line in (a) represent travel time contours of the tsunami inverse travel time.

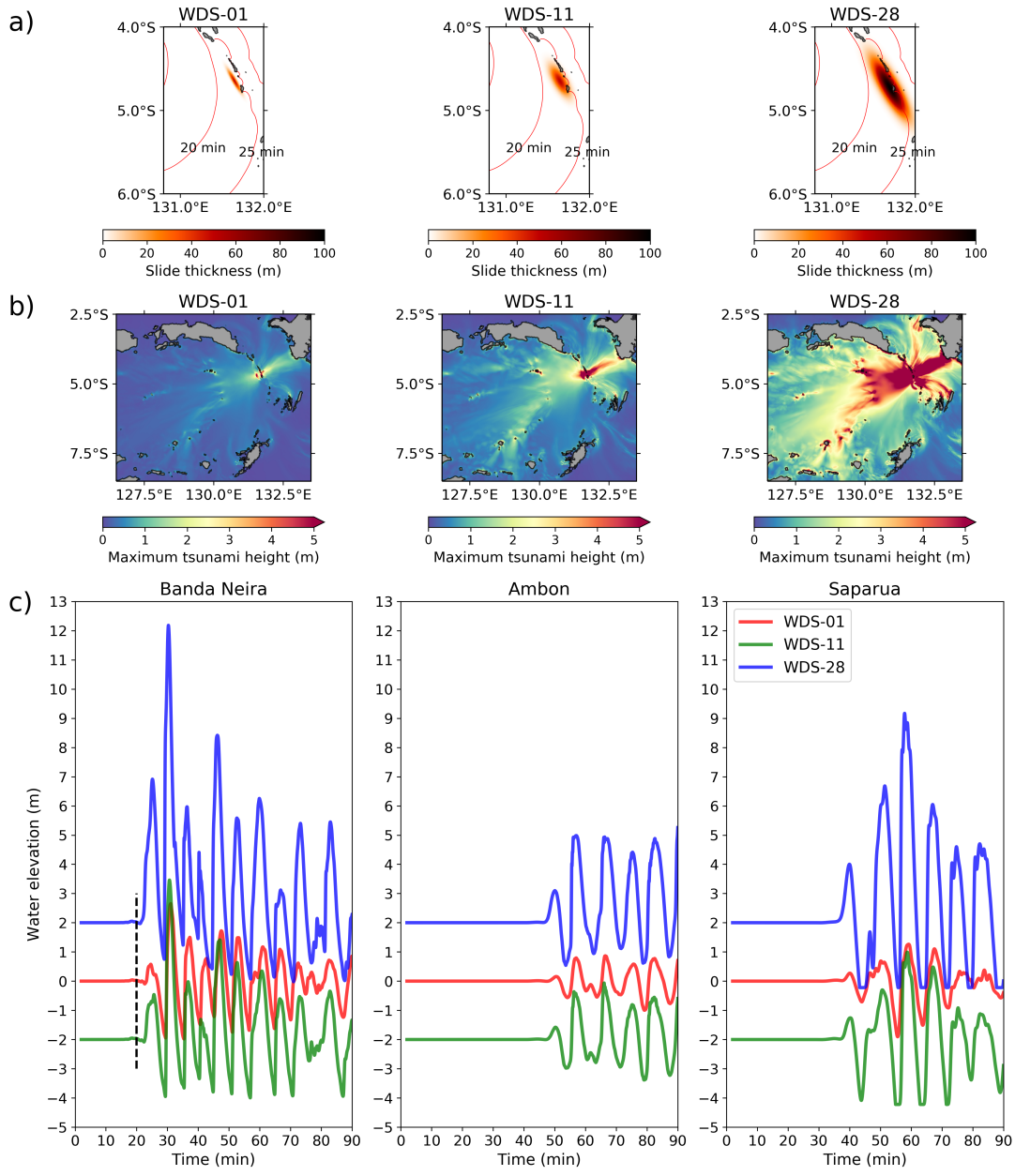

Figure B.6: Selected landslide-generating tsunami models of the WDS scenarios: a) landslide locations and their thickness layer ; b) simulated maximum tsunami height from scenarios in (a); c) simulated tsunami waveform at three virtual gauges. The red line in (a) represent travel time contours of the tsunami inverse travel time.

B.6 Criteria of the best model

The best earthquake or landslide scenario is selected according to three criteria. Firstly, the tsunami arrival time at the Banda Neira is approximately 20 minutes after the ground shaking stop. Second, the arriving tsunami has to be in a positive polarity phase. Lastly, 'very high' tsunami at Banda Neira (8 m) and 'high enough' at Ambon and Saparua. The first and second criteria are well confirmed from the Banda Detachment (all scenarios located at the south-west of Banda Neira) and the landslide (WDS) scenarios. However, only the WDS-11 scenario that we think explain well the third criteria. It is rather difficult to fit the simulated tsunami height against all the observations; data accuracy and no high-resolution elevation model is available for the simulation. Therefore, the best landslide scenario is subjective selected in this case.

Appendix C

Supplementary materials: Multi-Data-Type Source Estimation for The 1992 Flores Earthquake and Tsunami

In order to achieve a final source model, we consider the following approach to parameterisation. Firstly, we find a proper weighting and smoothing coefficient to balance the datasets. Then we adjust the hypocenter location and fault plane orientation. Lastly, we find the rupture propagation mechanism. In each step, we run tsunami modelling to validate run-up heights along the northern coast of Flores data from Tsuji et al. [1995b] and the waveform at Palopo tide gauge digitised from [Hidayat et al., 1995].

C.1 Weighting and smoothing

The teleseismic body and surface waves have about 3900 and 3200 data points (i.e., $N_s = 3900 + 3200$). In contrast, only eight uplift data available ($N_u = 8$). Therefore, we set the weight for body and surface waves at $\gamma_s = 1.0$. Then we test weighting for uplift (γ_u) from 1 to 500. Furthermore, a proper smoothing coefficient (β) between 0.01 and 1.0 are analysed to produce a spatially smooth slip distribution. Figure C.1 shows the variances result of this analysis for all datasets. Figure C.2 shows some slip distribution models correspond to the γ_u and β.

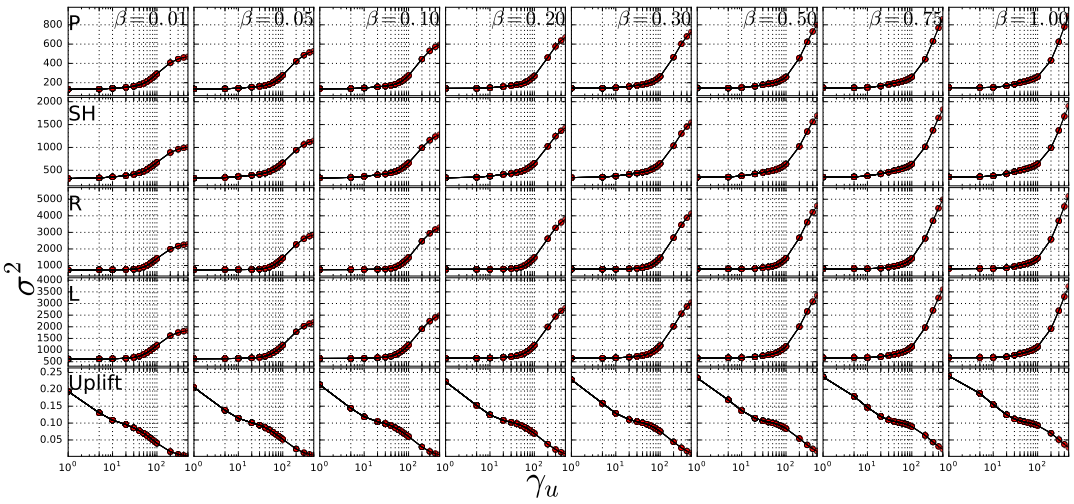

Figure C.1: Variance of weighting and smoothing

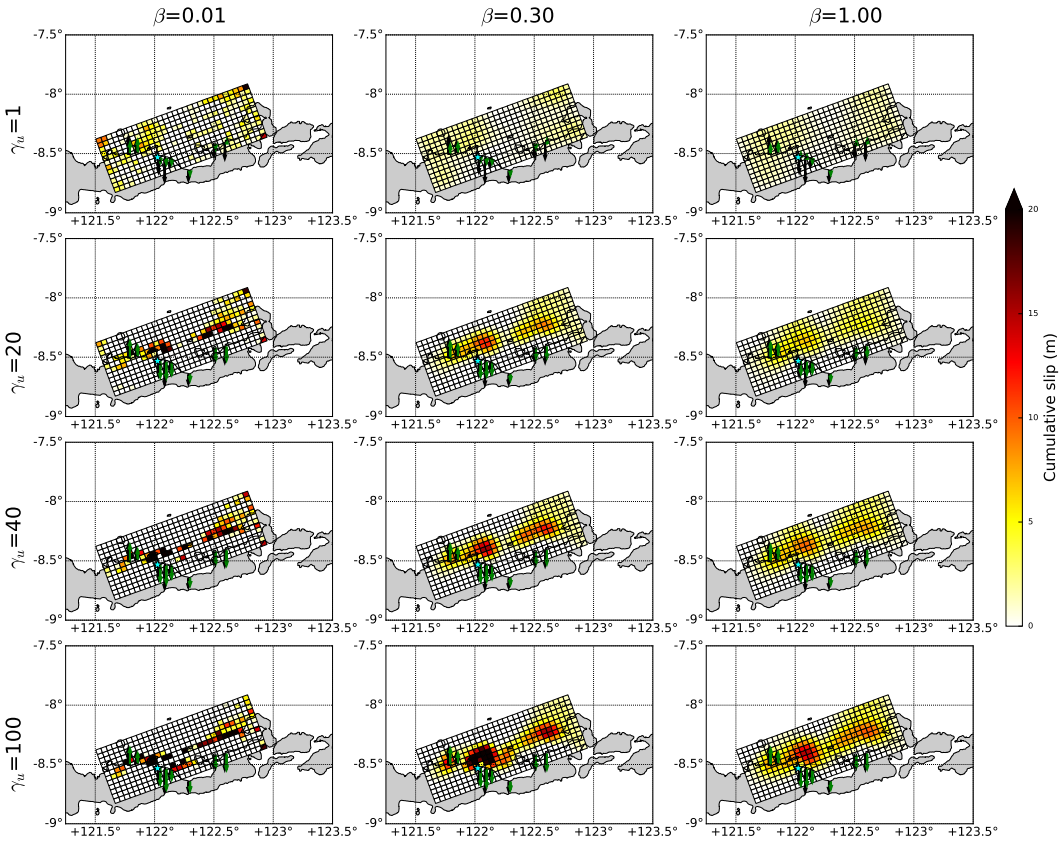

Figure C.2: Inverted cumulative slip from different γ_u and β. Black and green arrows are uplift data and predicted from the slip, respectively.

C.2 Effect of fault plane orientation

We also analyse the effect of moving the epicenter by 15 km from the original location in different directions. From previous the step, we decided that $\beta = 0.3$ is a good coefficient to produce smooth slips distributions. Since $\gamma_u = 20$ and $\gamma_{=}40$ are the limits between which both seismic and uplift data are fit well, we use both values for this analysis. Figure C.3 shows the variance values. Figure C.4 shows the uplift model. Figure C.5 and C.6 shows tsunami run-up heights and waveform comparisons.

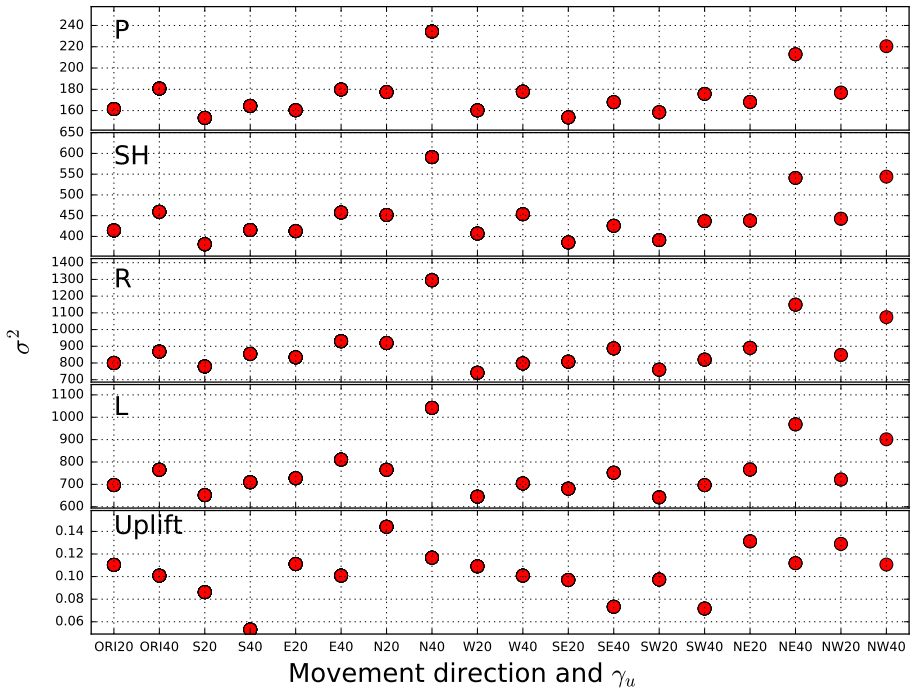

Figure C.3: Variance by moving the epicenter. *ORI* means original parameters. Letter(s) in front of the numbers show the direction. Numbers show the γ_u coefficient.

Furthermore, we analyse fault plane orientation: strike and dip angles together with epicenter depth (hypo depth) as well. We test strike angles of $50, 60, 70, 80, 90°$, dip angles of $18, 23, 28, 32, 37°$, and hypo depth of $10, 16, 20$ km. Figure C.7 and C.8 show the variances result. Figure C.9 shows the uplift modeled. Figure C.10 and C.11 show simulated tsunami run-up heights and waveform.

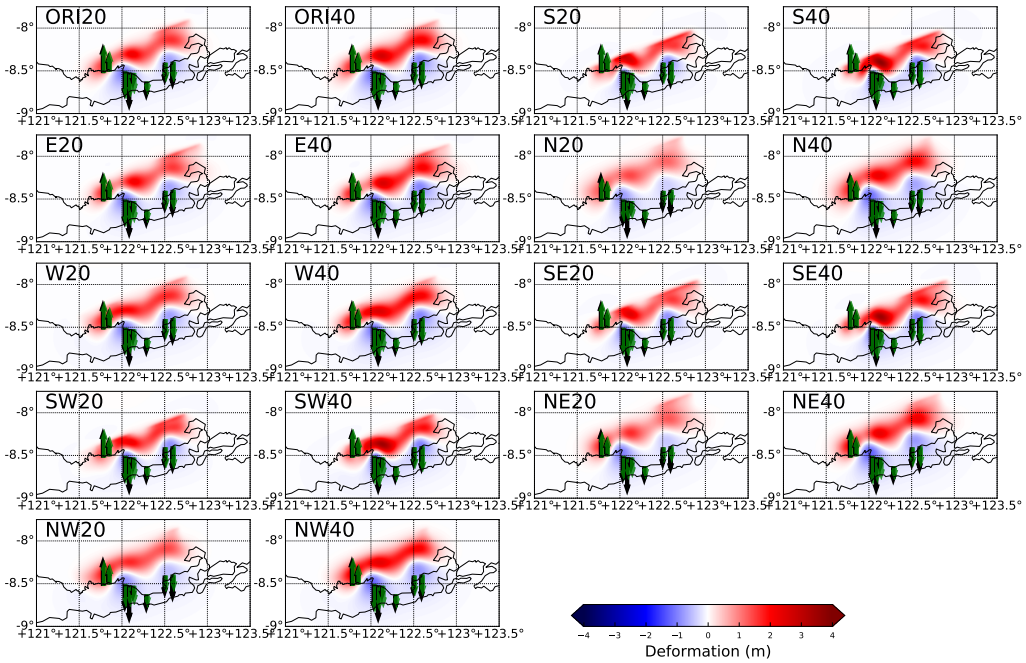

Figure C.4: Uplift models by moving the epicenter

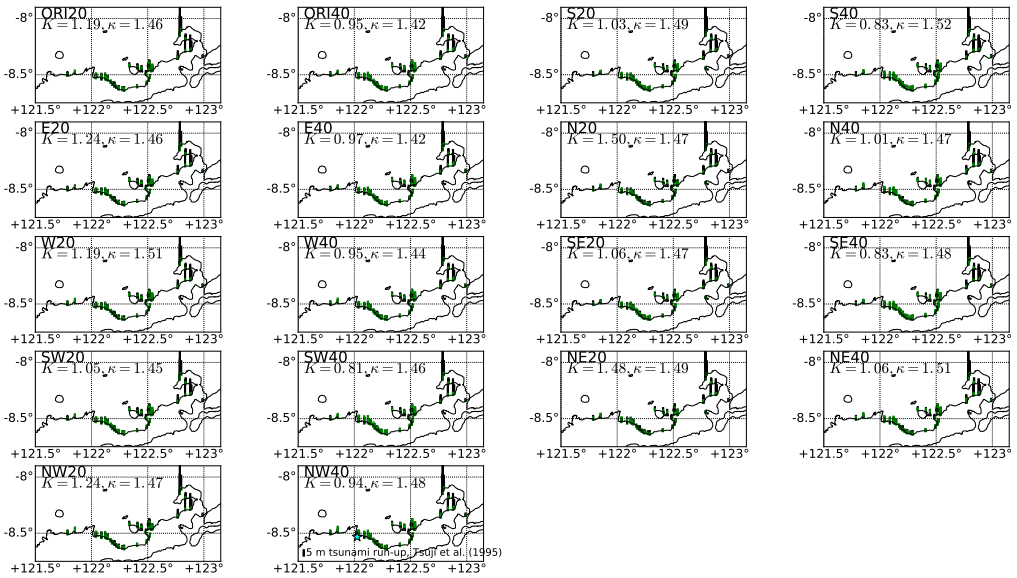

Figure C.5: Simulated tsunami run-up heights models by moving the epicenter. *ORI* = Original fault plane model, *S,E,NW,etc.* indicate the direction of the epicenter movement, and *20,40* are the γ_u. K and κ are Aida number (see Eq. 5.2.

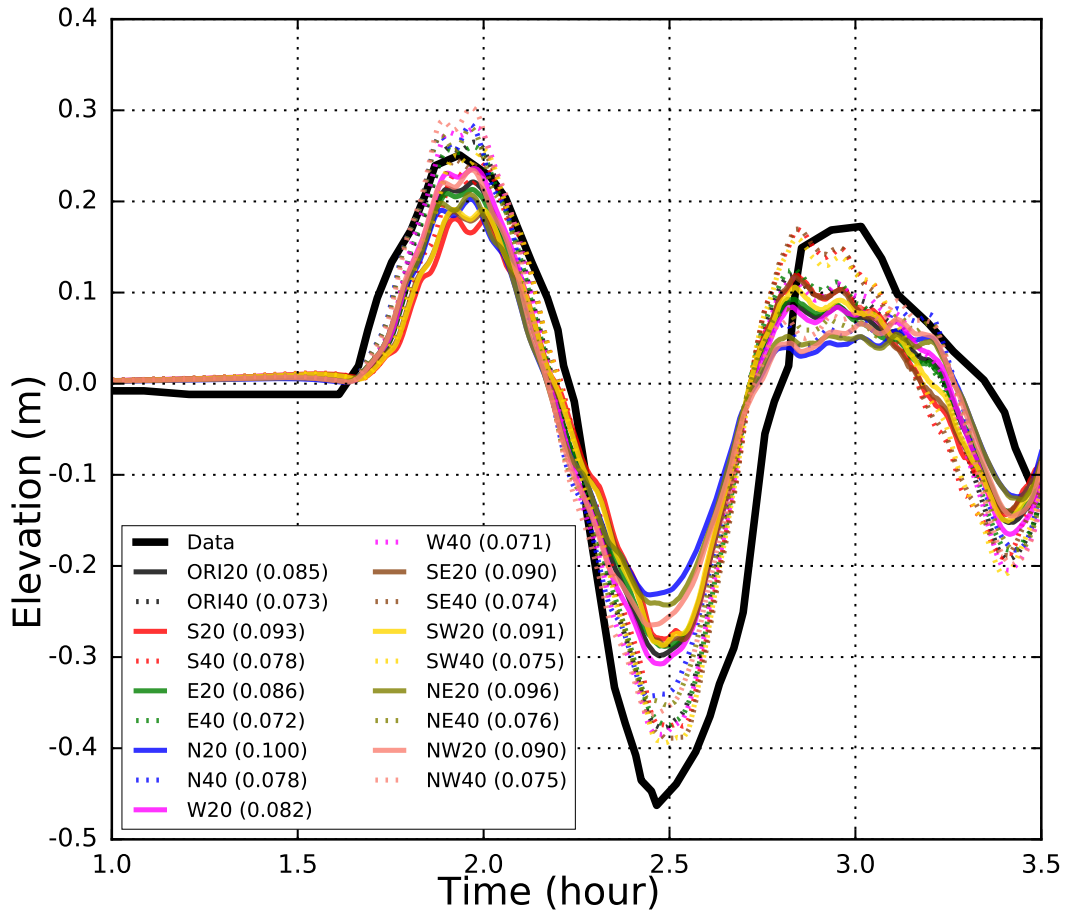

Figure C.6: Tsunami waveforms at Palopo tide gauge by moving the epicenter. Numbers on the legend are the RMS erros value for each models.

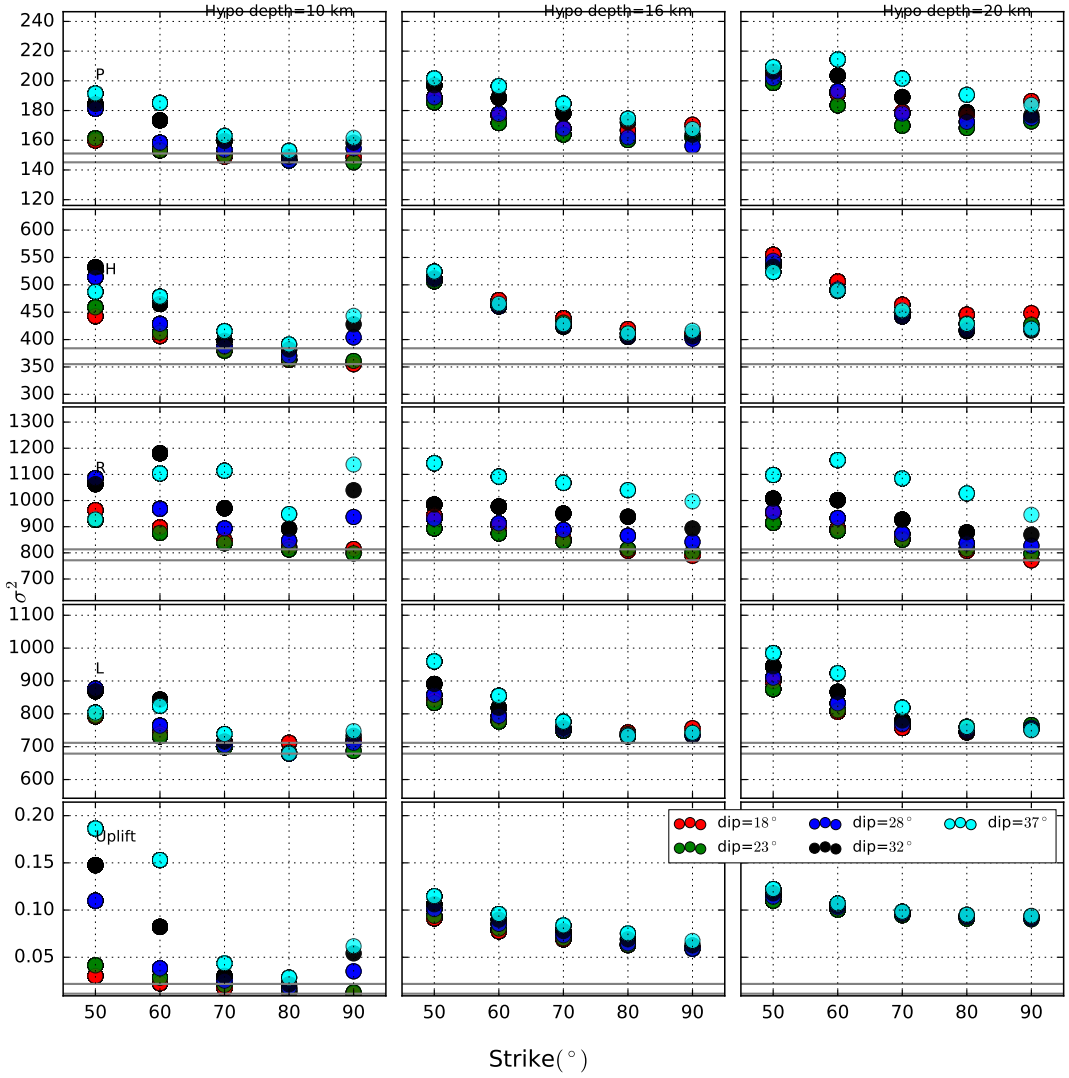

Figure C.7: Variances of the inversion by changing the fault plane orientation

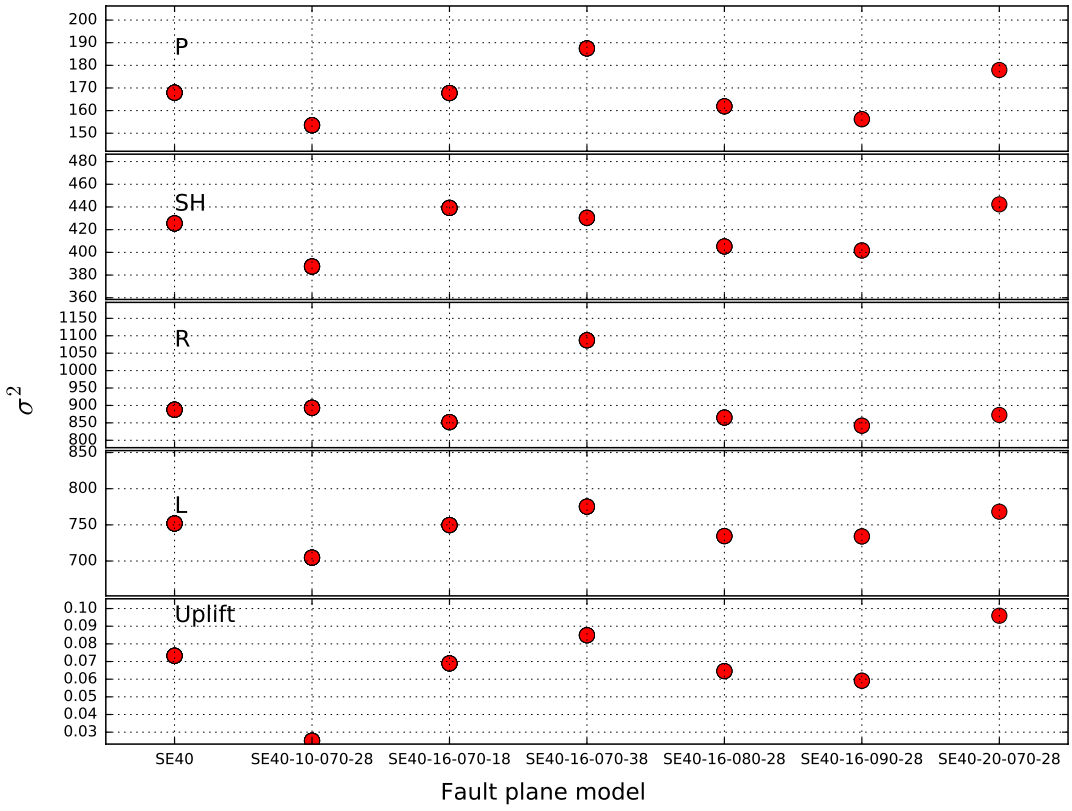

Figure C.8: Variance by varying the fault orientation. SE40 means original epicenter moved to SE with $\gamma = 40$. Numbers after this show *hypocenter depth - strike angle - dip angle*.

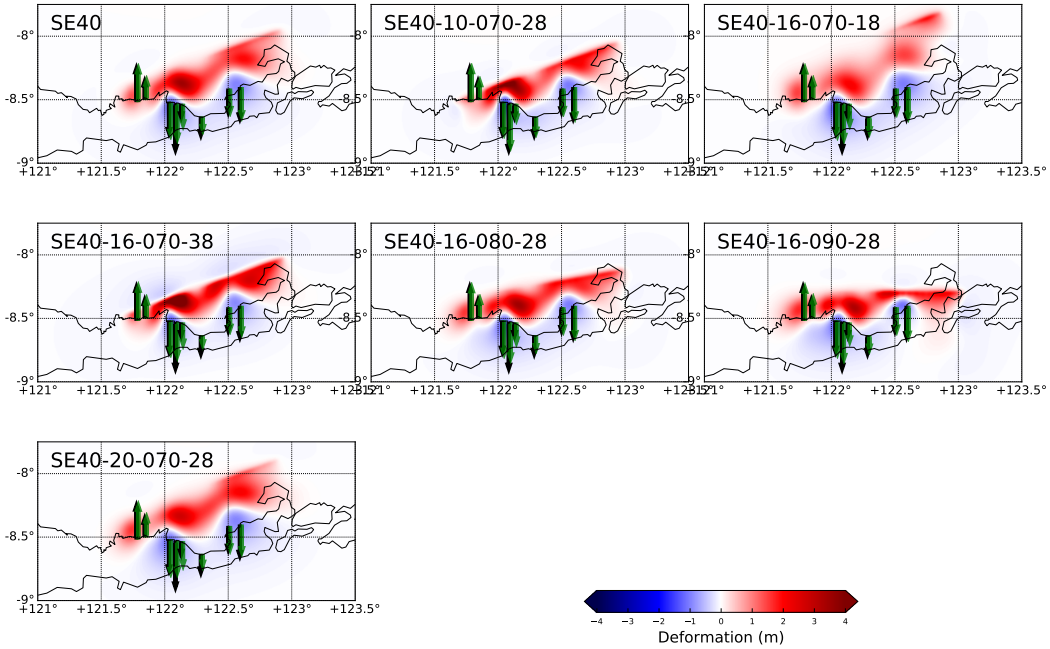

Figure C.9: Deformation models by changing the fault plane orientation

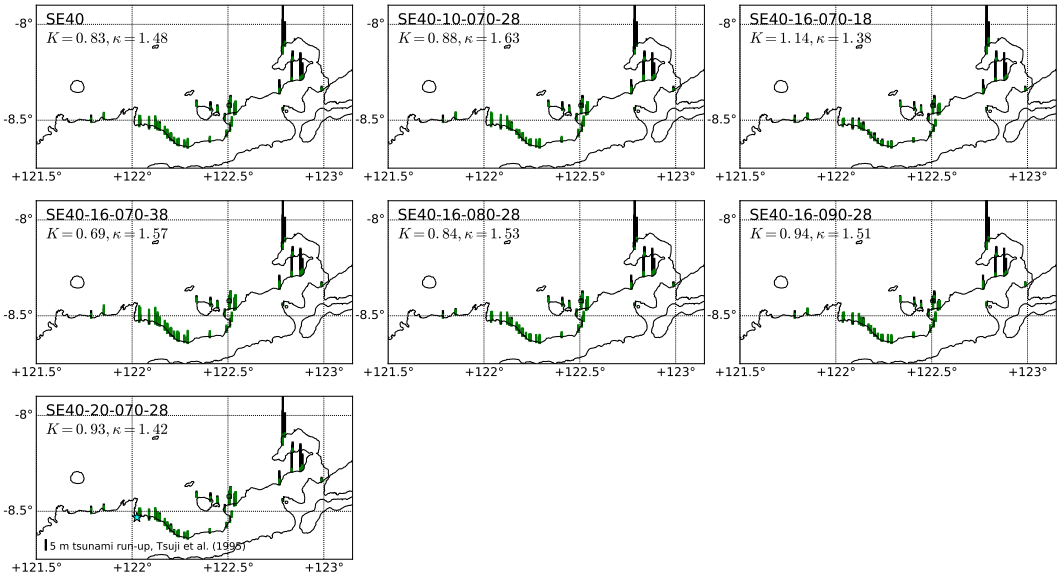

Figure C.10: Simulated tsunami run-up heights models by changing the fault plane orientation. *SE40* is the reference model, the result from moving the epicenter. Digits after *SE*40 are hypocenter depth - strike angle - dip angle. K and κ are Aida number (see Eq. 5.2).

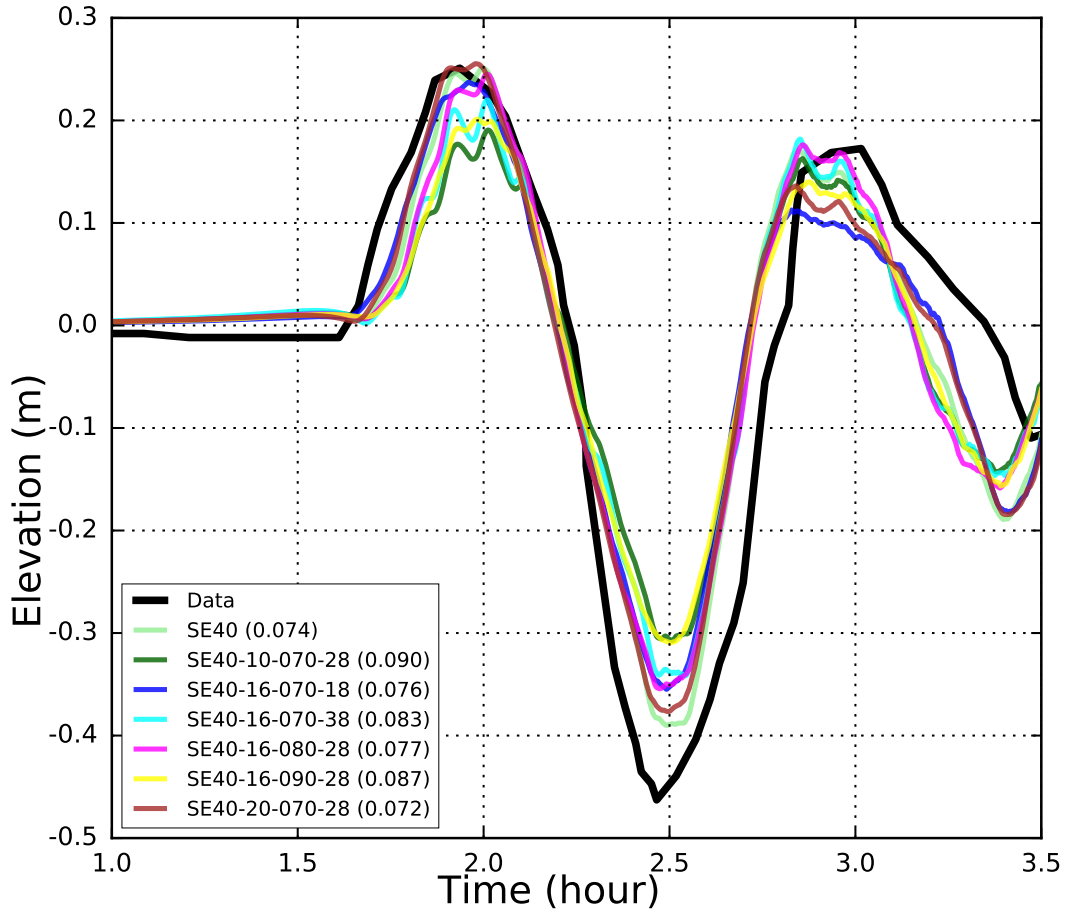

Figure C.11: Simulated tsunami waveforms at Palopo tide gauge by changing the fault plane orientation Numbers on the legend are the RMS erros value for each models.

C.3 Rupture propagation

Lastly, we analyse the rupture propagation parameters of NTW, Vr_{max}, and th. We test NTW = 3, 5, 7, 9, Vr_{max} = 1.5, 2.0, 2.5, 3.0, 3.5 $^{km}/_{s}$. Figure C.12 shows the variance results. Figure C.13 shows the estimated uplift model. Figure C.14 and C.15 are the simulated tsunami run-up heights and waveform.

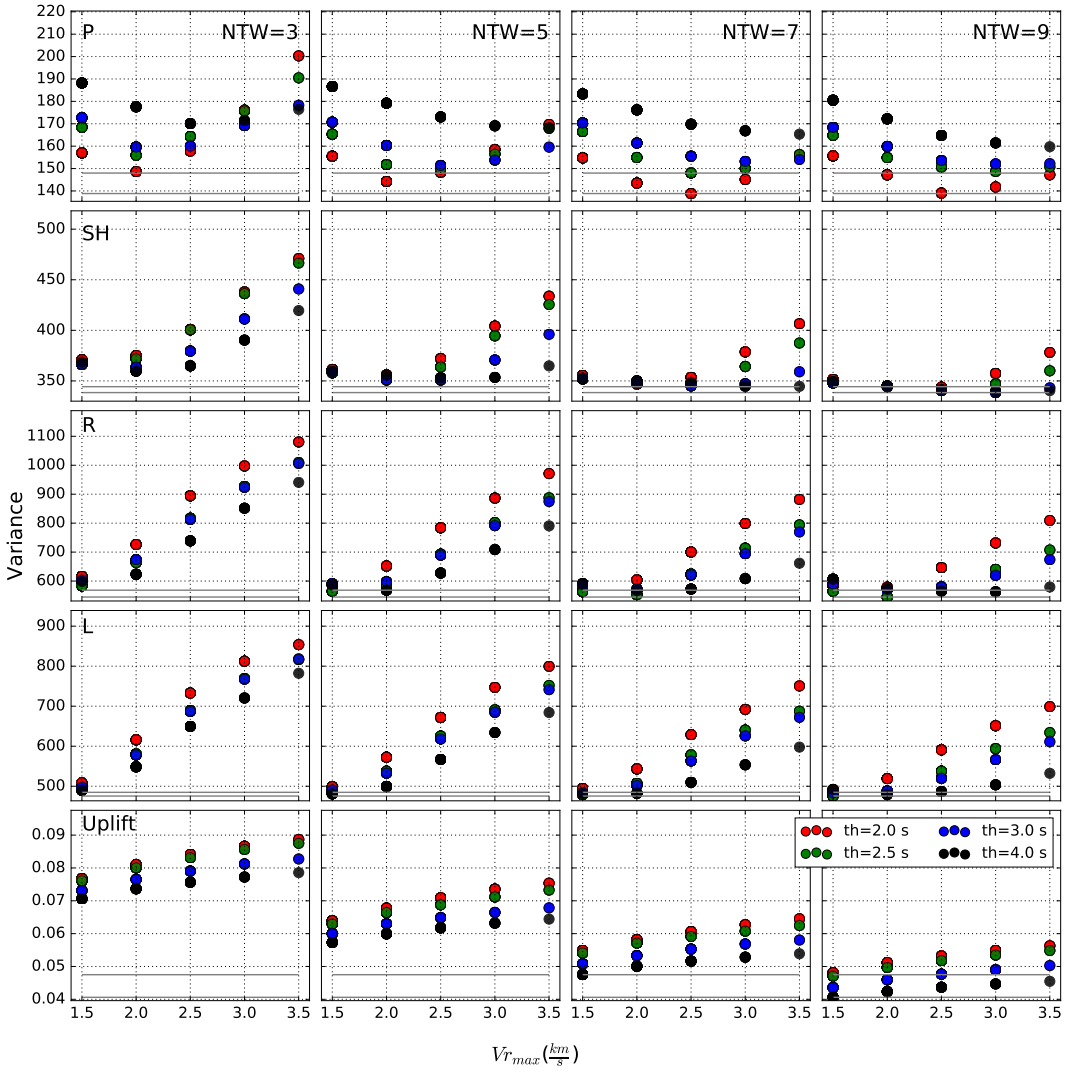

Figure C.12: Variance by varying the rupture propagation parameters

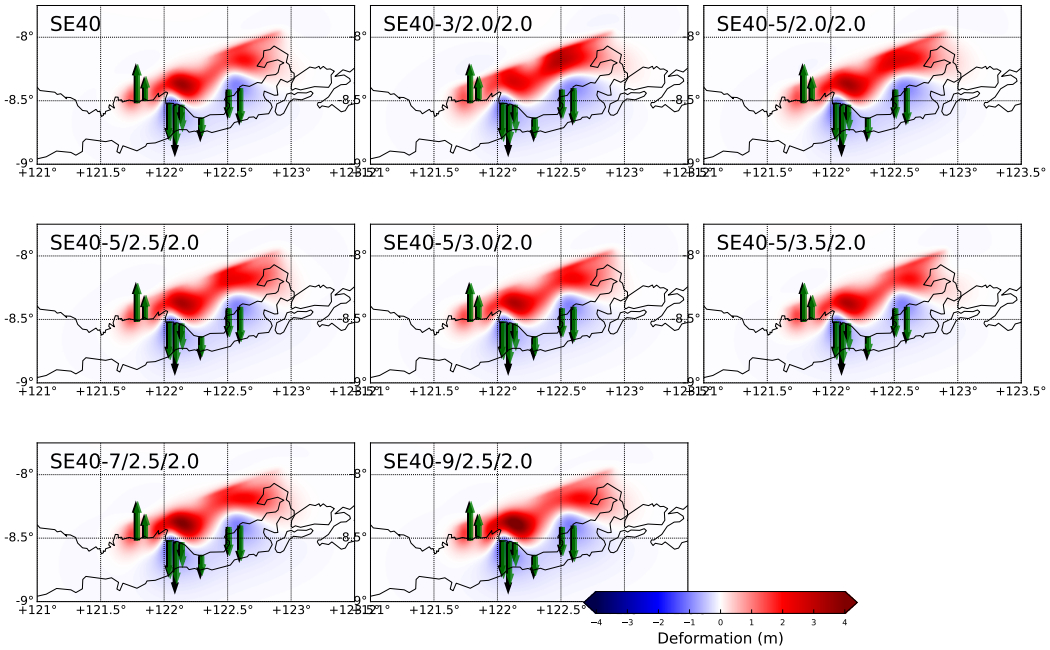

Figure C.13: Deformation models by changing the rupture propagation parameters

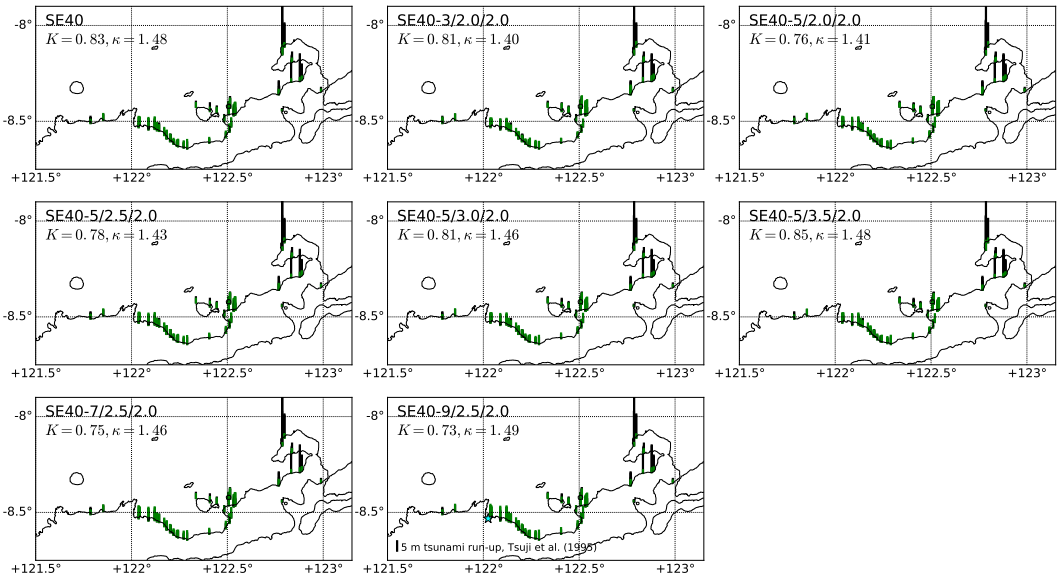

Figure C.14: Simulated tsunami run-up heights models by changing the rupture propagation parameters

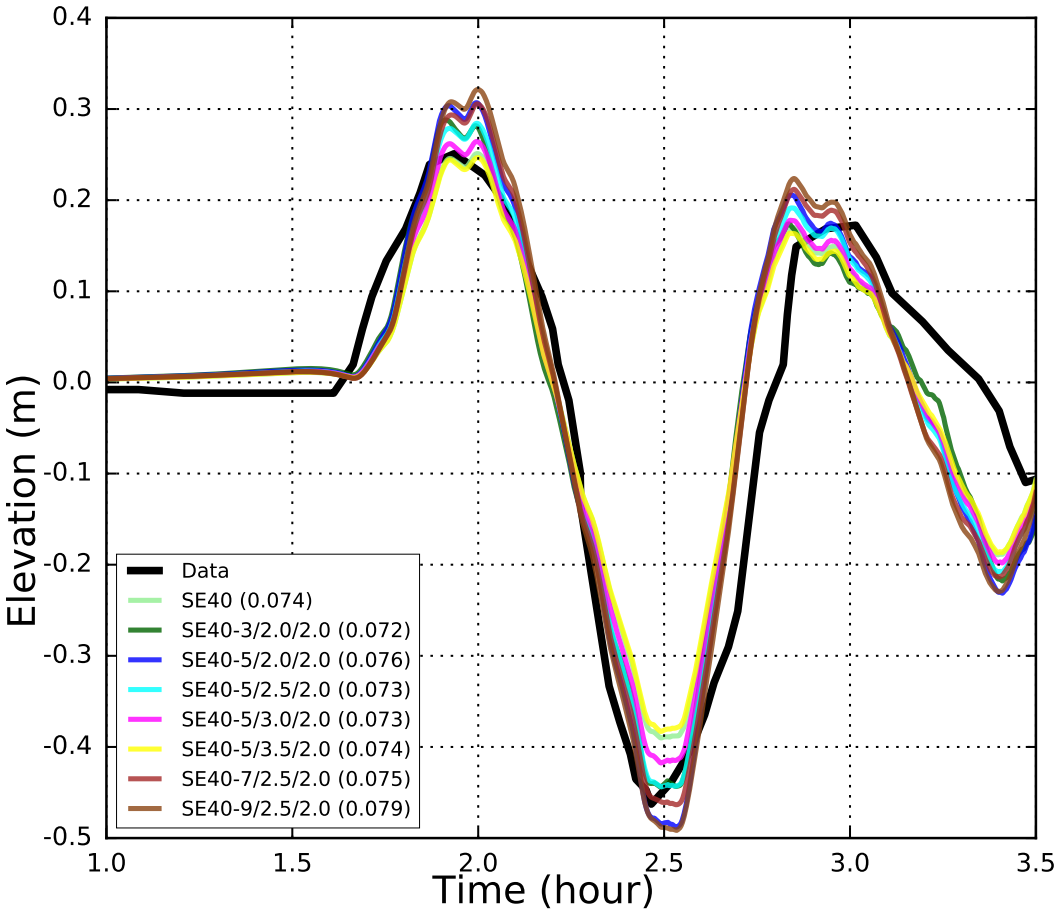

Figure C.15: Simulated tsunami waveforms at Palopo tide gauge by changing the rupture propagation parameters. Numbers on the legend are the RMS erros value for each models.

Bibliography

Abercrombie, R. E.; Antolik, M.; Felzer, K.; and Ekström, G., 2001. The 1994 Java tsunami earthquake: Slip over a subducting seamount. *Journal of Geophysical Research: Solid Earth*, 106, B4 (2001), 6595–6607. doi:10.1029/2000JB900403. (cited on page 28)

Abers, G. A., 1991. Possible seismogenic shallow-dipping normal faults in the Woodlark-Dentrecasteaux extensional province, Papua New Guinea. *Geology*, 19, 12 (Dec. 1991), 1205–1208. doi:10.1130/0091-7613(1991)019<1205:PSSDNF>2.3.CO;2. (cited on page 96)

Abers, G. A., 2001. Evidence for seismogenic normal faults at shallow dips in continental rifts. *Geological Society, London, Special Publications*, 187, 1 (2001), 305–318. doi:10.1144/GSL.SP.2001.187.01.15. (cited on page 96)

Abers, G. A.; Mutter, C. Z.; and Fang, J., 1997. Shallow dips of normal faults during rapid extension: Earthquakes in the Woodlark-D'Entrecasteaux rift system, Papua New Guinea. *Journal of Geophysical Research B: Solid Earth*, 102, B7 (Jan. 1997), 15301–15317. doi:10.1029/97JB00787. (cited on page 96)

Abrahamson, N.; Gregor, N.; and Addo, K., 2016. Bc hydro ground motion prediction equations for subduction earthquakes. *Earthquake Spectra*, 32, 1 (2016), 23–44. doi:10.1193/051712EQS188MR. (cited on page 131)

Aida, I., 1978. Reliability of a tsunami source model derived from fault parameters. *Journal of Physics of the Earth*, 26, 1 (1978), 57–73. doi:10.4294/jpe1952.26.57. (cited on page 108)

Allgeyer, S. and Cummins, P., 2014. Numerical tsunami simulation including elastic loading and seawater density stratification. *Geophysical Research Letters*, 41, 7 (2014), 2368–2375. doi:10.1002/2014GL059348. (cited on page 125)

Ammon, C. J.; Kanamori, H.; Lay, T.; and Velasco, A. A., 2006. The 17 July 2006 Java tsunami earthquake. *Geophysical Research Letters*, 33, 24 (2006). doi:10.1029/2006GL028005. (cited on pages 28 and 31)

Atkinson, G. M. and Kaka, S. I., 2007. Relationships between felt intensity and instrumental ground motion in the central united states and california. *Bulletin of the Seismological Society of America*, 97, 2 (2007), 497–510. doi:10.1785/0120060154. (cited on page 131)

Audley-Charles, M., 2011. Tectonic post-collision processes in Timor. *Geological Society, London, Special Publications*, 355, 1 (2011), 241–266. doi:10.1144/SP355.12. (cited on page 98)

Audley-Charles, M.; Carter, D.; Barber, A.; Norvick, M.; and Tjokrosapoetro, S., 1979. Reinterpretation of the geology of Seram: implications for the Banda Arcs and northern Australia. *Journal of the Geological Society*, 136, 5 (1979), 547–566. (cited on page 50)

Axen, G. J., 1999. Low-angle normal fault earthquakes and triggering. *Geophysical Research Letters*, 26, 24 (Dec. 1999), 3693–3696. doi:10.1029/1999GL005405. (cited on page 96)

Axen, G. J. and Karner, G., 2004. Mechanics of low-angle normal faults. *Rheology and deformation of the lithosphere at continental margins*, (2004), 46–91. (cited on page 96)

Baba, T.; Allgeyer, S.; Hossen, J.; Cummins, P. R.; Tsushima, H.; Imai, K.; Yamashita, K.; and Kato, T., 2017. Accurate numerical simulation of the far-field tsunami caused by the 2011 Tohoku earthquake, including the effects of Boussinesq dispersion, seawater density stratification, elastic loading, and gravitational potential change. *Ocean Modelling*, 111 (2017), 46–54. doi:10.1016/j.ocemod.2017.01.002. (cited on pages 66, 125, and 134)

Baba, T.; Cummins, P. R.; Thio, H. K.; and Tsushima, H., 2009. Validation and joint inversion of teleseismic waveforms for earthquake source models using deep ocean bottom pressure records: A case study of the 2006 Kuril megathrust earthquake. *Pure and Applied Geophysics*, 166, 1-2 (2009), 55–76. doi:10.1007/s00024-008-0438-1. (cited on page 107)

Baba, T.; Gon, Y.; Imai, K.; Yamashita, K.; Matsuno, T.; Hayashi, M.; and Ichihara, H., 2019. Modelling of a dispersive tsunami caused by a submarine landslide based on detailed bathymetry of the continental slope in Japan Nankai trough, southwest Japan. *Tectonophysics*, 768, 228182 (August 2019). doi:10.1016/j.tecto.2019.228182. (cited on pages 66, 90, 126, and 137)

Baba, T.; Takahashi, N.; Kaneda, Y.; Ando, K.; Matsuoka, D.; and Kato, T., 2015. Parallel implementation of dispersive tsunami wave modeling with a nesting algorithm for the 2011 Tohoku tsunami. *Pure and Applied Geophysics*, (Feb. 2015). doi:10.1007/s00024-015-1049-2. (cited on pages 66, 107, 125, and 134)

Beckers, J. and Lay, T., 1995. Very broadband seismic analysis of the 1992 Flores, Indonesia, earthquake (Mw = 7.9). *Journal of Geophysical Research: Solid Earth*, 100, B9 (1995), 18179–18193. doi:10.1029/95JB01689. (cited on pages 28, 97, 108, 109, 111, and 115)

Benavente, R. and Cummins, P. R., 2013. Simple and reliable finite fault solutions for large earthquakes using the w-phase: The Maule (Mw= 8.8) and Tohoku (Mw=

9.0) earthquakes. *Geophysical Research Letters*, 40, 14 (2013), 3591–3595. doi:10.1002/grl.50648. (cited on page 107)

Berninghausen, W., 1966. Tsunamis and seismic seiches seported from the regions adjacent to the Indian Ocean. *Bull, Seism. Soc. Am.*, 54 (1966), 439–442. (cited on page 18)

Berninghausen, W. H., 1969. Tsunamis and seismic seiches of Southeast Asia. *Bulletin of the Seismological Society of America*, 59, 1 (1969), 289–297. (cited on page 18)

Bevington, P. and Robinson, D. K., 1992. *Data reduction and error analysis for the physical sciences*. McGraw Hill, New York, New York, third edn. (cited on page 131)

BIG, B., 2018. Seamless Digital Elevation Model (DEM) dan Batimetri Nasional. online. www.tides.big.go.id/DEMNAS/. (cited on pages 128 and 134)

Bird, P., 2003. An update digital model of plate boundaries. *Geochemistry, Geophysics, Geosystems*, 4, 3 (March 2003). doi:10.1029/2001GC000252. (cited on pages xviii, 98, and 100)

BMKG, B., 2018a. *Katalog Gempa Bumi Merusak 1821-2017*. (cited on pages 8 and 19)

BMKG, B., 2018b. *Katalog Tsunami Indonesia Tahun 416-2017*. Jakarta. (cited on pages 19 and 28)

Boore, D. M.; Stewart, J. P.; Seyhan, E.; and Atkinson, G. M., 2014. Nga-west2 equations for predicting pga, pgv, and 5% damped psa for shallow crustal earthquakes. *Earthquake Spectra*, 30, 3 (2014), 1057–1085. doi:10.1193/070113EQS184M. (cited on page 131)

Borrero, J. C.; Weiss, R.; Okal, E. A.; Hidayat, R.; Arcas, D.; and Titov, V. V., 2009. The tsunami of 2007 September 12, Bengkulu Province, Sumatra, Indonesia: post-tsunami field survey and numerical modelling. *Geophysical Journal International*, 178, 1 (2009), 180–194. doi:10.1111/j.1365-246X.2008.04058.x. (cited on pages 28 and 31)

Bowin, C.; Purdy, G.; Johnston, C.; Shor, G.; Lawver, L.; Hartono, H.; and Jezek, P., 1980. Arc-continent collision in Banda Sea region. *AAPG Bulletin*, 64, 6 (1980), 868–915. (cited on page 79)

Breen, N. A.; Silver, E. A.; and Roof, S., 1989. The Wetar Back Arc Thrust Belt, eastern Indonesia: The effect of accretion against an irregularly shaped arc. *Tectonics*, 8, 1 (1989), 85–98. doi:10.1029/TC008i001p00085. (cited on pages xviii, 7, and 100)

Brouwer, H., 1921. Some relations of earthquakes to geologic structure in the East Indian Archipelago. *Bulletin of the Seismological Society of America*, 11, 3-4 (1921), 166–182. (cited on pages 61, 62, and 67)

Brune, S.; Babeyko, A.; Ladage, S.; and Sobolev, S., 2010. Landslide tsunami hazard in the Indonesian Sunda Arc. *Natural Hazards and Earth System Sciences*, 10, 3 (2010), 589–604. doi:10.5194/nhess-10-589-2010. (cited on page 122)

Chiou, B. S.-J. and Youngs, R. R., 2014. Update of the chiou and youngs nga model for the average horizontal component of peak ground motion and response spectra. *Earthquake Spectra*, 30, 3 (2014), 1117–1153. doi:10.1193/072813EQS219M. (cited on page 131)

Chlieh, M.; Avouac, J.-P.; Sieh, K.; Natawidjaja, D. H.; and Galetzka, J., 2008. Heterogeneous coupling of the Sumatran megathrust constrained by geodetic and paleogeodetic measurements. *Journal of Geophysical Research: Solid Earth*, 113, B5 (2008). doi:10.1029/2007JB004981. (cited on page 123)

Cipta, A.; Oman, A.; Supartoyo, S.; Minarno, P.; Solikhin, A.; Falah, F.; and Efendi, R., 2018. *Anomali perilaku gelombang tsunami*, chap. Di Balik Pesona Palu, 133–142. Badan Geologi, Bandung, Indonesia, 1 edn. (cited on pages 28 and 39)

Cipta, A.; Robiana, R.; Griffin, J.; Horspool, N.; Hidayati, S.; and Cummins, P. R., 2017. A probabilistic seismic hazard assessment for Sulawesi, Indonesia. *Geological Society, London, Special Publications*, 441, 1 (2017), 133–152. doi:10.1144/SP441.6. (cited on page 8)

Collettini, C. and Sibson, R. H., 2001. Normal faults, normal friction? *Geology*, 29, 10 (Oct. 2001), 927–930. doi:10.1130/0091-7613(2001)029<0927:NFNF>2.0.CO;2. (cited on page 96)

Coordinating Ministry for Economic Affairs, R. o. I., 2011. *Masterplan for acceleration and expansion of Indonesia economic development 2011 - 2025*. Coordinating Ministry for Economic Affairs, Indonesia. ISBN 978-979-3754-14-7. (cited on page 3)

Cox, D. C., 1970. Discussion of âĂIJtsunamis and seismic seiches of Southeast Asiaâ Ăİ by William H. Berninghausen. *Bulletin of the Seismological Society of America*, 60, 1 (1970), 281–287. (cited on page 18)

Daryono, M. R.; Natawidjaja, D. H.; Sapiie, B.; and Cummins, P., 2019. Earthquake geology of the Lembang Fault, West Java, Indonesia. *Tectonophysics*, 751 (2019), 180–191. doi:10.1016/j.tecto.2018.12.014. (cited on page 122)

Davies, G.; Griffin, J.; Løvholt, F.; Glimsdal, S.; Harbitz, C.; Thio, H. K.; Lorito, S.; Basili, R.; Selva, J.; Geist, E.; and Baptista, M. A., 2018. A global probabilistic tsunami hazard assessment from earthquake sources. *Geological Society, London, Special Publications*, 456, 1 (2018), 219–244. doi:10.1144/SP456.5. (cited on pages xv, 1, and 3)

Davies, H. L.; Davies, J. M.; Perembo, R. C. B.; and Lus, W. Y., 2003. *The Aitape 1998 Tsunami: Reconstructing the Event from Interviews and Field Mapping*, 1895–1922.

Birkhäuser Basel, Basel. ISBN 978-3-0348-7995-8. doi:{10.1007/978-3-0348-7995-8_7}. (cited on page 63)

de Wit, H. C., 1952. In memory of GE Rumphius (1702-1952). *Taxon*, (1952), 101–110. doi:10.2307/1217885. (cited on page 54)

DeMets, C.; Gordon, R. G.; and Argus, D. F., 2010. Geologically current plate motions. *Geophysical Journal International*, 181, 1 (2010), 1–80. doi:10.1111/j.1365-246X.2009.04491.x. (cited on page 7)

detikNews, 2018. BNPB ralat jumlah korban meninggal tsunami Selat Sunda jadi 426 orang. website. https://news.detik.com/berita/d-4362536/bnpb-ralat-jumlah-korban-meninggal-tsunami-selat-sunda-jadi-426-orang. Last accessed 1 July 2019. (cited on page 31)

Dowrick, D. and Rhoades, D., 2005. Revised models for attenuation of modified mercalli intensity in new zealand earthquakes. *Bulletin of the New Zealand Society for Earthquake Engineering*, 38, 4 (2005), 185–214. (cited on pages xviii, 85, and 87)

Ekström, G.; Nettles, M.; and Dziewoński, A., 2012. The global cmt project 2004–2010: Centroid-moment tensors for 13,017 earthquakes. *Physics of the Earth and Planetary Interiors*, 200 (2012), 1–9. doi:10.1016/j.pepi.2012.04.002. (cited on page 37)

Ekström, G.; Tromp, J.; and Larson, E. W., 1997. Measurements and global models of surface wave propagation. *Journal of Geophysical Research: Solid Earth*, 102, B4 (1997), 8137–8157. (cited on page 107)

Fisher, T. and Harris, R., 2016. Reconstruction of 1852 Banda Arc megathrust earthquake and tsunami. *Natural Hazards*, 83, 1 (2016), 667–689. doi:10.1007/s11069-016-2345-6. (cited on pages xviii, xx, 28, 47, 77, 79, 81, 84, 85, 87, 88, 89, 91, 92, 96, 119, 135, and 136)

Fritz, H. M.; Kongko, W.; Moore, A.; McAdoo, B.; Goff, J.; Harbitz, C.; Uslu, B.; Kalligeris, N.; Suteja, D.; Kalsum, K.; et al., 2007. Extreme runup from the 17 July 2006 Java tsunami. *Geophysical Research Letters*, 34, 12 (2007). doi:10.1029/2007GL029404. (cited on pages 28 and 31)

Fujii, Y. and Satake, K., 2008. Tsunami waveform inversion of the 2007 Bengkulu, southern Sumatra, earthquake. *Earth, planets and space*, 60, 9 (2008), 993–998. doi:10.1186/BF03352856. (cited on pages 28 and 31)

Fujii, Y.; Satake, K.; and Nishimae, Y., 2011. Observation and modeling of the January 2009 West Papua, Indonesia tsunami. *Pure and applied geophysics*, 168, 6-7 (2011), 1089–1100. doi:10.1007/s00024-010-0220-z. (cited on pages 28 and 46)

Giachetti, T.; Paris, R.; Kelfoun, K.; and Ontowirjo, B., 2012. Tsunami hazard related to a flank collapse of Anak Krakatau volcano, Sunda Strait, Indonesia.

Geological Society, London, Special Publications, 361, 1 (2012), 79–90. doi:10.1144/SP361.7. (cited on page 75)

Giyanto; Abrar, M.; Hadi, T. A.; Budiyanto, A.; Hafizt, M.; Salatalohy, A.; and Iswari, M. Y., 2017. *Status terumbu karang Indonesia 2017*. Pusat Penelitian Oseanografi - Lembaga Ilmu Pengetahuan Indonesia, Jakarta Utara, Indonesia. Bahasa Indonesia. (cited on page 123)

Glade, T.; Albini, P.; and FrancÃl's, F., 2001. An introduction to the use of historical data in natural hazard assessments. In *The use of historical data in natural hazard assessments* (Eds. T. Glade; P. Albini; and F. Frances), vol. 17. Kluwer Academic Publishers, Boston;Dordrecht;. ISBN 0792371542;9780792371540;. (cited on page 4)

Gomez, J.; Madariaga, R.; Walpersdorf, A.; and Chalard, E., 2000. The 1996 earthquakes in Sulawesi, Indonesia. *Bulletin of the Seismological Society of America*, 90, 3 (2000), 739–751. doi:10.1785/0119990055. (cited on page 28)

Gonzalez, F.; Sutisna, S.; Hadi, P.; Bernard, E.; and Winarso, P., 1993. Some observations related to the Flores Island earthquake and tsunami. In *TSUNAMI*. International Tsunami Symposium, Wakayama, Japan. (cited on page 103)

Grezio, A.; Babeyko, A.; Baptista, M. A.; Behrens, J.; Costa, A.; Davies, G.; Geist, E. L.; Glimsdal, S.; González, F. I.; Griffin, J.; et al., 2017. Probabilistic tsunami hazard analysis: Multiple sources and global applications. *Reviews of Geophysics*, 55, 4 (2017), 1158–1198. doi:10.1002/2017RG000579. (cited on page 123)

Griffin, J.; Latief, H.; Kongko, W.; Harig, S.; Horspool, N.; Hanung, R.; Rojali, A.; Maher, N.; Fuchs, A.; Hossen, J.; Upi, S.; Edi, D.; Rakowsky, N.; and Cummins, P., 2015. An evaluation of onshore digital elevation models for modelling tsunami inundation zones. *Frontiers in Earth Science*, 3 (2015). doi:10.3389/feart.2015.00032. (cited on pages xix, 28, 97, 103, 104, 111, 112, 113, 122, and 134)

Griffin, J.; Nguyen, N.; Cummins, P.; and Cipta, A., 2018. Historical earthquakes of the Eastern Sunda Arc: Source mechanisms and intensity-based testing of IndonesiaâĂŹs National Seismic Hazard Assessment. *Bulletin of the Seismological Society of America*, 109, 1 (2018), 43–65. doi:10.1785/0120180085. (cited on pages 85, 96, 99, and 131)

Grilli, S. T.; Tappin, D. R.; Carey, S.; Watt, S. F.; Ward, S. N.; Grilli, A. R.; Engwell, S. L.; Zhang, C.; Kirby, J. T.; Schambach, L.; et al., 2019. Modelling of the tsunami from the December 22, 2018 lateral collapse of Anak Krakatau volcano in the Sunda Straits, Indonesia. *Scientific reports*, 9, 1 (2019), 1–13. doi:10.1038/s41598-019-48327-6. (cited on page 31)

Gunawan, E.; Kholil, M.; and Meilano, I., 2016. Splay-fault rupture during the 2014 Mw7. 1 Molucca Sea, Indonesia, earthquake determined from GPS measurements. *Physics of the Earth and Planetary Interiors*, 259 (2016), 29–33. doi:10.1016/j.pepi.2016.08.009. (cited on pages 28 and 44)

Gusman, A.; Tanioka, Y.; Kobayashi, T.; Latief, H.; and Pandoe, W., 2010. Slip distribution of the 2007 Bengkulu earthquake inferred from tsunami waveforms and InSAR data. *Journal of Geophysical Research: Solid Earth*, 115, B12 (2010). doi:10.1029/2010JB007565. (cited on pages 28 and 31)

Gusman, A.; Tanioka, Y.; MacInnes, B.; and Tsushima, H., 2014. A methodology for nearâĂŘfield tsunami inundation forecasting: Application to the 2011 Tohoku tsunami. *Journal of Geophysical Research: Solid Earth*, 119, 11 (2014), 8186–8206. doi:10.1002/2014JB010958. (cited on page 108)

Gusman, A. R.; Nugraha, A. D.; and Shiddiqi, H. A., 2017a. Hypocenter relocations and tsunami simulation for the 15 November 2014 Northern Molucca Sea earthquake in Indonesia. *Jurnal Geofisika*, 15, 1 (2017), 1–9. https://jurnal-geofisika.or.id/index.php/jurnal-geofisika/article/view/29. (cited on pages 28 and 44)

Gusman, A. R.; Satake, K.; and Harada, T., 2017b. Rupture process of the 2016 wharton basin strike-slip faulting earthquake estimated from joint inversion of teleseismic and tsunami waveforms. *Geophysical Research Letters*, 44, 9 (2017), 4082–4089. doi:10.1002/2017GL073611. (cited on page 31)

Gusman, A. R. and Tanioka, Y., 2014. W-phase inversion and tsunami inundation modeling for tsunami early warning: Case study for the 2011 Tohoku event. *Pure and Applied Geophysics*, 171, 7 (2014), 1409–1422. doi:10.1007/s00024-013-0680-z. (cited on page 107)

Hall, R., 2011. Australia–SE Asia collision: plate tectonics and crustal flow. *Geological Society, London, Special Publications*, 355, 1 (2011), 75–109. doi:10.1144/SP355.5. (cited on page 93)

Hall, R., 2012. Late jurassic–cenozoic reconstructions of the Indonesian region and the Indian Ocean. *Tectonophysics*, 570 (2012), 1–41. doi:10.1016/j.tecto.2012.04.021. (cited on page 93)

Hall, R. and Spakman, W., 2015. Mantle structure and tectonic history of SE Asia. *Tectonophysics*, 658 (2015), 14–45. doi:10.1016/j.tecto.2015.07.003. (cited on pages 77, 78, and 79)

Hamilton, W., 1979. *Tectonics of the Indonesian region*. United States Government Printing Office, Washington, 4^{th} edn. (cited on pages xviii, 3, 7, 49, 50, 79, 98, and 100)

Hananto, N.; Boudarine, A.; Carton, H.; Singh, S. C.; Avianto, P.; Dyment, J.; Qin, Y.; Ghosal, D.; Zuraida, R.; Tapponnier, P. E.; Deplus, C.; and Sieh,

K., 2018. Evidence of pervasive trans-tensional deformation in the northwestern Wharton Basin in the 2012 earthquakes rupture area. *Earth and Planetary Science Letters*, 502 (2018), 174 – 186. doi:https://doi.org/10.1016/j.epsl.2018.09.007. http://www.sciencedirect.com/science/article/pii/S0012821X18305387. (cited on page 31)

Harig, S.; Immerz, A.; Weniza; Griffin, J.; Weber, B.; Babeyko, A.; Rakowsky, N.; Hartanto, D.; Nurokhim, A.; Handayani, T.; and Weber, R., 2019. The tsunami scenario datadata of the Indonesia Tsunami Early Warning System (InaTEWS): Evolution of the coverage and the involved modeling approaches. *Pure and Applied Geophysics*, (September 2019). doi:10.1007/s00024-019-02305-1. (cited on page 1)

Harris, R. and Major, J., 2017. Waves of destruction in the East Indies: the Wichmann catalogue of earthquakes and tsunami in the Indonesian region from 1538 to 1877. *Geological Society, London, Special Publications*, 441, 1 (2017), 9–46. doi:10.1144/SP441.2. (cited on pages 15, 17, 19, 34, 35, 36, 45, 50, 61, 81, and 118)

Hayes, G., 2017. Preliminary finite fault results for the Dec 12, 1992 Mw 7.7 - 8.5100,121.8900 earthquake (version 1). https://earthquake.usgs.gov/earthquakes/eventpage/usp0005j5a. (cited on pages xix, 111, 112, and 113)

Hébert, H.; Burg, P.-E.; Binet, R.; Lavigne, F.; Allgeyer, S.; and Schindelé, F., 2012. The 2006 July 17 Java (Indonesia) tsunami from satellite imagery and numerical modelling: a single or complex source? *Geophysical Journal International*, 191, 3 (12 2012), 1255–1271. doi:10.1111/j.1365-246X.2012.05666.x. (cited on page 31)

Heidarzadeh, M.; Krastel, S.; and Yalciner, A. C., 2014. The state-of-the-art numerical tools for modeling landslide tsunamis: A short review. In *Submarine mass movements and their consequences*, 483–495. Springer. doi:10.1007/978-3-319-00972-8_43. (cited on page 127)

Heidarzadeh, M. and Satake, K., 2014. Possible sources of the tsunami observed in the northwestern Indian Ocean following the 2013 September 24 Mw 7.7 Pakistan inland earthquake. *Geophysical Journal International*, 199, 2 (2014), 752–766. doi:10.1093/gji/ggu297. (cited on page 132)

Henry, C. and Das, S., 2002. The mw 8.2, 17 February 1996 Biak, Indonesia, earthquake: Rupture history, aftershocks, and fault plane properties. *Journal of Geophysical Research: Solid Earth*, 107, B11 (2002). doi:10.1029/2001JB000796. (cited on pages 28 and 46)

Hidayat, D.; Barker, J.; and Satake, K., 1995. Modeling the seismic source and tsunami generation of the December 12, 1992 Flores Island, Indonesia, earthquake. *Pure and Applied Geophysics*, 144, 3-4 (1995), 537–554. doi:10.1007/BF00874382. (cited on pages xix, 28, 97, 102, 103, 105, 111, 112, 113, and 143)

Hill, E. M.; Borrero, J. C.; Huang, Z.; Qiu, Q.; Banerjee, P.; Natawidjaja, D. H.; Elosegui, P.; Fritz, H. M.; Suwargadi, B. W.; Pranantyo, I. R.; et al., 2012.

The 2010 Mw 7.8 Mentawai earthquake: Very shallow source of a rare tsunami earthquake determined from tsunami field survey and near-field gps data. *Journal of Geophysical Research: Solid Earth*, 117, B6 (2012). doi:10.1029/2012JB009159. (cited on pages 28, 31, and 107)

Honthaas, C.; Réhault, J.-P.; Maury, R. C.; Bellon, H.; Hémond, C.; Malod, J.-A.; Cornée, J.-J.; Villeneuve, M.; Cotten, J.; Burhanuddin, S.; et al., 1998. A neogene back-arc origin for the Banda Sea basins: geochemical and geochronological constraints from the Banda ridges (East Indonesia). *Tectonophysics*, 298, 4 (1998), 297–317. doi:10.1016/S0040-1951(98)00190-5. (cited on page 50)

Hornbach, M. J.; Braudy, N.; Briggs, R. W.; Cormier, M.-H.; Davis, M. B.; Diebold, J. B.; Dieudonne, N.; Douilly, R.; Frohlich, C.; Gulick, S. P.; et al., 2010. High tsunami frequency as a result of combined strike-slip faulting and coastal landslides. *Nature Geoscience*, 3, 11 (2010), 783. doi:10.1039/ngeo975. (cited on page 9)

Horspool, N.; Pranantyo, I.; Griffin, J.; Latief, H.; Natawidjaja, D.; Kongko, W.; Cipta, A.; Bustaman, B.; Anugrah, S.; and Thio, H., 2014. A probabilistic tsunami hazard assessment for Indonesia. *Natural Hazards and Earth System Sciences*, 14, 11 (2014), 3105–3122. doi:10.5194/nhess-14-3105-2014. (cited on pages 1, 61, 66, 118, and 123)

Iida, K., 1983. Some remarks on the occurrence of tsunamigenic earthquakes around the Pacific. *Tsunamis: Their Science and Engineering*, (1983), 61–76. (cited on page 18)

Imamura, F. and Imteaz, M., 1995. Long waves in two-layers: governing equations and numerical model. *Science Tsunami Hazards*, 13 (1995), 3–24. (cited on pages 90, 126, 127, and 137)

Imamura, F. and Kikuchi, M., 1994. Moment release of the 1992 Flores Island earthquake inferred from tsunami and teleseismic data. *Science Tsunami Hazards*, 12 (1994), 67–76. (cited on pages xix, 97, 111, 112, and 113)

Imamura, F.; Subandono, D.; Watson, G.; Moore, A.; Takahashi, T.; Matsutomi, H.; and Hidayat, R., 1997. Irian Jaya earthquake and tsunami cause serious damage. *Eos, Transactions American Geophysical Union*, 78, 19 (1997), 197–201. doi:10.1029/97EO00128. (cited on pages xvi, 28, 45, and 46)

Indonesia Kaya, 2019. Satu benteng dan banyak kisah di dalamnya. Website. https://www.indonesiakaya.com/jelajah-indonesia/detail/satu-benteng-dan-banyak-kisah-di-dalamnya. Last accessed on 13 June 2019. (cited on pages xvii and 74)

Ioki, K.; Tanioka, Y.; Yanagisawa, H.; and Kawakami, G., 2019. Numerical simulation of the landslide and tsunami due to the 1741 oshima-oshima eruption in

hokkaido, japan. *Journal of Geophysical Research: Solid Earth*, 124, 2 (2019), 1991–2002. doi:10.1029/2018JB016166. (cited on page 127)

IRIS, I., 2018. Iris - wilber 3 dataset. www.iris.edu. (cited on page 108)

Irsyam, M.; Sengara, I.; Aldiamar, F.; Widyantoro, S.; Triyoso, W.; Natawidjaja, D.; Kertapati, E.; Meilano, I.; Suhardjono; Asrurifak, M.; and Ridwan, M., 2010. Summary of study: Development of seismic hazard maps of Indonesia for revision of hazard map in SNI 03-1726-2002. Technical report, Team for Revision of Seismic Hazard Maps of Indonesia, Bandung. (cited on pages 61, 66, 118, and 123)

ITIC, I., 2006. Seram Indonesia, Mw=6.7, 14 March 2006. http://itic.ioc-unesco.org/images/docs/overview_14mar2006_Seram_Indonesia.pdf. Last accessed 19 May 2019. (cited on pages 28 and 42)

Jarvis, A.; Reuter, H.; Nelson, A.; and Guevara, E., 2008. Hole-filled SRTM for the globe version 4, available from the CGIAR-CSI SRTM 90m Database. online. http://srtm.csi.cgiar.org/srtmdata/. (cited on pages 128 and 134)

Johnson, J. M.; Satake, K.; Holdahl, S. R.; and Sauber, J., 1996. The 1964 Prince William sound earthquake: Joint inversion of tsunami and geodetic data. *Journal of Geophysical Research: Solid Earth*, 101, B1 (1996), 523–532. doi:10.1029/95JB02806. (cited on page 107)

Kanamori, H. and Stewart, G. S., 1976. Mode of the strain release along the Gibbs fracture zone, Mid-Atlantic ridge. *Physics of the earth and planetary interiors*, 11, 4 (1976), 312–332. doi:10.1016/0031-9201(76)90018-2. (cited on page 107)

Kassi, A. M.; Bayraktar, H.; Khan, S. D.; and Kasi, A. K., 2017. Recurring emergence of the mud islands on shelf of the arabian sea along the makran coast of pakistan–historical perspective using remote sensing techniques. *Journal of the Geological Society of India*, 90, 2 (2017), 201–208. doi:10.1007/s12594-017-0700-1. (cited on page 85)

Kikuchi, M. and Kanamori, H., 1982. Inversion of complex body waves. *Bulletin of the Seismological Society of America*, 72, 2 (1982), 491–506. (cited on page 107)

Kikuchi, M. and Kanamori, H., 1986. Inversion of complex body waves - II. *Physics of the earth and planetary interiors*, 43, 3 (1986), 205–222. doi:10.1016/0031-9201(86)90048-8. (cited on page 107)

Kikuchi, M. and Kanamori, H., 1991. Inversion of complex body waves - III. *Bulletin of the Seismological Society of America*, 81, 6 (1991), 2335–2350. (cited on page 107)

KKP, K., 2017a. Maritim Indonesia, kemewahan yang luar biasa. https://kkp.go.id/artikel/2233-maritim-indonesia-kemewahan-yang-luar-biasa. Written by Elviana Roza. (cited on page 7)

KKP, K., 2017b. Refleksi 2017 dan outlook 2018 membangun dan menjaga ekosistem laut Indonesia bersama DITJEN Pengelolaan Ruang Laut. https://kkp.go.id/djprl/artikel/2798-refleksi-2017-dan-outlook-2018-membangun-dan-menjaga-ekosistem-laut-indonesia-bersama-ditjen-pengelolaan-ruang-laut. https://kkp.go.id/djprl/artikel/2798-refleksi-2017-dan-outlook-2018-membangun-dan-menjaga-ekosistem-laut-indonesia-bersama-d (cited on page 7)

Konca, A. O.; Hjorleifsdottir, V.; Song, T.-R. A.; Avouac, J.-P.; Helmberger, D. V.; Ji, C.; Sieh, K.; Briggs, R.; and Meltzner, A., 2007. Rupture kinematics of the 2005 Mw 8.6 Nias–Simeulue earthquake from the joint inversion of seismic and geodetic data. *Bulletin of the Seismological Society of America*, 97, 1A (2007), S307–S322. doi:10.1785/0120050632. (cited on page 107)

Koulali, A.; Susilo, S.; McClusky, S.; Meilano, I.; Cummins, P.; Tregoning, P.; Lister, G.; Efendi, J.; and Syafi'i, M. A., 2016. Crustal strain partitioning and the associated earthquake hazard in the Eastern Sunda-Banda Arc. *Geophysical Research Letters*, (2016), 1943–1949. doi:10.1002/2016GL067941. (cited on pages xviii, 7, 98, 99, and 100)

Kruschke, M., 2011. *Doing Bayesian data analysis: A tutorial with R and BUGS*. Else, Amsterdam, the Netherlands, second edn. (cited on page 131)

Lander, J. F.; Whiteside, L. S.; and Lockridge, P. A., 2003. Two decades of global tsunamis. *Science of Tsunami Hazards*, 21, 1 (2003), 3. (cited on pages 19, 28, and 42)

Lassa, J., 2009. Bencana yang terlupakan? mengingat kembali bencana Larantuka dan Lembata 1979-2009 (the forgotten disasters? remembering the larantuka and lembata disaster 1979-2009). *Journal of NTT Studies*, 1, 2 (2009), 159–184. (cited on pages 19, 28, and 36)

Latief, H.; Kodijat, A.; Ismoyo, D.; Bustamam, B.; Adyasar, D.; Nurbandika, N.; and Rahayu, H., 2016. *Air turun naik di tiga negeri*. United Nations Educational, Scientific, and Cultural Organization, Office Jakarta - Indian Ocean Tsunami Information Centre. In Indonesian. (cited on pages 28, 34, 54, and 67)

Latief, H.; Puspito, N. T.; and Imamura, F., 2000. Tsunami catalog and zones in Isndonesia. *Journal of Natural Disaster Science*, 22, 1 (2000), 25–43. (cited on pages xv, 4, 14, 16, 17, 18, 19, 28, 29, 39, 47, and 117)

Linthout, K.; Helmers, H.; Wijbrans, J. R.; and Van Wees, J. D. A., 1996. 40Ar/39Ar constraints on obduction of the Seram ultramafic complex: consequences for the evolution of the southern Banda Sea. *Geological Society, London, Special Publications*, 106, 1 (1996), 455–464. (cited on page 79)

Liu, P. L.-F.; Cho, Y.-S.; Briggs, M. J.; Kanoglu, U.; and Synolakis, C. E., 1995. Runup of solitary waves on a circular island. *Journal of Fluid Mechanics*, 302 (1995), 259–285. doi:10.1017/S0022112095004095. (cited on page 101)

Liu, Z. Y.-C. and Harris, R. A., 2014. Discovery of possible mega-thrust earthquake along the Seram Trough from records of 1629 tsunami in eastern Indonesian region. *Natural Hazards*, 72, 3 (2014), 1311–1328. doi:10.1007/s11069-013-0597-y. (cited on pages xviii, 28, 34, 79, 81, 87, 88, and 92)

Lorito, S.; Romano, F.; Piatanesi, A.; and Boschi, E., 2008. Source process of the September 12, 2007, Mw 8.4 southern Sumatra earthquake from tsunami tide gauge record inversion. *Geophysical Research Letters*, 35, 2 (2008). doi:10.1029/2007GL032661. (cited on pages 28 and 31)

Løvholt, F.; Harbitz, C. B.; Farrokh, N.; Birkmann, J.; Setiadi, N. J.; Bach, C.; and Fernando, N., 2014. Tsunami risk reduction: Are we better prepared today than in 2004? Input paper: Prepared for the global assessment report on disaster risk reduction 2015, UNISDR, Geneva, Switzerland. (cited on page 1)

Løvholt, F.; Kühn, D.; Bungum, H.; Harbitz, C. B.; and Glimsdal, S., 2012. Historical tsunamis and present tsunami hazard in eastern Indonesia and the southern Philippines. *Journal of Geophysical Research: Solid Earth*, 117, B9 (2012). doi:10.1029/2012JB009425. (cited on pages 50, 66, 77, 96, and 118)

Lynett, P. J.; Borrero, J. C.; Liu, P. L.-F.; and Synolakis, C. E., 2003. Field survey and numerical simulations: A review of the 1998 Papua New Guinea tsunami. In *Landslide Tsunamis: Recent Findings and Research Directions*, 2119–2146. Springer. doi:10.1007/978-3-0348-7995-8_16. (cited on page 128)

Maramai, A. and Tinti, S., 1997. The 3 June 1994 Java tsunami: A post-event survey of the coastal effects. *Natural Hazards*, 15, 1 (1997), 31–49. doi:10.1023/A:1007957224367. (cited on pages 28 and 31)

Marliyani, G.; Arrowsmith, J.; and Helmi, H., 2019. Evidence for multiple ground-rupturing earthquakes in the past 4000 years along the Pasuruan Fault, East Java, Indonesia: Documentation of active normal faulting in the Javan Backarc. *Tectonics*, (2019). doi:10.1029/2018TC005255. (cited on pages 84 and 85)

Martin Jr., O., 1967. *Science and the Sea*, chap. Underwater Disturbances, 53–60. U.S. Naval Oceanographic Office, Washington, D.C. (cited on page 35)

Matsutomi, H.; Shuto, N.; Imamura, F.; and Takahashi, T., 2001. Field survey of the 1996 Irian Jaya earthquake tsunami in Biak Island. *Natural Hazards*, 24, 3 (2001), 199–212. doi:10.1023?A:1012042222880. (cited on pages 28 and 45)

Mayberry, K., 2018. Indonesia quakes a 'wake-up call' on buildings' shaky foundations. Website. https://www.aljazeera.com/news/2018/10/indonesia-quakes-wake-call-buildings-shaky-foundations-181018015500435.html. Last accessed on 20 November 2019. (cited on page 8)

McCaffrey, R., 1988. Active tectonics of the eastern Sunda and Banda arcs. *Journal of Geophysical Research: Solid Earth*, 93, B12 (1988), 15163–15182. doi:10.1029/JB093iB12p15163. (cited on pages 3, 7, 49, and 81)

McCaffrey, R. and Nabalek, J., 1984. The geometry of back arc thrusting along the eastern Sunda Arc, Indonesia: Constraints from earthquake and gravity data. *Journal of Geophysical Research*, 89, B7 (Jul. 1984), 6171–6179. (cited on pages 98 and 114)

McCaffrey, R. and Nabalek, J., 1987. Earthquakes, gravity, and the origin of the Bali basin: An example of a nascent continental fold-and-thrust belt. *Journal of Geophysical Research*, 92, B1 (Jan. 1987), 441–460. (cited on page 7)

McCloskey, J.; Lange, D.; Tilmann, F.; Nalbant, S. S.; Bell, A. F.; Natawidjaja, D. H.; and Rietbrock, A., 2010. The September 2009 Padang earthquake. *Nature Geoscience*, 3, 2 (2010), 70. doi:10.1038/ngeo753. (cited on page 28)

Meade, B. J., 2007. Algorithms for the calculation of exact displacements, strains, and stresses for triangular dislocation elements in a uniform elastic half space. *Computers & geosciences*, 33, 8 (2007), 1064–1075. doi:10.1016/j.cageo.2006.12.003. (cited on pages 90 and 135)

Muhari, A.; Imamura, F.; Arikawa, T.; Hakim, A. R.; ; and Afriyanto, B., 2018. Solving the puzzle of the September 2018 Palu, Indonesia, tsunami mystery: Clues from the tsunami waveform and the initial field survey data. *Journal of Disaster Research*, (2018), sc20181108. doi:10.20965/jdr.2018.sc20181108. (cited on pages 28 and 39)

Nakamura, M., 2009. Fault model of the 1771 Yaeyama earthquake along the Ryukyu trench estimated from the devastating tsunami. *Geophysical Research Letters*, 36, 19 (2009). doi:10.1029/2009GL039730. (cited on page 108)

Natawidjaja, D. H.; Sieh, K.; Chlieh, M.; Galetzka, J.; Suwargadi, B. W.; Cheng, H.; Edwards, R. L.; Avouac, J.-P.; and Ward, S. N., 2006. Source parameters of the great Sumatran megathrust earthquakes of 1797 and 1833 inferred from coral microatolls. *Journal of Geophysical Research: Solid Earth*, 111, B6 (2006). doi:10.1029/2005JB004025. (cited on pages 28, 30, and 123)

Natawidjaja, D. H.; Sieh, K.; Ward, S. N.; Cheng, H.; Edwards, R. L.; Galetzka, J.; and Suwargadi, B. W., 2004. Paleogeodetic records of seismic and aseismic subduction from central Sumatran microatolls, Indonesia. *Journal of Geophysical Research: Solid Earth*, 109, B4 (2004). doi:10.1029/2003JB002398. (cited on pages 30 and 123)

Nathalia, T. and Ismar, A., 2009. Four killed as quake strikes Indonesia's Papua. Reuters. https://www.reuters.com/article/us-quake-indonesia/four-killed-as-quake-strikes-indonesias-papua-idUSTRE50304B20090104. Last accessed on 10 May 2019. (cited on page 46)

Newcomb, K. and McCann, W., 1987. Seismic history and seismotectonics of the Sunda Arc. *Journal of Geophysical Research: Solid Earth*, 92, B1 (1987), 421–439. doi:10.1029/JB092iB01p00421. (cited on pages 28, 30, and 31)

Newman, A. V.; Hayes, G.; Wei, Y.; and Convers, J., 2011. The 25 October 2010 Mentawai tsunami earthquake, from real-time discriminants, finite-fault rupture, and tsunami excitation. *Geophysical Research Letters*, 38, 5 (2011). doi:10,129/2010GL046498. (cited on pages 28 and 31)

NGDC/WDS, N. G. D. C. D. S., 2019. Global Historical Tsunami Database. Technical report, National Geophysical Data Center, NOAA. http://www.ngdc.noaa.gov/. Doi:10.7289/V5PN93H7. (cited on pages xv, 4, 14, 15, 16, 17, 19, 28, 41, and 42)

Nguyen, N.; Griffin, J.; Cipta, A.; and Cummins, P. R., 2015. Indonesia's historical earthquakes. Technical Report 23, Geoscience Australia. www.ga.gov.au. (cited on pages 47 and 122)

NOAA/NWS, N., 2004. Tsunami of 11 November 2004. NOAA / Natioanal Weather Service. https://www.tsunami.gov/previous.events/?p=11-11-04. Last accessed on 10 May 2019. (cited on page 37)

Nomanbhoy, N. and Satake, K., 1995. Generation mechanism of tsunamis from the 1883 Krakatau eruption. *Geophysical Research Letters*, 22, 4 (1995), 509–512. (cited on pages 10 and 28)

Nugroho, H.; Harris, R.; Lestariya, A. W.; and Maruf, B., 2009. Plate boundary reorganization in the active Banda Arc–continent collision: Insights from new GPS measurements. *Tectonophysics*, 479, 1-2 (2009), 52–65. doi:10.1016/j.tecto.2009.01.026. (cited on page 98)

OCHA/GVA, 2000. Indonesia - earthquake OCHA situation report No. 2. Reliefweb. https://reliefweb.int/report/indonesia/indonesia-earthquake-ocha-situation-report-no-2-0. (cited on page 42)

OCHA/GVA, 2002. Indonesia - earthquake OCHA situation report No. 3. Reliefweb. https://reliefweb.int/report/indonesia/indonesia-earthquake-ocha-situation-report-no-3-0. (cited on pages 28 and 46)

Okada, Y., 1985. Surface deformation due to shear and tensile faults in a half-space. *Bulletin of the Seismological Society of America*, 75, 4 (August 1985), 1135–1154. (cited on pages 66, 107, 108, 130, and 135)

Okal, E. A., 1999. Historical seismicity and seismotectonic context of the great 1979 Yapen and 1996 Biak, Irian Jaya earthquakes. In *Seismogenic and Tsunamigenic Processes in Shallow Subduction Zones*, 633–675. Springer. (cited on pages 28 and 45)

Okal, E. A. and Reymond, D., 2003. The mechanism of great Banda Sea earthquake of 1 February 1938: Applying the method of preliminary determination of focal mechanism to a historical event. *Earth and Planetary Science Letters*, 216, 1-2 (2003), 1–15. doi:10.1016/S0012-821X(03)00475-8. (cited on pages 28, 35, 62, 63, 64, and 92)

Okal, E. A. and Synolakis, C. E., 2004. Source discriminants for near-field tsunamis. *Geophysical Journal International*, 158, 3 (2004), 899–912. doi:10.1111/j.1365-246X.2004.02347.x. (cited on pages 63 and 64)

Olson, A. H. and Apsel, R. J., 1982. Finite faults and inverse theory with applications to the 1979 Imperial Valley earthquake. *Bulletin of the Seismological Society of America*, 72, 6A (1982), 1969–2001. (cited on page 107)

Pagani, M.; Monelli, D.; Weatherill, G.; Danciu, L.; Crowley, H.; Silva, V.; Henshaw, P.; Butler, L.; Nastasi, M.; Panzeri, L.; et al., 2014. Openquake engine: An open hazard (and risk) software for the global earthquake model. *Seismological Research Letters*, 85, 3 (2014), 692–702. (cited on pages 112 and 131)

Pairault, A. A.; Hall, R.; and Elders, C. F., 2003. Structural styles and tectonic evolution of the Seram Trough, Indonesia. *Marine and Petroleum Geology*, 20, 10 (2003), 1141–1160. doi:10.1016/j.marpetgeo.2003.10.001. (cited on page 50)

Paris, R.; Switzer, A. D.; Belousova, M.; Belousov, A.; Ontowirjo, B.; Whelley, P. L.; and Ulvrova, M., 2014. Volcanic tsunami: a review of source mechanisms, past events and hazards in Southeast Asia (Indonesia, Philippines, Papua New Guinea). *Natural Hazards*, 70, 1 (2014), 447–470. doi:10.1007/s11069-013-0822-8. (cited on pages xv, 2, 9, 10, 12, 14, 16, 19, 28, and 42)

Patria, A. and Hall, R., 2017. The Origin and Significance of the Seram Trough, Indonesia. (2017). (cited on page 50)

Patton, J.; Stein, R.; and Sevilgen, V., 2018. Sunda Strait tsunami launched by sudden collapse of Krakatau volcano into the sea. Temblor. http://doi.org/10.32858/temblor.001. (cited on pages xv, 2, 10, 32, and 75)

Pelinovsky, E.; Yuliadi, D.; Prasetya, G.; and Hidayat, R., 1997. The 1996 Sulawesi tsunami. *Natural Hazards*, 16, 1 (1997), 29–38. doi:10.1023/A:1007904610680. (cited on pages xvi, 28, 39, and 40)

Peregrine, D. H., 1972. Equations for water waves and the approximations behind them. *Waves on beaches and resulting sediment transport*, (1972), 95–121. (cited on page 125)

Pownall, J.; Hall, R.; and Lister, G., 2016. Rolling open Earth's deepest forearc basin. *Geology*, (2016). doi:10.1130/G38051.1. (cited on pages xvii, 50, 51, 77, 78, 79, 80, 90, 93, 119, 120, 122, 135, and 137)

Pownall, J.; Hall, R.; and Watkinson, I., 2013. Extreme extension across Seram and Ambon, eastern Indonesia: evidence for Banda slab rollback. *Solid Earth*, 4, 2 (2013), 277–314. doi:10.5194/se-4-277-2013. (cited on pages 3, 7, 49, 50, 77, 78, and 79)

Pownall, J. M.; Forster, M. A.; Hall, R.; and Watkinson, I. M., 2017. Tectonometamorphic evolution of Seram and Ambon, eastern Indonesia: Insights from 40Ar/39Ar geochronology. *Gondwana Research*, 44 (2017), 35–53. doi:10.1016/j.gr.2016.10.018. (cited on page 79)

Pranantyo, I. R. and Cummins, P. R., 2019. Multi–Data–Type Source Estimation for the 1992 Flores Earthquake and Tsunami. *Pure and Applied Geophysics*, 176, 7 (Jan 2019), 2969–2983. doi:10.1007/s00024-018-2078-4. (cited on pages 7, 28, 37, and 75)

Prasetya, G.; De Lange, W.; and Healy, T., 2001. The Makassar Strait tsunamigenic region, Indonesia. *Natural Hazards*, 24, 3 (2001), 295–307. doi:10.1023/A:1012297413280. (cited on pages 28 and 39)

Pribadi, K.; Kusumastuti, D.; and Rildova, 2008. Learning from recent Indonesian earthquakes: An overover to improve structural performance. In *The 14th World Conference on Earthquake Engineering*. Beijing, China. (cited on page 8)

PUSGEN, T., 2017. Peta sumber dan bahaya gempa Indonesia tahun 2017. Technical report, Pusat Litbang Perumahan dan Permukiman, Kementerian Pekerjaan Umum dan Perumahan Rakyat, Jalan Panyaungan, Cileunyi Wetan, Kabupaten Bandung. In Bahasa Indonesia. (cited on page 123)

Reclus, J. J. É., 1885. *The earth and its inhabitants: The universal geography*, vol. XIV (Australasia). JS Virtue & Co., London. https://archive.org/details/universalgeograp14recl. Edited by Keane, A.H. (cited on pages xx and 134)

Reid, A., 2015. History and seismology in the Ring of Fire: Punctuating the Indonesian past. In *Southeast Asia in the Longue Durée*, 62–77. JSTOR. (cited on page 29)

Rhodes, B.; Tuttle, M.; Horton, B.; Doner, L.; Kelsey, H.; Nelson, A.; and Cisternas, M., 2006. Paleotsunami research. *Eos, Transactions American Geophysical Union*, 87, 21 (2006), 205–209. doi:10.1029/2006EO210002. (cited on page 122)

Rumphius, G. E., 1675. *Waerachtigh Verhael van de Schuckelijcke Aerdbebinge*. BATAVIA. Translated by Beekman, E.M. and Foss, F. (1997) as "True history of the terrible earthquake", published and edited by Buijze, W. (cited on pages xxiii, 4, 14, 15, 19, 28, 34, 50, 52, 54, 57, 62, 71, 74, and 117)

Sandiford, M., 2008. Seismic moment release during slab rupture beneath the Banda Sea. *Geophysical Journal International*, 174, 2 (2008), 659–671. doi:10.111/j.1365-246X.2008.03838.x. (cited on page 98)

Sandiford, M., 2010. Geodynamics: Complex subduction. *Nature Geoscience*, 3, 8 (2010), 518. doi:10.1038/ngeo928. (cited on pages 7 and 78)

Sandwell, D.; Gille, S.; and Smith, W., 2002. Bathymetry from Space: Ocean, Geophysics, and Climate. Technical report, Geoscience Professional Services, Bethesda,

Maryland. https://www.geo-prose.com/pdfs/bathy_from_space.pdf. (cited on page 128)

Sassa, S. and Takagawa, T., 2019. Liquefied gravity flow-induced tsunami: first evidence and comparison from the 2018 Indonesia Sulawesi earthquake and tsunami disasters. *Landslides*, 16, 1 (2019), 195–200. doi:10.1007/s10346-018-1114-x. (cited on pages 1 and 75)

Satake, K., 1987. Inversion of tsunami waveforms for the estimation of a fault heterogeneity: Method and numerical experiments. *Journal of Physics of the Earth*, 35, 3 (1987), 241–254. doi:10.4294/jpe1952.35.241. (cited on page 107)

Satake, K., 1993. Depth distribution of coseismic slip along the Nankai Trough, Japan, from joint inversion of geodetic and tsunami data. *Journal of Geophysical Research: Solid Earth*, 98, B3 (1993), 4553–4565. doi:10.1029/92JB01553. (cited on page 107)

Satake, K., 2002. Tsunamis. In *International Handbook of Earthquake and Engineering Seismology, Part A* (Eds. W. H. Lee; H. Kanamori; P. C. Jennings; and C. K. linger), vol. 81 of *International Geophysics*, 437 – 451. Academic Press. doi:https://doi.org/10.1016/S0074-6142(02)80231-5. http://www.sciencedirect.com/science/article/pii/S0074614202802315. (cited on page 125)

Satake, K., 2015. Tsunamis. In *Treatise on Geophysics (Second Edition)* (Ed. G. Schubert), 477 – 504. Elsevier, Oxford, second edition edn. ISBN 978-0-444-53803-1. doi:https://doi.org/10.1016/B978-0-444-53802-4.00086-5. http://www.sciencedirect.com/science/article/pii/B9780444538024000865. (cited on pages xv and 10)

Satake, K. and Imamura, F., 1995. Introduction to âĂIJtsunamis: 1992–94âĂİ. In *Tsunamis: 1992–1994*, 373–379. Springer. doi:10.1007/978-3-0348-7279-9_1. (cited on page 28)

Satake, K.; Nishimura, Y.; Putra, P. S.; Gusman, A. R.; Sunendar, H.; Fujii, Y.; Tanioka, Y.; Latief, H.; and Yulianto, E., 2013. Tsunami source of the 2010 Mentawai, Indonesia earthquake inferred from tsunami field survey and waveform modeling. *Pure and Applied Geophysics*, 170, 9-10 (2013), 1567–1582. doi:10.1007/s00024-012-0536-y. (cited on pages 28 and 31)

Schindelé, F.; Reymond, D.; Gaucher, E.; and Okal, E., 1995. Analysis and automatic processing in near-field of eight 1992–1994 tsunamigenic earthquakes: Improvements towards real-time tsunami warning. *pure and applied geophysics*, 144, 3-4 (1995), 381–408. doi:10.1007/BF00874374. (cited on page 28)

Sexton, J.; Johnson, C.; and Blewett, S., 2011. Tsunami: Teacher notes and student activities. Geoscience Australia, Canberra. 2nd edn. Record No.2011/27. (cited on pages xv, 10, and 11)

Silver, E. A.; Breen, N. A.; and Prasetyo, H., 1986. Multibeam study of the Flores Back-Arc thrust belt, Indonesia. *Journal of Geophysical Research*, 91, B3 (March 1986), 3489–3500. doi:10.1029/JB091iB03p03489. (cited on pages xviii, 7, 98, 100, and 114)

Silver, E. A.; Reed, D.; and McCaffrey, R., 1983. Back arc thrusting in the Eastern Sunda arc, Indonesia: A consequence of arc-continent collision. *Journal of Geophysical Research*, 88, B9 (Sep. 1983), 7429–7488. doi:10.1029/JB088iB09p07429. (cited on pages xviii, 7, 98, and 100)

Singh, S. C.; Hananto, N.; Qin, Y.; Leclerc, F.; Avianto, P.; Tapponnier, P. E.; Carton, H.; Wei, S.; Nugroho, A. B.; Gemilang, W. A.; et al., 2017. The discovery of a conjugate system of faults in the Wharton Basin intraplate deformation zone. *Science advances*, 3, 1 (2017), e1601689. doi:10.1126/sciadv.1601689. (cited on pages 28 and 31)

Socquet, A.; Simons, W.; Vigny, C.; McCaffrey, R.; Subarya, C.; Sarsito, D.; Ambrosius, B.; and Spakman, W., 2006. Microblock rotations and fault coupling in SE Asia triple junction (Sulawesi, Indonesia) from GPS and earthquake slip vector data. *Journal of Geophysical Research: Solid Earth*, 111, B8 (2006). doi:10.1029/2005JB003963. (cited on page 8)

Soloviev, S.; Go, C.; and Kim, X., 1986. Catalog of tsunamis in the Pacific Ocean, 1969-1982. *Moscow, MGC, 163p*, (1986). (cited on pages xv, 4, 14, 15, 17, 18, 19, 28, 39, 45, 47, and 75)

Soloviev, S. and Go, C. N., 1974. Catalog of tsunamis in western coast of the Pacific Ocean. *Academy of Sciences, USSR, Izdat. Nauka*, (1974), 1–130. English translation by Sidney O. Wigen, Institute of Ocean Sciences, Department of Fisheries and Oceans, 5077, Sidney, Canada, 1984. (cited on pages xv, 4, 14, 15, 17, 18, 19, 28, 34, 35, 36, 38, 39, 40, 41, 42, 44, 45, 47, 50, 52, 54, 61, 75, 77, 81, 88, 91, 92, and 94)

Spakman, W. and Hall, R., 2010. Surface deformation and slab–mantle interaction during Banda arc subduction rollback. *Nature Geoscience*, 3, 8 (2010), 562. doi:10.1038/NGEO917. (cited on pages 3, 7, 49, 50, 61, 77, 78, 79, 81, and 98)

Storchak, D. A.; Di Giacomo, D.; Bondár, I.; Engdahl, E. R.; Harris, J.; Lee, W. H.; Villaseñor, A.; and Bormann, P., 2013. Public release of the ISC–GEM global instrumental earthquake catalogue (1900–2009). *Seismological Research Letters*, 84, 5 (2013), 810–815. doi:10.1785/0220130034. (cited on pages 34, 35, 38, 39, 41, 42, 44, and 45)

Sull-Teng, K. H., 2019. Gempa dan tsunami Banggai, 4 Mei 2000. Website. http://komunitashistoriasul-teng.simplesite.com/430649051/6706224/posting/. Last accessed on 10 May 2019. (cited on pages 28 and 42)

Synolakis, C.; Imamura, F.; Tsuji, Y.; Matsutomi, H.; Tinti, S.; Cook, B.; Chandra, Y.; and Usman, M., 1995. Damage, conditions of East Java tsunami of 1994

analyzed. *EOS, Transactions American Geophysical Union*, 76, 26 (1995), 257–257. doi:10.1029/95EO00150. (cited on page 28)

Synolakis, C. E., 1991. Green's law and the evolution of solitary waves. *Physics of Fluids A: Fluid Dynamics*, 3, 3 (1991), 490–491. doi:10.1063/1.858107. (cited on page 71)

Synolakis, C. E.; Bardet, J.-P.; Borrero, J. C.; Davies, H. L.; Okal, E. A.; Silver, E. A.; Sweet, S.; and Tappin, D. R., 2002. The slump origin of the 1998 Papua New Guinea tsunami. *Proceedings of the Royal Society of London. Series A: Mathematical, Physical and Engineering Sciences*, 458, 2020 (2002), 763–789. doi:10.1098/rspa.2001.0915. (cited on page 63)

Tanioka, Y.; Satake, K.; and Ruff, L., 1995. Total analysis of the 1993 Hokkaido Nansei-Oki earthquake using seismic wave, tsunami, and geodetic data. *Geophysical research letters*, 22, 1 (1995), 9–12. (cited on page 107)

Tappin, D.; Watts, P.; McMurtry, G.; Lafoy, Y.; and Matsumoto, T., 2001. The Sissano, Papua New Guinea tsunami of July 1998âĂŤoffshore evidence on the source mechanism. *Marine Geology*, 175, 1-4 (2001), 1–23. doi:10.1016/S0025-3227(01)00131-1. (cited on page 63)

Tappin, D. R., 2017. Tsunamis from submarine landslides. *Geology Today*, 33, 5 (2017), 190–200. doi:10.1111/gto.12200. (cited on page 63)

Tappin, D. R.; Matsumoto, T.; Watts, P.; Satake, K.; McMurtry, G. M.; Matsuyama, M.; Lafoy, Y.; Tsuji, Y.; Kanamatsu, T.; Lus, W.; et al., 1999. Sediment slump likely caused 1998 papua new guinea tsunami. *Eos, Transactions American Geophysical Union*, 80, 30 (1999), 329–340. doi:10.1029/99EO00241. (cited on page 63)

ten Brink, U.; Lee, H.; Geist, E.; and Twichell, D., 2009. Assessment of tsunami hazard to the U.S. East Coast using relationships between submarine landslides and earthquakes. *Marine Geology*, 264 (2009), 65âĂŞ73. doi:10.1016/j.margeo.2008.05.011. (cited on page 93)

The New Humanitarian, 2009. Indonesia: Quake devastation exposes poor building standards. Website. https://reliefweb.int/report/indonesia/indonesia-quake-devastation-exposes-poor-building-standards. Last accessed 20 November 2019. (cited on page 8)

Trifunac, M., 1974. A three-dimensional dislocation model for the San Fernando, California, earthquake of February 9, 1971. *Bulletin of the Seismological Society of America*, 64, 1 (1974), 149–172. (cited on page 107)

Tsuji, Y.; Imamura, F.; Matsutomi, H.; Synolakis, C. E.; Nanang, P. T.; Harada, S.; Han, S. S.; Arai, K.; Cook, B.; et al., 1995a. Field survey of the East Java earthquake and tsunami of June 3, 1994. In *Tsunamis: 1992–1994*, 839–854. Springer. doi:10.1007/978-3-0348-7279-9_25. (cited on page 28)

Tsuji, Y.; Matsutomi, H.; Imamura, F.; Takeo, M.; Kawata, Y.; Matsuyama, M.; Takahashi, T.; Sunarjo; and Harjadi, P., 1995b. Damage to coastal villages due to the 1992 Flores Island earthquake tsunami. *Pure and Applied Geophysics*, 144, 3-4 (1995), 481–524. doi:10.1007/BF00874380. (cited on pages xvi, xviii, xix, xxiii, 28, 37, 97, 99, 101, 102, 103, 104, 112, 113, and 143)

UNISDR, 2015. Making development sustainable: The future of disaster risk management. Global assessment report on disaster risk reduction, United Nations Office for Disaster Risk Reduction (UNISDR), Geneva, Switzerland. (cited on pages xv, 1, and 2)

U.S. Geological Survey, 2019. Earthquake catalog. USGS website. https://earthquake.usgs.gov/earthquakes/search/. Last accessed on 11 May 2019. (cited on pages xv, 9, and 34)

Usna, I.; Tjokrosapoetro, S.; and Wiryosujono, S., 1979. Geological interpretation of a seismic reflection profile across the Banda Sea between Wetar and Buru islands. *Bull. Geol. Res. Dev. Centre*, 1 (1979), 7–15. (cited on page 7)

Vernes, D., 1978. Slope movements type and processes. *Landslide analysis and control, Special Report*, 176 (1978), 11–33. (cited on page 10)

Vinogradova, N. T.; Ponte, R. M.; Quinn, K. J.; Tamisiea, M. E.; Campin, J.-M.; and Davis, J. L., 2015. Dynamic adjustment of the ocean circulation to self-attraction and loading effects. *Journal of Physical Oceanography*, 45, 3 (2015), 678–689. doi:10.1175/JPO-D-14-0150.1. (cited on page 125)

Ward, S. N. and Day, S., 2003. Ritter island volcanoâĂŤlateral collapse and the tsunami of 1888. *Geophysical Journal International*, 154, 3 (2003), 891–902. (cited on page 128)

Watkinson, I. M. and Hall, R., 2017. Fault systems of the eastern Indonesian triple junction: Earth'svaluation of Quaternary activity and implications for seismic hazards. *Geological Society, London, Special Publications*, 441, 1 (2017), 71–120. doi:10.1144/SP441.8. (cited on pages 51, 61, 62, 67, and 122)

Watts, P.; Grilli, S.; Tappin, D. R.; and Fryer, G. J., 2005. Tsunami generation by submarine mass failure II: Predictive equations and case studies. *Journal of Waterway, Port, Coastal, and Ocean Engineering*, (November/December 2005), 298–310. doi:10.1061/ASCE)0733-950X(2005)131:6(298). (cited on pages 113, 127, and 130)

Wells, D. L. and Coppersmith, K. J., 1994. New empirical relationships among magnitude, rupture length, rupture width, rupture area, and surface displacement. *Bulletin of the seismological Society of America*, 84, 4 (1994), 974–1002. (cited on page 62)

Wernicke, B., 1995. Low-angle normal faults and seismicity: A review. *Journal of Geophysical Research: Solid Earth*, 100, B10 (1995), 20159–20174. doi:10.1029/95JB01911. (cited on page 96)

Wichmann, A., 1918. *Die Erdbeben Des Indischen Archipels Bis Zum Jahre 1857*. Joahnnes Muller, Amsterdam. (cited on pages xv, 4, 14, 15, 17, 19, 28, 34, 35, 36, 42, 45, 47, 54, 75, 77, 81, 85, 88, 91, 92, 131, and 132)

Wichmann, A., 1922. *Die Erdbeben Des Indischen Archipels von 1858 bis 1877*. Uitgave van de Koninklijke Akademie van Wetenschappen, Amsterdam. (cited on pages xv, 4, 14, 15, 17, 19, 28, 42, 44, 47, 75, 88, and 92)

Williams, R.; Rowley, P.; and Garthwaite, M. C., 2019. Reconstructing the anak krakatau flank collapse that caused the december 2018 indonesian tsunami. *Geology*, 47, 10 (2019), 973–976. doi:10.1130/G46517.1. (cited on page 31)

World Bank, 1993. Indonesia Flores earthquake reconstruction project. Report, The World Bank. (cited on page 97)

Xiao, L.; Ward, S. N.; and Wang, J., 2015. Tsunami squares approach to landslide-generated waves: application to gongjiafang landslide, three gorges reservoir, china. *Pure and Applied Geophysics*, 172, 12 (2015), 3639–3654. doi:10.1007/s00024-015-1045-6. (cited on page 127)

Yalciner, A.; Hidayat, R.; Husrin, S.; Prasetya, G.; Annunziato, A.; Dogan, G.; Zaytsev, A.; Omira, R.; Proietti, C.; Probst, P.; Paparo, M.; Wronna, M.; Pronin, P.; Giniyatullin, A.; Putra, P.; Hartanto, D.; Ginanjar, G.; Kongko, W.; and Pelinovsky, E., 2018. The 28^{th} September 2018 Palu earthquake and tsunami - post tsunami field survey report. Technical report, ITST. (cited on pages xvi, 28, 39, and 41)

Yamanaka, Y. and Tanioka, Y., 2017. Estimating the topography before volcanic sector collapses using tsunami survey data and numerical simulations. *Pure and Applied Geophysics*, 174, 8 (2017), 3275–3291. doi:10.1007/s00024-017-1589-8. (cited on page 127)

Yeh, H.; Imamura, F.; Synolakis, C.; Tsuji, Y.; Liu, P.; and Shi, S., 1993. The Flores Island tsunamis. *EOS, Transactions, American Geophysical Union*, 74, 33 (Aug. 1993), 369. doi:10.1029/93EO00381. (cited on pages 28, 36, 97, 102, and 113)

Yudhicara, Y.; Bani, P.; and Darmawan, A., 2015. Geothermal System as the Cause of the 1979 Landslide Tsunami in Lembata Island, Indonesia. *Indonesian Journal on Geoscience*, 2, 2 (2015), 91–99. (cited on pages 28 and 36)

Zhao, J. X.; Zhou, S.; Zhou, J.; Zhao, C.; Zhang, H.; Zhang, Y.; Gao, P.; Lan, X.; Rhoades, D.; Fukushima, Y.; et al., 2016. Ground-motion prediction equations for shallow crustal and upper-mantle earthquakes in japan using site class and simple geometric attenuation functions. *Bulletin of the Seismological Society of America*, 106, 4 (2016), 1552–1569. doi:10.1785/0120150063. (cited on page 131)